VOL. 24 • NO. 2 • MID-FEBRUARY 1984

IGM83-000-381
CNRC 26447

Polymer ENGINEERING AND SCIENCE

POLYMER TOPICS

NRCC/IMRI
Mini-Symposium Series
Polymer Blends—'83

CONTENTS

69 Preamble/L.A. UTRACKI, Guest Editor

70 J. NOOLANDI/Recent Advances in the Theory of Polymeric Alloys

79 I.C. SANCHEZ/On the Nature of Polymer Interfaces and Interphases

87 M.A. WINNIK/Fluorescence Techniques in the Study of Polymer Colloids

98 S. VARENNES, G. CHARLET, and G. DELMAS/Use of the Lower Critical Solution Temperature for the Characterization of Polymer Mixtures and the Study of Their Compatibility: Application to Polyethylenes, Polypropylene, and Their Copolymers

104 S. BYWATER/Block Polymers. Characterization and Use in Polymer Blends

112 A. GARTON/Some Observations on Kinetic and Steric Limitations to Specific Interactions in Miscible Polymer Blends

117 M.M. DUMOULIN, L.A. UTRACKI, and J. LARA/Rheological and Mechanical Behavior of the UHMWPE/MDPE Mixtures

127 P. DEMONT, D. CHATAIN, and C. LACABANNE/Thermally Stimulated Creep of Polyethylene, Polypropylene, Copolymers, and Blends

135 P.R. COUCHMAN/The Composition-Dependent Glass Transition: Relations Between Temperature, Pressure, and Composition

144 T.M. MALIK and R.E. PRUD'HOMME/Dielectric Properties of Poly(α-Methyl-α-N-Propyl-β-Propiolactone)/Poly(Vinyl Chloride) Blends

153 J.M. OTTINO and N. SHAH/Analysis of Transient Sorption and Permeation of Small Molecules in Multiphase Polymer Systems

PUBLISHED BY THE SOCIETY OF PLASTICS ENGINEERS, INC.

Polymer ENGINEERING AND SCIENCE

Published by the Society of Plastics Engineers

EDITOR—Roger S. Porter
℅ Polymer Science and Engineering
University of Massachusetts
Amherst, Mass. 01003

GUEST EDITOR—L. A. Utracki
℅ Industrial Materials Research Institute
National Research Council of Canada
75, Boul. De Mortagne
Boucherville, Quebec
Canada J4B 6Y4

ASSOCIATE EDITOR—Richard E. Ball
℅ Western New England College
Springfield, Mass. 01119

ADVISORY BOARD

E. Baer
Case Institute of Technology
J. A. Biesenberger
Stevens Institute of Technology
D. M. Bigg
Battelle Columbus Laboratories
L. L. Blyler, Jr.
Bell Laboratories
L. J. Broutman
Illinois Institute of Technology
E. S. Clark
University of Tennessee
A. N. Gent
University of Akron
H. B. Hopfenberg
North Carolina State University
J. F. Johnson
University of Connecticut
M. R. Kamal
McGill University
R. P. Kambour
General Electric Company
J. R. Knox
Amoco Chemicals Corporation
S. Matsuoka
Bell Telephone Laboratories
B. Maxwell
Princeton University
C. L. McCormick
University of Southern Mississippi
D. R. Paul
University of Texas
J. R. A. Pearson
Imperial College of Science & Technology
D. H. Reneker
National Bureau of Standards
C. E. Rogers
Case Western Reserve University
R Salovey
University of Southern California
N. S. Schneider
Army Materials and Mechanics Research Center
T. L. Smith
IBM Research Center
Z. Tadmor
Israel Institute of Technology
M. Takayanagi
Kyushu University

PUBLICATIONS COMMITTEE

D. W. Riley, Chairman
Extrusion Engineers

R. P. Braddicks, Jr.
Plastics Consultant
R. D. Forger
Society of Plastics Engineers
J. C. Haarsma
S/C Electric Co.
J. L. Hull
Hull Corporation
D. Jesiolowski
Owens Illinois
M. A. Mendelsohn
Westinghouse Electric Corp.
R. S. Porter
University of Massachusetts
A. A. Schoengood
Society of Plastics Engineers
R. F. Staats-Westover
Bell Telephone Labs
G. R. Thom
Regal Plastics Company
A. M. Varner
Moldflow USA, Inc.
A. E. Whitney, Jr.
Goodyear Chemical

Copyright by the Society of Plastics Engineers, Inc., 1984. Reproduction in whole or in part without written permission is strictly prohibited.

Polymer Engineering and Science (ISSN 0032-3888) is printed at Waverly Press, Easton, MD 21601. Address changes, undeliverable copies and orders for subscriptions should be sent to Circulation Manager, Society of Plastics Engineers, 14 Fairfield Dr., Brookfield Center, Conn. 06805. Published monthly except for February, April, June, August, October, and December when published semi-monthly. Second-class postage paid at Brookfield Center, Conn., and additional entry offices. Accepted at special postal rate provided in P.M. Sec. 132.122.

Neither the Society of Plastics Engineers, Inc., nor **Polymer Engineering and Science** is responsible for the views expressed by individual contributors either in articles published in **Polymer Engineering and Science** or in technical papers presented at meetings of the Society.

Subscription rates for 1984. SPE members, 1 year—$70, 2 years—$125, 3 years—$175. Nonmembers (U.S. and North America), 1 year—$95, 2 years—$170, 3 years—$225. Corporate, Institutional or library, 1 year—$250. Postage charge for all subscriptions outside North America—$18 per year. Air delivery outside North America—$50 per year.

SOCIETY OF PLASTICS ENGINEERS, INC.
Business and Executive Offices, 14 Fairfield Dr., Brookfield Center, Conn. 06805

Robert D. Forger
Publisher
Gerald D. Neal
Circulation Manager
Janice E. Alexander
Production Manager
Jeannette M. Piastuch
Copy Editor

OFFICERS OF THE SOCIETY

Robert J. Schaffhauser
President
William C. Kuhlke
President-elect
Richard G. Johnson
First Vice President
Greg R. Thom
Second Vice President
Jacques de Craene
Vice President for International Affairs
John R. Kretzchmar
Secretary
Bruce A. Petersen
Treasurer
Robert D. Forger
Executive Director

POLYMER ENGINEERING & SCIENCE is indexed by:—Chemical Abstracts—Engineering Index, Inc.

PREAMBLE

This symposium, held April 12, 1983, was the eighth one organized and sponsored by the Industrial Materials Research Institute of the National Research Council of Canada, the third one on "Polymer Blends", and the last to be held in the old building. In the next few months we will be moving to the new, permanent location at 75 Blvd. de Mortagne in Boucherville, Quebec.

Judging by the experience of the past three years, the decision to concentrate the Institute's activities on mathematical modeling of plastics processing, polymer blends, and polymer composites, was a wise one. The responses of the national and international, as well as the commercial and academic communities, have been quite favorable. With the aid of the three annual symposia on these topics we are gradually developing a significant "in house" expertise as well as encouraging research and application on these commercially important subjects.

By publishing the proceedings of these meetings in *Polymer Engineering and Science* and in *Polymer Composites* we have been able to reach a very wide audience.

To date the proceedings of the first six symposia have been published and the seventh is in the final stage of review. Beginning with the last meeting (February 8, 1983) on mathematical modeling we will be storing the complete recordings of each symposium (lectures and discussions) for two years.

Of the eleven papers presented during this meeting the first four concentrate on thermodynamics: phase equilibria and compatibilization (Noolandi), properties of interphases (Sanchez), morphology and dynamics of phase separation (Winnik) and the use of the lower critical solubility temperature as an analytical tool for studying polymer blends and copolymers (Delmas-Patterson). The next two papers: on compatibilization by polymer blends (review by Bywater) and on morphology of blends (Garton) form a bridge to the remaining five presentations dealing with the rheology and transport properties of polymer blends in the molten and solid states. Here the flow and mechanical properties of polyethylenes (Dumoulin), the amorphous phase transitions in polyethylene-polypropylene systems (Lacabanne), the glass transition (Couchman), the relaxational properties of miscible polymer blends, PVC/PMPPL (Prud'homme) and the gas permeability through a multiphase film with complex morphologies (Ottino) were discussed.

Due to the nature of our Institute, the "applied" nature has been particularly stressed in these publications. It is especially gratifying to see that the theoretical calculations are reaching a stage of advancement which should be of direct interest to commercial R/D personnel.

L. A. Utracki
Symposium organizer and chairman,
and Guest Editor

Recent Advances in the Theory of Polymeric Alloys

JAAN NOOLANDI

Xerox Research Centre of Canada
2660 Speakman Drive
Mississauga, Ontario L5K 2L1
Canada

The theory of multicomponent polymeric systems, termed "polymeric alloys", composed of block copolymers, homopolymers and solvents is discussed. We first review the microscopic interfacial properties of polymeric mixtures, highlighting the interfacial activity of block copolymers as emulsifying agents in incompatible homopolymer blends. We then turn to some interesting features of the phase diagrams, such as homopolymer-induced mesophase formation and the existence of *eutectic* points, similar to those for metallurgical alloys. Finally, we address problems in polymer dynamics and present some recent new theoretical results based on the tube model.

INTRODUCTION

The use of polymeric alloys and composites in modern technological applications is greatly increasing in importance. While strong and lightweight materials have always been in demand by the aircraft industry, current research in automobile design and manufacture is directed towards replacing all metal parts in an automobile, including the engine block, by ceramics and plastics. The urgent requirement for specialty polymers with unique properties presents exciting challenges to the technologist and fascinating opportunities to the basic researcher.

This paper gives a brief overview of some of the recent advances in the theory of multicomponent polymeric systems. The phase diagrams of these systems show a rich variety of features similar to those encountered in physical metallurgy, and hence the use of the term "alloys". With the refinement of experimental tools such as small-angle X-ray and neutron scattering, considerable microscopic information about the microstructure of polymeric alloys is becoming available. It is appropriate, therefore, to encourage the theoretical development of this field, both for clarifying questions of practical importance, as well as developing new insights into polymer physics in general.

We first review the nature of the interphase between two immiscible homopolymers and follow with a description of the microdomain structure of pure block copolymers and block copolymers diluted with solvent. The remarkable interfacial activity of small amounts of block copolymer added to immiscible homopolymers is then discussed, and some examples of the phase diagrams of homopolymer-block copolymer mixtures are given. The paper concludes with a short excursion into polymer dynamics.

BLOCK COPOLYMER MICRODOMAIN STRUCTURE

A discussion of inhomogeneous polymeric systems, whether composed of homopolymers and/or block copolymers, naturally begins with a discussion of the interface. In *Fig. 1*, we show the interface between two immiscible homopolymers of infinite molecular weight, the simplest possible case. The lower half of the figure shows the density profiles of the two homopolymers through the interphase region. The physical principles governing the thickness of this region, a, and the interfacial tension, γ, are very simple. For a sharp interfacial profile we have the least number of contact points between the two different polymers and the enthalpic or interaction energy contribution to the total free energy is minimized. However, the entropic contribution to the free energy arising from the turning-back entropy of the polymer chains is also smallest for a narrow interphase, leading to an increase in the total free energy. A broad interphase, on the other hand, leads to an increase in the turning-back entropy but also increases the interaction energy. The optimum interphase thickness is of course determined by a balance between the entropy and the enthalpy, and the corresponding interfacial tension γ (obtained by dividing the interfacial free energy by the interfacial area) can be shown to be given by:

$$\gamma \sim Aa + \frac{B}{a}, \qquad (1)$$

where A is proportional to χ, the Flory-Huggins interaction parameter between segments of unlike polymers, and $B \sim b^2$, where b is an average segment length. Minimizing *Eq 1* with respect to a results in

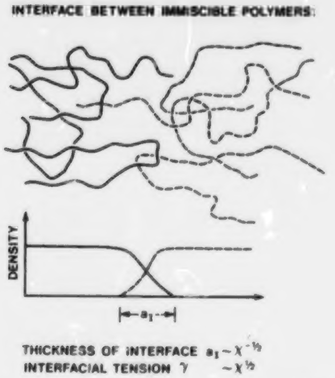
INTERFACE BETWEEN IMMISCIBLE POLYMERS:
DENSITY
a_I
THICKNESS OF INTERFACE $a_I \sim \chi^{-1/2}$
INTERFACIAL TENSION $\gamma \sim \chi^{1/2}$

Fig. 1. Interfacial density profile between immiscible homopolymers of infinite molecular weight.

$$a_I \sim \chi^{-1/2}, \qquad \gamma \sim \chi^{1/2}, \tag{2}$$

where both the enthalpic and entropic terms contribute equally to γ. These results were first obtained by Helfand and Tagami (1).

As shown earlier by Meier (2), we may apply the same principles to determine the interfacial properties of a diblock copolymer system as shown in *Fig. 2*. The situation here is somewhat more complicated than shown in *Fig. 1* because of the constraint introduced by tying the two blocks together chemically. Consequently, we must correctly take into account the reduction in the total entropy of the system arising from this constraint. In particular, the reduction in the entropy corresponding to the localization of the joints must be included in the free energy. A diblock copolymer system of roughly equal lengths for the two blocks forms a lamellar domain structure shown in the bottom half of *Fig. 2*. In this kind of structure, the chains inside the domains may be somewhat stretched to maintain an overall constant density in the system. This leads to an additional reduction in the total entropy.

The equilibrium domain spacing has been obtained theoretically by Meier (2, 3) and Helfand and Wasserman (4), by minimizing the total free energy in a mean field calculation, and generally good agreement with experiment has been obtained. An interesting feature of the pure block copolymer system is that depending on the ratio of the lengths of the two blocks, the microdomain structure may show different shapes as illustrated in *Fig. 3*. With short chains for one of the blocks, a spherical structure is found, and with increasing length of the minor block the spherical domains join to form cylinders. For equal lengths of the two blocks, the cylinders join to form lamellae. Of course, this simple set of structures is repeated in reverse as the other block decreases in length. The pure block copolymer system has been studied intensively both theoretically (1–6) and experimentally (6–10) over the last few years. Our main interest here is to look at mixtures of block copolymers with homopolymers and solvents. Thus, we first focus on a simple mixture consisting of an almost non-selective solvent such as toluene with a diblock copolymer such as isoprene-styrene.

The result of the detailed calculation by Noolandi and Hong (11) for the structure of such a system is shown in *Fig. 4*. For an increasing volume fraction of the solvent, the change of this structure can be easily understood by looking at the dominant terms in the free energy. The main contributions to the free energy per unit volume arise from the interfacial tension and the entropy of stretching of the two blocks,

$$\mathscr{F} = 2\gamma/d + \Phi_P C d^2 \tag{3}$$

where Φ_P is the volume fraction of polymer, and C is a constant. Minimizing the free energy with respect to the domain spacing gives the following simple result:

$$d^3 \propto \frac{\gamma(\Phi_P)}{\Phi_P} \tag{4}$$

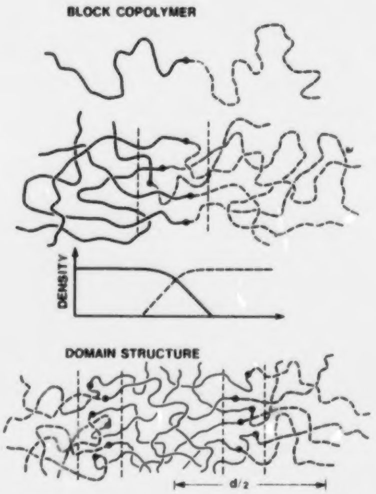

Fig. 2. Lamellar domain structure for diblock copolymers, showing interphase region.

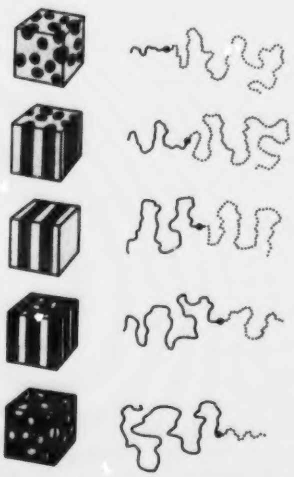

Fig. 3. Different microdomain structures for diblocks of varying composition.

For most immiscible polymers, the interfacial tension depends linearly on Φ_P through the overall amount of polymer in the system, and on $\Phi_P^{0.5}$ through the dilution of the strength of the interaction between unlike segments, giving in total $\gamma \sim \Phi_P^{1.5}$. *Equation 4* therefore predicts that the domain spacing should decrease with decreasing volume fraction of polymer, corresponding to more interpenetration of chains into dissimilar domains. This result has recently been observed by Hashimoto, *et al.* (12). The results for a detailed numerical calculation with different polymer-polymer interaction parameters are shown in *Fig. 5*. For fixed degree of polymerization of the two blocks, increasing the χ parameter for the interaction between block *A* and block *B* increases the equilibrium domain spacing, since the different blocks experience less interpenetration. However, upon dilution, the system dissolves into a homogeneous phase at the same value of the domain spacing, although a larger volume fraction of solvent is required to achieve this for the system with the larger χ parameter. This result illustrates another case of the "dilution" of the interaction discussed earlier, where the effect of the solvent can be accounted for by replacing the interaction parameter by $\chi\Phi_P$ (13). The verification of many of these theoretical predictions experimentally gives us confidence in applying the same theory to more complicated multi-component systems.

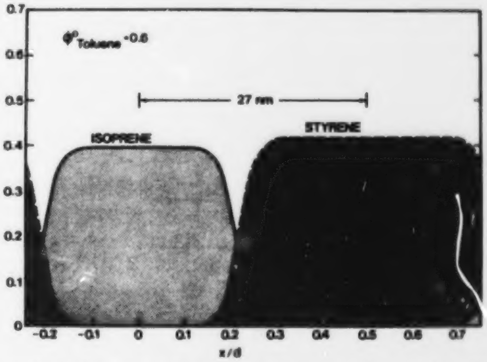

Fig. 4. Volume fractions of isoprene and styrene through lamellar microdomains for solvent volume fraction $\Phi^\circ_{Toluene} = 0.6$. The degree of polymerization of the polystyrene is $Z_{PS} = 587$ and $Z_{PI} = 647$. The different χ parameters are given in Ref. 11. d/2 is the spacing between the midpoints of neighboring microdomains.

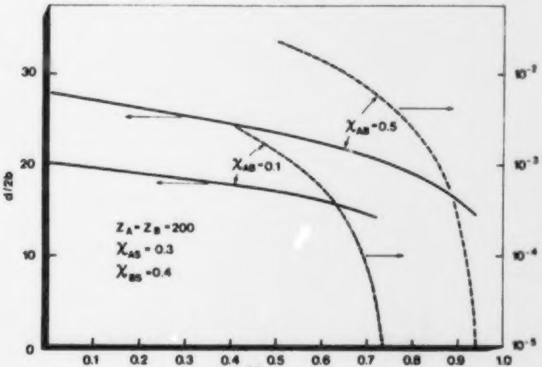

Fig. 5. Spacing (d/2) between midpoints of neighboring microdomains for diblock copolymers with lamellar structure in units of the Kuhn length b (left-hand scale) as a function of solvent volume fraction. The right-hand scale gives the free energy difference between the ordered and (hypothetical) uniform state. The density of the pure solvent is ρ_{0S}.

BLOCK COPOLYMERS AS EMULSIFYING AGENTS

A very important and interesting area in the subject of block copolymer-homopolymer mixtures is the study of block copolymers as emulsifiers for immiscible homopolymers. As is well known, the total free energy of a two-phase system is given by a bulk and interfacial contribution,

$$\mathcal{F} = \sum_i N_i\mu_i + \gamma A \qquad (5)$$

where μ_i is the chemical potential of component *i*, and *A* is the interfacial area. For a large interfacial tension γ, the interfacial area is usually a planar surface between the two phases. If an emulsifier is added to the system, the interfacial tension is decreased considerably, and it may be easy to increase the interfacial area. Thus, the system often breaks up into smaller microscopic droplets when it is subjected to agitation.

As shown originally by Riess, *et al.* (14), in the case of two immiscible homopolymers block copolymers may be used as the emulsifying agent. When the block copolymer is added to the system, some of it becomes localized at the interface and it is the nature of the interfacial activity resulting in the small interfacial tension which is of interest to us. Although the detailed theory of this effect by Noolandi and Hong (15) is quite complicated, some qualitative insight into the problem may be gained by considering the various contributions of a total free energy.

In *Fig. 6*, the table shows the various enthalpic and entropic contributions to the total free energy. Localization of some of the block copolymer at the interface (see *Fig. 7*) results in a lowering of the interaction energy between the two immiscible homopolymers. In addition, the region of the interphase between the homopolymers is considerably broadened, leading to an increase in the turning-back entropy of the polymer chains. The net effect of both contributions is to decrease the total free energy. Localization of the copolymer, on the other hand, results in a decrease in the entropy and ultimately limits the amount of copolymer present at the interphase. The separation of the two blocks into the corresponding homopolymer phases gives a decrease in the energy of interaction of the two blocks with each other as well as a large decrease in the interaction energy of the oriented blocks with the homopolymers, both with respect to the corresponding interactions when the copolymer is in either of the bulk phases. The separation of the blocks also results in a small decrease of the entropy. Finally, there is an additional decrease in entropy due to the stretching of the blocks of the

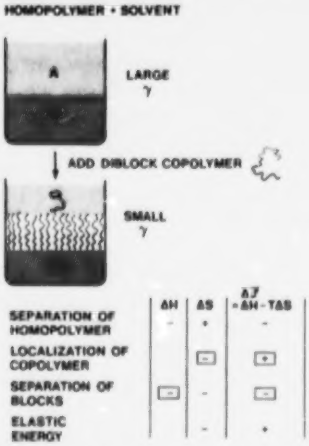

Fig. 6. Contributions of various terms to total free energy for system consisting of two immiscible homopolymers (including solvent) with diblock copolymer added as an emulsifying agent. The boxed terms indicate the main contributions to γ, the interfacial tension.

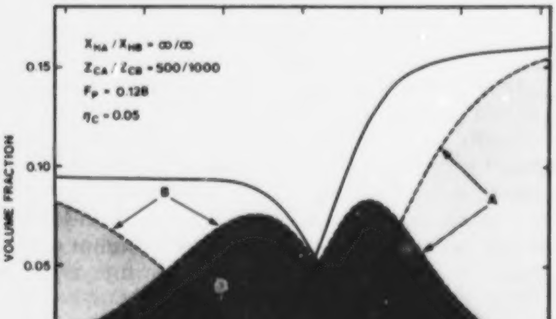

Fig. 7. Interfacial density profiles of styrene homopolymer (A: upper dashed curve), styrene blocks of copolymer (A: lower dashed curve), butadiene homopolymer (B: left dashed curve), butadiene blocks of copolymer (B: right dashed curve). The solid lines correspond to the total volume fractions of the A and B components, and the length through the interphase region is measured in units of the average Kuhn length, b. The degrees of polymerization of the homopolymers are denoted by X_{HA}, X_{HB} and the corresponding quantities for the blocks are Z_{CA}, Z_{CB}. F_P is the initial weight fraction of homopolymer present and η_C is the weight fraction of copolymer with respect to one of the (equal weight) homopolymers.

copolymer—the so-called elastic energy—resulting in an increase in the total free energy. The sum of all these contributions must be carefully evaluated in order to determine the effect on the surface tension between the two phases.

In *Fig. 7*, we show the interfacial density profiles of an immiscible homopolymer system to which block copolymer has been added. It should be noted that the overall density profiles of the *A* and *B* units of the two polymers remain almost invariant, with the block copolymer density almost completely replacing the reduced homopolymer density. However, there is considerable broadening of the homopolymer interphase region, as shown in the *figure*. The decreased interaction energy of the localized block copolymers with the homopolymers due to the separation of the blocks is mainly responsible for the reduction in the interfacial tension. Detailed calculations based on this theory have been carried out by Noolandi and Hong (15) for the polystyrene-polybutadiene and styrene system, with added polystyrene polybutadiene block copolymer. Many of the results are in agreement with experiment, but a lack of detailed microscopic information about the system makes comparison with theory difficult. At present, only the spinning-drop technique has been used by Gaillard, *et al.* (16) to measure the interfacial tension of these complicated systems. Hopefully, more sophisticated microscopic probes of the interface will be devised in the future.

PHASE EQUILIBRIA IN POLYMERIC ALLOYS

In order to study the phase diagrams of homopolymer-block copolymer mixtures of arbitrary composition, it is instructive to consider again the case of a symmetric block copolymer *A* and *B* in a non-selective solvent. If $Z_A = Z_B$, $Z_C = Z_A + Z_B$, and $\chi_{AS} = \chi_{BS}$, it has been shown by Noolandi and Hong (17) that microdomains are formed if the following generalized Leibler criterion (6) is satisfied:

$$\chi_{AB} Z_C \Phi_C \geq 10.5 \qquad (6)$$

where Φ_C is the total volume fraction of block copolymer. The reduction of the total free energy below the corresponding value for the homogeneous phase is then given by:

$$\Delta = -0.27\chi_{AB}(\Phi_C - 10.5/Z_C\chi_{AB})^2 \qquad (7)$$

In *Fig. 8*, we show a schematic diagram of the total free energy of the block copolymer solvent system in which mesophase formation takes place for polymer volume fractions greater than a critical value Φ^*. The overall phase separation behavior of such a system can be determined in the usual way making use of the tangent construction. The complete temperature composition phase diagram obtained by this method is shown in *Fig. 9* for a symmetric block copolymer in a poor, nonselective solvent. Note the existence of four different phases: *H* (homogeneous), *M* (mesophase), *HM* (homogeneous-mesophase), *HH* (homogeneous-homogeneous). The tangent constructions for different constant values of the temperature as a function of the

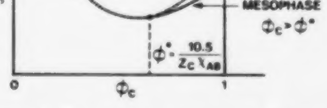

Fig. 8. Schematic diagram of homogeneous Flory-Huggins free energy $\mathcal{F}_{FH}$ (solid line to the left of Φ^* and dotted line to the right of Φ^*) and inhomogeneous free energy (solid line to the right of Φ^*). Φ^* is the smallest copolymer volume fraction for which mesophase formation is possible.

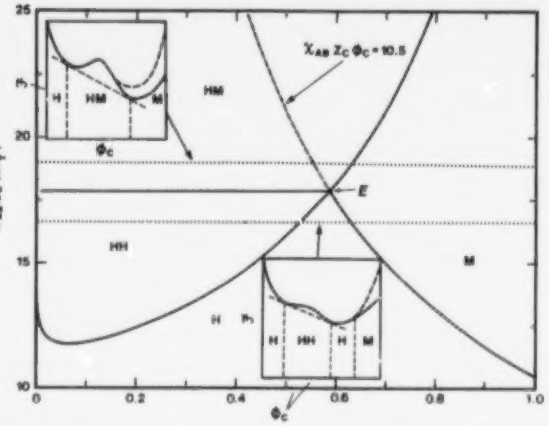

Fig. 9. Phase diagram of a mixture of a diblock copolymer and a non-selective solvent. The degree of polymerization Z_A, Z_B of each block is 100, $Z_C = Z_A + Z_B$ and $\chi_{AS} = \chi_{BS} = 10\ \chi_{AB}$. The different regions are indicated by M (mesophase), H (homogeneous), HM (homogeneous-mesophase), and HH (homogeneous-homogeneous). E represents the eutectic point. The boundary between M and H is the spinodal for microphase separation and the continuation of the spinodal beyond the point E is indicated by the dashed line. The solid lines enclosing the regions HM and HH are the binodals. The inserts show the schematic variation of the free energy with polymer volume fraction Φ_C for trajectories with different values of the temperature T.

copolymer volume fraction are also shown in the *figure*.

In the region *M*, the system remains as a single phase consisting of microdomains (the mesophase), whereas in the region *H*, the system exists as a single homogeneous phase. The boundary between *M* and *H* is the spinodal for microphase separation and in this part of the phase diagram it represents the direct transition line between the mesophase *M* and the homogeneous phase *H*. The continuation of the spinodal beyond the point *E* is indicated by the dashed line.

The boundary between *M* and *H* can be interpreted as follows: for a solution with constant copolymer concentration (say $\Phi_C = 0.9$) we look at the effect of changing the temperature (i.e., varying χ_{AB}), and therefore consider the vertical line at $\Phi_C = 0.9$ in the diagram. Starting at a low temperature (say $\chi_{AB} Z_C = 20$), when the system is initially in *M*, a single phase with microdomains, and raising the temperature, we move downwards until the region *H* is reached (at $\chi_{AB} Z_C = 11.7$) and the system becomes a single homogeneous phase. The transition line thus gives the melting curve of the microdomain structure. On the other hand, if we keep the temperature constant (say, at $\chi_{AB} Z_C = 15$), then the corresponding horizontal line describes the effect of adding solvent to the block copolymer. Starting from the pure block copolymer ($\Phi_C = 1$) in *M* we move horizontally to the left as solvent is added. When the transition is reached (at $\Phi_C = 0.7$ or 30 percent solvent concentration) the microdomain structure disappears. The boundary line therefore determines the amount of solvent required to dissolve the microdomain structure, or equivalently, gives the critical copolymer concentration required for microphase separation.

If we maintain the same temperature (at $\chi_{AB} Z_C = 15$) and keep on adding solvent, we obtain a homogeneous copolymer solution in the range $0.44 < \Phi_C < 0.70$ (i.e., in region *H*). However, as we enter the region *HH*, the system demixes, with an almost pure solvent phase separating from a homogeneous polymer solution with $\Phi_C = 0.44$. This is to be expected since we have assumed a poor nonselective solvent. The left and right boundaries of *HH* correspond to the usual binodal curves determined from the Flory-Huggins theory.

At a lower temperature (say, $\chi_{AB} Z_C = 20$) than that indicated by *E* ($\chi_{AB} Z_C = 17.9$), the situation is somewhat different. Here, on dilution of the concentrated polymer solution, we have a single mesophase until we enter the region *HM*. Then an almost pure solvent phase separates out, and the remaining polymer solution is sufficiently concentrated ($\Phi_C = 0.67$) that it stays in the mesophase, and the microdomain structure is maintained. The binodals for the region *HM* deviate from those determined by the Flory-Huggins theory but in this particular case the polymer-solvent interaction dominates over the polymer-polymer interaction and the deviation is small. In general, however, this will not be the case.

Finally, we note that the temperature corresponding to *E* ($\chi_{AB} Z_C = 17.9$) may be identified as a eutectic temperature, being the lowest temperature at which a homogeneous solution, besides the almost pure solvent, can exist. At this temperature we can have three phases in equilibrium: viz. the almost pure solvent, the homogeneous polymer solution at $\Phi_C = 0.59$, and the mesophase at $\Phi_C = 0.59$. For this particular case, the latter two phases are indistinguishable, but in general, coexistence of three distinct phases at the eutectic temperature will occur. The composition corresponding to *E* ($\Phi_C \simeq 0.59$) may be called the eutectic composition in the sense that, aside from the almost pure solvent, a mixture with concentration $\Phi_C = 0.59$ remains a homogeneous solution all the way down to the eutectic temperature, whereas mixtures with other compositions would demix or undergo microphase separation earlier. The existence of eutectic points is, of course, well known from other fields such as physical metallurgy.

Phase diagrams similar to *Fig. 9* may be constructed for block copolymer-homopolymer mixtures. A particular case is shown in *Fig. 10* for a symmetric block copolymer with a homopolymer corresponding to one of the blocks of the copolymer. One interesting feature of this diagram is the prediction of the phenomenon of homopolymer induced mesophase formation. From the right hand side of the diagram it can be seen that Leibler's 10.5 rule (6) for microdomain formation by the diblock copolymer is violated when about 20 percent of homopolymer (similar in composition to one of the blocks) is added. In this case, the enthalpic contribution to the free energy clearly favors microdomain formation in order to "shield" the ho-

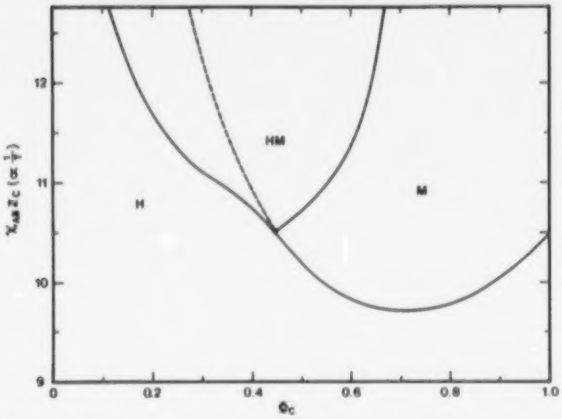

Fig. 10. Phase diagram of a diblock copolymer-homopolymer mixture. The volume fraction of copolymer is Φ_C, and the degrees of polymerization of the blocks are equal, $Z_{CA} = Z_{CB}$, with $Z_{HA} = Z_{CA}$ for the homopolymer. Only one interaction parameter, χ_{AB} is required to characterize this system, since the interaction between one of the blocks and the homopolymer vanishes. The solid lines represent the binodals between the region M (ordered mesophase), H (homogeneous), and HM (homogeneous-mesophase). The dotted line shows the continuation of the spinodal for microphase separation. In general, the topology of the phase diagrams for copolymer-homopolymer mixtures is the same as for copolymer-solvent mixtures (Fig. 9), allowing for shifts and deformation of the binodals.

mopolymer from "adverse" interactions, even at the expense of some entropy loss due to the localization of the homopolymers and block copolymers in a domain structure. In general, the detailed experimental study of such phase diagrams is just beginning (18, 19) and it will be some time before the predictions of the theory can be checked.

POLYMER DYNAMICS AND THE EARTHWORM MODEL

Finally we turn to the interesting question of polymer dynamics in multi-component systems. Relatively little theoretical or experimental work has been carried out in this area up to the present, but in the next few years we expect a lot of activity. Consequently, we feel it is appropriate to discuss some of the emerging concepts in this paper.

Before complicated problems such as spinodal decomposition can be addressed, it is advisable to have a good understanding of polymer dynamics in a single component system. For this reason, we will discuss a certain type of intra-chain diffusion controlled reaction, called the cyclization reaction. A detailed discussion of this interesting field may be found in the papers by Winnik, *et al.* (20, 21). The experiment is shown schematically in *Fig. 11*. An organic chromophore unit is first attached to each end of a long polymer chain. One of the end molecules is excited by light, and if the two ends of the polymer happen to diffuse together, the two molecules will temporarily form an excited unit which will emit light at a different wave length from the single molecule fluorescence. The monitoring of the weak fluorescence from the $(PP)^*$ excimer allows one to determine the important cyclization rate constant, k_{cyc}. Usually the reverse rate constant k_{-1} is small. The rate equation for the excimer density is given by:

$$\frac{dn_{(PP)^*}}{dt} = k_{cyc} n_{PP^*} - k_{-1} n_{(PP)^*} \qquad (8)$$

In dilute solution, k_{cyc} is found experimentally by Winnik, *et al.* (20) to depend upon the degree of polymerization N of the polymer as $N^{-1.35}$, and the value of the exponent is somewhat lower than theoretical predictions. In a polymer melt, however, the corresponding experiment has yet to be done. A technical difficulty is that because of the much slower rate of reactions, a long-lived excited chromophore P^* has to be found and tied to a polymer chain.

Theoretically, however, it is possible to make a prediction for the cyclization rate based on the recent tube model of Edwards (22) and de Gennes (23). In *Fig. 12*, we give a pictorial representation for the one-dimensional diffusion of a single polymer chain. The chain is supposed to be surrounded by a mean field tube defined roughly by the entan-

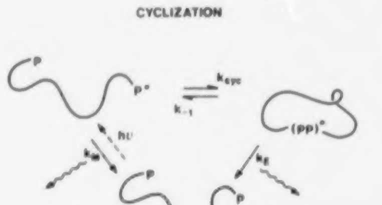

Fig. 11. Schematic diagram showing cyclization reaction in polymer solution or melt, with various rate constants.

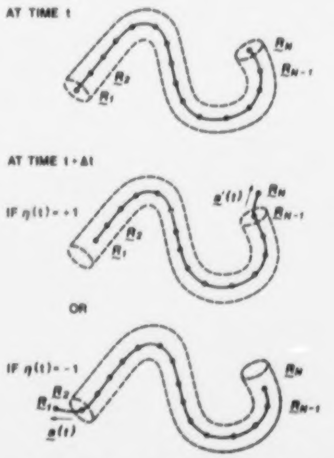

Fig. 12. Pictorial representation of Edwards-de Gennes reptation model for polymer chains in a melt. The upper panel shows a model polymer chain in its confining tube at time t. The solid circles represent the universal joints of an N-bead chain. The lower two panels show the forward or backward motion of the chain along the tube, depending on whether a stochastic function $\eta(t)$ takes on values of +1 or −1 at random. The beads that get out of the tube (B_N or B_1) move a distance a but in random directions as indicated by the stochastic vectors $g'(t)$ or $g(t)$. The tube is allowed to evolve in random directions only from the two ends, with tube leakage from the middle being neglected.

glement points surrounding the polymer. The central part of the tube is assumed to remain immobile until such time as the polymer chain has completely disengaged from the original tube by Brownian motion. The process of tube renewal is allowed to take place only from the ends as the polymer chain slides back and forth in response to the fluctuating forces in the melt. An important feature of the model is the assumption of one-dimensional diffusion so that tube renewal other than from the ends is ignored. Obviously, it is of great importance to have a direct test of this hypothesis.

Recently, an exact solution of the earthworm equations describing the motion shown in *Fig. 12* has been obtained by Bernard and Noolandi (24). In particular, it is possible to obtain an exact expression for the memory function $S(t)$. This quantity gives the probability that two chain ends come together at time t, given that they were together at time $t = 0$. The cyclization rate constant can be shown to be the inverse of the integral over time of the transient part of this memory function. The memory function itself shows an interesting behavior as a function of time. For short times, it behaves as a power law, $S(t) \sim (t/\tau_{rep})^{-3/4}$, where τ_{rep} is the tube disengagement time. In de Gennes terminology (25), the early time behavior is compact, meaning that the chain ends explore all possible points in the course of their random walk. At longer times, however, the memory function becomes exponential as the chain ends explore only a fraction of possible points during their random walk, and this is called non-compact behavior.

It is worth noting that for very short times (less than the time for equilibration of the "gas" of diffusing length-storing "kinks" inside the tube), we do not see the $t^{-3/8}$ behavior for $S(t)$ predicted by de Gennes (26). This is presumably because the earthworm equations of Doi and Edwards (27) assume a *rigid* model polymer chain, in which local chain fluctuations are ignored. Unfortunately, the $t^{-3/4}$ short time behavior for $S(t)$ obtained from the earthworm equations is not characteristic of the reptation model alone, since a similar behavior is found for the Rouse model (28), which allows for all random motions of the flexible chain.

The integral of the memory function shown in *Fig. 13* gives the result that the cyclization rate is inversely proportional to the time taken for the polymer chain to completely disengage from its original tube. According to de Gennes (23) the reptation time is proportional to the cube of the molecular weight. This result for the cyclization rate, however, is only valid in limit of the molecular weight becoming very large. For finite molecular weight, we find a fractional power law dependence. This naturally leads to the interesting speculation that the fractional power law discussed by Graessley (29) for the zero shear rate viscosity as a function of molecular weight may also be due to finite chain effects. We are currently pursuing this idea with more detailed calculations.

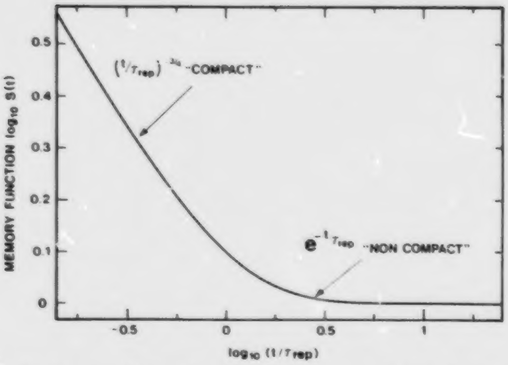

Fig. 13. Universal intrachain memory function S(t) in the continuum limit, giving the conditional probability of end-to-end encounters at time t for a reptating polymer chain whose ends were in contact at $t = 0$. τ_{rep} is the fundamental reptation or tube disengagement time. The integral of the transient part of S(t) is proportional to the inverse of the cyclization rate constant.

In conclusion, recent work on the detailed predictions of the Edwards-de Gennes tube model should allow for definitive tests of reptation. If the theory survives in its present form, it can be extended to study more complicated cases such as spinodal decomposition in multi-component systems.

ACKNOWLEDGEMENTS

I have greatly benefited from discussions with my colleagues Drs. K. M. Hong and D. A. Bernard at the Xerox Research Centre of Canada.

REFERENCES

1. E. Helfand and Y. Tagami, *J. Polym. Sci.*, **B9**, 741 (1971).
2. D. J. Meier, *J. Polym. Sci.*, **C26**, 81 (1969).
3. D. J. Meier, *Polym. Prepr., Am. Chem. Soc., Div. Polym. Chem.*, **11**, 400 (1970).
4. E. Helfand and Z. R. Wasserman, *Macromolecules*, **9**, 879 (1976).
5. S. Krause, "Block and Graft Copolymers", J. J. Burke and V. Weiss, eds., Ch. 8, Syracuse Univ. Press, Syracuse, New York (1973).
6. L. Leibler, *Macromolecules*, **13**, 1602 (1980).
7. T. Inoue, T. Soen, T. Hashimoto, and H. Kawai, *J. Polym. Sci., Part A-2*, **7**, 1283 (1969).
8. P. Grosius, Y. Gallot, and A. Skoulios, *Makromol. Chem.*, **127**, 94 (1969).
9. T. Hashimoto, A. Todo, H. Itoi, and H. Kawai, *Macromolecules*, **10**, 377 (1977).
10. G. Hadziioannou and A. Skoulios, *Macromolecules*, **15**, 267 (1982).
11. J. Noolandi and K. M. Hong, *Ferroelectrics*, **30**, 117 (1980).
12. T. Hashimoto, M. Shibayama, and H. Kawai, *Polym. Prepr., Am. Chem. Soc., Div. Polym. Chem.*, **23**, 21 (1982).
13. K. M. Hong and J. Noolandi, *Macromolecules*, **14**, 736 (1981).
14. G. Riess, J. Kohler, C. Tournut, and A. Banderet, *Makromol. Chem.*, **101**, 58 (1967).
15. J. Noolandi and K. M. Hong, *Macromolecules*, **15**, 482 (1982).
16. P. Gaillard, M. Ossenbach-Sauter, and G. Riess, *Makromol. Chem., Rapid Commun.*, **1**, 771 (1980).
17. J. Noolandi and K. M. Hong, *Polym. Bull.*, **7**, 561 (1982).
18. G. C. Eastmond and D. G. Phillips, *Polymer*, **20**, 1501 (1979).
19. R. J. Roe, W.-C. Zin, and M. Fishkis, "Proc. of 28th IUPAC Macromolecules Meeting, Amherst, Mass.", p. 662, IUPAC (1982).
20. M. A. Winnik, T. Redpath, and D. H. Richards, *Macromolecules*, **13**, 328 (1980).

21. S.-T. Cheung, M. A. Winnik, and T. Redpath, *Makromol. Chem.*, **183**, 1815 (1982).
22. S. F. Edwards, *Proc. Phys. Soc., London*, **92**, 9 (1967).
23. P. G. de Gennes, *J. Chem. Phys.*, **55**, 572 (1971).
24. D. A. Bernard and J. Noolandi, *Phys. Rev. Lett.*, **50**, 253 (1983).
25. P. G. de Gennes, *J. Chem. Phys.*, **76**, 3316 (1982).
26. P. G. de Gennes, *J. Chem. Phys.*, **76**, 3322 (1982).
27. M. Doi and S. F. Edwards, *J. Chem. Soc., Faraday Trans. 2*, 74, 1789 (1978).
28. P. E. Rouse, *J. Chem. Phys.*, **21**, 1273 (1953).
29. W. W. Graessley, *Adv Polym. Sci.*, **16**, 1 (1974).

DISCUSSION

M. Grmela: I would like to ask you if you have tried to make a link between the dynamical point of view, as discussed in the second part of your talk, and the equilibrium considerations of the first part. For example, you introduced the unstable, metastable states etc. Are they stable or unstable from the dynamical point of view?

J. Noolandi: We are in the midst of doing this. In particular an interesting problem is spinodal decomposition. We would like to calculate the rate of spinodal decomposition for multicomponent systems using reptation theory. Theoretical work has been done in this area, for example, de Gennes has done some calculations, corrected by Pincus. It turns out to be a rather complicated calculation and it is now believed that there is nothing unusual about the spinodal decomposition of polymers. In fact, it is very much like spinodal decomposition of atoms in metallurgy, for example. What is different is the magnitude of the diffusion constants. Basically the system is believed to scale in the same way, but this prediction remains to be checked by detailed studies using neutron scattering. In fact, some results of neutron scattering experiments have come out recently, but they are still not good enough to check the detailed predictions based on reptation theory, so I guess this question is unresolved at the moment.

I. Sanchez: Two comments and a question. You did a superb job of presenting a very difficult subject this morning and you should be congratulated. Now the questions. In the phase diagram where you have a eutectic point, is the eutectic defined by a common tangent between the mesophase free energy and the homogeneous fluid phase? (Answer: Yes). O.K. The last point is a comment about one of your diagrams, in which you showed a series of pictures where you have a two phase system of high surface tension and of low surface tension. For the low surface tension you showed that it is a finely dispersed phase. I think that this diagram was a little bit misleading; the way that I would picture it is that in all cases the system (regardless of the value of the interfacial free energy) would tend to go to a state where you minimize the area, even if the interfacial tension is small. Therefore, lowering the interfacial tension does not help promote the creation of a finely dispersed system because that system is still metastable with respect to the most stable state of the system, which is one of minimum free area. In fact, in the absence of gravity, you would not even see a binary; you would see a single, very large, spherical particle.

J. Noolandi: I agree with you. In many cases I oversimplified. On the other hand, in practice, when we are working with some kind of polymerization reaction, we do wish to disperse one phase very finely in another. In this case we are not dealing with an equilibrium situation; we are always agitating the system to maintain finely dispersed particles. Having a low interfacial tension makes this process very much easier. I think that the two aspects of the problem are related in this way.

J. M. Ottino: I agree there is nothing mysterious about the phenomenon of spinodal decomposition in polymers. When you compare it with spinodal decomposition of metal atoms say, they should, more or less, scale in the same way, although in some cases there are internal topological constraints in copolymers that may make them different. In spinodal decomposition one always has the concept that the phase will tend to be bicontinuous. However, for phase separation in blends, one draws pictures like spheres, cylinders, lamellae, and so on. What comments do you have in this respect? Sometimes it is known that by allowing bicontinuity, one can decrease the total contact area between the two phases. For example, if you have constant volume fraction, let's say 50 percent spheres dispersed in a cubic lattice and somehow you fuse them together, allowing bicontinuity, you can decrease the area by about 15%. How do you see the problem of bicontinuity and other kinds of morphologies developing in polymer blends? When you approach this from the point of spinodal decomposition, it seems that bicontinuity is the normal occurrence, not an exception.

J. Noolandi: I agree, I think it will occur, but again, there has been no theoretical calculation as far as I know. There have been no detailed experimental studies either, and that is another problem. I think it could be calculated within the framework of these theories. However, I would hesitate to do it until there are very good microscropic studies in spinodal decomposition. This may take place in the next few years.

P. R. Couchman: At one point, when you were talking about the block copolymer thickness of the interphase region, you mentioned that this goes as $Z_c^{1/2}$ (Z_c is the degree of polymerization of the copolymer). One can conceive two extrema: it might go between Z_c and $Z_c^{1/2}$. Why, in particular, did you use $Z_c^{1/2}$?

J. Noolandi: For the case of large homopolymer molecular weights, the reduction of the interfacial tension is only a function of the concentration and molecular weight of the block polymer. As an example, we took the simplest possible case for the dependence of the copolymer thickness on Z_c. Better estimates may be obtained by comparison with the detailed numerical analysis of the mean-field equations. When this is done the simple theory agrees very well with the numerical solution. However, this does not mean that either of them is correct. There is a more complicated possibility, where the surfactant goes to the interface and forms a localized ordered phase. It is known from the study of polar surfactants that this may occur. Unfortunately, it complicates the theoretical situation immeasurably, in part because we are not dealing with a periodic, ordered system. If our simple model proves to be inadequate, we will tackle the more complicated case.

L. A. Utracki: I have a small point to raise. Let us consider the simple but industrially important blend of polyethylene with polypropylene. According to your equation, one would have two choices to compatibilize such a system—either to use a relatively high concentration of small molecular weight block polymer, or, conversely, a small amount of very high molecular weight block polymer of ethylene propylene. This must have a significant effect on the profitability of an industrial operation. Obviously you would like to have a very high molecular weight block and add very little. Am I reading your conclusions correctly? Something does not seem to be right, because if you go to the extreme of very high molecular weight, the number of crossing points between the two domains will be very limited. In such an extremal case, you are not going to achieve your goal.

J. Noolandi: If the molecular weight becomes very high, the large molecules of copolymer will form micelles. We can estimate roughly what this concentration is, and we should always be working on the edge of it. I did not get into that aspect of the problem, but what we want to do is work with as low a concentration and as high a molecular weight as possible, without forming micelles. The formation of micelles wastes the surfactant because it is not going to the interface where it is needed. In a practical situation there are a lot of other constraints to consider, namely cost, polydispersity, chemical structure, and so on.

On the Nature of Polymer Interfaces and Interphases

ISAAC C. SANCHEZ

Center for Materials Science
National Bureau of Standards
Washington, D.C. 20234

An abbreviated review of the current state of knowledge of polymer interfacial phenomena is given. Classical thermodynamics treats the interfacial zone (the interphase) as a "black box" and yields rigorous relationships among interfacial quantities. A recent reformulation of interphase thermodynamics, which eliminates the use of a Gibbs dividing surface, is shown to be an invaluable tool for investigating interfacial properties. Microscopic theories, such as the gradient theory, yield more details about what is in the black box, but the information is only approximate. The gradient theory has been used to: (1) relate the surface tension of a polymer liquid to its isothermal compressibility, (2) develop a quantitative theory of polymer liquid surface tension, and (3) determine the interfacial tension between two immiscible polymer liquids. The gradient theory will be shown to be in harmony with the microscopic theory of Helfand and co-workers although the latter treats polymer interfaces from a completely different point of view.

INTRODUCTION

Polymer interfaces play an important role in polymer technology through the processes of wetting, adsorption, adhesion, and through their effects on the kinetics of phase separation and mechanical mixing of molten polymers. The latter is especially important for polymer blends. In polymer blends, where multiphase structures can form, the dispersion and morphology of the component phases are controlled by the kinetics of phase separation. The kinetics depend crucially on the energetic cost of developing concentration gradients (interfaces) (1). Moreover, the mechanical properties of such a multiphase polymer blend are directly related to interfacial energies (2).

In *Fig. 1* a planar interface for a binary mixture is schematically illustrated. The dashed lines define the interfacial zone or "interphase." The position of the dash lines is somewhat arbitrary, a point that shall be discussed in detail in the next section. In a finely dispersed polymer blend, the interphase may represent a non-negligible fraction of the system.

INTERPHASE AS A BLACK BOX

Classical thermodynamics treats the interphase as a "black box." It describes what is in the box, but not how the material is distributed within the box. In this sense the information is limited. The power of the thermodynamic description is that it establishes rigorous relationships among the interfacial properties. Microscopic theories can yield more information about what is in the box (for example, concentration profiles), but the results are usually approximate in nature. The rigorous results of thermodynamics can be used as a standard to judge the validity and self-consistency of microscopic theories.

Thermodynamics offers a second advantage. If an interfacial property is difficult to measure, thermodynamics can suggest alternative properties to measure so that the difficult property of interest can be determined. As will be shown later, for example, the adsorption of a third component to the interphase of a binary mixture is related to the variation of the interfacial tension with temperature, $(\partial\sigma/\partial T)$, and the variation of the critical temperature with the addition of the third component, $(\partial T_c/\partial C_3)$. The adsorption of the third component is difficult to measure, but $\partial\sigma/\partial T$ and $\partial T_c/\partial C_3$ are by comparison easily measured.

Although the thermodynamic description of an interphase is an invaluable tool, it is rarely used. The reason for this neglect is largely pedagogical. The traditional approach of Gibbs requires the use of a dividing surface to which interfacial properties are referenced. This method is burdened with notational and conceptual difficulties. Recently, an alternative but equivalent method of treating interphase thermodynamics has been developed by Cahn (3) which avoids many of the pitfalls of the traditional approach. Cahn's method has received little attention, so it is briefly reviewed here.

Cahn's Interphase Thermodynamics

Consider a two phase system of n components with a planar interface of surface area A and interfacial tension σ. For such a system the combined first and second laws of thermodynamics yields:

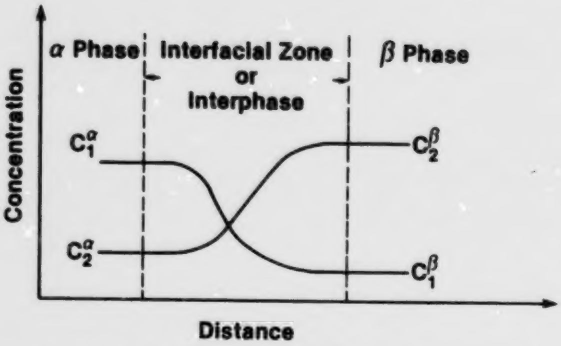

Fig. 1. A schematic of the concentration profiles through an interface for a two-component mixture.

$$dE = TdS - PdV + \sum \mu_i dN_i + \sigma dA \qquad (1)$$

where all symbols have their customary thermodynamic meanings. The Euler relation associated with *Eq 1* is

$$\sigma = (E - TS + PV - \sum N_i\mu_i)/A \qquad (2)$$

Since $E - TS + PV$ is the Gibbs free energy of the two phase system with an interphase and $\sum N_i\mu_i$ is the Gibbs free energy of the same system without an interphase (recall that the μ_i are identical in both bulk phases), σ is an excess free energy associated with the presence of the interphase. When the total differential of *Eq 2* is taken and compared with *Eq 1*, a Gibbs-Duhem relation is obtained:

$$Ad\sigma = -SdT + VdP - \sum N_i d\mu_i \qquad (3a)$$

In the interphase, the extensive variables (E, S, V, and the N_i) will have values dependent on how the interphase is defined. Let $[X]$ represent the amount of the extensive variable X per unit area that is contained in the interphase. Thus, *Eq 3a* can be rewritten as

$$d\sigma = -[S]dT + [V]dP - \sum [N_i]d\mu_i \qquad (3b)$$

which is one version of the Gibbs adsorption equation. The quantity $[X]$ is not an excess quantity; it is the actual amount of X in the interphase. Thus, the surface variable $[X]$ depends on how the interphase is defined; i.e., it depends on where the dashed lines in *Fig. 1* are drawn. However, certain combinations of these variables are independent of how the interphase is defined. For example, *Eq 2* can be expressed as

$$\sigma = [E] - T[S] + P[V] - \sum [N_i]\mu_i \qquad (4)$$

Since the interfacial tension is independent of how the interphase is defined, the combination of surface variables on the *RHS* of *Eq 4* must likewise be independent. *All important interphase thermodynamic equations must exhibit this invariance.*

What Cahn has shown is that through the judicious choice of a reference system, *Eq 3a* can be rewritten so that the coefficients of dT, dP, and the $d\mu_i$ become excess surface variables which possess the desired invariance. Cahn's generalized adsorption equation for a two phase system is

$$d\sigma = -[S/XY]dT + [V/XY]dP - \sum_{i=1}^{n} [N_i/XY]d\mu_i \qquad (5)$$

where, for example

$$[S/XY] \equiv \frac{\begin{vmatrix} [S] & [X] & [Y] \\ S^\alpha & X^\alpha & Y^\alpha \\ S^\beta & X^\beta & Y^\beta \end{vmatrix}}{\begin{vmatrix} X^\alpha & Y^\alpha \\ X^\beta & Y^\beta \end{vmatrix}} \qquad (6)$$

and where X and Y are any two distinct members of the set $\{S, V, N_i\}$. The α and β superscripts refer to the α and β phases of the two phase system. Note that because the numerator is zero when two columns of the determinant are the same, two of the coefficients on the *RHS* of *Eq 5* vanish. For example, if N_1 and N_2 are chosen for X and Y, then

$$d\sigma = -[S/N_1N_2]dT + [V/N_1N_2]dP - \sum_{i=3}^{n} [N_i/N_1N_2]d\mu_i \qquad (7)$$

since $[N_1/N_1N_2]$ and $[N_2/N_1N_2]$ are identically zero. The number of non-zero terms on the *RHS* of *Eq 5* will always equal the system's degrees of freedom as determined by the Gibbs phase rule.

To better understand the significance of the coefficients in *Eq 5*, take a units of the α phase and b units of the β phase and combine them to form a hypothetical system which, hereafter, is called the *reference system.* The amount of X in the reference system is $aX^\alpha + bX^\beta$ and the amount of Y is $aY^\alpha + bY^\beta$. Now in the actual system the interphase is defined by the placement of two surfaces, the two dashed lines in *Fig. 1*, chosen so that

$$[X] = aX^\alpha + bX^\beta \qquad (8a)$$

$$[Y] = aY^\alpha + bY^\beta \qquad (8b)$$

It is obvious that when the interphase is defined in this manner, $[X]$ and $[Y]$ have zero excess relative to the reference system. However, any other surface variable $[Z]$ in general has a non-zero excess when compared to the reference system, i.e.,

$$[Z] = aZ^\alpha + bZ^\beta + \Delta Z \qquad (9)$$

and it is easily shown that the excess, ΔZ, is given by

$$\Delta Z = [Z/XY] \qquad (10)$$

Thus, the coefficients in *Eq 5* have a simple physical interpretation. For example, $[V/N_1N_2]$ is the excess volume in the interphase compared to the volume of a reference system in which $[N_1]$ and $[N_2]$ have zero excess. With this interpretation in mind, it is now obvious that quantities such as $[N_1/N_1N_2]$ and $[N_2/N_1N_2]$ must equal zero by definition. The salient point is that the arbitrary bounds of the interphase that determine the surface concentrations $[X]$ and $[Y]$ also define the appropriate reference system, or equivalently, the a,b pair in *Eq 8* that make $[X]$ and $[Y]$ have zero excess. The remaining excess variables are invariant to the arbitrary location of the interphase boundaries, or equivalently, the magnitudes of $[X]$ and $[Y]$. This invariance follows directly from the properties of determinants. The value of a determinant remains unchanged when a multiple of one row is added to another. Moving the a interphase boundary further into a phase is exactly this operation. It adds to the first row a multiple of the row corresponding to the phase into which the boundary is moved. The excess variables defined by *Eq 10* have the necessary characteristics of a physical surface variable, invariance to location of interphase boundaries.

Equation 5 can also be generalized to treat systems that exhibit three or more simultaneous phases (3).

Applications

Consider a liquid-vapor interface in a binary mixture in which the second component is a minor one. A useful version of *Eq 5* for this system is

$$d\sigma = -[S/VN_1]dT - [N_2/VN_1]d\mu_2 \qquad (11)$$

If the concentration C_2 of component 2 is small enough, then $d\mu_2 = RTdlnC_2$ and *Eq 11* becomes

$$(\partial\sigma/\partial lnC_2)_T = -RT[N_2/VN_1] \qquad (12)$$

Thus, if the surface excess of the minor component is positive, addition of the minor component lowers the surface tension; if the surface excess is negative, indicative of a rejection of the minor component from the interphase, then addition of the minor component raises the surface tension. These predictions agree with physical intuition, but *Eq 12* also indicates how surface adsorption can be quantitatively estimated by measuring $(\partial\sigma/\partial C_2)_T$.

For a liquid-liquid interface in a binary mixture, *Eq 5* can be written as

$$d\sigma = -[S/N_1N_2]dT + [V/N_1N_2]dP \qquad (13)$$

Thus,

$$(\partial\sigma/\partial T)_P = -[S/N_1N_2] \qquad (14)$$

Now for a system that exhibits an upper critical solution temperature (UCST), $\partial\sigma/\partial T$ is negative which implies by *Eq 14* that the excess entropy of the interphase is positive for a UCST type mixture. For a mixture with a lower critical solution temperature (LCST), as observed in many polymer mixtures, $\partial\sigma/\partial T$ is positive which implies that the excess entropy of the interphase is negative. These results are consistent with the conclusions that the excess bulk entropy of mixing is positive at a UCST and negative at a LCST (4).

At constant temperature, *Eq 13* yields

$$(\partial\sigma/\partial P)_T = [V/N_1N_2] \qquad (15)$$

Since $d(\text{LCST})/dP > 0$ in all known cases (5), *Eq 15* suggests that the surface excess volume is always negative for a LCST type mixture.

As a final example of how *Eq 5* can be applied, the adsorption of a minor third component to a liquid-liquid interface is considered. For a ternary mixture, a useful form of *Eq 5* is

$$d\sigma = -[S/N_1N_2]dT + [V/N_1N_2]dP - [N_3/N_1N_2]d\mu_3 \qquad (16)$$

The quantity of interest is $[N_3/N_1N_2]$ since it represents the excess amount of the third component that is adsorbed into the interphase. At constant σ and P, *Eq 16* yields

$$(\partial T/\partial\mu_3)_{\sigma,P} = -[N_3/N_1N_2]/[S/N_1N_2] \qquad (17)$$

If the concentration of the third component is sufficiently small, $d\mu_3 = RTdlnC_3$, and *Eq 17* becomes

$$[N_3/N_1N_2] = C_3(\partial\sigma/\partial T)_P(\partial T_c/\partial C_3)/RT \qquad (18)$$

where $[S/N_1N_2]$ has been replaced by $(\partial\sigma/\partial T)_P$ of the binary mixture and $(\partial T/\partial C_3)_\sigma$ has been replaced by $\partial T_c/\partial C_3$ (the $\sigma = 0$ path) where T_c is the critical temperature. *Equation 18* is unique because it relates a surface excess quantity to the critical point depression (or elevation), a phase diagram property that pertains to the bulk phases. *Equation 18* was first derived by Rice (6) by a much different procedure.

Because of the conceptual simplicity of Cahn's reformulation of interphase thermodynamics, it will surely see more application in future studies of interfacial phenomena.

MICROSCOPIC THEORIES

Liquid-Vapor Interfaces

A first principles calculation of the interfacial tension requires the determination of the free energy of the interphase. In a single component fluid with a flat liquid-vapor interface, the molecular number density, $n(x)$, varies with position, x, through the interphase. In the bulk phases, $n(x)$ has the constant values of n_l in the liquid phase and n_g in the gas phase. When the Helmholtz free energy density $\Psi(x)$ at the point x is expanded in a series, there obtains (7–9)

$$\Psi(x) = \Psi_o(n) + \tfrac{1}{2}A(n)(dn/dx)^2 + \ldots \qquad (19)$$

where $\Psi_o(n)$ is the free energy density of a uniform fluid of density $n(x)$; $\Psi_o(n_l) + P = n_l\mu$ and $\Psi_o(n_g) + P = n_g\mu$ where μ is the equilibrium chemical potential and P is the bulk pressure. The coefficient of the square gradient term, $A(n)$, is related to a second moment of an Ornstein-Zernike direct correlation function $c(r,n)$ of a uniform fluid of density n. It is given by

$$A(n) = \frac{kT}{6}\int r^2c(r,n)d^3r \qquad (20)$$

Recently, Kayser and Raveché (10) have determined the fourth order correction terms in *Eq 19*.

Truncating the series in *Eq 19* at the square gradient term is known as the *gradient approximation*. Combining the gradient approximation with the thermodynamic definition of the interfacial tension *Eq 2*, yields three equivalent relations for the surface tension (8, 9, 11).

$$\sigma = 2\int \Delta\Psi dx = \int A(n)(dn/dx)^2 dx = \int_{n_g}^{n_l} (2A\Delta\Psi)^{1/2} dn \qquad (21)$$

where

$$\Delta\Psi \equiv \Psi_o(n) + P - n\mu \qquad (22)$$

and is schematically illustrated in *Fig. 2*.

The density profile can be determined by integrating the following differential equation:

$$\Delta\Psi = \tfrac{1}{2}A(n)(dn/dx)^2 \qquad (23)$$

Of the three relations for σ given in *Eqs 21*, the one involving the integral over density is the most useful because it does not require explicit knowledge of the density profile. However, it does require knowledge of A and $\Delta\Psi$. The value of A can be easily evaluated in a mean field approximation because the direct correlation function $c(r,n)$ can be replaced by the molecular pair potential, $\epsilon(r)/kT$, and then the defining integral for A, *Eq 20*, can be evaluated. In a mean field approximation A is a constant independent of density and *Eqs 21* become the well-known Cahn-Hilliard relations (12). In principle, $\Delta\Psi$ can be evaluated using any model free energy function.

Poser and Sanchez (13, 14) have used the lattice fluid (LF) model (15, 16) to evaluate $\Delta\Psi$ and a mean field approximation for A to determine the surface tensions of simple liquids as well as polymer liquids. The only parameters required to calculate a surface tension are obtained from the bulk thermodynamic properties of the liquid. The theory is surprisingly accurate. For non-polar and slightly polar liquids the surface tension can be calculated from the triple point to 0.7 of the gas-liquid critical temperature with an error of less than 5 percent (experimental errors are of the order of 1 to 2 percent). Polymer liquid surface tensions satisfy a corresponding states principle and can be estimated for many polymers with an error of less than 10 percent. In *Fig. 3* this theory is compared with experimental surface tension data for polyisobutylene and with three other methods (17–19) of estimating polymer surface tensions.

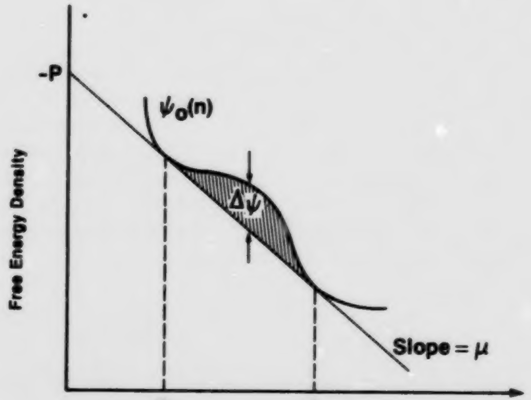

Fig. 2. Geometric interpretation of $\Delta\Psi$ for a liquid-vapor interface (see Eqs 21 and 22).

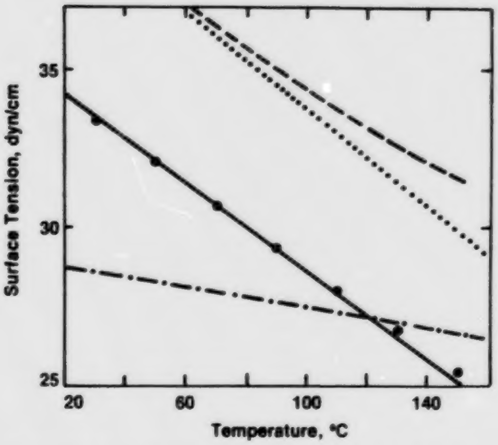

Fig. 3. Comparison of experimental surface tension data for polyisobutylene (solid circles) with gradient/lattice fluid theory (solid line), empirical parachors (dotted line), solubility parameters (dot-dash line), and corresponding states theory (dash line). From Ref. 14.

An advantage of the lattice fluid model is that the free energy and equation of state depend explicitly on the size of the molecule. Thus, the effects of molecular size or chain length on bulk and surface thermodynamic properties can be investigated. It is well known that the surface tension of chain liquids, such as the normal alkanes, are molecular weight (M) dependent. The lattice fluid model in conjunction with the mean field versions of *Eqs 21* quantitatively correlates the surface tension variation of the *n*-alkanes with both M and temperature.

Surface tensions are inherently M dependent because liquid densities are inherently M dependent. The density of a polymeric liquid may be 10 to 20 percent larger than the density of a low M homologue at the same temperature. This occurs because the favorable free energy change associated with creating vacancies (increasing the liquid volume) in a polymeric liquid is smaller than in a low M homologue. Energetically the cost is approximately the same, but entropically there is an appreciable difference. Creating vacancies in a polymeric liquid results in a smaller entropy increase than occurs in a low M homologue. The increase in entropy associated with an incremental volume increase depends on the ability of the system to utilize the extra volume. Because more monomer units are chemically connected to one another in a polymeric liquid, the increase in configurational entropy is smaller for the polymeric liquid. Therefore, at equilibrium, a polymeric liquid will possess a smaller number of vacancies and will be denser than a low M homologue. A density difference of 20 percent can result in a 100 percent difference in surface tension.

Experimentally, the excess surface entropy, $-(\partial\sigma/\partial T)_p = [S/NV]$, of a polymeric liquid is smaller than for a low M homologue. The excess surface entropy of a polymeric liquid is typically about a factor of 2 smaller than a corresponding low M homologue. For example, it is 0.110 dyne/cm-K for *n*-pentane and 0.057 for linear polyethylene. The primary reason for this phenomenon can again be related to density variations. A polymeric liquid has a smaller thermal expansion coefficient than a low M homologue because entropy increases associated with volume expansion are smaller for a polymeric liquid. Since the polymer liquid density varies more slowly with temperature, $-(\partial\sigma/\partial T)_p$ is smaller for the polymeric liquid. A second possible reason why the excess surface entropy might be smaller is that the surface restricts the number of polymer conformations. However, Hong and Noolandi (20) have concluded that this effect is only of secondary importance.

The combination of the lattice fluid model and gradient approximation have also been successfully applied in describing the liquid-vapor interfacial tension of polymer/solvent pairs (21).

Very recently this author has used *Eqs 21* to relate the surface tension of a liquid to its isothermal compressibility (κ) and mass density (ρ). The equation is (22)

$$\sigma = (A_o\rho/\kappa)^{1/2} \tag{24}$$

in the normal liquid range and where A_o is a constant. The constant A_o has three important properties: (1) it is temperature independent, (2) it is an invariant for a large class of organic liquids, and (3) it can be estimated from Lennard-Jones force constants. The first property indicates that all of the temperature dependence of a liquid's surface tension is imbedded in its compressibility and density. The second property is really surprising. For fifty organic liquids that include aliphatic and aromatic hydrocarbons, alcohols, amines, acids, as well as other oxygen and nitrogen containing organics, $A_o^{1/2} = (2.78 \pm 0.13) \times 10^{-4}$ in units of $(\text{erg-cm}^2/\text{g})^{1/2}$. This correlation for these 50 organic liquids is shown in *Fig. 4*. Among these 50 organics ρ varies by a factor 3, σ by a factor of 5, and κ by an order of magnitude, yet the average deviation in $A_o^{1/2}$ is only 5 percent. Among polymer liquids A_o is still temperature independent, but its variability is greater than that exhibited by the 50 organics as illustrated in *Table 1* and *Fig. 5*.

A semi-empirical formula has been derived for A_o relating it to the parameters ϵ_o and σ_o that characterize the molecular pair interaction potential; ϵ_o is related to the depth of the potential energy well and σ_o is a measure of the repulsive core of the potential. For a Lennard-Jones 6–12 potential it has been shown that (22)

$$A_o^{1/2} = 0.26(\epsilon_o\sigma_o^2/M)^{1/2} \tag{25}$$

where M is molecular weight. This result implies that $\epsilon_o\sigma_o^2 \sim M$ and that the parameter combination $(\epsilon_o\sigma_o^2/M)$ is an invariant for the 50 organics in *Fig. 4*. The physical implications of this result still remain unclear.

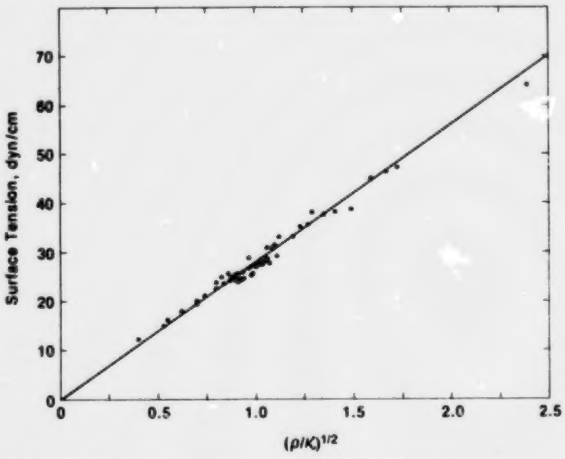

Fig. 4. Surface tensions of 50 organic liquids plotted as a function of $(\rho/\kappa)^{1/2}$. The straight line has a slope of $A_o^{1/2} = 2.78 \times 10^{-4}$ (erg − cm^2/g)$^{1/2}$. From Ref. 22.

Liquid-Liquid Interfaces

Helfand and Tagami (23, 24) and Helfand and Sapse (25) have developed a theory of interfacial tension between polymer pairs of infinite molecular weight. Their approach differs from the gradient theory discussed in the previous section. A polymer chain is assumed to satisfy a modified diffusion equation in which a meandering monomer unit is under the influence of a mean field created by neighboring chains. The surface tension is given by

$$\sigma = (\chi/6)^{1/2} b\rho_o kT \tag{26}$$

and interfacial thickness, l, is given by

$$l = 2b/(6\chi)^{1/2} \tag{27}$$

where χ is the usual Chi interaction parameter, b is a segment length and ρ_o is the monomer number density. Similar equations are obtained when b and ρ_o are different for the two polymers (25). These equations can also be derived by a simple heuristic argument (26, 27).

Although the theory of Helfand and co-workers is conceptually quite unlike the gradient theory, both theories lead formally to the same set of equations for the interfacial tension. This similarity between the two theories is demonstrated below.

When the gradient theory is applied to a multicomponent mixture, the result is (8, 28)

$$\begin{aligned}\sigma &= \sum_{ij} \int_{-\infty}^{\infty} A_{ij}(dn_i/dx)(dn_j/dx)dx \\ &= 2\int_{-\infty}^{\infty} \Delta\Psi dx\end{aligned} \tag{28}$$

where

Table 1. Polymeric Liquids*

Liquid	t (°C)	ρ (g/cm^3)	$\kappa \times 10^{10}$ (cm^2/dyn)	σ (dyn/cm)	$A_o^{1/2} \times 10^4$ (erg-cm^2/g)
poly(dimethylsiloxane)	20	0.971	1.16	19.8	2.16
	100	0.905	1.89	15.9	2.30
	140	0.870	2.41	14.0	2.33
	200	0.826	3.25	11.1	2.20
poly(isobutylene)	0	0.930	0.435	35.0	2.39
	50	0.940	0.550	31.8	2.48
	100	0.879	0.690	28.6	2.53
	150	0.854	0.851	25.4	2.53
poly(n-butyl methacrylate)	100	1.004	0.673	26.5	2.17
	140	0.975	0.833	24.1	2.23
	180	0.947	1.03	21.7	2.26
poly(methyl methacrylate)	140	1.136	0.556	32.0	2.24
poly(vinyl acetate)	30	1.185	0.474	35.8	2.26
	70	1.153	0.565	33.2	2.32
	100	1.128	0.639	31.2	2.34
l-polyethylene	140	0.805	0.972	28.8	3.16
	180	0.765	1.17	26.5	3.28
a-polystyrene	120	1.013	0.614	33.5	2.61
	180	0.982	0.749	29.2	2.55

* From Ref. 22.

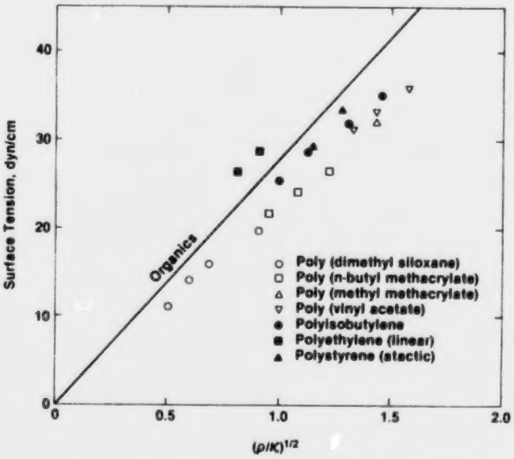

Fig. 5. Surface tensions of 7 polymer liquids in Table 1 are plotted as a function of $(\rho/\kappa)^{1/2}$.

$$\begin{aligned}\Delta\Psi &= \Psi_o + P - \sum n_i(x)\mu_i \\ &= \tfrac{1}{2} \sum_{i,j} A_{ij}(dn_i/dx)(dn_j/dx)\end{aligned} \tag{29}$$

and A_{ij} is the generalization of *Eq 20*:

$$A_{ij}(\{n\}) = \frac{kT}{6} \int r^2 c_{ij}(r, \{n\}) d^3r \tag{30}$$

where $\{n\}$ denotes the set of the densities, n_i.

The molecular weight and density dependence of the diagonal coefficients, A_{ii}, can be determined by the following argument (22): The dependence of surface tension on compressibility and mass density is not significantly different for n-pentane than for its high M analog, linear polyethylene. There is a M dependence, but it is implicit and buried in the slight dependence of κ and ρ on M. The effect of M on the surface tension can be seen by inspection of *Eq 21*:

$$\begin{aligned}\sigma &= \int A(n)(dn/dx)^2 dx \\ &= M^{-2} \int A(d\rho/dx)^2 dx\end{aligned} \tag{31}$$

In order for σ not to depend explicitly on M, $A(n)$ must vary as $M^{2-\alpha}/n^\alpha$ so that $M^{-2}A = \rho^{-\alpha}$. For $\alpha = 1$, *Eq 31* becomes

$$\sigma \sim \int \rho^{-1}(d\rho/dx)^2 dx \tag{32}$$

which is explicitly independent of M and implies that

$$A(n) \sim M/n = M^2/\rho \tag{33}$$

Although other choices of α yield the desired type of relation, the choice $\alpha = 1$ is reasonable on other grounds. For a polymer it becomes meaningless to use a molecular pair potential. Instead, if a pair potential is assigned to each monomer unit or any convenient group of atoms (the sub-molecule) of mass M_o, the direct correlation function for a polymer could be approximated as

$$c(r,n) \simeq (M/M_o)c_o(r,n) \tag{34}$$

where c_o is the effective direct correlation function for one of the monomers or sub-molecules. In this approximation *Eq 20* yields $A \sim M$ which implies that $\alpha = 1$.

The above arguments suggest that the diagonal coefficients A_{ii} in *Eq 28* should vary as $M_i/n_i = M_i^2/\rho_i$.

In contrast, the cross terms, A_{ij}, will have a much different dependence on M than the diagonal terms. The reason is simple. The *ii* interactions are strongly correlated because the i monomers in a given polymer are chemically bonded to one another. In comparison, the *ij* interactions are weakly correlated because the i and j monomers belong to different molecules—the constraint of chain connectivity is absent. Thus, it is expected that c_{ij} is independent of the M of component i or j and *a cross term such as*

$$A_{ij}M_i^{-1}M_j^{-1}(d\rho_i/dx)(d\rho_j/dx)$$

will be negligible compared to any diagonal term if either i or j component is a polymer. So whenever a cross term involves a polymer component, it can be ignored! This is a convenient simplification. For example, for a polymer/solvent or polymer/polymer binary, *Eqs 28* and *29* become

$$\sigma = 2\int_{-\infty}^{\infty} \Delta\Psi dx \qquad (35)$$

and

$$2\Delta\Psi = A_{o(1)}\rho_1^{-1}(d\rho_1/dx)^2 + A_{o(2)}\rho_2^{-1}(d\rho_2/dx)^2 \qquad (36)$$

where the constants $A_{o(i)}$ are defined by *Eq 24. Equations 35* and *36* are identical in functional form to *Eqs 2.13* and *3.2* of the Helfand and Sapse paper (25). Thus, the gradient theory is in harmony with the theory of Helfand and co-workers save for the interpretation of the numerical coefficients of the square gradient terms.

Helfand has recently reviewed his diffusion equation approach to polymer/polymer interfaces (27). This author has also recently reviewed other aspects of polymer/polymer interfaces, such as their behavior near the critical point and their role in spinodal decomposition, that have not been considered herein (1).

SUMMARY

This abbreviated review of polymer interfaces and interphases has attempted to summarize and reconcile the current state of theoretical knowledge in this field.

It has been shown that Cahn's reformulation of interphase thermodynamics avoids many of the difficulties of the traditional approach of Gibbs and is an invaluable tool when investigating interfacial properties. When the interphase is defined by the placement of two boundary surfaces (shown as the dashed lines in *Fig. 1*), an appropriate reference system can always be defined for a two-phase system so that any two of the extensive variables in the set $\{E, V, S, N_i\}$ will have zero excess relative to the reference system. The reference system is composed of appropriate amounts of each bulk phase. All other remaining extensive variables will, in general, have a non-zero excess relative to the reference system. These excess surface variables are invariant to how the interphase is defined. For example, moving the boundary layers in *Fig. 1* deeper into the bulk phases merely redefines the reference system for which two of the extensive variables must have a zero excess. The excess of the remaining variables remains invariant to the movement of the boundary layers. Cahn has shown that a generalized adsorption equation, *Eq 5*, can be written in terms of these invariant excess surface variables. Some applications of this useful equation were developed.

Gradient theories of polymer interfaces were briefly reviewed. Gradient theory has been used to develop a quantitative theory of polymer liquid surface tension and to relate the surface tension of a liquid to its isothermal compressibility and mass density. Although the theory of Helfand and coworkers for polymer/polymer interfaces adopts a point of view that is different from that of the gradient theory, it has been shown that both theories yield the same set of fundamental equations for the interfacial tension. The physical interpretation of numerical coefficients differs, but otherwise the equations are identical.

REFERENCES

1. I. C. Sanchez, *Ann. Rev. Mater. Sci.*, **13,** 387 (1983).
2. S. Wu, in "Polymer Blends," Vol. I, D. R. Paul and S. Newman, eds., Ch. 6, Academic Press, New York (1978).
3. J. W. Cahn, in "Segregation to Interfaces," J. J. Blakely and W. C. Johnson, eds., pp. 3–23, ASM Seminar Series, Cleveland (1978).
4. I. C. Sanchez, in "Polymer Compatibility and Incompatibility: Principles and Practice," K. Solc, ed., MMI Symp. Ser., Vol. 2, pp. 59–76. Harwood, Cooper Station, NY (1982).
5. J. S. Rowlinson, "Liquids and Liquid Mixtures," pp. 143–149. Plenum Press, New York (1969).
6. O. K. Rice, *J. Chem. Phys.*, **64,** 4362 (1976).
7. D. G. Triezenberg and R. Zwanzig, *Phys. Rev. Lett.*, **28,** 1183 (1972).
8. V. Bongiorno, L. E. Scriven, and H. T. Davis, *J. Coll. Interf. Sci.*, **57,** 462 (1976).
9. A. J. M. Yang, P. D. Fleming, and J. H. Gibbs, *J. Chem. Phys.*, **64,** 3732 (1976).
10. R. F. Kayser and H. J. Raveché, "Extension of the Square-Gradient Theory to Fourth Order," *Physica* (in press).
11. J. S. Rowlinson and B. Widom, "Molecular Theory of Capillarity," Ch. 3. Clarendon Press, Oxford (1982).
12. J. W. Cahn and J. E. Hilliard, *J. Chem. Phys.*, **28,** 258 (1958).
13. C. I. Poser and I. C. Sanchez, *J. Coll. Interf. Sci.*, **69,** 539 (1979).
14. I. C. Sanchez and C. I. Poser, in "Physiochemical Aspects of Polymer Surfaces," Vol. 1, pp. 173–182. K. L. Mittal, ed., Plenum, New York (1983).
15. I. C. Sanchez and R. H. Lacombe, *Nature*, **252,** 381 (1974).
16. I. C. Sanchez and R. H. Lacombe, *J. Phys. Chem.*, **80,** 2352 (1976).
17. S. Sugden, *J. Chem. Soc.*, **125,** 32 (1924).
18. K. S. Siow and D. Patterson, *Macromolecules*, **4,** 26 (1971).
19. D. Patterson and A. K. Rastogi, *J. Phys. Chem.*, **74,** 1067 (1970).
20. K. M. Hong and J. Noolandi, *Macromolecules*, **14,** 1229 (1981).
21. C. I. Poser and I. C. Sanchez, *Macromolecules*, **14,** 361 (1981).
22. I. C. Sanchez, *J. Chem. Phys.*, **79,** 405 (1983).
23. G. Helfand and Y. Tagami, *Polym. Lett.*, **9,** 741 (1971).
24. G. Helfand and Y. Tagami, *J. Chem. Phys.*, **56,** 3592 (1972).
25. G. Helfand and A. M. Sapse, *J. Chem. Phys.*, **62,** 1327 (1975).
26. G. Helfand, *Acct. Chem. Res.*, **8,** 295 (1975).
27. G. Helfand in "Polymer Compatibility and Incompatibility: Principles and Practices," K. Solc, ed. MMI Symp. Ser., Vol. 2, pp. 143–163. Harwood, Cooper Station, NY (1982).
28. P. D. Fleming, A. J. M. Yang, and J. H. Gibbs, *J. Chem. Phys.*, **65,** 7 (1976).

I. SANCHEZ

J. Noolandi: On your last view graph (see *Eqs 28* and *29*) it seems that one could make this analogy quantitative by simply taking the diffusion equation of Helfand and letting the molecular weight of the polymer to become infinite since then you will have only these gradient terms left, I believe that in this case your non-diagonal A_{ij} terms would be exactly zero.

I. Sanchez: Yes. That is exactly what I argued, that in limit of high molecular weight these cross terms (A_{ij}) go to zero.

M. Grmela: I am thinking about the actual shapes of the interfaces. In fact, if you have two components, what is the preferable topological arrangement of the two phases? I think that this program can be predicted by starting from the gradient theory. My question is whether you have done this kind of study.

I. Sanchez: The answer to the first question is yes; you can get information as to what is happening at the interface. For example, the density profiles can be calculated from the theory. The answer to your second question is no; we have not done any detailed calculations of what is happening. This equation (*Eq 23*) allows you to calculate the density profile for a pure fluid. For example, $\Delta\Psi$, is a thermodynamic quantity that depends on the chemical potential. Using an appropriate model free energy function, $\Delta\Psi$ can be determined and then the density profile can be calculated. For a multicomponent system, this equation (*Eq 29*) along with the individual Euler-Lagrange equations for each component (not shown) can be used to calculate density profiles. Alternatively, one can make certain assumptions about how these density variables (ρ_i) are related to one another. For example, say that ρ_1 plus ρ_2 is equal a constant (incompressible approximation) and that gives me an equation of how the density should vary with x. I can integrate this equation (*Eq 29*) to get the density profile. Other approximations are possible. Everything in principle can be calculated from the gradient theory or from the diffusion equation approach.

L. A. Utracki: You showed a very beautiful graph with a theoretical calculation plotted versus experimental data for variety of liquids. Could you point out the salient points of the theoretical calculations.

I. Sanchez: The relationship is arrived at by a combination of physical and dimensional arguments. Basically, what you find is that this coefficient, A, which is the second moment of the correlation function, has to be proportional to the two parameters of a pair potential. If I have Lennard-Jones pair potential, the depth of the energy well is ϵ_o and the repulsive core is of size σ_o. For this type of potential, or any potential of this general shape, the coefficient has to be proportional to ϵ_o and σ_o^2, divided by the molecular weight of the species. It turns out that the proportionality constant is a universal constant, that is, I can use the same constant and can calculate what I call A_o from this expression (see *Eq 25*). For that one curve that I showed for helium and water, and a bunch of other liquids in between, I went to the literature and pick-out the ϵ_o and σ_o values for these different molecules and evaluated this product (*Eq 25*). The fact that the "experimental" and "theoretical" values of A_o agree so well has a very special implication. It says that these two parameters (ϵ_o and σ_o) are not independent and that they are coupled in a very special way. The product, $\epsilon_o\sigma_o^2$, is proportional to molecular weight. For example, if you look at all the organic molecules this combination $(\epsilon_o\sigma_o^2/M)^{1/2}$ is almost invariant; a constant for all the organics (not containing halogens).

J. Noolandi: I have a question regarding the use of the Lennard-Jones potential for something like methane as compared to helium. The Lennard-Jones potential is, of course, averaged spherically symmetric. I am a little surprised that this correlation holds because the ϵ_o that I would get by averaging the methane interaction potential, which is highly directional, is not as well defined parameter as perhaps σ_o, the hard core of the interaction. My question is: do you find that for the organics, and for things like methane and water, there is a considerable contribution for ϵ_o or is it merely a size effect for these more complicated molecules? Is σ_o, in fact, giving you most correlation or is ϵ_o even there doing something for you?

I. Sanchez: I do not know if I can answer your question. However, I can make a statement that may shed some light on your question. If you look in the literature for values of ϵ_o and σ_o for something like butane you will find very disparate values given. The ϵ_o's and σ_o's are not the same because these parameters are determined in different ways: from second virial and coefficients or viscosities. It is interesting that I can take these different sets of values, form this combination $(\epsilon_o\sigma_o^2/M)^{1/2}$ and I still get nearly the same value of A_o. So, there is compensation between these two in a very special way; they are coupled. They are not independent.

Fluorescence Techniques in the Study of Polymer Colloids

MITCHELL A. WINNIK

Lash Miller Laboratories
Department of Chemistry
and Erindale College, University of Toronto
Toronto, Ontario, Canada M5S 1A1

Applications of fluorescence techniques to the study of polymer colloids are reviewed, with emphasis on excimer and exciplex forming probes and fluorescence energy transfer processes. In these experiments non-aqueous dispersions covalently labelled with naphthalene or anthracene were examined by a variety of techniques in order to elucidate aspects of core morphology with a resolution of about 10Å. The current "concentric sphere" or "core-shell" model of colloid structure was found to be inconsistent with the results of the luminescence experiments. A new "microphase" model is proposed which overcomes these difficulties. In this model, the core structure is seen to be made up of phase-separated microdomains of core and stabilizer chains.

In polymer blends, in certain composite materials, in thin films and in colloidal particulates, the relevant spacial scales which determine the properties of the materials are very small. They range from molecular dimensions in monolayer films to distances 10 to 100 times the molecular radii of gyration for polymer films and colloids. In such systems one must ask questions about the molecular morphology, and the design process becomes one of molecular engineering.

Appropriate tools are needed for the study of these materials. These tools must be able to resolve morphological and dynamic features on the scale of several to several hundred Angstroms. One needs to be able to measure the size, shape, and composition of microphases, as well as the characteristics of interfaces. Information is needed about the orientation of individual molecules and multimolecular ordering. Dynamic relaxation processes need to be understood on this scale, including the dynamics of small molecule penetration into, and diffusion within, each microphase.

These kinds of problems are very similar to those faced by immunologists and membrane biochemists in elucidating the structural and dynamic features of complex biological systems. To some extent, scientists studying synthetic and biopolymer systems have used similar tools, e.g. electron microscopy and nmr. In other ways their approaches have been very different. Much of the important molecular-level information about synthetic polymer systems, over the last ten years, has come from neutron scattering studies of deuterium labelled chains (1). Over the same period of time, those studying biopolymer systems have come to rely increasingly on luminescence experiments (2), examining the fluorescence and phosphorescence properties of dyes bound or attached to sites in the system.

There is no intrinsic reason why luminescence techniques cannot provide information of similar richness about systems composed of synthetic polymers. The question of which techniques achieve prominence in a field, and in what order, is due largely to the accidents of history and the personal proclivities of those working in the field.

Polymer scientists are beginning to discover the power of luminescence techniques (3). This review examines some of the recent advances in the application of these techniques to the study of microphase morphology and interface phenomena in polymer colloids.

BACKGROUND

These are seven techniques which form the basis of luminescence spectroscopy. Molecules fluoresce from singlet states, phosphoresce from triplet states, and these emissions are polarized. In steady state, emission wavelengths are scanned at fixed excitation to obtain *fluorescence spectra* and *phosphorescence spectra*; excitation wavelengths are scanned for a given emission to determine the *excitation spectrum*. Under steady state illumination, using polarized light, *the mean polarization* of a sample is measured. Transient techniques measure *fluorescence decay*, *phosphorescence decay*, and *polarization decay* at individual wavelengths. In addition, there are bimolecular processes such as energy transfer, excimer and exciplex formation, and quenching phenomena which provide added dimensions to these techniques. These techniques and processes are summarized in *Table 1*.

Excimer Formation and Self-Quenching

Good insights into the nature of these phenomena, and how they are affected if the luminescent

Table 1. Luminescence Measurements

A. **Techniques**		
steady state measurements	*transient techniques*	*time scale*
fluorescence spectra	fluorescence decay	nanoseconds
phosphorescence spectra	phosphorescence decay	nanoseconds to seconds
polarization	polarization decay	nanoseconds to seconds
excitation spectra		
B. **Processes**		
reaction	*observation*	*spacial scale*
energy transfer		
$A^* + B \rightarrow B^* + A$	emission from B	10 Å to 80 Å
excimer and exciplex formation		
$A^* + A \rightarrow (AA)^*$ $A^* + D \rightarrow (AD)^*$	new emission from (AA)* or (AD)*	5 Å
quenching and self-quenching	decreased emission intensity; shorter decay time	5 Å to 15 Å
$A^* + Q \rightarrow A + Q$ $A^* + A \rightarrow 2A$		

dye is attached to a polymer, can be gained from careful consideration of *Figs. 1* and *2*. *Figure 1* presents the fluorescence and phosphorescence spectra of the naphthalene derivative 1-naphthylmethyl pivalate (1), at two different concentrations in methylcyclohexane solution. *Figure 2* shows the fluorescence spectra of a corresponding naphthalene derivative (2) covalently attached to the poly(methyl methacrylate) [PMMA] chains of a PMMA particle, sterically stabilized by polyisobutylene. Both solutions have been frozen in liquid nitrogen to yield transparent glasses which suppress molecular motion.

These spectra provide examples of two luminescence phenomena, excimer emission and self-quenching (4), which are very useful in the study of polymer systems. Excimers (4b) (and exciplexes (4c)) are electronically excited bimolecular complexes between species that normally do not form complexes in their ground state. Excimer emission is red-shifted with respect to emission from the corresponding locally excited molecule. This emission usually requires a planar sandwich-like orientation of the chromophores in the excimer.

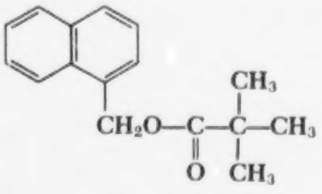

1

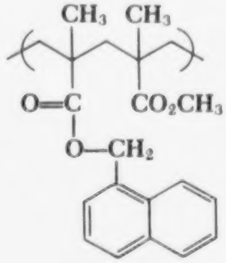

2

An example of naphthalene excimer formation is shown in *Fig. 1*, where the process can be described as

$$N^* + N \rightarrow (NN)^*. \qquad (1)$$

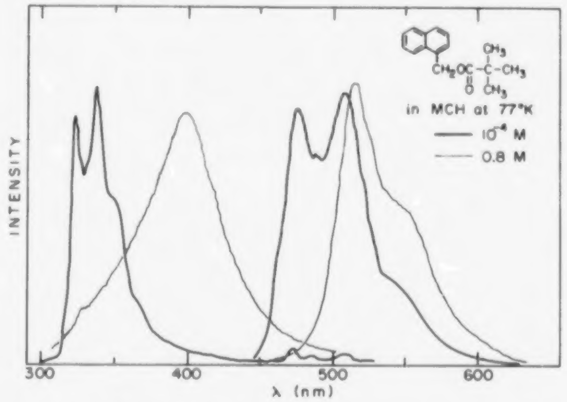

Fig. 1. The fluorescence and phosphorescence spectra of 1-naphthylmethyl pivalate in a methylcyclohexane (MCH) glass at 77 K. The heavy line refers to a nominal (room temperature) concentration of 1 × 10⁻⁴ M; the light line, to 0.8 M.

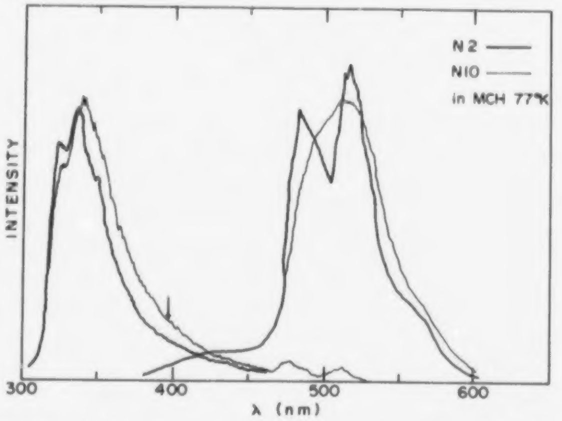

Fig. 2. The fluorescence and phosphorescence spectra of methylcyclohexane dispersions of N2 and N10 (approximately 3 mg/ml) frozen rapidly to 77 K.

At low concentrations one sees two emissions. Fluorescence is observed between 315 and 400 nm. Its decay, measured separately, is exponential, with a fluorescence lifetime ($^1\tau$) of 84 nsec. At longer wavelengths, phosphorescence is observed. Its decay is also exponential, with a lifetime ($^3\tau$) under these conditions of 2.2 sec.

At higher concentrations, 0.8 M, these emissions are shifted to longer wavelength. The locally excited naphthalene [N] fluorescence has been replaced by naphthalene excimer [$(NN)^*$] fluorescence. Since molecular diffusion is prevented in the glassy matrix, excimer emission must result from preformed pairs of N molecules in the sandwich geometry necessary for excimer formation. The phosphorescence is also red-shifted. The new emission is probably due to triplet excimer phosphorescence. Triplet excimers (5) are not as well characterized as singlet excimers.

Figure 2 shows the fluorescence and phosphorescence from two colloidal systems dispersed in methylcyclohexane, measured at 77 K. The dispersions differ only in the amount of N groups which are incorporated into the cores of the particles. $N10$ is a PMMA particle containing 10 mol percent N groups (as a copolymer of 1-naphthylmethyl methacrylate and methyl methacrylate). Its local [N] concentration is estimated to be 0.7 M. $N2$ is a similar particle containing 2 mol percent N groups, with a local [N] concentration within the core of 0.17 M.

While the emission spectra of $N2$ and $N10$ differ in detail, they are on the whole very similar. Little excimer fluorescence is seen in either sample. The vertical arrow at 395 nm points to a small contribution of N-excimer fluorescence in the $N10$ sample. The implication is that in $N2$ and $N10$ the naphthalene groups are close enough to interact, but because of their attachment to the polymer chains, they cannot achieve the proper orientation to emit excimer fluorescence. This interaction results in shortening of the fluorescence and phosphorescence lifetimes in the dispersion of higher local [N] concentration, a process referred to as self-quenching.

Self-quenching, or "concentration quenching," is defined as any interaction between an excited state molecule and a corresponding ground state molecule which decreases the luminescence intensity and shortens the corresponding intensity decay time of the excited species. Excimer formation is a kind of self-quenching phenomenon. The general process for naphthalene self-quenching can be expressed as

$$N^* + N \rightarrow 2N. \tag{2}$$

As we will see below, this process can provide a very important means of measuring swelling or contraction of microdomains within a material, since these processes lead to changes in the local [N] concentration.

Non-Radiative Energy Transfer

An electronically excited molecule (the donor) can transfer its energy to another molecule (the acceptor) over substantial distances by a dipole coupling mechanism if certain criteria are met (6). The fluorescence spectrum of the donor must overlap the absorption spectrum of the acceptor molecule. For transfer from N^* to anthracene (A), the process can be written

$$N^* + A \xrightarrow{k_{ET}} N + A^*. \tag{3}$$

The appropriate emission and absorption spectra for a substituted naphthalene derivative and a substituted anthracene derivative are shown in *Fig. 3*. There is also a dependence on the mutual orientation of donor and acceptor molecules (6–8)

According to the theory of Förster (7, 8), the characteristic distance R_o between donor and acceptor chromophores at which half the excitation energy is transferred is given by the expression

$$R_o^6 = 8.8 \times 10^{-25} J n^{-4} \kappa^2 \Phi_D^o \tag{4}$$

where J is the overlap integral (e.g. integrated over the shaded portion of the spectrum in *Fig. 3)*, n is the index of refraction of the medium, κ is an orientational parameter, and Φ_D^o is the fluorescence quantum yield of donor fluorescence in the absence of acceptor. R_o pertains to a pair of chromophores where energy transfer occurs faster than molecular diffusion. The rate of energy transfer varies as the inverse sixth power of the distance, viz.

$$k_{ET} = k_F \left(\frac{R_o}{r}\right)^6 \tag{5a}$$

where k_F is the rate constant for fluorescence of the donor; and the efficiency E of the energy transfer depends upon

$$E = \frac{r^{-6}}{r^{-6} + R_o^{-6}} \tag{5b}$$

In favorable cases, R_o may be as large as 50 to 60Å. For the specific case of N^* transferring energy to A, the R_o value is 22Å, with alkyl substituents on either A or N having only a very small effect on the magnitude of R_o. Since energy transfer can be detected for distances up to approximately 1.8 R_o, fluorescence energy transfer in static systems serves as a "spectroscopic ruler" (8) for measuring distances of 20 to 100Å, depending upon the choice of chromophore pairs.

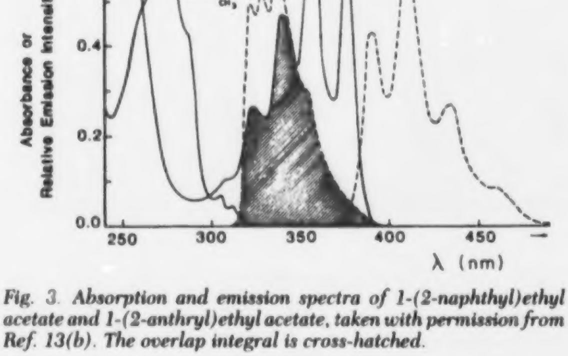

Fig. 3. Absorption and emission spectra of 1-(2-naphthyl)ethyl acetate and 1-(2-anthryl)ethyl acetate, taken with permission from Ref. 13(b). The overlap integral is cross-hatched.

POLYMER COLLOIDS

The term polymer colloids refers to particles of an organic polymer of colloidal dimensions, dispersed in an aqueous or non-aqueous medium (9). Aqueous dispersions are normally stabilized by coulombic interactions between surface charges on the particles. Non-aqueous dispersions (NAD's) are normally "sterically-stabilized" by cilia of soluble polymer chains which protrude from their surface. Sterically stabilized aqueous dispersions have also been prepared. In addition, aqueous polystyrene dispersions containing fluorescent dyes have been prepared and are available commercially.

Our concern is with the application of luminescence techniques to map out the microscopic morphology and dynamics of these particles. In our work we examined non-aqueous dispersions of PMMA particles stabilized by polyisobutylene [PIB]. Particles labelled with *N* groups or *A* groups in the PMMA phase were prepared by adding 1-naphthylmethyl methacrylate or 9-anthrylmethyl methacrylate, respectively, to methyl methacrylate during the preparation of the particles. By scanning electron microscopy, these particles had radii of approximately 1 μm. By BET analysis, they were found to be non-porous (10). Photographs of the sample *A*2, after freeze drying, are shown in *Fig. 4*. We believe that both the necking between particles and the surface crazing are caused by radiation damage during particle examination in the electron microscope.

Analysis of *solutions* of the polymer in $CDCl_3$ by ^1H nmr indicated the monomer mole ratio of *IB*/*MMA*/*N* or *A* to be 13/100/2 in the particles identified as *A*2 and *N*2, and 13/100/10 in those referred to as *A*10 and *N*10. The near unity values of the reactivity ratios indicate that the *N* or *A* groups are randomly distributed along the PMMA chains (10, 11).

Attempts to measure the molecular weights of the polymers making up the dispersions were not very successful. By gel permeation chromatography (gpc) in tetrahydrofuran solution, the material had a biphasic molecular weight distribution with a long retention time consistent with a very low molecular weight (less than 20,000). On the other hand, preliminary fractional precipitation studies indicate the presence of very little homopolymer, since each fraction showed both PMMA and PIB signals in the ^1H nmr. These observations are consistent with an MW significantly less than 10^5, but with interactions between PIB and the PS beads in the gpc column being responsible for the long retention times. These results are important because they affect the model one develops for the internal structure of the dispersions.

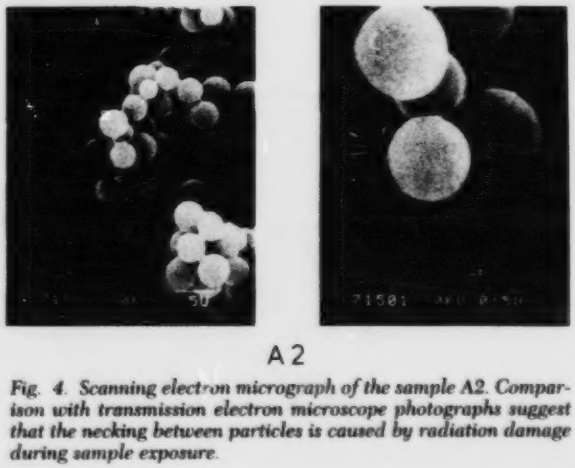

Fig. 4. Scanning electron micrograph of the sample A2. Comparison with transmission electron microscope photographs suggest that the necking between particles is caused by radiation damage during sample exposure.

Dispersions of *N*2 and *N*10 in isooctane show typical *N* fluorescence. Careful examination of the *N* fluorescence decay curve $I_N(t)$, measured at 337 nm, shows a small component of shorter lifetime, $\tau_{N,sh}$ = 12 ns. An example can be seen in *Fig. 5* (where $I_N(t)$ is measured for an isooctane dispersion of *N*10 in the presence of a trace of anthracene). The short component conveys important information about the system. It arises from static concentration fluctuations of *N* groups within the PMMA phase of the dispersion, which, for proximate *N*/*N* pairs, shorten the fluorescence decay by the process of self-quenching.

Models for Sterically Stabilized Polymer Colloids

In dispersion polymerization of vinyl monomers in non-aqueous media (10), the monomer must initially be soluble in the dispersion medium. After initiation of the polymerization, the chain grows to a critical molecular weight and phase separates from the solution to form the nucleus of a particle. Provided that an amphipathic block or graft copolymer is present in the reaction mixture, the nuclei formed are stabilized by adsorption of the amphipathic copolymer at the surface of the nuclei, which then grow into discrete particles. Numerous hypotheses of the detailed mechanism of particle nucleation and growth have been proposed, (10) although no definitive conclusions have been drawn.

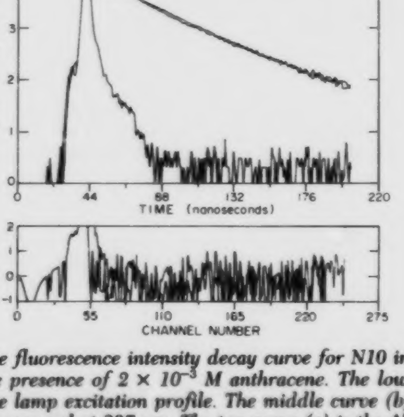

Fig. 5. The fluorescence intensity decay curve for N10 in isooctane in the presence of 2 × 10^{-3} M anthracene. The lowermost curve is the lamp excitation profile. The middle curve (b) is the N^* decay measured at 337 nm. The top curve (a) is the A^* decay measured at $\lambda > 450$ nm. Reproduced with permission from Ref. 12.

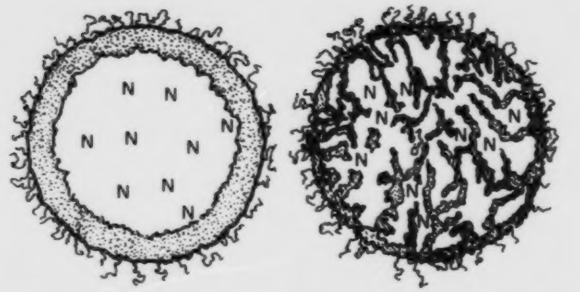

Concentric Sphere Model

Microdomain Blend Model

Fig. 6. Models for the morphology of polymer colloids.
(a) The concentric sphere or core-shell model. Core homopolymer plus core polymer components of the dispersant form a spherical interior phase covered by a spherical shell of stabilizer chains. For N10 and N2, the particle diameters are approximately 2 μm, implying that the stabilizer shell is 350Å thick.
(b) The microphase model. Segments of the stabilizer chains, grafted to the core polymer, phase separate in the interior of the core. These form an interconnecting network of threads and pools, as well as a thin surface layer which serves to stabilize the dispersion.

The presumption that the core of the particle so formed is essentially pure homopolymer has led to a model for particle morphology, *Fig. 6a* which we refer to as the concentric sphere or core-shell model. There is some evidence in support of this model from the work of Dawkins when the amphipathic dispersant is a block copolymer (11). For various reasons which will be developed below, we have found this model to provide an unacceptable description of the morphology of non-aqueous dispersions stabilized by graft copolymer dispersants. We have therefore proposed a new model, *Fig. 6b*, the *microphase model*, to explain our experimental results.

Energy Transfer Studies. The 40Å Ruler

When anthracene is added to isooctane dispersions of N2 or N10, both N and A fluorescence can be observed upon excitation of the sample at 280 nm (12). At this wavelength, *Fig. 3*, the N groups are excited preferentially. Energy transfer from N^* to A was established by fluorescence decay measurements using the time-correlated single photon counting technique. A in isooctane has a fluorescence lifetime $\tau_A = 5.4$ ns. When the fluorescence decay of A is measured at $\lambda \geq 450$ nm upon excitation of N in N2 or N10, the decay curve can be resolved into two components. An example is given in *Fig. 5*. The short component, $\tau_{A,sh} = 5.4$ ns, is due to direct absorption light by A at 280 nm. The long component $\tau_{A,l} = 38.8$ ns is due to energy transfer from N^*. This interpretation is confirmed by finding that the long component of the N^* fluorescence measured at 337 nm, $\tau_{N,l} = 39.2$ ns, has the same value within experimental error.

When the anthracene concentration in the isooctane medium is varied, the naphthalene lifetime changes. In addition, the system follows the behavior predicted by the Stern-Volmer equation

$$\frac{1}{\tau_{N,l}} = \frac{1}{\tau_{N,l,o}} + k_{ET}[A] \qquad (6)$$

where $\tau_{N,l,o}$ is the naphthalene lifetime in the absence of A (see *Fig. 7*). This surprising result demonstrates both a diffusion component to the energy transfer process and, even more significantly, that the A groups can reach all of the N groups contributing to the 39 ns lifetime with *equal probability*. The anthracene concentrations we examine are too small to affect those N groups with 12 ns lifetimes. Since the long component represents the majority of N groups in the 2 μm diameter particle, it implies penetration of the A molecules deep within the particle.

The slope of the Stern-Volmer plot for N10 + A is 2×10^9 m^{-1} s^{-1}. This compares with a value of $k_{ET} = 1.4 \times 10^{10}$ m^{-1} s^{-1} for energy transfer from 1-naphthylmethyl pivalate (1) to anthracene, two small molecules in isooctane solution. Energy transfer occurs by a diffusion controlled process.

The magnitude of k_{ET} is related to the diffusion coefficients of the interacting species by the expression (6, 13)

$$k_{ET} = \frac{4\,\pi\,N\,D\,R_f}{1000} \qquad (7)$$

where N is Avogadro's number, D is the sum of the diffusion coefficients of the interacting species, and R_f is the radius of a characteristic diffusion cross-section. According to the treatment of Gösele (14), R_f is not a constant for a pair of reactants. For Förster energy transfer, when the mean diffusion length is larger than R_o, R_f depends upon D, R_o, and the fluorescence lifetime of the donor (τ_o) in the absence of acceptor, so that with increasingly rapid diffusion R_f decreases in magnitude, approaching a value typical of molecular dimensions at large D.

From *Eq 7* we can calculate a value of $D_{AN} = 2.4 \times 10^{-5}$ cm^2 s^{-1} for A and 1 in isooctane, a value typical of small molecule diffusion in solution. Correspondingly, we calculate a value $D_{coll} = 1.8 \times 10^{-6}$ cm^2 s^{-1} for N10 + A. This value is too large by more than 8 orders of magnitude for the diffusion

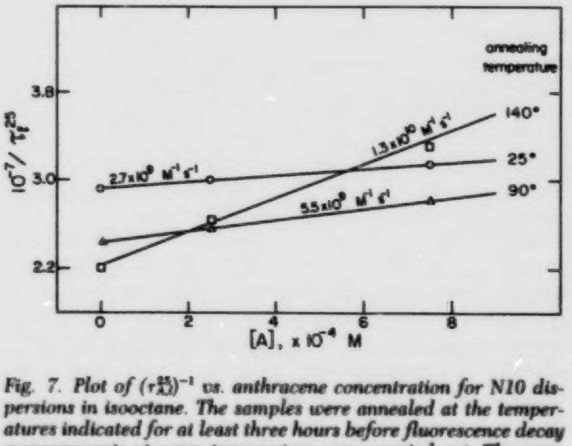

Fig. 7. Plot of $(\tau_{N,l}^{25})^{-1}$ vs. anthracene concentration for N10 dispersions in isooctane. The samples were annealed at the temperatures indicated for at least three hours before fluorescence decay measurements at room temperature were carried out. The magnitudes of the slopes [k_{ET}, Eq 6] are indicated on the plot.

of *A* to *N* groups embedded in a PMMA matrix below its glass transition temperature.

Three processes contribute to the magnitude of D_{coll}. These are anthracene diffusion, D_A, segmental diffusion associated with the *N* groups, $D_{loc,N}$, and exciton diffusion between *N* groups, Λ_N. While exciton diffusion is important for chlorophyll molecules in a chloroplast, where the R_o for self-energy transfer in chlorophyll is approximately 50Å, it should not be very important in *N*2 and *N*10: the local concentration of chromophores is low, and the R_o for self-energy transfer is only 8Å (6). Although one writes $D_{coll} = D_A + D_{loc,N} + \Lambda_N$, it seems reasonable to conclude that the D_A term makes the major contribution to D_{coll}. One should note, *Eq. 6*, that the absolute magnitude of D_{coll} depends upon the concentration of *A* within the colloids, which is assumed to be the same as that in the isooctane solvent.

Temperature Effects on Non-Radiative Energy Transfer

If samples of *N*2 or *N*10 in isooctane are heated for several hours and then cooled to room temperature, irreversible changes occur both in the naphthalene fluorescence decay profiles and in the rate of energy transfer between N^* and *A* (15). Stern-Volmer plots for three annealing temperatures are presented in *Fig. 7*. The effect of heating and recooling the dispersion is to increase the rate of energy transfer and to increase as well the fluorescence lifetimes of the naphthalene groups, $\tau_{N,l,o}^{25}$.

The slopes of these plots are indicated, and the rate constants for energy transfer under a variety of conditions are presented in *Fig. 7*. The upper curve in *Fig. 8* describes the temperature dependence of k_{ET} for energy transfer from *N*10 to *A* for experiments carried out at the temperature indicated (k_{ET}^T). The lower curve, where we focus our attention, describes the behavior of k_{ET}^{25} determined at 25°, after annealing the samples successively at each of the temperatures indicated.

The changes in k_{ET}^{25} are modest up to temperatures of 60 to 70°. Subsequently, large increases are observed. Above 125°, the k_{ET}^{25} values appear to level off. The temperature range where k_{ET}^{25} begins to increase corresponds to the temperature where one observes a pronounced response in differential scanning calorimetry [DSC] measurements of the freeze-dried *N*10 powder, both in the presence or absence of isooctane. We refer to the onset temperature as T_c, and interpret this behavior and the increase in k_{ET} as manifestations of the glass transition in the core of the dispersion.

We attribute the large increases in k_{ET}^T and k_{ET}^{25} values above T_c to the onset of large amplitude motion of the *N* groups in the core, coupled with the increased penetration of solvent into the PMMA phase. Upon cooling, much of this solvent gets trapped in the core, increasing both the amount of *A* present and its mobility. It is interesting to note that after annealing above 125°, the value of k_{ET}^{25} obtained is essentially identical to that found for free 1^* and *A* in isooctane solution.

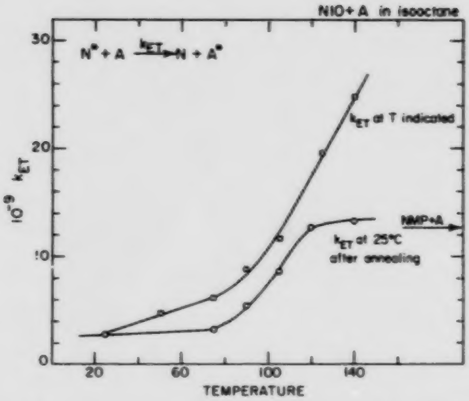

Fig. 8. The temperature dependence of k_{ET}. The upper curve describes k_{ET} values obtained from high temperature fluorescence decay measurements (k_{ET}^T). The lower curve describes k_{ET}^{25} values after annealing the samples at the temperatures indicated.

The Microphase Model

Polyisobutylene comprises 9 percent of the dry volume of *N*10 and *N*2. In terms of the concentric sphere model, it would form a layer 350Å deep on the surface of a 2 μm diameter particle. This layer would be swollen by alkane solvents, permitting anthracene in isooctane to penetrate to the PIB/PMMA interface. According to this model, only *N* groups within 40 to 60Å of the surface would be able to transfer energy to A. The other *N* groups, when excited, would have the same fluorescence lifetime as in the absence of *A*. These represent all but a small fraction of *N* groups in the core, and this prediction of the concentric sphere model is inconsistent with our observations.

In the microphase model, we envision threads and pools of PIB penetrating as an interconnected network throughout the PMMA phase (15). These threads, typically 100Å in diameter, form a discrete phase which can be swollen by alkane solvents which are incapable of penetration into the PMMA domains. In this way, solvents can carry *A* groups deep within the colloid core without affecting T_c of the PMMA phase (see *Fig. 6*).

Other factors lend support to this model. The absence of homopolymer in the fractional precipitation studies argues against a pure PMMA core. So, too, does the relatively low molecular weight of the constituent polymers. The chemical connectivity between PIB and PMMA chains of these lengths lead one to anticipate that there would be substantial amounts of PIB in the core of the colloid. More recently we have found with new systems containing phenanthrene or pyrene groups in the stabilizer part of the dispersant chains, that some of the chromophores are protected against oxygen quenching (16). This too suggests that some of these groups, and parts of the stabilizer chains, are buried deep within the core of the particle.

The key feature of microphase model is that it permits *A* to approach within 40 to 60Å of the majority of *N* groups in the particle. It suggests that a different probe, one that requires 4 to 5Å proximity to the *N* groups for its presence in the core to be detected, would give results that were very different.

Exciplex Formation. The 4Å Ruler

N,N-dimethyl aniline (DMA) forms an intensely emissive exciplex with anthracene and its derivative. When a hexadecane dispersion of *A*2 or *A*10 is incubated with 0.5M DMA, exciplex formation takes place over a period of seven days (17). Typical results are shown in *Fig. 9*. *Figure 10* shows that there is a cooperative aspect to dimethylaniline penetration into the core. Exciplex formation is initially slow. After approximately a week, the floodgates open and the system comes to equilibrium.

Two features distinguish this experiment from the energy transfer experiments with *N*10. First, studies on small molecules suggest that exciplexes form with interchromophore separations of typically 3.5Å (4c, 18). Exciplex emission in the *A*10/DMA system requires the DMA to diffuse to within approximately 3.5Å of the *A* groups. Second, DMA itself is a good solvent for PMMA and a poor solvent for PIB. One might presume that DMA is reasonably soluble in the PMMA phase and can act as a plasticizer for it, whereas it might be poorly soluble in PIB. It may be that its poor solubility in PIB, as well as the glassy nature of the PMMA phase, act to retard its approach to the *A* groups in the particle.

SWELLING AND CONTRACTION IN THE PMMA MICROPHASES

Phosphorescence Self-Quenching

Naphthalene derivatives such as 1 have triplet lifetimes in rigid matrices which are insensitive to solvent, mildly sensitive to temperature, and very sensitive to chromophore concentration. For example, when solutions of 1 in methylcyclohexane [MCH] are frozen rapidly to liquid nitrogen temperature to form transparent glassy solutions, the phosphorescence lifetimes decrease with increasing [*N*] concentration (19). One can interpret these results in terms of the "active-sphere" quenching model, originally proposed by Perrin (20a) and modified by Inokuti and Hirayama (20b). In this model, N^* can be quenched by immobile neighboring *N* groups with a rate constant that depends upon the chromophore separation *r*. As in the Förster model, a critical distance $r = R_o$ is defined as the chromophore separation where the rate of energy transfer equals the reciprocal triplet lifetime at infinite dilution $(1/{}^3\tau_o)$ (19).

Based upon this model, the phosphorescence intensity $I_p(t)$ is predicted to decay as

$$I_p(t) = I_{p,o} \exp\left(-t/{}^3\tau_o - [N]/[N]_o\right) \qquad (8)$$

with $[N]_o = {}^3/_4\, \pi(R_o)^3$. With increasing [*N*], the decay rates increase. The form of the decay is no longer exponential, but the deviations from exponentiality might be imperceptibly small. Under these circumstances, and with [*N*] significantly smaller than $[N]_o$, the mean decay time ${}^3\bar{\tau}$ can be shown to depend upon [*N*] according to

$$\frac{{}^3\tau_o}{{}^3\bar{\tau}} = 1 - \frac{[N]}{[N]_o}. \qquad (9)$$

In *Fig. 11* we plot measured values of ${}^3\tau_o/{}^3\bar{\tau}$ *vs.* [*N*] for 1, and obtain a linear plot. The [*N*] values used refer to the concentration at room temperature. Upon freezing to a glass, MCH contracts approximately 16 percent in volume so that the actual concentrations are about 16 percent higher. In addition, we can estimate the local concentration of *N* in *N*2 and *N*10 from the measured number of moles per gram of *N* groups and the density of the *N*-containing microphase. This density depends upon both the copolymer density at room temperature and the extent to which its volume contracts upon cooling. Neither of these is known. We choose as an estimated density that of pure PMMA at 298 K. This choice gives values of [*N*] whose τ values for the freeze-dried powder fall on the plot for 1 in

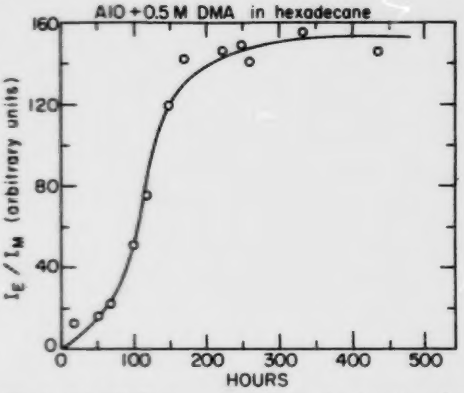

Fig. 10. A plot of I_E/I_M for an A10 dispersion in n-hexadecane in the presence of 0.5 M dimethylaniline as a function of the exposure time.

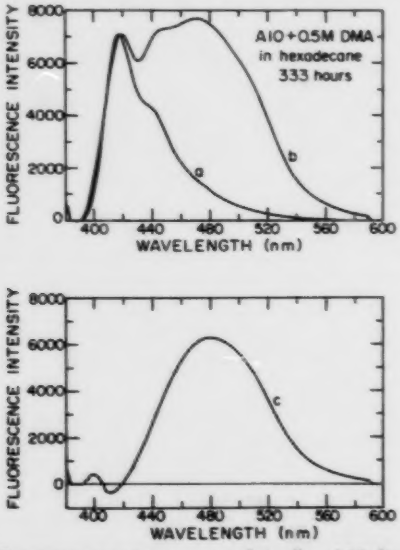

Fig. 9. Fluorescence spectra, upper plot, of an A10 dispersion in isooctane (a) and of a similar dispersion after exposure to 0.5 M N,N-dimethylaniline for 14 days (b). The lower curve (c) is the difference spectrum showing the exciplex fluorescence (I_E).

Fig. 11. The agreement between these sets of values suggests that we have underestimated the local density of the powder at 298 K in a way which compensates for the different extents of contraction of MCH and the copolymer upon cooling to 77 K.

From the slope of *Fig. 11* we calculate an R_o value of 7.2Å for triplet self-quenching in 1. This value is smaller than that of 12.9Å which Inokuti and Hirayama (20b) calculated from Ermolaev's data on naphthalene itself (21). The smaller value for 1 is probably related to the presence of the bulky t-butyl group.

Figure 11 serves as a calibration curve for interpreting the phosphorescence lifetimes measured for MCH dispersions and methanol suspensions of $N2$ and $N10$ at 77 K. From each lifetime we can obtain a corresponding $[N]$ concentration, which reflects the volume change in the PMMA microdomains due to the presence of MCH or methanol. For the dispersions in MCH, the calculated $[N]$ concentrations of 0.14 and 0.49 M, respectively, for $N2$ and $N10$, correspond to a 37 percent increase in volume for the N-group environment relative to that of the freeze-dried powders. In methanol suspensions, these concentrations drop to 0.10 and 0.31 M, corresponding to a 2.2-fold dilution of the N groups (19).

If the volume changes were isotropic, the particle radii would be 1.16 times larger in MCH and 1.30 times larger in methanol than in the dry solid. It is not necessary and perhaps unlikely that these volume changes would occur uniformly throughout the particle. The triplet self-quenching process is sensitive to interactions on the scale of distances of approximately 10Å (R_o = 7.2Å). Since the chromophores are bound to the PMMA chains, our observations pertain specifically to the PMMA microdomains within the particle. The effects of MCH and methanol may be to cause local swelling or to retard the extent of contraction of the PMMA microphases when the samples are cooled rapidly to 77 K.

Fluorescence Self-Quenching

The fluorescence lifetimes of naphthalene derivatives depend sensitively upon temperature, solvent, and concentration. The temperature and solvent sensitivity is related primarily to factors which alter the rate of triplet formation from the excited singlet state, whereas the concentration dependence involves self-quenching. As *Figs. 2* and *3* indicate, if excimers are involved, they need not be of an emissive form.

The fluorescence lifetimes of $N2$ and $N10$ are different, and both are significantly shorter than that of 1 in dilute solution. The fluorescence lifetimes of $N2$ and $N10$ change irreversibly when the powder samples or the dispersions in alkane solvents are heated and then cooled to room temperature. Results for $N10$ powder and its dispersions in isooctane and hexadecane are shown in *Fig. 12* (22).

The behavior of the powder is significantly different from that of the dispersions. In the powder, the $\tau_{N,l}^{25}$ values are only modestly affected by annealing up to 60 to 70°. Above that temperature these values decrease. The $\tau_{N,l}^{25}$ values of the dispersions are only modestly affected by annealing temperatures up to 60 to 70°, but these values *increase* suddenly for samples heated successively to higher temperatures and then cooled. These observations suggest an increase in the self-quenching efficiency for powder samples and a decrease in the self-quenching efficiency for the alkane dispersions for samples heated above 60 to 70° and then cooled to room temperature.

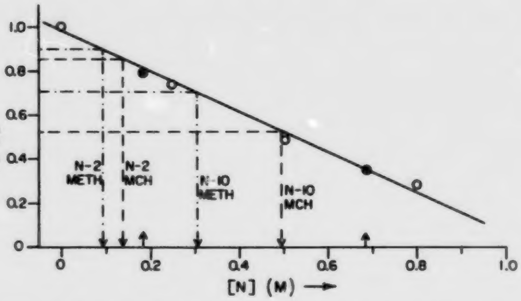

Fig. 11. A plot according to Eq 9 of the mean triplet lifetime vs. the (room temperature) concentration of 1 in methylcyclohexane (○) frozen to a glass at 77 K. Values are also shown (●) for powder samples of N2 and N10 at 77 K. The solid line is treated as a calibration curve relating $^3\bar{\tau}$ to [N]. N2 and N10 samples exposed to methanol (METH) and methylcyclohexane (MCH) before freezing have longer $^3\bar{\tau}$ values. This curve is used to infer the corresponding local [N] concentration.

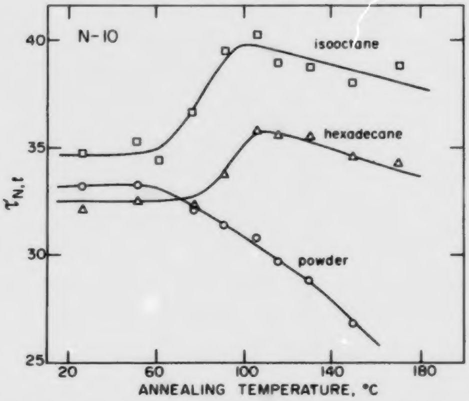

Fig. 12. The $\tau_{N,l}^{25}$ values of N10 samples after annealing for three hours at the temperatures indicated. The isooctane and hexadecane dispersions contain 3 mg/ml. The powder samples were heated under vacuum. The results are shown for samples progressively treated by annealing at a given temperature, cooling to room temperature where $I_N(t)$ was measured, and then reheating to the next annealing temperature.

In a previous section on energy transfer experiments it was suggested that heating alkane dispersions of $N10$ and $N2$ above T_c resulted in important changes in the permeability of the PMMA microphases to solvent and to A molecules. As shown in *Fig. 12*, that heating the particles also causes changes in the mean N-group concentrations within the PMMA microdomains. In the powder, the effect of heating is to cause a volume contraction leading to a decrease in $\tau_{N,l}^{25}$. In the dispersions, a swelling occurs, leading to an increase in $\tau_{N,l}^{25}$.

The extent of swelling or contraction can be made quantitative by application of the active-sphere quenching model. Proper account can be taken, as well, for the short component in the $I_N(t)$ fluorescence decay. These topics are beyond the scope of this report and form the basis of a forthcoming manuscript (22). Two further observations should be noted here. First, the degree of swelling of the PMMA phase in isooctane dispersions of $N10$ is so large that in some samples $\tau_{N,l}^{25}$ achieves essentially its zero concentration value. Second, the degree of swelling as inferred from $I_N(t)$ measurements depends in some important and as yet poorly understood way on the history of the sample; $\tau_{N,l}^{25}$ values undergo much more pronounced changes for samples that have been dispersed in solvent for long periods of time. These effects are currently under study.

SUMMARY

Applications of fluorescence techniques to the study of polymer colloids are discussed. These focus on non-aqueous dispersions of PMMA particles stabilized by a PMMA-polyisobutylene graft copolymer, containing naphthalene groups covalently linked to the PMMA chains. Fluorescence energy transfer experiments between excited N^* groups in the core of the dispersion and anthracene molecules in isooctane solution give results inconsistent with the concentric sphere model, *Fig. 6*, normally used to describe particle morphology. A new model, the microphase model, is developed to explain the data.

Both fluorescence and phosphorescence lifetime measurements can be used to measure the extent of swelling or contraction of the PMMA microphases when the particles are heated, cooled, or treated with non-solvents for PMMA. These experiments detect an important change in the volume and permeability of the PMMA phase when samples are heated above 60 to 70°. This corresponds to a pronounced response in the DSC scan of the particles, suggesting that the sample has its glass transition temperature in this range.

ACKNOWLEDGMENT

The author thanks NSERC Canada for a Co-op Grant which initiated this work, and to the donors of the Petroleum Research Fund administered by the American Chemical Society for their financial support. Dr. M. D. Croucher (Xerox, Canada) played a major role in this research and his contributions and ideas are cited in the appropriate references. I wish to express my special appreciation for the contributions of Professor O. Pekcan, Department of Physics, Hacettepe University, Ankara, Turkey, who, as a visiting scientist, carried out many of the experiments described here; and to Mr. Luke Egan, whose experimental contributions and helpful comments were important in the development of this project.

REFERENCES

1. (a) Cotton, J. P., Decker, D., Benoit, H., Farnoux, B., Higgins, J., Jannink, G., Ober, R., Picot, C., and des Cloizeaux, J., *Macromolecules*, **7**, 863 (1974).
   (b) Daoud, M., Cotton, J. P., Farnoux, B., Jannink, G., Sarma, G., Benoit, H., Duplessix, R., Picot, C., and de Gennes, P.-G., *ibid*, **8**, 804 (1975).
2. (a) Badley, R. A., in "Modern Fluorescence Spectroscopy," Wehry, E. L., ed., Plenum Press, New York, (1976).
   (b) See chapters by Schiller, P. W., Shearer, W. T. and Parker, C. W., Cathou, R. E. and Bungin, J. R., and by Yoo, T. J. in "Biochemical Fluorescence," Chen, R. F. and Edelhoch, H., eds., Marcel Dekker, New York, (1975).
3. Morawetz, H., *Science*, **203**, 405 (1979), Beaven, S. W., Hargreaves, J. S., and Phillips, D., *Advances in Photochem.*, **11**, 207 (1979); DeSchryver, F. C., *Makromol. Chem. Suppl.*, **3**, 85 (1979).
4. (a) Birks, J. B., "Photophysics of Aromatic Molecules," Wiley, New York, (1971).
   (b) Birks, J. B., *Rep. Prog. Phys.*, **38**, 903 (1975).
   (c) Reference 4(a), Ch. 9, and "The Exciplex," Gordon, M. and Ware, W., eds., Academic Press, (1975).
5. Langelaar, J., Jansen, G., Rettschnick, R. P. H., and Hoytink, *Chem. Phys. Lett.*, **12**, 86 (1971).
6. Berlman, I. B., "Energy Transfer Parameters of Aromatic Compounds," Academic Press, New York, (1973).
7. Förster, T., *Ann. Physik*, **2**, 55 (1948).
8. Stryer, L., *Ann. Rev. Biochem.*, **47**, 819 (1978).
9. Vincent, B. and Whittington, S. G., *Surface and Colloid Science*, **12**, 1 (1982). "Polymer Colloids 2." R. M. Fitch, ed., Plenum Press, New York, (1980).
10. Barrett, K. E. J., ed., "Dispersion Polymerization in Organic Media," Wiley Interscience, London, (1975).
11. Dawkins, J. V. and Taylor, G., *J. C. S. Faraday 1.*, **76**, 1263 (1980).
12. Pekcan, O., Winnik, M. A., Egan, L., and Croucher, M. D., *Macromolecules*, **16**, 699 (1983).
13. Birks, J. B. and Georghiou, S., *J. Phys. B., (Proc. Phys. Soc.). Ser.* 2, **1**, 958 (1968).
14. Göselle, U., Hauser, M., Klein, U. K. A., and Frey, R., *Chem. Phys. Letters*, **34**, 519 (1975); Klein, U. K. A., Frey, R., Hauser, M., and Göselle, U., *ibid.*, **41**, 139 (1976).
15. Pekcan, O., Winnik, M. A., and Croucher, M. D., *J. Polym. Sci. Polym. Lett.*, **21**, 1011 (1983).
16. Egan, L. and Winnik, M. A., unpublished observations.
17. Winnik, M. A., Hua, M. H., Hougham, B., and Williamson, B., *Macromolecules*, in press (1984).
18. (a) Beens, H. and Weller, A., in "Organic Molecular Photophysics," Vol. 2, Birks, J. B., ed., Wiley, London, (1975).
    (b) For a recent discussion of anthracene-dimethylaniline exciplexes, see Watkins, A. R., *J. Phys. Chem.*, **83**, 1892 (1979).
19. Pekcan, O., Winnik, M. A., and Croucher, M. D., *J. Coll. Inter. Sci.*, **95**, 420 (1983).
20. (a) Perrin, F., *Compte Rend.*, **178**, 1978 (1924); *Ann. Chem. Phys.*, **17**, 283 (1932).
    (b) Inokuti, M. and Hirayama, F., *J. Chem. Phys.*, **43**, 1978 (1965).
21. Terenin, A. and Ermolaev, V., *Izv. Akad. Nauk, SSSR, Ser. Fiz.*, **26**, 121 (1962), English translation, *Bull. Acad. Sci. USSR, Phys. Ser.*, **26**, 21 (1962).
22. Pekcan, O. and Winnik, M. A., to be published.

DISCUSSION

J. Noolandi: Do you think that poly(iso-butylene) is stuck in the core by entanglements?

M. Winnik: No, I think it is in there by covalent attachment.

L. Piche: Is there another way of measuring the parameter which would give you the interaction or the distance between two spins—I am thinking of NMR where you could measure T_1 and T_2. Would the T_2 give you the distance between two defects by means of the coupling?

M. Winnik: I do not understand your question. What distances would you like to determine?

L. Piche: You have been talking about the distance between the naphthalenes or between naphthalene and anthracene. Is there no other way of measuring this, of getting some more information on this coupling of chromophores? I think that NMR would give the information on this.

M. Winnik: I do not see how NMR would provide information in the case of naphthalene and anthracene, because if our model is correct, their interaction involves a diffusion process. I just do not see how that would come out of an NMR experiment. In the experiment where one looks at the communication between a naphthalenes, one can consider using the ESR of the naphthalene triplet state to obtain similar kinds of information, but again one would be looking at the excited triplet state of a molecule.

I. Sanchez: This is a very powerful technique for looking at the problem of miscibility, or compatibility, in polymer blends. Work of this type is going on in our laboratory at NBS, where we have tagged PMMA and ethyl methacrylate with the anthracene and naphthalene. We look at the efficiency of energy transfer between blends involving methyl and ethyl methacrylates. Of course that system is incompatible, so the energy transfer is very poor between the two chromophores. If you add a third polymer, PVF_2, which is compatible with both ethyl and methyl methacrylates, then you start seeing an increase in energy transfer. I think this may answer the question that was raised earlier, that by looking at the efficiency of energy transfer you get a qualitative if not a quantitative measure of the average distance of separation between the anthracene and naphthalene chromophores. I think this technique is the only one that is not ambiguous in determining whether you have a one or a two phase system in polymer blends.

M. Winnik: It is just a question of resolution. The resolution that you get in that kind of measurement is about 20 Å or more. I was unaware of these experiments. I would urge you to carry them out by fluorescent decay techniques, because the amount of information obtained is much richer than with steady state methods.

I. Sanchez: For the record, I would like to mention that the person who is doing this at NBS is Francis Wang.

L. A. Utracki: You are very enthusiastic about the method and it seems that it has quite a bit of potential, but I think that we should be quite cautious. The information which you gave us today on the effect of annealing of the powder, in the absence of solvent, is ambiguous. I do not see the effect explainable in logical terms. Something funny is happening with the system in question.

M. Winnik: What we call "logical" is really limited by our experience and our imagination, isn't it?

L. A. Utracki: No, because the so called "phase ripening effect" is known. But here, in explaining these phenomena, you are virtually saying that opposite effects would be involved. You are introducing certain concentration of highly aromatic groups into the polymer matrix. How do these groups affect the matrix? The glass transition temperature of PMMA being around 70°C seems rather low.

M. Winnik: The glass temperature of the system as measured by DSC seems to be the same whether the aromatic groups are there or not. As far as we can ascertain the perturbation of the T_g from that normally associated with PMMA is due to the small nature of the micro-phases, coupled with some aspects of the interfaces. It is due to the structure of the material which has poly(isobutylene) intimately mixed with the poly(methyl methacrylate). It is not a consequence of the presence of the aromatic chromophores.

L. A. Utracki: But if you would mold the specimen, would the glass transition temperature be raised or stay the same?

I. Sanchez: The percent of tagging is very small, is it not?

M. Winnik: Well, it is not that small. In *N*2, it is relatively small, but in *N*10 it is really quite substantial: it is ten mole percent of the methymethacrylate. But what I am saying to you, and this is really important, is that the DSC behavior of these materials seems to be independent of the presence of the chromophores.

L. A. Utracki: Could you for the benefit of those of us who are working with industrial materials, point out the fluorescent method that you would recommend using to study industrial blends.

M. Winnik: Well, there are two ways of studying this kind of problem. You can passively dissolve a chromophore into one of the components of a blend. This is called the "probe" method. These are relatively easy experiments to do. You would learn something, but you would be stuck with the ambiguity of not being certain that you know where the chromophore was. In "labelling" experiments, the chromophores are attached covalently to the components of one or both of the phases. One then knows where the "labels" are. If I were going to study polyethylene/polypropylene, which is a nice problem, I think I would take advantage of the advantageous carbonyl groups present in both and use those as a handle to chemically attach different chromophores. Then I think you could study the blend, in films or in bulk, for essentially any kind of industrial processing that you want to do. You could take a sample of that material, put it in the fluorescence spectrometer, and carry out a measurement. I see this as a general kind of technique.

P. Couchman: To return to the glass temperature of PMMA. A change of about 30°C would be hard to account for simply by the size effect. Frankly, these particles have radius of about 20,000 A. It is a bit large; the size effect should essentially be trivial.

M. Winnik: I am talking about the size of the individual microdomaines.

P. Couchman: I thought you meant the whole particle.

M. Winnik: I suspect that there is a lot more grafting than the original model of the colloid scientist would lead us to believe. We have indications that much of the PMMA is not homopolymer but in fact is a graft co-polymer with PIB. That I suspect is the source of the discrepancy; the composition of the material is not what one supposes.

P. Couchman: That is an attractive and imaginative explanation.

L. A. Utracki: But is it logical?

P. Couchman: It may be even that.

B. Thycher: Just a general question. Do you see any hope for use of the fluorescence techniques to try to understand the entanglement spacing in polymer melts?

M. Winnik: I discussed this problem with Jaan Noolandi and with other people like Professor de-Gennes. It is basically a question of time resolution and spatial resolution. There are some really nice experiments by Barton Smith at IBM involving the motion of a fluorescent-tagged polymer in a transparent matrix. He studies the melt diffusion of poly(propylene oxide) and can determine the diffusion coefficient unambiguously. He is using the fluorescence of the material simply as a tracer, and is not limited by the fluorescence life time. In the cyclization experiments that Jaan Noolandi mentioned briefly this morning, one is more limited because the fluorescent group is really a stop watch. When it runs out of time, you run out of measurement.

Use of the Lower Critical Solution Temperature for the Characterization of Polymer Mixtures and the Study of Their Compatibility: Application to Polyethylenes, Polypropylene, and Their Copolymers

SUZANNE VARENNES, GÉRARD CHARLET, *and* GENEVIÈVE DELMAS

Chemistry Department, UQAM
C.P. 8888, Succ. A, Montreal H3C 3P8
Canada

The Lower Critical Solution Temperature (LCST) of polyethylene (PE), polypropylene (PP), and ethylene-propylene block and random copolymers have been measured in heptanes. A thermogram related to the variation of the turbidity of the solution is obtained between 100 and 210°C. The temperature of the onset of the turbidity peak is defined as the LCST of the system. The width and the area of the turbidity peaks are tentatively associated with the polymer polydispersity and the amount of polymer involved in the phase separation. The thermograms of solutions containing both homopolymers show two distinct turbidity peaks situated at a 70°C interval. Correlations of molecular orientations in the concentrated phase, possible in PE systems but not in PP solutions, are at the origin of the lower LCST values for PE solutions. The LCST of copolymers are situated between those of the homopolymers but the dependence of the LCST on the copolymer ethylene content is different for block and random copolymers. Examples of thermograms are also given for mixtures of copolymers with PE and PP. By analysis of their thermograms, some commercial block EP copolymers were also found to contain PE and PP. This method seems well suited for characterizing polymer mixtures.

INTRODUCTION

The Lower Critical Solution Temperature (LCST) in Polymer Solutions

The phase separation of a polymer solution at relatively high temperature, i.e., above the boiling point of the solvent, has been found to be a general phenomenon (1–4). This decrease of polymer-solvent compatibility when the temperature is raised is not due to the disappearance of a favorable interaction but to the dominant effect of a negative contribution to the entropy of mixing. The latter comes from the contraction of the expanded solvent when it is mixed with the dense polymer liquid. The usually negative volume of mixing of a polymeric liquid such as polyisobutylene and a nonpolar solvent (5) is a manifestation of the fact that the solvent contracts more readily than the polymeric liquid expands. Equation of state theories based on Prigogine's early work (6) can predict the LCST of non-polar systems using the molecular sizes (2a) of the two components or their thermal expansion coefficients (2b, c). In general, the trends of the LCST for a polymer in a series of solvents or for different polymers have been successively predicted if not their exact values.

LCST and Correlations of Molecular Orientations

Experimental results have confirmed that the LCST is lower when the free volume dissimilarity, i.e., the difference in expansion between the polymer and the solvent is larger. Accordingly, the LCST increases for a given polymer when the solvent boiling point increases. On the other hand, comparison of the LCST of several polymers in the same solvent gives an indication of their relative degrees of expansion. As an example, the LCST of a stiff-chain polymer, polyisobutylene (PIB) in *n*-pentane is 76°C while it is 150°C for the more flexible polydimethylsiloxane (PDMS) in the same solvent. The expansion coefficients of these two polymers are respectively $0.55 \times 10^{-3} K^{-1}$ (PIB) and $0.887 \times 10^{-3} K^{-1}$ (PDMS). Only a few papers have been published in the last ten years (3, 4) on LCST determination, probably because it was felt that no unexpected effects were likely to occur. However, the analysis of systematic LCST measurements of polyethylene (PE), polypropylene (PP), and random EP copolymers in nonpolar solvents (7) has shown that the free volume or equation of state difference between the polymers was not sufficient to explain the values of the LCST of the PE solutions which could be as much as 90° lower than those for PP in the same solvent.

The presence of correlations in molecular orientations (CMO) in a liquid lowers the free energy while its destruction by mixing with a second component raises the free energy of the system, i.e., the χ parameter. The phase separation in a PE solution is favored because it creates a concentrated polymer phase in which the CMO have more chances to occur than in the one-phase dilute system. Such a favorable situation does not exist for PP or other polyolefins because the side groups on their chains prevent extensive CMO. In consequence, the LCST of PE solutions are consistently lower than those of polymers having branched segments. Furthermore, the sensitivity of CMO to the branching of a polymer may be used to correlate the LCST's of PE of different densities (8). The χ parameter is found to be lower (9) for branched PE than for linear PE, which emphasizes the importance of CMO in the thermodynamics of mixing. In the later experiments, a globular solvent is a better solvent for the branched PE since the branched PE melt contains fewer CMO to be destroyed through the mixing than does the linear PE. The ability of PE melt and PE solutions to keep CMO at high temperature may appear surprising but compares well with the stability of CMO in other systems. CMO have been shown to be (10) a function of the degree of thermal expansion which can be calculated to be the same for PE at 170°C as for n-C_{16} at 50°C. Since n-C_{16} loses its order at 50°C, the CMO in PE are likely to remain until 170°C (7b). The fact that PE solutions have LCST's which are much lower than those of the other polyolefins, particularly in branched volatile alkanes, means that PE may be conveniently detected in mixtures by using the LCST method.

The abbreviation EP-S-62 will be used for the ethylene-propylene statistical copolymer containing 62 mole percent of PE. The same abbreviation, with B instead of S, will serve for the corresponding block copolymer.

EXPERIMENTAL

The LCST determinations were made as in *Ref. 7*. The turbidity measurements are described below.

Turbidity Measurements

The glass tube containing the solution to be studied was sealed and placed in an oven whose temperature was slowly increased (0.5 to 1.5 degree per minute). A beam of light was directed on a photoelectric cell after its passage through the solution. When a solution is undergoing a critical state, its turbidity increases in a dramatic way as can be seen visually. At the same time, the light transmitted through the solution decreases. The signal from the photocell and that from a thermocouple placed in the oven were fed respectively to the Y and X galvanometers of an X-Y recorder. The variation with temperature of the light transmitted by a polymeric solution is related to the thermodynamic states of this solution and is called a thermogram. *Figure 1* is a typical thermogram of a binary polymer mixture (EP-S-62) + 2,4-dimethylpentane (2,4 DMP)). The sharp increase of turbidity at T_c which is read as a decrease in transmitted light, defines the LCST. The integrated value of the turbidity, brought about by the phase separation is related to the ratio ξ:

$$\xi = \text{area (abca)/area } (a\, T_cT'_cca)$$

Below T_c the mixture is homogenous while above T'_c there are two phases in the tube. The concentrated phase which usually falls at the bottom of the tube has, at T'_c, a volume about ten times smaller than that of the dilute phase for the range of concentration studied.

BINARY SYSTEMS

LCST and Polymer Concentration

Figure 2 gives an example of the variation with ϕ_2 (ϕ_2 being the total polymer volume fraction) of the phase separation temperature, T_c, for the system EP-S-62 + 2,4-DMP. The temperature of the minimum in the $T_c(\phi_2)$ curve, in this case 155°C for $\phi_2 = 0.020$, is taken to be the LCST for the system. Each point in *Fig. 3*, for instance, is the minimum temperature of curves similar to that of *Fig. 2*. However, in order to avoid defining another term, the term LCST (or T_c) has been used in this work for the temperature of phase separation, as in *Fig. 1*, even if is not the temperature of the minimum of the $T_c(\phi_2)$ curve. Analysis of the turbidity curves, similar to that of *Fig. 1*, permitted the correlation of the turbidity with polymer concentration as shown in the bottom curve where $\ln(1-\xi)$ is plotted against the amount m_p of the polymer in the solution. (A similar correlation can be obtained using the volume fraction of the precipitating polymer instead of m_p).

Dependence of the LCST on Molecular Weight

The effect of molecular weight similar at both the LCST and the upper critical solution temperature (UCST) or θ temperature. The LCST of smaller molecular weight polymers is higher because they are more soluble. The Flory-Huggins theory pre-

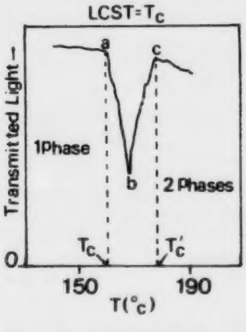

Fig. 1. *Typical thermogram of a binary polymer solution: EP-S-62 + 2,4 DMP, at $\phi_2 = 0.03$ and heating rate 0.5° per minute. The integrated value of the turbidity brought about by the phase separation is related to the ratio ξ = area (abca)/area ($aT_cT'_cca$).*

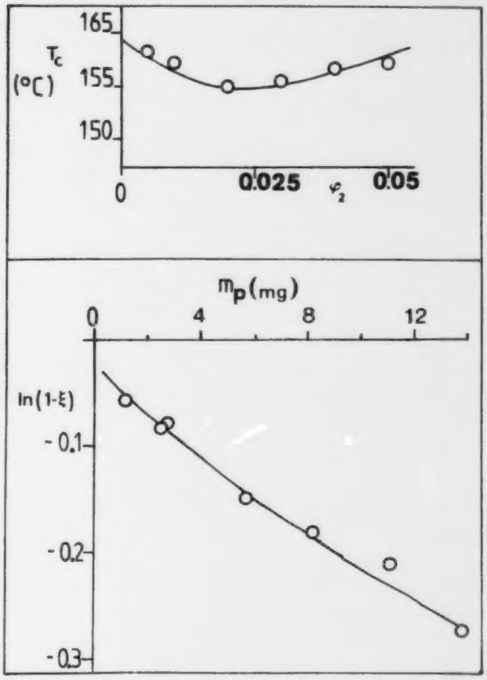

Fig. 2. Dependence of the T_c and the turbidity on polymer concentration: ϕ_2. The minimum of the upper curve temperature, 155°C, is the value reported as the LCST for this system. The integrated turbidity, ln $(1 - \xi)$ is plotted against m_p instead of ϕ_2 as explained in the text.

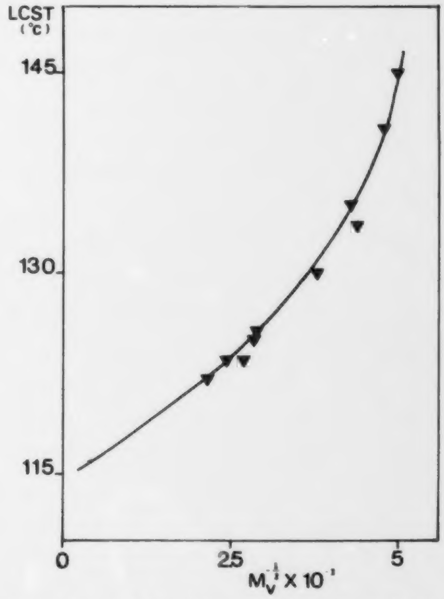

Fig. 3. Dependence of the LCST on molecular weight (M_v). The LCST of ten polyethylene samples (d = 0.96) in 2,2-dimethylpentane are plotted against $M_v^{-1/2}$. The LCST for M infinite is found to be 115°C for this system.

dicts T^{-1} (UCST) to be proportional to $M^{-1/2}$. Since the χ parameter, near the LCST, increases with T while it decreases with T at the UCST, T rather than T^{-1} should be used to correlate the LCST with $M^{-1/2}$. Over a small temperature interval, however, the $T^{-1}(M^{-1/2})$ or $T(M^{-1/2})$ correlations are equally valid. *Figure 3* presents the LCST, in 2,2-dimethylpentane, for ten PE samples (d = 0.96) whose molecular weights vary between 44,000 and 213,000. The LCST extrapolated to infinite molecular weight $(\mathrm{LCST})_\infty$ is found to be 115°C for this system. The M_v have been obtained from the intrinsic viscosity $[\eta]$ in decalin at 135°C and the relation (11): $[\eta](dl \cdot g^{-1}) = 67.7\ 10^{-5}\ M^{0.67}$.

Dependence of the LCST on Polymer Composition

The LCST were obtained for 2,2-dimethylpentane solutions of seven polymer samples having very similar molecular weights (around 200,000). Two are the pure PE and PP and five are statistical ethylene-propylene copolymers of different ethylene contents.

In *Fig. 4*, the LCST have been plotted against the sample ethylene content. One can visualize the large difference in LCST between PE and PP and also the almost linear dependence of the LCST on the polymer chemical composition. Because of these features, LCST determination can be a rapid method for analyzing the ethylene content of a statistical copolymer.

Thermogram Shape and Sample Polydispersity

Since the low molecular weight chains have a higher LCST, their presence in a sample will presumably spread the temperature interval during which phase separation occurs. This effect is discussed elsewhere (8), using analysis of LCST thermograms of polyisobutylene and polystyrene of various polydispersities.

Comparison of EP Block and Statistical Copolymers

The thermodynamic properties of a copolymer in solution depend not only on the mean ethylene

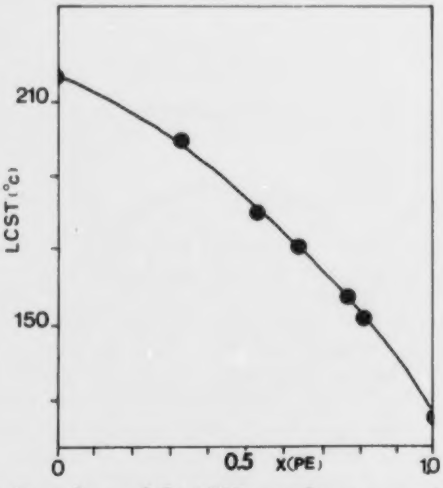

Fig. 4. Dependence of the LCST on polymer composition for random copolymers. Due to the large difference in the LCST of the two homopolymers in 2,2 DMP, the ethylene content of an EP statistical copolymer can be obtained with good accuracy by LCST determination. (Taken from Ref. 7).

content of the chain but also on the length of the PE or PP sequences. This effect can be seen to its maximum by comparing the LCST of block and random copolymers of the same molar content of ethylene. The long ethylene sequences of the block copolymers will allow more correlations of orientations to be formed than in its statistical counterpart and will thus lower the LCST. The thermograms in *Fig. 5* show that the LCST of a block copolymer is 30° lower than that of the statistical sample of about the same ethylene content (40 *vs.* 33 percent). The thermogram also indicates a larger polydispersity in the block copolymer.

TERNARY SYSTEMS

Ternary Systems: One Polymer and Two Solvents

A mixture of two liquids behaves as one liquid whose free volume is intermediate between those of the pure liquids. As shown in *Fig. 6*, the LCST of a PIB sample ($M_v = 1.4\ 10^6$) in a mixture of two heptanes depends linearly on the solvent composition. The higher solvent quality of n-C_7 compared to 2,4-dimethylpentane is partly due to its lower expansion coefficient and partly to its molecular shape. Discussion of the effect on the LCST of the expansion coefficient, the molecular shape, and the number of gauche conformations of the solvent are presented in *Ref. 7*.

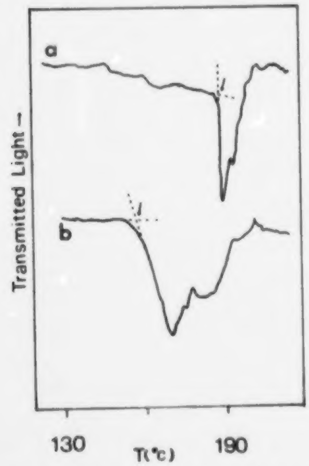

Fig. 5. Comparison of the LCST of a random (EP-S-33) (curve a) and a block (EP-B-40) (curve b) copolymer in 2,4-dimethylpentane.

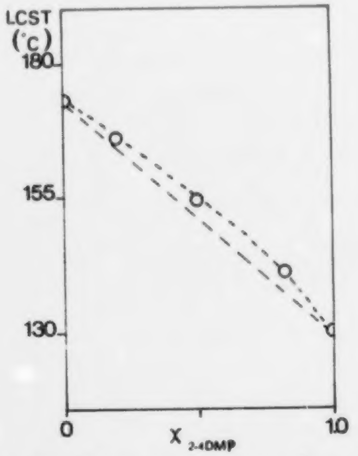

Fig. 6. The LCST of a ternary mixture: one polymer + 2 solvents: The LCST of this PIB sample ($M_v = 1.4\ 10^6$) in n-heptane + 2,4 DMNP is seen to depend linearly on the solvent composition.

Ternary Systems: Two Polymers and One Solvent

Several ternary systems with different combinations of PE, PP statistical and block copolymers of different ethylene content have been studied in 2,4-DMP. From the thermograms and from visual observations of the phases, the following general features of the ternary systems can be drawn:

1. Two T_c's can be seen on the thermogram.
2. The two T_c's of the ternary mixture are very close to those obtained in the binary mixtures.
3. The two concentrated phases formed respectively at T_c (A) and T_c (B) may remain distinct at $T > T_c$ (B) resulting in a three phase system, or mix with time resulting in a two phase system depending on the nature of A and B.

The thermograms given here are for three ternary systems:

1. PE + PP with $X(\mathrm{PE}) = m_{\mathrm{PE}}[m_{\mathrm{PE}} + m_{\mathrm{PP}}]^{-1} = 0.4$
2. EP-S-62 + PP with $X = 0.5$
3. EP-S-62 + PE with $X = 0.5$

Figure 7 gives the thermogram of the ternary mixture of PE, PP ($X(\mathrm{PE}) = 0.4$) and 2,4 DMP at $\phi_2 = 0.03$ (curve a). The T_c of PP is the same as in a binary mixture but that of PE is lowered by 10°. The thermogram of the same PE (Marlex) in a binary solution is given for comparison (curve b). The narrow PP peak is typical and occurs in binary and ternary mixtures in the heptanes.

The following systems have been selected because the difference in T_c of the pure polymers is smaller than that for the previous mixture of PE + PP. In *Fig. 8*, EP-S-62 is mixed ($X = 0.5$) with PE (curve a). Although the two turbidity curves overlap, the presence of two distinct polymers in the mixture is shown clearly by the thermogram. The turbidity curves will overlap less using PE of smaller polydispersity whose thermogram is narrower. In

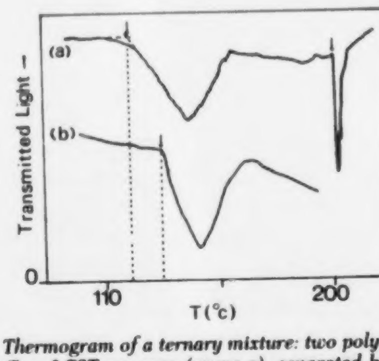

Fig. 7. Thermogram of a ternary mixture: two polymers and one solvent. Two LCST are seen (curve a), separated by 82° on this thermogram of a mixture of PE and PP (X = 0.4) in 2,4 DMP at $\phi_2 = 0.03$. The thermogram for the same PE sample in 2,4-DMP is shown for comparison (curve b).

curve b, PP has been mixed ($X = 0.5$) with the same copolymer. The LCST of the polymer forming a separate phase is not altered by the presence of the other polymer. For PP, this result may indicate that, at T_c for PP, the solution contains verylittle PE. At T_c for PE, this effect could be related to a partial compatibility between the copolymer and PE which is diminished in PP + PE mixtures. Investigation of these thermodynamic differences in being pursued currently. Note also that the interval between the T_c and T_c' for the copolymer is larger in the ternary than in a binary solution (*Fig. 1*).

A general picture of the PE and PP LCST behavior in binary and ternary mixtures is given in *Fig. 9* where the T_c are plotted against the ethylene composition of the mixture. The two curves in the middle part of the diagram correspond to the LCST of binary solutions, either of a block copolymer (■) or of a random copolymer (★). Obviously, one LCST is recorded for these systems. The LCST for the block copolymers are consistently lower than for the random ones. The two curves at the lower and upper part of the diagram depict the position of the two LCST in a ternary system made by mixing different amounts of PE and PP. The LCST of PP in the ternary mixtures are about the same as in the binary solution (point at $X(\mathrm{PE}) = 0$). On the other hand, the LCST of PE are about 10°C lower than for the pure PE solution (point at $X(\mathrm{PE}) = 1.0$).

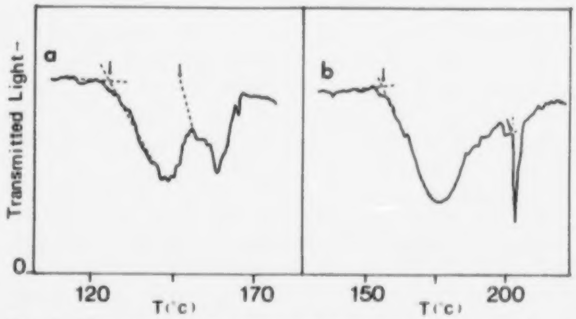

Fig. 8. Thermogram of a ternary mixture: two polymers and one solvent (2,4 DMP). Curve a: PE + EP-S-62. Curve b: PP + EP-S-62.

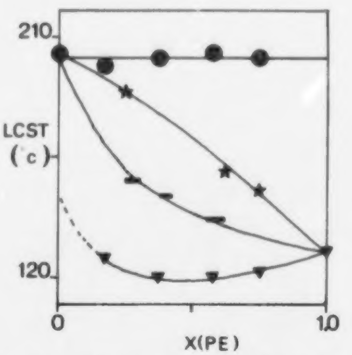

Fig. 9. LCST and copolymer composition: LCST in 2,4-DMP of PP, PE, block (■) and statistical (☆) copolymers and PP + PE mixtures plotted against the average ethylene content of the polymers. The binary mixtures (■, ☆) have one LCST while the ternary systems show the PE (▼) and PP (●) LCST.

Analysis of a Block Copolymer with a Low Ethylene Content

The T_c of the block copolymers of low ethylene content have not been reported in *Fig. 9* due to the complexity of their composition. *Figure 10* shows a thermogram of a PE block copolymer with a nominal ethylene content of 15 percent. Apart from the large polydispersity of the sample, the thermogram shows a distinct T_c at the temperature of PP. The proper T_c for the copolymer is not easy to locate but is probably at 170°C. By adding a small amount (m_p) of PP to the mixture and by correlating the values of ξ with m_p, the amount of PP has been estimated to be 15 percent. The change of turbidity at the T_c of PE also reveals the presence of PE in the sample. It is interesting to note that a small amount of PE is probably sufficient to lower the first temperature where turbidity changes. From its thermogram, (curve b) the (EP-B-63) appears to also contain polymeric impurities (PP).

Polymer Compatibility at the LCST in Semi-Concentrated Solutions

In a ternary solution whose thermogram shows two turbidity peaks, visual observation of the tube content above the higher T_c, T_{c2}, indicates the presence of three separate phases corresponding respectively to the concentrated solution of polymer 1 formed at $T_{c,1}$, that of polymer 2 formed at $T_{c,2}$ and the dilute solution. After a few hours at $T_{c,2}$ only two phases remain when the initial solution is

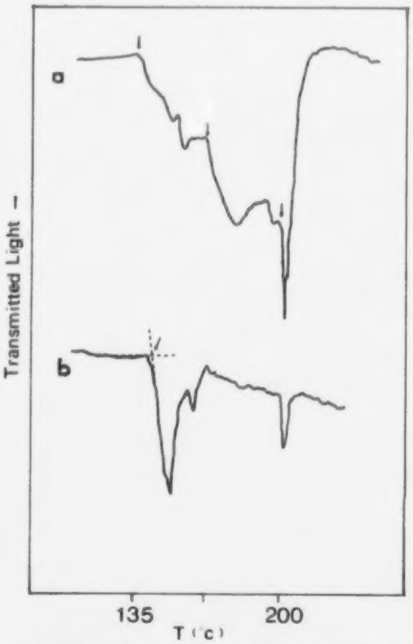

Fig. 10. Thermogram of a block copolymer a (EP-B-15) in 2,4-DMP (without polymeric addition). The changes of turbidity at the LCST of PE and PP (↓) indicate the presence of these homopolymers in the sample. From its thermogram (curve b), the copolymer (EP-B-58) is less heterogeneous but contains some PP as well.

made with PP and EP-S-62. On the other hand, the incompatibility of PP and PE in semi-concentrated solution persists above 210°C since three phases are observed indefinitely at this temperature.

The assumption behind any quantitative interpretation of the thermograms is that the turbidity at each temperature is a function of the amount of the polymer, of a given molecular weight, involved in the phase separation at the temperature of observation. The thermogram of PE (Marlex) shown in *Fig. 7* (curve b) is quite symmetrical and may indeed reflect the molecular weight distribution of this sample. However, the lack of symmetry of the turbidity-temperature curves of *Fig. 5* (curves a and b) suggests a non-equilibrium value of the turbidity. Any quantitative comparison of thermograms with a molecular weight distribution curve such as is given by gel permeation chromatography should be attempted on thermograms obtained at a much lower heating rate, particularly when the molecular weight distribution is expected to be narrow. The LCST method presented here should be particularly useful for characterizing polymer mixtures since the chemical nature of the polymer and not its molecular weight only determine the value of the LCST. The prospect of polydispersity evaluation, if confirmed, is particularly attractive for crystalline polymers whose characterization by other methods requires expensive equipment. The rapidity and simplicity of the method makes it well adapted for small laboratories or production units.

ACKNOWLEDGEMENTS

We would like to thank J. Chauvette (Hercules Canada, Varennes P.Q.), L. Utracki (IMRI, Montréal), and Du Pont of Canada for the gifts of polymer samples. The salary of S. V. was supported by the Canadian Department of Manpower.

REFERENCES

1. Freeman, P. I. and Rowlinson, J. S., *Polymer*, **1**, 20 (1960).
2. a) Delmas, G., Patterson D., and Somcynsky, T., *Polym. Sci.*, **57**, 79 (1962).
   b) Patterson, D., Delmas, G., and Somcynsky, T., *Polymer*, **8**, 503 (1966).
   c) Bardin, J. M. and Patterson, D., *Polymer*, **10**, 247 (1969).
3. De Saint-Romain, P. and Delmas, G., *Eur. Polymer, J.*, **10**, 1133 (1974).
4. Hamada, F., Fujisawa, K., and Hakajima A., *Polymer J.*, **4**, 316 (1973).
5. Hamada, F., Shiomi, T., Fujisawa K., and Nakajina, A., *Macromolecules*, **13**, 729 (1980).
6. Prigogine, I., with the collaboration of Mathot, V. and Bellemans, A. "The Molecular Theory of Solutions", *North Holland Publishing Co.* Amsterdam (1957).
7. a) Charlet, G. and Delmas, G., *Polymer*, **22**, 1181 (1981).
   b) Charlet, G., Ducasse, R., and Delmas, G., *Polymer*, **22**, 1190 (1981).
8. Varennes, S., Charlet, G., and Delmas, G., to be published.
9. Schreiber, H. P., Tewari, Y. B., and Patterson, D., *J. Polym. Sci., Polym. Phys. Ed.*, **11**, 15 (1973).
10. Croucher, M.D., and Patterson, D., *J. Chem. Soc. Faraday Trans. II*, **20**, 1479 (1974).
11. J. Brandrup and E. H. Immergut, "Polymer Handbook," Wiley, New York (1975).

DISCUSSION

A Winnik: I compliment you for showing us the richness of information that you can get from what looks like a relatively simple technique. I want to ask you how reproducible are the traces that you get. I am also concerned about the interpretation of the area parameter, ξ. In my mind, it seems that this is a kinetic parameter, related to the size of the phases that are separated and to the kinetic of phase separation.

J. Ottino: Extrapolation to zero heating rate could indeed give valuable information for these thermodynamic measurements.

G. Delmas-Patterson: Using the same heating rates and the same cell geometry, the thermograms are reproducible. The assumption behind the interpretation of the thermograms is that the scattered light is a function of the amount, m_p, of polymer participating in the formation of the concentrated phase in equilibrium with the dilute phase at a given temperature. If the phase separation is produced at quasi constant temperature, using small temperature increments, ΔT_i, the turbidity peaks are spread over only short times (of the order of minutes, and variable with ΔT_i) suggesting fast equilibrium:

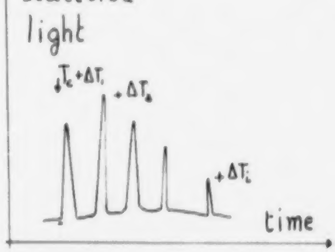

The comparison of the total area, ξ, of turbidity obtained in isothermal conditions with that of the thermograms will indeed help to differentiate between kinetic and equilibrium effects.
On the other hand, if the previous assumption is too simplistic, the method can be useful in a semi-quantitative way to separate mixtures of polymer and copolymers whose characterization by other methods (IR, GPC, DSC) is difficult or too onerous for a small laboratory.

L. A. Utracki: I understand that you can distinguish the structure of polyethylenes by this technique. The thermogram is different for linear low density than for high density or low density.

G. Delmas-Patterson: The polyethylenes (PE) of high and low density give indeed different LCST-M_v relationships in volatile solvents. To characterize the linear low density PE (LLDPE), the LCST can also be used, either by establishing correlations similar to that of *Fig. 3* (LCST, M_v) or of *Fig. 4* (LCST, composition). However, if the parent homopolymer were present, even in traces, in LLDPE, it would be seen on the thermogram and so characterize the LLPDE.

Block Polymers. Characterization and Use in Polymer Blends

S. BYWATER

Chemistry Division
National Research Council of Canada
Ottawa, Canada
K1A 0R9

Polymer blends, because of the well-known immiscibility of polymers, generally show phase separation. Block polymers can be considered as simple models of two-phase systems. Because unlike segments are connected by covalent bonds, the phase separation is on a smaller scale and takes rather unusual forms. The types of block polymers of commercial importance are described with a consideration of the morphologies which result from particular compositions. Their use as solubilizing agents to increase the compatibility of the corresponding homopolymers is also discussed.

INTRODUCTION

Block polymers, i.e. those copolymers which contain relatively long segments of homopolymer joined at one or more junction points to other homopolymers may be considered as "microcomposites" (1). The typical phase separation observed in composite materials can be observed, albeit in sub-microscopic form. As well, block polymers can be used to form more conventional composite materials when blended with one or more homopolymers (2). There is now extensive literature on these materials; the most recent book on the subject (3) contains several thousand references. The present article can therefore only describe the most commonly used block polymer systems.

PREPARATION

These polymers can be divided (somewhat arbitrarily) into four types A-B, A-B-A, A-B-C, and (A-B)$_n$ types where A represents a sequence A-A-A-A-A of identical monomer units, and similarly for B,C. (A-B)$_n$X are radial block polymers with n di-block sequences coupled to a central X unit. All the classical methods of homopolymerization, free radical, cationic, anionic, Ziegler, and condensation types have been used to prepare some types of block polymers. A concise review of these methods is available (4). Most of them are not really suitable for the production of block polymers in any reasonable degree of purity. The presence of chain tranfer and/or termination processes in free radical, cationic or Ziegler systems will inevitably result in products which are mixtures. In principle, only the anionic and condensation mechanisms will produce the required high yields of block polymer. These systems are, in fact, the ones used commercially to produce block polymers. The former method is normally used to produce A-B, A-B-A, and (A-B)$_n$X types and although in principle it can be used to prepare (A-B)$_n$ types, the latter method is normally used to produce them. In fact, it is claimed (5) that the first thermoplastic elastomer developed was a segmented polyurethane of the latter type. Such linear multiblock polymers are commonly prepared by reacting a preformed di-hydroxy terminated rubbery polymer of molecular weight in the 1000 to 3000 range (commonly a polyester or polyether) with a di-isocyanate and a low molecular weight chain extender (usually a diol). The rubbery prepolymer forms the soft phase and the polyurethane segments the hard (crystalline) phase, i.e. structures of the type:

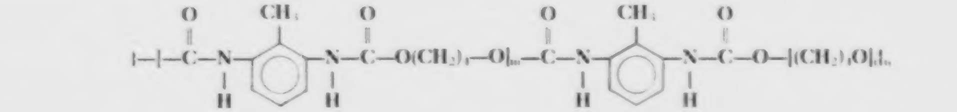

are formed. Materials of similar structure can also be prepared from polyesters, for example by trans esterification of dimethylterephthalate, butanediol, and poly(tetramethylene ether) glycol (hydroxyl terminated poly THF) to give:

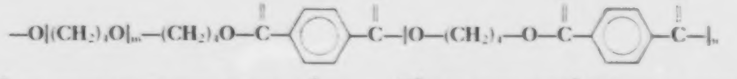

These two syntheses are essentially modifications of normal polycondensations but involving as one component a low molecular weight prepolymer to provide the soft (rubbery) matrix. Block lengths are short, and this factor, together with inevitable polydispersity in block lengths, results in relatively poorly-defined morphology.

Undoubtedly, the most versatile method of preparation involves anionic polymerization. The absence of termination or transfer processes with nonpolar monomers enables, in principle, the preparation of products with near-monodisperse blocks and hence well-defined morphology. Commercial production of styrene-diene materials by this method accounts for the remaining source of industrial block polymers. In practice, due to the extreme sensitivity of the systems to moisture, oxygen and carbon dioxide, many samples contain impurities (e.g. in tri-block polymers, some di-block material and homopolymer (5)). Polar monomers often undergo unwanted side reactions although ethylene oxide, methyl methacrylate, vinyl pyridine, and the siloxanes have been used to form two-block material with suitable precautions if necessary. Three-block polymers are more difficult to produce (6) because the anion-pairs of polar monomers will not add styrene or diene monomers. Even with diene monomers their anion-pairs only add styrene relatively slowly which results in some polydispersity in the final block of S-B-S or S-I-S polymers. (S = styrene, B = butadiene, I = isoprene.) The formation of two-block material followed by coupling can be used to circumvent problems of this type. It can be carried out on the active system itself or after conversion of the active centers to suitable functional groups. Difunctional initiators offer another solution although hydrocarbon soluble systems necessary for retention of the desirable 1,4 structure in polydienes still appear to have problems (7, 8). If one of the components is totally unsuited to anionic polymerization, e.g. ethylene, other methods are available (6). Simple hydrogenation of polydiene containing polymers produces polyolefinic blocks. More generally, methods have been developed (9) to transform anion-pairs into groups which will initiate, or act as co-catalysts for subsequent radical, cationic or Ziegler polymerization. Together with the above described post-procedures, anionic polymerization provides a powerful tool for block polymer preparation.

CHARACTERIZATION

For well-defined block polymers, contamination of the product by homopolymer or material having a different number of blocks can be determined by gel-permeation chromatography (5) or by density gradient ultracentrifugation (10). Molecular weights can be determined by osmotic pressure measurement. They are, of course, number average values but can be considered representative for anionically prepared samples where the polydispersity is not large. Weight average molecular weights can be determined using light scattering techniques. Again, these will be essentially correct for well-defined polymers; only if compositional heterogeneity occurs will the results be in error (11). Gel-permeation chromatography is probably the most widely used technique for molecular weight determination. The so-called "universal calibration" method (12) which involves plotting log $[\eta]\cdot M$ *vs.* elution volume appears to work well for block polymers. An alternative method (13), based on the suggestion that the logarithm of the molecular weight is given by the weighted average of the molecular weights of the homopolymers having the same elution volume, supposes that the hydrodynamic volumes of the sequences are additive (14). This is a reasonable approximation for styrene-diene block polymers (15) in good solvents for each block and hence only small differences are observed in measured molecular weights between the two methods (16). The approximation is not necessarily always correct; some deviations have been observed in styrene-siloxane block polymers (17), so that caution is required in the application of this method.

MORPHOLOGY

The homopolymers comprising the blocks of virtually all block polymers are incompatible so that phase separation will occur in solid samples and even in moderately concentrated solutions, except possibly for very low molecular weight polymers. As the constituent blocks are connected, this phase separation must take rather special forms. For styrene-diene block polymers, the morphology and its variation with composition have been amply described in numerous publications (18). Spheres of the minor component are formed in a matrix of the major component when its volume fraction is low, followed at higher volume fractions by rods of the minor component until finally at roughly equal composition alternate lamellae are found (*Fig. 1*). Morphology is often determined on thin, solvent cast films preferentially stained by OsO_4. Structures close to the above equilibrium morphology are obtained by slow evaporation of a dilute solution in a good solvent for both components (19). Faster evaporation leads to less well-defined structures, and selective solvents result in unrepresentative morphology. Annealing of the samples is useful in order to obtain the characteristic morphology and also to increase the grain size. Some difficulties can occur in differentiation between spherical and cylindrical morphology by examination of thin films in the electron microscope (20). These can be ob-

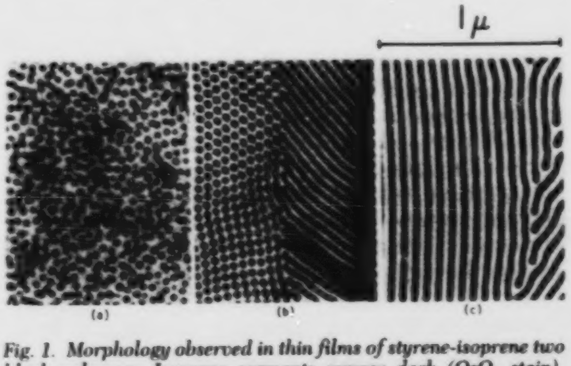

Fig. 1. Morphology observed in thin films of styrene-isoprene two block polymers. Isoprene segments appear dark (OsO_4 stain). Polymer composition a) 22 percent, b) 35 percent, c) 42 percent isoprene, Ref. 18.

viated by sectioning the material in two perpendicular directions, or indeed by use of small angle X-ray scattering techniques. Extrusion of bulk material gives even better ordered oriented structures approaching a pseudo single crystal type (21). Similar results can be obtained with an apparatus which subjects a sheet to numerous shearing movements above T_g of the hard domains (22).

The domain sizes increase with increasing molecular weight of the corresponding block, as would be expected.

Most block polymers have total molecular weights in the range 10^4 to 10^5 which produces domains in the size range of 10 to 50 nm. They are therefore optically transparent. At molecular weights ~10^6, however, domain sizes become large enough to be an appreciable fraction of the wavelength of visible light. Interference effects then produce iridescent colors in block polymer films and solutions (23, 24).

Theoretical treatments of block polymer morphology are well developed (25–29). They predict, at least semiquantitatively, the changes in morphology with composition and variation of domain size with molecular weight. Basically, three important structure-determining factors must be taken into account. First, there is an entropy loss caused by the restriction of the junction points to the interfacial region. Secondly, this concentration of link points causes a further entropy loss because to maintain a uniform density in the domains, the polymer chains must stretch, and so cannot retain their (smaller) unperturbed end-to-end distances. Both of these factors increase the free energy as domain size increases. The third factor concerns the repulsive energy of unlike segments constrained to be in the interfacial region. This causes a decrease in free energy at larger domain sizes, since larger domains produce a lower surface area per unit volume. A minimum exists, therefore, in the free energy at a certain domain size which depends on the particular morphology. Spherical morphology has the lowest energy minimum at the most extreme compositions, followed by rod-like domains in the intermediate region and lamellae at near equal compositions. Domain sizes are predicted to vary at about the two thirds power of molecular weight (*Fig. 2*), with an interfacial thickness of the order of 1.5 to 3 nm not greatly dependent on molecular weight. In general, the experimental results are in reasonable agreement with theory for lamellar morphology (18, 30) both in regard to domain size and interfacial thickness (~2 nm). Where spherical domains occur, the agreement is less good (18, 31). Smaller than expected polyisoprene spheres were found in solvent cast films of styrene-isoprene two block polymers. It was emphasized that with this morphology, equilibration during solvent evaporation requires transport of chains through the matrix which may have a reasonably large energy barrier. Whether annealing would correct this discrepancy is not clear. The effect of various heat treatments on a similar polymer has been reported (32). Little change in sphere diameter was found but sharper interfaces were observed (down to ~0.75 nm) on slow cooling from 140°C. In this case, the matrix was polyisoprene containing spherical polystyrene domains which may be a more favorable case for the diffusion process than is the reversed morphology.

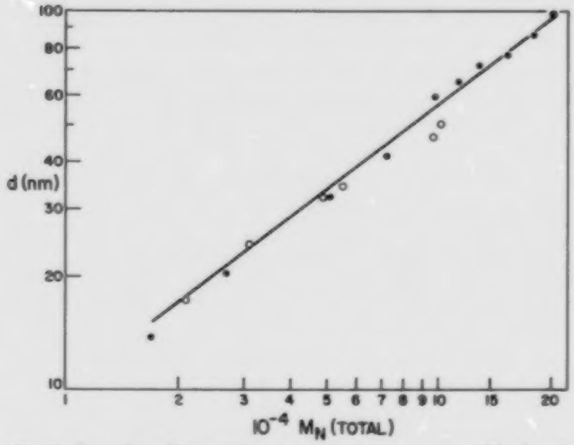

Fig. 2. Inter-lamellar spacing in styrene-isoprene two block polymers as a function of total molecular weight ○ ref. 30, ● Hadziioannu, thesis Strasbourg 1980. slope = 0.75.

The morphology of $(A\text{-}B)_n$ multi-block polymers of the styrene-diene type appears not to have been described. Only that of segmented polyurethanes and polyesters has received attention. Tobolsky, in a comparison of viscoelastic properties of segmented polyurethanes with those of S-B-S block copolymers, was first to suggest that the former must have a similar two phase morphology (33). Electron microscopy of preferentially stained sections confirmed this hypothesis (34). The morphology resembled that of styrene-diene block polymers of poorly developed and smaller domain structure with no long-range order. The existence of crystallizability offers a further degree of complexity to the morphology. Whereas the small domains described above are presumably crystallites of the hard segments, upon suitable sample treatment a spherulitic superstructure can be developed (35, 36). The morphology of these materials is therefore not well-defined, depends strongly on specimen preparation, and probably on the two segment types as discussed below.

The presence of two phases implies the occurrence of two glass transition temperatures as well as melting transitions in crystallizable materials. A number of transitions have been observed in multiblock segmented polyesters and polyurethanes (37). Depending on the composition and segment type, T_g's of soft and hard segments may be observed together with crystal melting endotherms. In addition, endotherms attributed to the disruption of ordered non-crystalline segments can appear whose temperature depends on sample pre-treatment (38). Soft segment crystallinity is suppressed at shorter segment lengths and at higher proportions of hard segment. Evidence exists in some cases for the presence of hard segments in the soft phase in segmented polyurethanes as shown by a soft phase T_g which increases with higher proportions of hard segments. Better separation gives a constant T_g approaching that of the pure soft segment material. Mixing is favored by lower soft segment molecular weights and seems more evident with polyester than with polyether segments (37). Corresponding measurements on a polyether-polyester segmented copolymer (39) indicate that the amorphous phase consists of mixed polyether and polyester segments together with a crystalline polyester phase.

Anionically-prepared two and three block polymers have better defined morphologies and, in most cases, are amorphous so their transition behavior is limited to two T_g's. For styrene-siloxane block polymers, for example, the upper T_g is close to that of homopolystyrene but drops below this value at low block molecular weights (40, 41) (*Fig. 3*). The lower T_g remains essentially constant at ~150 K throughout the range close to the value expected for homopolydimethylsiloxane. This is a general phenomenon with styrene containing block polymers; the T_g of the hard phase is more sensitive to decreases in molecular weight than is that of the soft phase. Indeed, with some styrene-diene block polymers it appears that the styrene segment T_g never reaches that expected of high molecular weight homopolymer (42). Other samples show T_g's which approach the polystyrene value much more rapidly as molecular weight increases (43) (*Fig. 3*). The latter samples were of different composition (~70 percent styrene and hence with a polystyrene matrix) whereas the former contained only ~30 percent styrene so that polystyrene domains would be expected in a diene matrix. Sample composition may, therefore, be an important parameter. The sample pretreatments were, however, also different. In general, too little attention has been paid to these factors.

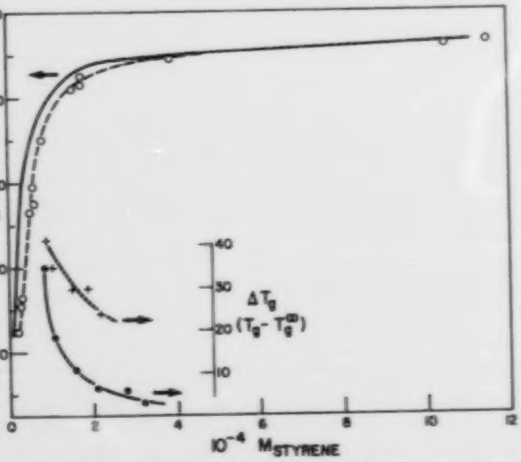

Fig. 3. T_g of the styrene segments in styrene-siloxane two block polymers as a function of their molecular weight. Full line T_g of homopolystyrene. (left axis) Ref. 41. ΔT_g of the styrene segments in; ● S-I-S block polymers (70 percent styrene segments), Ref. 43. + S-B-S block polymers (30 percent styrene segments), Ref. 42 (right axis).

The reason for the abnormal decrease of the T_g of the hard component at lower block molecular weights is not entirely understood. T_g's of homopolymers decrease at lower molecular weights, a phenomenon usually attributed to increased free volume of chain ends. The segments of block polymers have at most one free chain end so this factor does not explain the observed results. Some authors (44, 45) have attributed the effect to increasing amounts of a mixed phase at lower block molecular weights. Others (46–48) have suggested that although the linking points are not free chain ends, the higher mobility of the chains of the soft segment will induce prematurely molecular motions in the hard phase. Domain sizes in the low molecular weight region are, of course, quite small and the interfacial region, which should involve segment mixing, of roughly constant size, will become more important at low molecular weights. Until recently no evidence of transitions caused by a mixed phase could be detected. With a series of S-I-S tri-block polymers containing ~30 percent polyisoprene segments, however, the presence of a third intermediate transition was observed (43) in two polymers with polystyrene blocks of molecular weights of 8500 and 11,000. Above these molecular weights only the expected polyisoprene and polystyrene segment transitions were observed and below them only a single mixed transition. It is evident that further progress will require a more detailed investigation involving different sample pre-treatments and with samples of different morphology.

With block polymers of the lowest molecular weights (especially with styrene-diene block polymers, styrene-siloxane block polymers have segments which are much less compatible) only a single glass transition is observed at a temperature expected of a polymer mixture (43, 48, 49). The region of miscibility depends strongly on block polymer composition. Styrene-isoprene two block polymers containing equal weights of each component give evidence for two phases with block molecular weights as low as 1300. As the percentage of isoprene segments is decreased, however, increasingly high styrene segment molecular weights are required to produce a two phase system (*Fig. 4*). Unfortunately, there are no data available on block polymers having isoprene (or butadiene) segment molecular weights less than 20,000 and shorter styrene segments. Therefore, it is not yet possible to assess the degree of solubilization of short styrene segments in such block polymers. There is also some evidence that in two-block styrene-isoprene copolymers (48, 49) the lowering of T_g of the styrene blocks (in two phase systems) at a constant molecular weight increases as the molecular weight of the attached isoprene block decreases. Again the effect of composition cannot be neglected.

COMPATIBILIZATION

Block polymers have the potential to act as compatibilizers for one or both of their constituent homopolymers. Early work by Riess and co-workers (50, 51) showed that transparent films could be obtained in certain composition regions with polystyrene/polymethylmethacrylate or polystyrene/polyisoprene mixtures with the corresponding two-block polymers (*Fig.* 5). It was found that for best results block polymers of a 50/50 composition ratio were necessary and that the molecular weights of the homopolymers should be less than that of the corresponding blocks. Of course, the occurrence of transparent films does not mean that true compatibility has been achieved but simply that the domains are smaller than approximately one-fifth of the wavelength of visible light. As emphasized by Molau (52) the effect of block polymers in such systems is colloidal in nature.

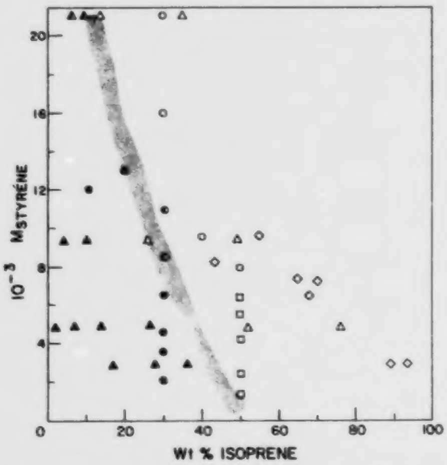

Fig. 4. Phase separation in styrene-isoprene two block polymers as a function of styrene segment molecular weight and composition. Open symbols, two phases. Closed symbols, one phase: ○, Ref. 43 (◒ intermediate mixed phase observed). □, Ref. 48. △, Ref. 49. ◇, styrene-butadiene three block polymers, Ref. 42. The hatched area indicates the boundary between one phase and two phase systems.

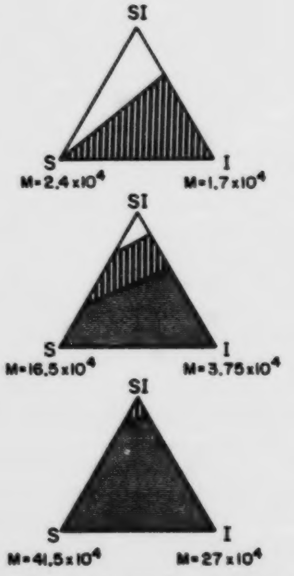

Fig. 5. Ternary diagrams of mixtures of polystyrene and polyisoprene and a two block styrene-isoprene copolymer ($M_N = 2 \times 10^5$, 44.4 percent polystyrene). Clear areas denote transparent films. Vertical hatching, slightly cloudy films. Horizontal hatching, opaque films, Ref. 51.

They provide finer dispersions of one phase in another as indicated by dissolution of a styrene-butadiene block polymer in styrene monomer followed by its subsequent polymerization. The spherical butadiene domains observed in the original block polymer were retained in size in the mixture but diluted in the polystyrene matrix. Addition of polybutadiene increased the domain size.

A more systematic study of films of various styrene-isoprene two block polymers (53) prepared in presence of the two homopolymers defined the morphologies more exactly. For block polymers having a morphology consisting of spherical isoprene domains in a styrene matrix, addition of the homopolymers in the same ratio as in the block polymer produced increased domain sizes and dispersion but retained the original basic structure even though the polystyrene was somewhat higher in molecular weight than the styrene blocks. Addition of homopolymers to a block polymer having a lamellar morphology was more disruptive of domain structure particularly when polybutadiene was added (*Fig. 6A*). Block polymers having a high isoprene content and hence normally showing a domain structure of styrene segment spheres in an isoprene segment matrix showed similar behavior to the first case except when the homopolystyrene added was of higher molecular weight, in which case large spherical polystyrene domains were present in an unchanged block polymer phase (*Fig. 6B*). Higher molecular weight homopolyisoprene, however was simply absorbed into the matrix separating the styrene domains of the block polymer. The effects of homopolymer incorporation are therefore dependent on the structure of the block polymer, the relative molecular weights of homopolymer and the corresponding block, and whether the homopolymer is compatible with the matrix or the domains.

The presence of two distinct phases of one polymer in block polymer/homopolymer blends has also been demonstrated by dynamic mechanical spectroscopy (54, 55). The block polymers were tri-block S-B-S types containing about 30 percent styrene segments. Addition of high molecular weight polystyrene caused two polystyrene type transitions to occur, the one from the block component being as usual at lower temperature. A similar effect was produced by the addition of high molecular weight polybutadiene to the block polymer, where two low temperature polybutadiene type transitions were found. In this type of block polymer the continuous phase is composed of polybutadiene segments. The ability, observed in some cases, of the matrix material to take up a higher molecular weight homopolymer must therefore be restricted to two block systems where the constraints of connection of both chain ends to the other phase are not present. DSC and refractive index measurements of the styrene type T_g in blends of polystyrene and styrene-siloxane two block polymers (56) indicate that the polystyrene mixes with the styrene block phase whether or not the former has a molecular weight much higher or lower than that of the block styrene component. Only a single T_g was observed which, if taken from the refractive index measurements (slow cooling), was in the expected region for a mixture of molecular weights. The DSC measurements also gave a single T_g but either close to that expected of the styrene block or nearer to that of the homopolymer. The results from the refractive index measurements were considered to be closer to equilibrium conditions. The DSC measurements, which were carried out on samples previously cooled rather rapidly from above T_g, could indicate a two phase styrene system with one transition so broadened as to be invisible (56). Many of the block polymers used contained 86 to 88 percent styrene segments so that the matrix would consist of polystyrene. The rest had close to 50 percent so that a mixed styrene phase is not entirely unexpected.

The ability of block polymers to prevent phase separation on a gross scale, together with their tendency to locate at phase interphases and hence improve inter-phase adhesion, suggests they should be of value in the preparation of polymer blends of enhanced physical properties (57). Early experiments by Riess and co-workers attempted to define the conditions required to produce high impact materials from blends of styrene-isoprene two block polymers and the corresponding homopolymers. Morphology was estimated by phase contrast microscopy on thin sections. In general, blends showing a granularity 1 to 2 μm in size under the microscope gave the best results. Similar studies were carried out on blends of polystyrene with an S-B-S triblock polymer (2, 59) with electron microscopy of stained sections giving a better definition of the morphology. High molecular weight block polymers ($M \sim 250{,}000$) of approximately equal styrene and butadiene contents were found to give the highest impact resistance when added to the extent of ~25 percent. Electron microscopy of these samples showed elastomer rich domains of ~1 μm average diameter embedded in the polystyrene matrix. Block polymers of lower molecular weight produced smaller domains and lower impact strength. The morphology of the best samples bore a strong resemblence to that of standard high impact polystyrene.

Polyolefines comprise another class of polymers to which block polymers could be added to improve impact resistance or to facilitate blending with other polymers. The use of tri-block S-B-S polymers in improving impact resistance in polypropylene and polyethylene has been described (60). Neither component of the block polymer is compatible with

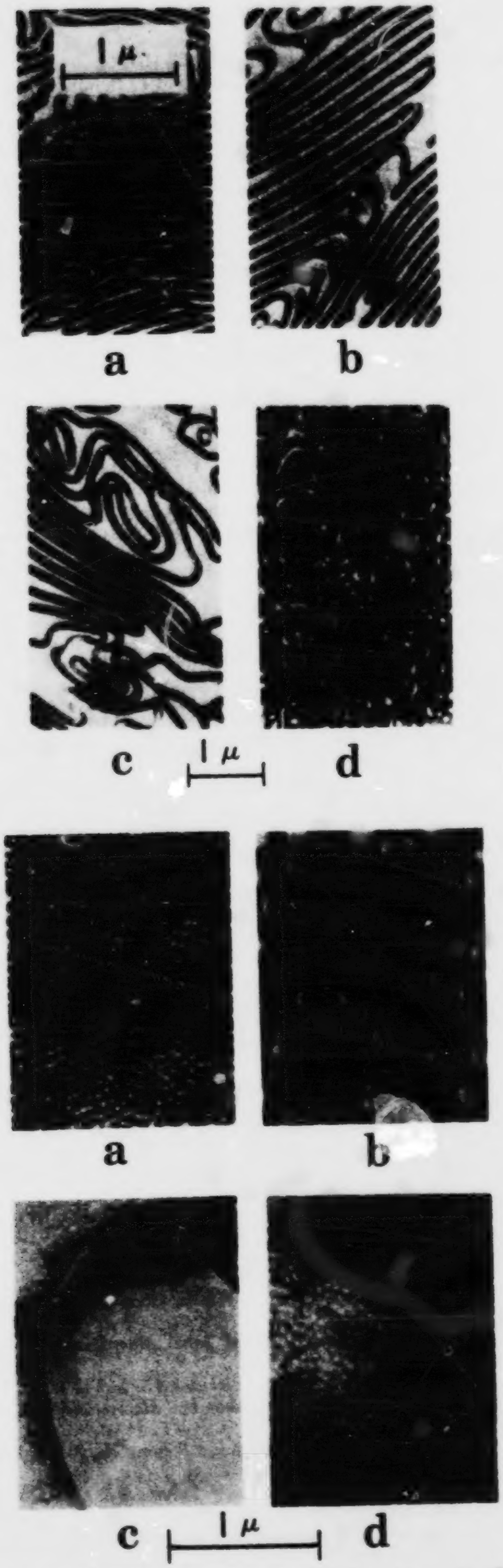

Fig. 6. Morphology observed in the electron microscope of thin films of a styrene-isoprene two block polymer mixed with polystyrene and polyisoprene (65).

A) 43/57 block ($M_S = 23 \times 10^4$, $M_I = 31 \times 10^4$). a) original, b) + 30 percent polystyrene ($M = 18 \times 10^4$), c) + 70 percent polystyrene ($M = 18 \times 10^4$), d) + 30 percent polyisoprene ($M = 40 \times 10^4$).

B) 18/82 block ($M_S = 5 \times 10^4$, $M_I = 22.7 \times 10^4$). a) original, b) + 20 percent polystyrene $M = 3.3 \times 10^4$, c) + 20 percent polystyrene ($M = 60 \times 10^4$), d) + 30 per cent polyisoprene ($M = 40 \times 10^4$).

polyolefines but low molecular weight S-B-S block polymers can apparently be blended successfully with them. Generally, however, the use of their hydrogenated counterparts has received most attention. The hydrogenation of styrene-butadiene block polymers yields blocks of what is essentially an ethylene-butene-1 copolymer since the usual polybutadiene microstructure is mostly 1,4 but does contain 10 to 15 percent vinyl units. These blocks might be more compatible with polyolefines.

Experiments on blending on a two roll mill, low density polyethylene and polystyrene in the presence of 9 percent two-block styrene-(ethylene-butene) (S-EB) polymers showed improved dispersion of the two polymers and its retention on subsequent compression molding (61, 62). Microscopic examination showed that polystyrene particles as small as 1 μm existed in the polyethylene rich region and a fine semicontinuous to continuous two phase structure in polystyrene rich blends. Two-block polymers were found to be more effective than three-block polymers. A "tapered" two-block polymer (in which some mixed sequences occur at the block center) was more effective than a pure two-block polymer of the same molecular weight. It was suggested that the tapered block polymer, because of its structure, stabilizes a diffuse interface between pure polyethylene and polystyrene phases, acting more as a solubilizing agent for the homopolymers than an anchoring agent. In all cases, however, enhanced strength was observed in the blends, particularly in the polystyrene rich composition region where the ductility was also improved.

High density polyethylene-polystyrene blends have also been studied in presence of such block polymers. The addition of 20 percent of a tri-block S-EB-S polymer to the polymer mixture converted brittle, cheesy blends to ductile materials but of lower modulus and yield strength (63). Better results appear to have been obtained with two block polymers (64) particularly at higher polystyrene content. Better dispersion was observed in presence of the block polymer together with higher strength and ductility than polystyrene itself. The number of variables in such systems (molecular weights of individual homopolymers, and the blocks, block polymer type, and blending techniques) is rather large so that a very systematic study will be required to delineate the best conditions for useful materials. The preliminary results do, however, suggest some promise for the use of block polymers in blends.

REFERENCES

1. S. L. Aggarwal, R. A. Livigni, L. F. Marker, and T. J. Dudek, "Block and Craft Copolymers", Ch. 9, Syracuse University Press, Syracuse, N.Y. (1973).
2. S. L. Aggarwal and R. A. Livigni, *Polym. Eng. Sci.*, **17**, 498 (1977).
3. A. Noshay and J. E. McGrath, "Block Copolymers-Overview and Critical Survey", Academic Press, New York (1977).
4. N. R. Legge, G. Holden, S. Davison, and H. E. DeLaMare, "Applied Polymer Science", Ch. 29, A.C.S. Organic Coatings, Plastics Chemistry Division, Washington D.C. (1975).
5. P. Dreyfuss and L. J. Fetters, *Rubber Chem. Technol.*, **153**, 728 (1980).
6. S. Bywater, *Prog. Polym. Sci.*, **4**, 27 (1974).
7. G. Beinert, P. Lutz, E. Franta, and P. Rempp, *Makromol. Chem.*, **179**, 551 (1978).
8. L. J. Fetters, C. W. Kamienski, R. C. Morrison, and R. N. Young, *Macromolecules*, **12**, 344 (1979).
9. D. H. Richards, *Br. Polym. J.*, **12**, 89 (1980).
10. J. Prudhomme and S. Bywater, "Block Polymers", p. 11, Plenum Press, New York (1970).
11. W. Bushuk and H. Benoit, *Can. J. Chem.*, **36**, 1616 (1958).
12. Z. Grubisic, P. Rempp, and H. Benoit, *J. Polym. Sci., Polym. Lett. Ed.*, **5**, 753 (1967).
13. L. H. Tung, *J. Appl. Polym. Sci.*, **13**, 2359 (1969).
14. N. Ho-Duc and J. Prud'homme, *Macromolecules*, **6**, 472 (1973).
15. J. Prud'homme, J. E. L. Roovers, and S. Bywater, *Eur. Polym. J.*, **8**, 901 (1972).
16. L. H. Tung, *J. Appl. Polym. Sci.*, **24**, 953 (1967).
17. J. G. Zilliox, J. E. L. Roovers, and S. Bywater, *Macromolecules*, **8**, 573 (1975).
18. T. Hashimoto, M. Shibayama, M. Fujimura, and H. Kawai, *Mem. Fac. Eng. Kyoto Univ.*, **43**, 184 (1981).
19. P. R. Lewis and C. Price, *Polymer*, **13**, 20 (1972).
20. E. Pedemonte, A. Turturro, U. Bianchi, and P. Devetta, *Polymer*, **14**, 145 (1973).
21. A. Keller, E. Pedemonte, and F. M. Willmouth, *Nature (London)*, **225**, 538 (1970).
22. G. Hadziioannou, A. Mathis, and A. Skoulios, *Colloid Polym. Sci.*, **257**, 136 (1979).
23. F. B. Bradford and E. Vanzo, *J. Polym. Sci. Part A1*, **6**, 1661 (1968).
24. S. Bywater and P. M. Toporowski, *Polymer*, **22**, 29 (1981).
25. D. J. Meier, *J. Polym. Sci. Part C*, **26**, 81 (1969).
26. D. J. Meier, *Am. Chem Soc. Div. Polym. Chem., Polym. Prepr.*, **11**, 400 (1970).
27. D. J. Meier, "Block and Graft Copolymers" Burke and Weiss, eds., Ch. 6, Syracuse University Press, Syracuse, N.Y. (1973).
28. E. Helfand, *Accts. Chem. Res.*, **8**, 295 (1975).
29. E. Helfand and Z. R. Wasserman, *Polym. Eng. Sci.*, **17**, 582 (1977).
30. T. Hashimoto, M. Shibayama, and H. Kawai, *Macromolecules*, **13**, 1237 (1980).
31. T. Hashimoto, M. Fujimura, and H. Kawai, *Macromolecules*, **13**, 1660 (1980).
32. U. Siemann and W. Ruland, *Colloid Polym. Sci.*, **260**, 999 (1982).
33. S. L. Cooper and A. V. Tobolsky, *Textile Res. J.*, **36**, 800 (1966).
34. J. A. Koutsky, N. V. Hien, and S. L. Cooper, *J. Polym. Sci. Part B*, **8**, 353 (1970).
35. M. Shen, U. Mehra, and M. Niinomi, *J. Appl. Phys.*, **45**, 4182 (1974).
36. Y-J. P. Chang and G. L. Wilkes, *J. Polym. Sci., Polym. Phys. Ed.*, **13**, 455 (1975).
37. J. W. C. Van Bogart, A. Lilaonitkul, and S. L. Cooper, *Adv. Chem. Ser.*, **176**, 3 (1979).
38. J. W. C. Van Bogart, D. A. Bluemke, and S. L. Cooper, *Polymer*, **22**, 1428 (1981).
39. A. Lilaonitkul, J. C. West, and S. L. Cooper, *J. Macromol. Sci. Part B*, **12**, 563 (1976).
40. S. Krause, M. Iskandar, and M. Iqbal, *Macromolecules*, **15**, 105 (1982).
41. Z. Lu and S. Krause, *Macromolecules*, **15**, 112 (1982).
42. S. Krause, Z. Lu, and M. Iskandar, *Macromolecules*, **15**, 1076 (1982).
43. G. C. Meyer and J. M. Widmaier, *J. Polym. Sci., Polym. Phys. Ed.*, **20**, 389 (1982).
44. G. Kraus and K. W. Rollmann, *J. Polym. Sci., Polym. Phys. Ed.*, **14**, 1133 (1976).
45. P. L. Kumler, S. E. Keinath, and R. F. Boyer, *Polym. Eng. Sci.*, **17**, 613 (1977).
46. U. Bianchi, E. Pedemonti, and A. Turturro, *Polymer*, **11**, 268 (1970).
47. G. E. Wardell, V. J. McBrierty, and D. C. Douglass, *J. Appl. Phys.*, **45**, 3341 (1974).

48. B. Morèse-Séguéla, M. St. Jacques, J. M. Renaud, and J. Prud'homme, *Macromolecules*, **13,** 100 (1980).
49. P. M. Toporowski and J. E. L. Roovers, *J. Polym. Sci., Polym. Chem. Ed.*, **14,** 2233 (1976).
50. G. Riess, J. Kohler, C. Tournut, and A. Banderet, *Makromol. Chem.*, **101,** 58 (1967).
51. J. Kohler, G. Riess, and A. Banderet, *Eur. Polym. J.*, **4,** 173 (1968).
52. G. E. Molau and W. M. Wittbrodt, *Macromolecules*, **1,** 260 (1968).
53. T. Inoue, T. Soen, T. Hashimoto, and H. Kawai, *Macromolecules*, **3,** 87 (1970).
54. L. Toy, M. Niinomi, and M. Shen, *J. Macromol. Sci. Phys.*, **11,** 281 (1975).
55. G. Kraus, "Polymer Blends", Ch. 18, Vol. 2 Academic Press, New York (1978).
56. Z. Lu, S. Krause, and M. Iskandar, *Macromolecules*, **15**, 367 (1982).
57. D. R. Paul, "Polymer Blends", Ch. 12, Vol. 2 Academic Press, New York (1978).
58. J. Kohler, G. Riess, and A. Banderet, *Eur. Polym. J.*, **4,** 187 (1968).
59. R. M. Durst, R. M. Griffith, A. J. Urbanic, and W. J. Van Essen, *Adv. Chem. Ser.*, **154,** 239 (1976).
60. A. L. Bull and G. Holden, *Elastomers Plast.*, **9,** 281 (1977).
61. R. Fayt, R. Jérôme, and Ph. Teyssié, *J. Polym. Sci., Polym. Lett. Ed.*, **19,** 79 (1981).
62. R. Fayt, R. Jérôme, and Ph. Teyssié, *J. Polym. Sci., Polym. Phys. Ed*, **20,** 2209 (1982).
63. C. R. Lindsey, D. R. Paul, and J. W. Barlow, *J. Appl. Polym. Sci.*, **26,** 1 (1981).
64. R. Fayt, R. Jérôme, and Ph. Teyssié, *J. Polym. Sci., Polym. Phys. Ed.*, **19,** 1269 (1981).
65. T. Inoue, T. Soen, T. Hashimoto, and H. Kawai, "Block Polymers", S. L. Aggarwal Ed., Plenum Press, N.Y. (1970).

DISCUSSION

I. Sanchez: I would like to make a comment that may be relevant to the variations of glass temperature that you showed. It concerns some experiments at NBS by Charles Han (neutron scattering experiments). He looked at the lamellar form of the styrene/isoprene block polymers and measured the radius of gyration of the styrene chains in the interlamellar domains. What he found was that these are highly oriented, that the chains are oriented perpendicular to the lamellar planes, which perhaps is not so surprising. What is surprising is that when the block co-polymer was blended with styrene homopolymer, in the part of the phase diagram where the styrene goes into the domains, that is, where the homopolymer actually dissolves within the lamellar domains, he found that this styrene also orients perpendicular to the domains. So the styrene in the interlamellar domains is quite different from the bulk polystyrene; it is highly oriented and one would expect the glass transition temperatures to be different due to that effect alone.

S. Bywater: I presume that you are referring to the high molecular weight limit of T_g. This may be a factor, but would not explain why the results are dependent on sample type (styrene-siloxane or styrene-diene). Many samples do contain impurities e.g. two-block material and homopolymer in three-block samples. There is also no standard sample treatment to ensure good phase separation, and some samples show poorly organized structures in electron microscopic examination. I do not know if this will affect T_g or not, i.e., if the differences observed are a matter of sample treatment or if sample composition is an important factor in some cases. Krause has certainly found differences in behavior in T_g's determined by refractive index measurements or D.S.C. measurements where the sample pre-treatment was different for the two techniques. It might be helpful but rather laborious to check phase separation in each case.

B. Thycher: I am just wondering about the styrene-EB block copolymer. Is that a commercially viable process to hydrogenate the butadienes?

S. Bywater: Apparently it is, such materials are sold by Shell under the trade-name Kraton-G.

Some Observations on Kinetic and Steric Limitations to Specific Interactions in Miscible Polymer Blends

ANDREW GARTON

Division of Chemistry
National Research Council of Canada
Ottawa, Ontario K1A OR6

This note describes the application of infrared spectroscopy to determine the proportion of ester groups of poly(ϵ-caprolactone) which are involved in specific interactions with the hydroxyl groups of the poly(2-hydroxypropyl ether of bisphenol A) (Phenoxy, Union Carbide) in a series of miscible blends of the two polymers. Even with a fifteen-fold excess of hydroxyl groups, only about 50 percent of the ester groups of poly(ϵ-caprolactone) are hydrogen-bonded, presumably reflecting steric restrictions to the ester-hydroxyl interactions. Partially miscible blends of these two polymers may also be prepared by a suitable choice of casting solvent, and infrared spectroscopy may then be used to follow the kinetics of miscibility when the partially miscible blend is heated.

The occurrence of polymer-polymer miscibility is frequently rationalized in terms of specific interactions between groups on the two polymers (1–3). Fourier Transform Infrared (FT-IR) spectroscopy is a very sensitive tool for studying molecular interactions because of its ability to detect the small perturbations of IR absorptions which occur when such interactions take place. Unfortunately, IR absorptions in solid polymers are relatively broad and this has restricted the quantitative use of the IR technique. Recently, however, it was demonstrated that IR spectroscopy has the potential for determining the *number* of interactions occurring in some miscible blends by separating the absorptions of the interacting and non-interacting groups (4, 5).

When studying low molecular weight compounds in dilute solution, it can reasonably be assumed that all the possible interacting centers are equally accessible. For example, the proportion of methyl acetate ester groups which interact with, for example, chloroform, can be calculated simply from the equilibrium constant associated with that interaction (5, 6). In solid polymers, steric factors may restrict the interaction between the polymers to such a degree that not all of the interacting centers (e.g. ester groups) of a polymer are accessible to the second polymer. To fully understand the interactions between polymers (or between a polymer and an additive) it is therefore necessary to examine the accessibility of interacting centers in solid polymers.

The ideal experimental situation would be if the absorptions of the interacting and non-interacting groups were completely separated. The proportion of the groups involved in specific interactions could be calculated simply from the areas of the well resolved absorptions and a knowledge of their relative extinction coefficients. In practice, complete separation of the absorptions does not usually occur because of the weakness of the perturbation produced by the interaction. Slight band asymmetry may then result but reliable separation of the two bands is not possible.

In some cases, however, particularly those involving a hydroxyl-carbonyl interaction, the perturbation of the absorption is significantly greater, making separation easier. *Figure 1a* shows the carbonyl stretch absorption at 25°C of poly(ϵ-caprolactone) (PCL) in a 10:90 (by weight) PCL-Phenoxy blend. Phenoxy is the poly(2-hydroxypropyl ether of bisphenol A) of structure 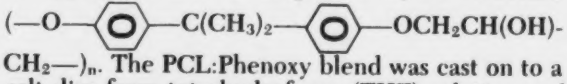. The PCL:Phenoxy blend was cast on to a salt disc from tetrahydrofuran (THF) solution and vacuum annealed at 100°C. Such blends are optically transparent and exhibit a single T_g and may therefore be classed as miscible. The carbonyl stretch absorption now is markedly asymmetric (*Fig. 1a*). The two absorptions are more clearly resolved if the sample is cooled to −150°C (*Fig. 1b*). This is because of the general sharpening of IR absorptions which occurs at low temperatures, and because decreasing interatomic distances increase the perturbation of the carbonyl group by the hydrogen bond. Apparent resolution may be further enhanced by processing the spectra through the Fourier self-deconvolution procedure of Kauppinen, *et al* (7) (*Fig. 1c*). This procedure is helpful in locating the position of absorption maxima, although some distortion of band areas occurs if the

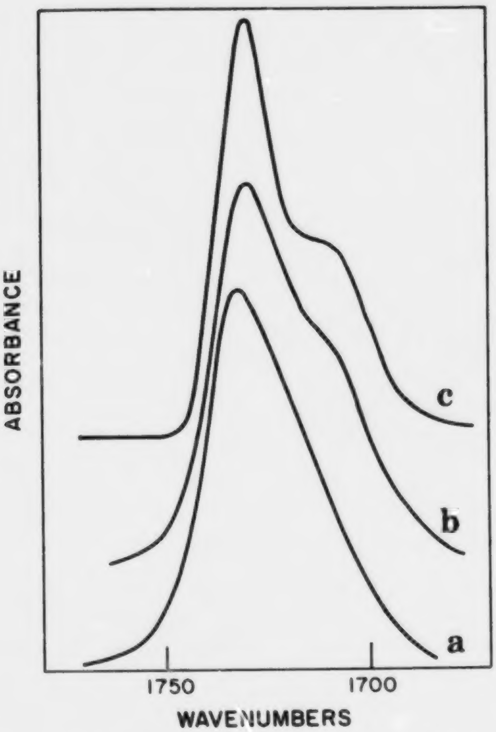

Fig. 1. The Carbonyl Stretch Absorption of PCL in a 10:90 PCL:Phenoxy Blend:
a) at 25°C
b) at −150°C
c) after Fourier self-deconvolution.

band profiles are not Lorentzian. *Figure 1* is therefore consistent with there being two components to the carbonyl stretch absorptions. At −150°C, the higher frequency component (presumably corresponding to noninteracting carbonyl groups) is centered at ~1730 cm^{-1}, with a broader, lower frequency component (presumably the hydrogen bonded carbonyl groups) centered at ~1712 cm^{-1}.

Three possible complications to this very simple interpretation of the spectra should be commented upon. Crystallization of the PCL obviously would perturb the IR spectrum. Crystalline PCL at −150°C has a characteristically sharp carbonyl stretch absorption centered at 1723 cm^{-1}. The broad low frequency component of the carbonyl stretch in blends (~1712 cm^{-1}) cannot therefore be associated with PCL crystallization. It can also be speculated that −150°C is below the upper critical solution temperature (UCST) of the blend [if such a phenomenon can occur in solid polymer blends (8)] and that phase separation may result on cooling. The blends are, however, glassy solids at room temperature (T_g ~ 50°C) and phase separation on cooling is unlikely for kinetic reasons. Finally, the Phenoxy is not of a particularly high molecular weight (~25,000) and so the possibility of interactions between PCL and the Phenoxy end groups should be considered. However, as is shown below, a fourfold increase in the Phenoxy:PCL relative concentration (10 percent PCL to 2.6 percent PCL) had little effect on the proportions of the two components of the PCL carbonyl stretch, indicating that interactions with end groups was not responsible for the splitting of the carbonyl absorption. As further confirmation, 8 percent of 2,2 bis-(4-hydroxyphenyl) propane (bisphenol A, a model for phenolic end groups in Phenoxy) was added to a 10:90 PCL: Phenoxy blend. At −150°C, the hydrogen-bonded component of the carbonyl stretch then occurred at a significantly lower frequency (1709 cm^{-1}).

Before examining the effect of blend composition on the proportion of ester groups involved in specific interactions, it is necessary to demonstrate that the samples are at an equilibrium state of interaction. This is demonstrated in *Fig. 2*, where blends of constant composition (10 percent PCL) were prepared by four different methods. As is well known (8, 9) (and is further demonstrated below), polymer-solvent interactions can result in some degree of phase-separation of miscible polymers when prepared as solvent-cast films. The three solvents produced films with different degrees of polymer-polymer interaction (as evidenced by their IR absorptions). However, when the three films were annealed at ≥100°C, the shapes of the carbonyl stretch absorptions of the PCL became identical (*Fig. 2*) and also similar to that of a film prepared

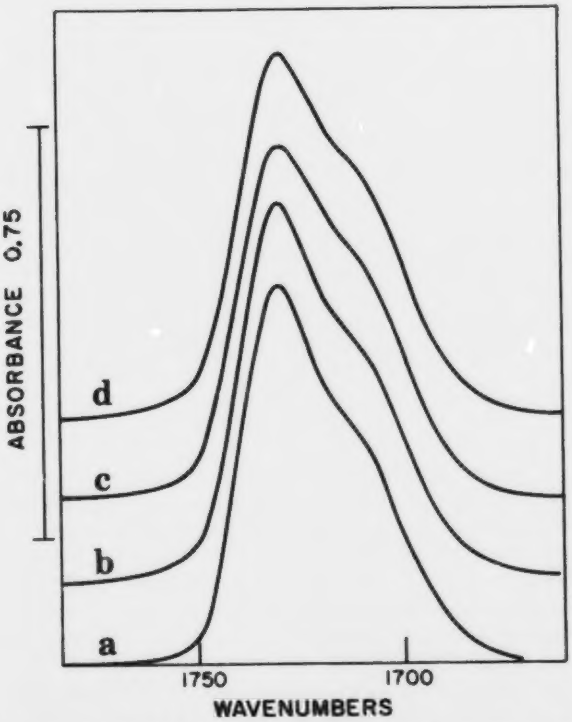

Fig. 2. The Carbonyl Stretch Absorption of PCL at −150°C in 10:90 PCL:Phenoxy Blends, Cast from Various Solvents and Annealed at ≥100°C.
a) from THF
b) from dioxane
c) from chloroform
d) quenched from 200°C melt.

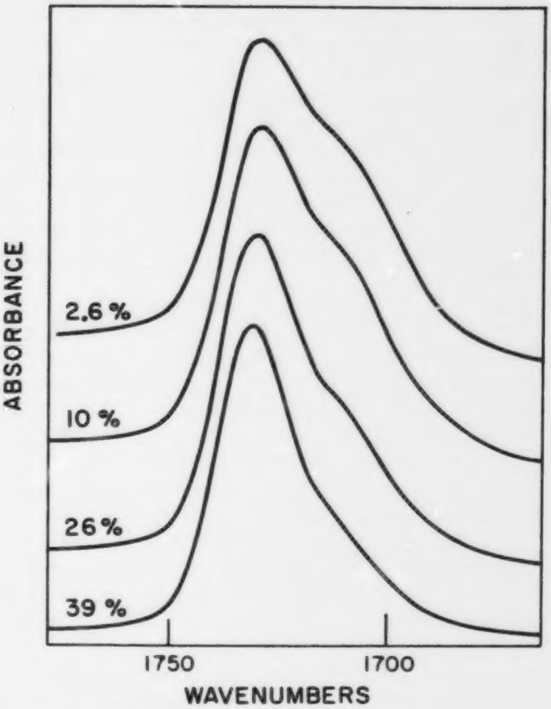

Fig. 3. The Carbonyl Stretch Absorption of PCL at −150°C in PCL:Phenoxy Blends of Various Compositions. Legends refer to percentage by weight of PCL.

by quenching from a 200°C melt. It may, therefore, reasonably be assumed that the blends under study had reached an equilibrium degree of polymer-polymer interaction.

Once these conditions for attaining equilibrium are established, it may be concluded from *Fig. 3* that the proportion of carbonyl groups which, at equilibrium, are hydrogen bonded (ie. the 1712 cm^{-1} component) increases as the polyester content decreases. This would be expected where the interaction were treated as a simple competitive equilibrium (ie. the Phenoxy and the PCL competing for interaction with the PCL ester groups) but once the association state data are quantified, it becomes clear that the interaction is more complex than a simple equilibrium.

The deconvolution procedure for separating the two absorptions is less precise than the procedure for spectra of model compounds described previously, (5, 6) because of a larger number of floating variables in the curve fitting procedure. The association state data in *Fig. 4*, therefore, have correspondingly large error bars. The initial step was to set a baseline, which was straightforward in this spectral region after subtraction of small absorptions due to the Phenoxy. The number of absorptions is defined as two by the model, and their maxima were defined by Fourier self-deconvolution or double differentiation (5–7). The floating variables in the least squares curve fitting are then band shapes (25 percent Lorentzian/75 percent Gaussian gave the best fit), band widths (although the higher frequency component was kept at a constant width and less than the width of the lower frequency component) and peak heights. In a separate experiment, where the spectral changes accompanying the development of PCL-Phenoxy interactions were examined, it was determined that the extinction coefficient of the hydrogen bonded carbonyl stretch (based on area) was 1.23 times the extinction coefficient of the unassociated carbonyl.

Figure 4 shows that even with a 15-fold excess of hydroxyl groups relative to ester groups, only about 50 percent of the carbonyl groups are hydrogen bonded. This observation presumably reflects steric limitations on the interaction caused by a mismatch in the polymer repeat distances and conformational limitations to the access of interacting groups. At higher polyester content, the proportion of hydrogen bonded carbonyl groups decreases (<30 percent at 39 percent PCL). These data are limited to blends containing <40 percent PCL because at higher concentrations crystallization of the PCL occurs.

If polymer blends are prepared in a non-equilibrium state of interaction by a suitable choice of casting solvent, the kinetics of miscibility may also be followed by IR spectroscopy. *Figure 5* shows that when a thin film of PCL:Phenoxy is cast onto a salt disc from THF solution and the solvent removed at room temperature (>4 weeks at <1 kPa vacuum, IR detects no residual solvent) relatively few specific interactions occur, ie. the 1712 cm^{-1} component is relatively small. Heating the film close to the T_g of the Phenoxy causes a marked increase in the number of interactions within ten minutes. At 130°C and higher, the equilibrium situation (cf. *Fig. 2*) is attained rapidly.

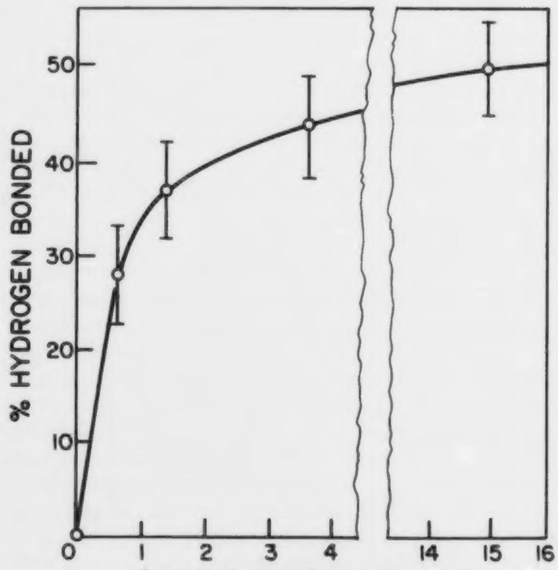

Fig. 4. The proportion of Carbonyl Groups of PCL which are Hydrogen-Bonded in PCL:Phenoxy Blends of Various Compositions.

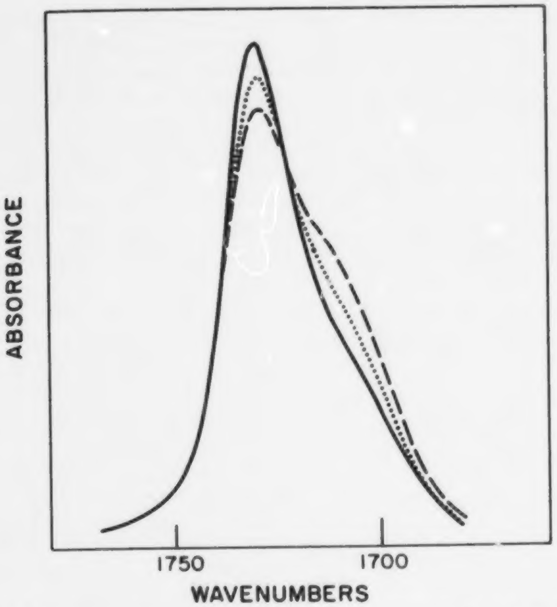

Fig. 5. Spectral Changes Accompanying Annealing of a 3.6:96.4 PCL:Phenoxy Blend Cast from THF.
—— as cast
– – – – 10 min. at 100°C
……. 10 min. at 130°C.

The kinetic and steric limitations to specific interactions described here will have several important consequences. Any attempt to define the thermodynamics of miscibility which includes an enthalpy of interaction term must make assumptions about the number of possible interacting centers. It is shown here that this number need not equal the number of polymer repeat units. Empirical predictions of polymer miscibility based on the interactions of model compounds must also consider these restrictions in solid polymers if they are to be realistic. Further, other polymer interactions such as plasticization will also be influenced by steric and kinetic limitations, and this IR technique may be useful in understanding such effects. The most obvious limitation of the technique is that when the IR absorption cannot reliably be resolved into two components, the reason may be either that the perturbation caused by the specific interaction is too small, or that the interaction is less specific in nature and there is a homogeneous population of interacting groups in the blend. IR spectroscopy cannot distinguish between these two cases.

EXPERIMENTAL

The Phenoxy (Union Carbide, PKHH) was kindly supplied by L. Pacala of Union Carbide. The intrinsic viscosity of the Phenoxy was 46.5 cm^3/g in THF at 25°C. PCL was purchased from Aldrich and had an intrinsic viscosity of 32.4 cm^3/g in THF at 25°C. All solvents were reagent grade and were redistilled before use. Thin films of the blends were cast from dilute solution on to salt discs in the conventional manner. The film thickness was controlled to keep the intensity of the carbonyl stretch absorption of the PCL at 0.85 ± 10 percent absorbance units. IR spectra were obtained at 1 cm^{-1} resolution using a Nicolet 7199 FT-IR as described previously (5, 6). T_g determinations (as a criterion of blend miscibility) were carried out using a DuPont 910 differential scanning calorimeter.

REFERENCES

1. J. W. Barlow and D. R. Paul, *Polym. Eng. Sci.*, **21**, 985 (1981).
2. R. E. Prud'homme, *Polym. Eng. Sci.*, **22**, 90 (1982).
3. O. Olabisi, *Macromolecules*, **8**, 316 (1975).
4. S. R. Fahrenholtz and T. K. Kwei, *Macromolecules*, **14**, 1076 (1981).
5. A. Garton, *Polym. Eng. Sci*, **23**, 12 (1983).
6. A. Garton, P. Cousin, and R. E. Prud'homme. *J. Polym. Sci., Polym. Phys. Ed.*, **21**, 2275 (1983).
7. J. K. Kauppinen, D. J. Moffatt, H. H. Mantsch, and D. G. Cameron, *Appl. Spectrosc.*, **35**, 271 (1981).
8. D. Patterson, *Polym. Eng. Sci.*, **22**, 64 (1982).
9. C. C. Hsu and J. M. Prausnitz, *Macromolecules*, **7**, 320 (1974).

DISCUSSION

M. Winnik: I am curious about the small fraction, apparently of hydrogen bonded carbonyls, when the ratio of OH groups to carbonyls is so high. I am wondering if you know anything about the oscillator strength of the carbonyl absorption, essentially the extinction coefficient for absorption.

A. Garton: There is not a large difference between the bonded versus non-bonded carbonyls in terms of the area of the absorption band. From *Fig.* 5, the extinction coefficient of the hydrogen bonded carbonyls is only 23 percent larger than the non-bonded carbonyls.

M. Winnick: I am sorry, I did not understand. Does that mean that you can convert the area ratios directly to mole ratios?

A. Garton: Yes, that is right.

R. E. Prud'Homme: Since you are looking at an interaction between the OH group of the phenoxy with the carbonyl group of the polyester, it would seem possible to look not only at the carbonyl group by infrared but also at the OH group. Have you tried to do that? Do you think that it would be possible to crosscheck your results?

A. Garton: No, and I do not think it is. You cannot differentiate spectroscopically between —OH hydrogen bonded to a carbonyl group and OH hydrogen bonded to another OH group. This is a complication which does not occur with the carbonyl stretch absorption.

I. Sanchez: I would like to make a comment. It concerns the idea that in miscible polymer blends we have a negative heat of mixing. There has been a tendency to try to identify these specific interactions, as you have done, to learn more about how we can get these negative heats of mixing. Recently Don Paul has made a very interesting observation. I think it gave an insight into why we sometimes observe compatibility in systems that should be immiscible. It has nothing to do with specific interactions but with the fact that in many compatible systems one of the polymers may be considered as a random co-polymer. If you look through the literature you will see that this is a general phenomenon, that in many of the compatible pairs one can be considered a random copolymer. Paul's proposal helps to explain compatibility in many systems. It is a very simple idea; if you take two copolymers, one that is polar and one that is nonpolar and make a random copolymer out of it, you have forced two polymers to mix. But they did not want to mix, so they melt with a high potential energy in comparison to what it would be if these comonomers are not forced to mix. Now, if another polymer is added to this copolymer, then a negative heat of mixing results simply because you are able to dilute these unfavorable interactions between the comonomers. It is this dilution effect that leads to the negative heat of mixing and not specific interaction. This may explain why people who investigated systems, like poly(caprolactone) and PVC, and looked for some specific interaction were not very successful in finding them. It may be that this dilution effect is operable, rather than specific interactions driving things toward a single phase.

A. Garton: Yes, no comments other than that the polymers studied here are not copolymers.

Rheological and Mechanical Behavior of the UHMWPE/MDPE Mixtures

M. M. DUMOULIN, L. A. UTRACKI *and* J. LARA

Industrial Materials Research Institute
National Research Council of Canada
750, rue Bel-Air, Montréal, Québec H4C 2K3

An attempt was made to melt incorporate ultra high molecular weight polyethylene, UHMWPE, into medium density polyethylene, MDPE. The behavior of the mixtures, containing up to 6 wt percent of UHMWPE, was examined using mechanical and rheological testing. The mechanical test results were found to contain large experimental errors, which makes interpretation very difficult. On the other hand, melt rheology studies, using dynamic and extensional deformations, gave direct insight into the extent and effect of blending. Degradation during the processing was evaluated by size exclusion chromatography. The degree of dispersion of the UHMWPE was examined under the optical microscope.

INTRODUCTION

The wide use of plastics is due largely to the broad range of their mechanical properties. The influence of molecular weight, MW, and the molecular weight distribution, MWD, on the melt rheology and the mechanical properties of solid plastics has been recognized as of the utmost importance for both the resin manufacturers and the processor. However, relatively recently the importance of the very high MW tail, VHMWT, in the MWD has come to be suspected. The reason for this is the instrumental development, especially in the area of the size exclusion chromatography, GPC, coupled with the low angle laser light scattering, LALS; first of all, the high efficiency GPC columns had to be able to separate the VHMWT, then LALS had to be able to detect it (the mass detector, e.g., differential refractometer, does not have the required sensitivity). In particular, in two areas the VHMWT should be of particular importance: extensional melt flow and long term creep behavior of the solid polymer, at a constant level of crystallinity.

In general, the mechanical properties improve as the molecular weight increases (1, 2). The usual explanation is based on the concept of the MW dependent entanglement concentration. However, in semi-crystalline polymers above certain value of MW, the crystallinity starts to decrease and these facts, coupled with increased problems in polymerization and processing, makes this route not very attractive. For polyethylenes, PE, the improvement of properties on increase of MW is not very pronounced (3). Furthermore, since some properties, like the yield stress, depend primarily on the degree of crystallinity (4), a too large increase of MW may in fact be detrimental. The effects of MW on mechanical properties of high density PE, HDPE, were discussed by Margolies (5), who concluded that these reach the optimum value at weight average molecular weight $M_w \cdot 10^{-6} = 1.5$ to 1.75. Ten years later (6) the range of MW: $3.5 \leq M_w \cdot 10^6 \leq 7$ was investigated. While the density and the impact strength were shown to decrease even in this range of ultra high MW PE, UHMWPE, at the same time the tensile strength and the abrasion resistance improved. In fact, the UHMWPE shows outstanding properties and compares quite well with other engineering thermoplastics (6). Unfortunately, its use is severely limited by the difficulties encountered in processing.

In short, the relation between mechanical properties, and the MW, and MWD is rather complex, especially for semi-crystalline polymers, but definite improvements can be achieved if the effective MW is increased, without causing detrimental effects on the degree of crystallinity and processability. This brings back the concept of the VHMWT.

This paper deals with the effects of VHMWT on melt flow and the mechanical properties of commercial grades of PE's. To control the VHMWT, small amounts of the UHMWPE were added to a pipe-grade PE resin.

EXPERIMENTAL

Materials

Two commercial PE resins were used: medium density PE, MDPE, and UHMWPE. Their basic properties are listed in *Table 1*. The resins were blended using the equipment and blending conditions listed in *Table 2*. The samples thus prepared contained: 0, 0.2, 0.6, 2.0, 6.0, and 100 (wt percent) of UHMWPE. As a reference, one sample containing 1.8 wt percent of UHMWPE was prepared by dissolving both PE's in 1, 2, 4-trichlorobenzene, TCB, at 145°C then co-precipitating with methanol.

Following blending, the samples were granulated then compression molded (160°C for 8 min) into 4 mm thick sheets. From these the appropriate specimens were cut for rheological and mechanical tests. The latter samples were annealed for 48 hrs at 90°C then conditioned for >48 hrs at 23°C and 50 percent relative humidity (ASTM-D638). For the extensional tests, the samples were transfer-molded from the granulated materials.

Rheological Measurements

The shear properties of the samples at 190°C were determined in the steady state and dynamic modes using the Rheometrics Mechanical Spectrometer, RMS, Model 605. For each sample, first the strain, γ, and time, t, tests, at two frequencies $\omega = 0.1$ and 10 (rads/s), were done. In all cases the linear viscoelastic region of γ within a stable response time period was found.

The extensional properties were determined in the Rheometrics Extensional Rheometer, RER. The instrument was used in constant elongation rate, $\dot{\epsilon}$, and constant extensional stress, σ_{11}, mode. The samples were transfer-molded under vacuum, annealed, and then affixed with epoxy (overnight curing) to the aluminum ties. The initial length and diameter of the samples were respectively: $L_o = 21.0 \pm 0.5$ and $D_o = 5.54 \pm 0.05$ (mm). The specimens did not show any shape change on immersion in hot, $T \leq 190$°C, silicon oil. For the test the samples were mounted in the instrument and immersed in poly(dimethylsiloxane) oils, Dow 200 or 210 H (see *Table 3*). The density of PE's at 190° was calculated as 0.751 (g/cm^3). The oil-polymer density difference, $\Delta < 0.08$, was too small to cause any detectable deformation of specimens. The testing started when the maximum temperature difference (as read by three thermocouples placed at different heights in the sample chamber) did not exceed 0.2 (°C). To achieve this, it took 7 to 10 min. In order to determine the effect of the residence time, t_R, the samples were evaluated in RER for up to 30 min, and tested for weight gain/loss in silicon oil outside RER for up to 23 hrs (7).

Size Exclusion Chromatography

The molecular parameters of the samples were determined by the size exclusion chromatography using a Waters Scientific GPC-150C instrument at 135°C with TCB as a solvent. The four μ-styragel columns (10^3, 10^4, 10^5, and 10^6 Å) were calibrated using 24 polystyrene, PS, standard samples in TCB at 135°C. The results are listed in *Tables 1* and *4*. To prevent oxidative degradation of PE, 0.2 wt percent of antioxidant (Santonox-R) was added to TCB (8). The solutions containing 0.02 to 0.1 wt percent of PE's were used.

Mechanical Testing

The tensile behavior of the samples was measured with an Instron Tensile Tester Model 1125, equipped with a 10 ton Instron load cell. Dumbbell shaped specimens (ASTM D638, type I) were die cut from compression molded plates, annealed, and conditioned. All tests were conducted under the conditions: gauge length—90 mm, rate of deformation—20 mm/min.

In addition, the long-term creep/environmental stress rupture type III test (ASTM-D2552) at 50°C in Igepal CO-630 was carried out. The preliminary results (test continues) indicate that this method is of dubious value—there are different modes of

Table 1. The Properties of PE Resins

No	Property	MDPE	UHMWPE
1	Manufacturer	DuPont	Hercules
2	Application	extrusion of pressure-rated pipe for water or natural gas	General use
3	Density, (kg/L)	0.941	0.94
4	MI^c (dg/min)	0.25	<0.01
5	$\bar{M}_w \times 10^{-6}$	0.283^a (±2.9%)	2.75^b
6	Zero-shear viscosity at 190°C, $\eta_o \times 10^{-4}$ (Pa.s)	7.1 ± 0.5	—

[a] Determined by GPC in TCB at 135°C ($\bar{M}_w/\bar{M}_n = 6.45 \pm 3.6\%$).
[b] Viscosity average molecular weight, M_v as calculated from intrinsic viscosity, $[\eta] = 1.8$ (L/g).
[c] Melt index at 190°C with a load of 2.16 kg.

Table 3. Properties of Silicon Oils

Property	at T°C	Units	DOW 200	DOW 210H
density	21	kg/L	0.960	0.968
density	150	kg/L	0.810	0.830
viscosity	25	cm^2/s	5	10
flash point	—	(°C)	280	300

Table 2. The Equipment and Conditions Used for Blending

	Equipment			Conditions		
					Mixing Energy	
No	Type	Code	Manufacturer	Temperature (°C)	Time (min)	Input × 10^{-3} (J/g)
1	Two Roll Mill	RM	C. W. Brabender, Model PM 2000	175	10	
2	Gelimat^a	G	Werner-Pfleiderer,	195 to 215	0.5	
3	Banbury	B	Farrell	185 to 200	10	2.6–5.1
4	By solution	S	—	145°C in TCB	60	

[a] After the high speed mixing, the blends were formed on a differential speed roll mill at 190°C for 3 min.

failure and the results are not consistent. Similarly, the Taber abrasion test (ASTM-D1044) gave virtually the same results for all samples within a very large range of experimental error (see also Ref. 5). The results of these two methods will not be discussed here.

Density

The density of the PE-specimens was measured by the density-gradient method (ASTM-D1505) using the test pieces cut out from the compression-molded sheet.

Microscopy

In order to check the uniformity, the PE mixtures were observed under the optical microscope (cross-polarized light, magnification ≤ 310 ×) and in the scanning electron microscope, SEM. In the first case, the specimens were microtomed from the RMS or RER test samples. No other treatment was used. In the second case, the specimens were prepared by fracturing the RER samples under liquid N_2, then metallization. In the SEM micrographs there was no evidence of any heterogeneity caused by the presence of the UHMWPE.

RESULTS

RMS Results

The data were collected within the linear viscoelastic region (see *Fig. 1*) and a span of time in which the most sensitive to changes, G', remained constant (*Fig. 2*). The results were repeated and accepted only if the difference between them was less then 5 percent. The strain of 2.5 percent and time $t < 20$ min were used in this study. For a more detailed description of the procedure, see e.g. (7), (9).

RER Results

It was found that within the experimental time of testing the samples were not affected by the silicon oils (7). The experimental error (maximum spread) of the elongational viscosity, η_e, was 6 percent. Both the constant strain rate, $\dot{\epsilon}$ and the constant stress, σ_{11}, test methods were used. Examples of these are shown respectively in *Figs. 3* and *4*.

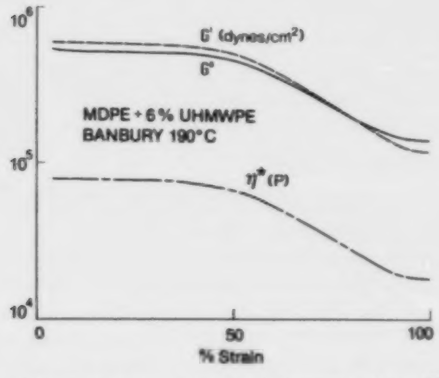

Fig. 1. The strain sweep, $\gamma = 0$ to 100 percent, at $\omega = 10$ (rad/s) and $T = 190°C$, for the sample B-6.

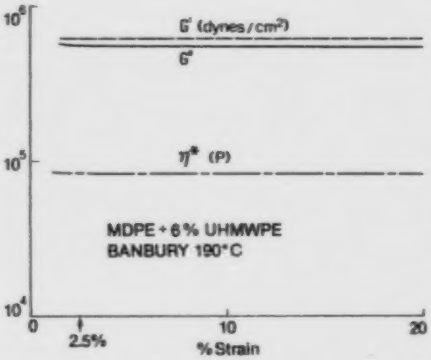

Fig. 2. The strain sweep, $\gamma = 0$ to 20 percent, at $\omega = 10$ (rad/s) and $T = 190°C$, for the sample B-6. Time of the test: 16 min.

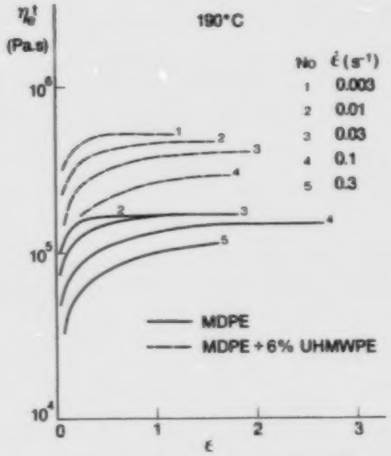

Fig. 3. The time dependent elongational viscosity for constant strain rates, $\dot{\epsilon}$, vs. deformation, for samples RM-0 and B-6, at 190°C.

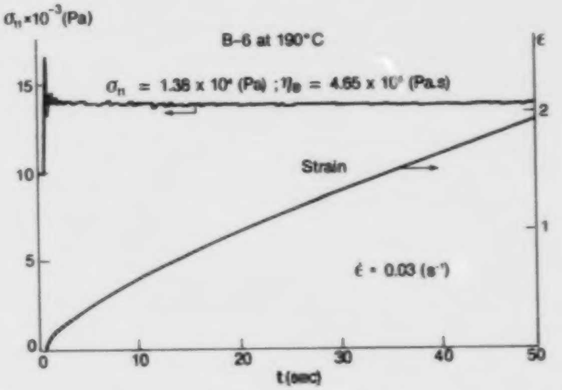

Fig. 4. The strain, ε, vs. time at a constant stress, σ_{11}, for sample B-6 at 190°C.

As observed previously (7), during the experiments with $\dot{\epsilon}$ = const., the viscosity was time dependent. In order to distinguish these transient viscosities from their steady state, plateau values, two different symbols are used: η_e^t to indicate the time dependent viscosity and η_e, its steady state values. It is of interest to note that the form of the η_e^t *vs.* ϵ curves resembles those of the previously tested high density, HDPE, or linear low density, LLDPE, PE (7).

It is known that the steady state deformation can be reached sooner under the constant stress condition than at $\dot{\epsilon}$ = const. This mode is particularly useful for HDPE for which, at σ_{11} = const., a wider range of deformation can be observed than for LDPE.

Comparative Rheological Data

In 1906 Trouton measured extensional viscosity, η_e, of tar, pitch and wax, finding $\eta_e \cong 3\eta_o$, where η_o is the zero shear viscosity.
The ratio:

$$R^\circ_T = \eta_e/3\eta_o \tag{1}$$

is called the Trouton ratio. Since

$$\lim_{\omega \to 0} \eta' = \eta_o \tag{2}$$

it will be convenient to redefine R_T as $\eta_e/3\eta'$. Obviously R_T depends on the rate of deformation and only at the limit:

$$\lim_{\omega, \dot{\epsilon} \to 0} R_T = R^\circ_T. \tag{3}$$

To compare the RMS and RER results it is useful to plot η' *vs.* ω and $\eta_e/3$ *vs.* $\dot{\epsilon}$ on the same graph. Examples of these dependencies are given in *Figs. 5–7* for MDPE, MDPE + 2 percent UHMWPE and MDPE + 6 percent UHMWPE respectively. The transient effects of the same samples are measured in RMS and RER are presented respectively in *Figs. 8* to *10*. The transient shear viscosity, η^t, was measured in cone-and-plate configuration at the lowest accessible shear rate: $\dot{\gamma} = 10^{-2}$ (s^{-1}). The η_e^t were determined in the constant strain rate experiments (*Fig. 3*).

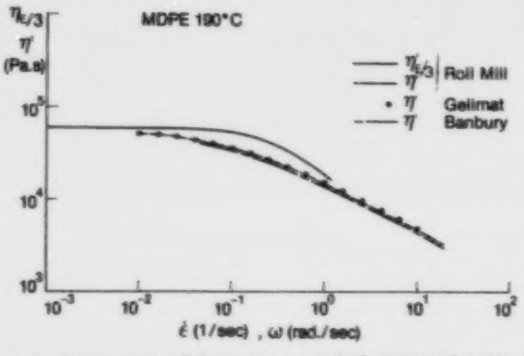

Fig. 5. Comparison of dynamic, η', and elongational, $\eta_e/3$, viscosities vs. frequency, ω, and strain rate, $\dot{\epsilon}$, respectively, for MDPE samples, at 190°C.

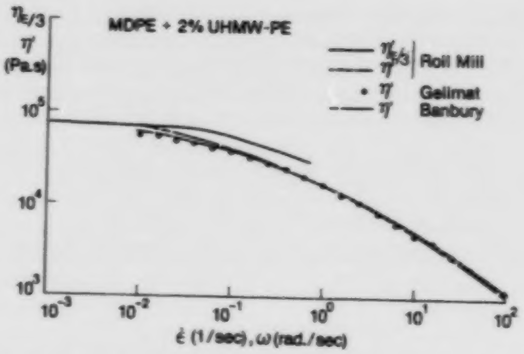

Fig. 6. Comparison of dynamic, η', and elongational, $\eta_e/3$, viscosities vs. frequency, ω, and strain rate, $\dot{\epsilon}$, respectively, for MDPE samples containing 2 percent UHMWPE, at 190°C.

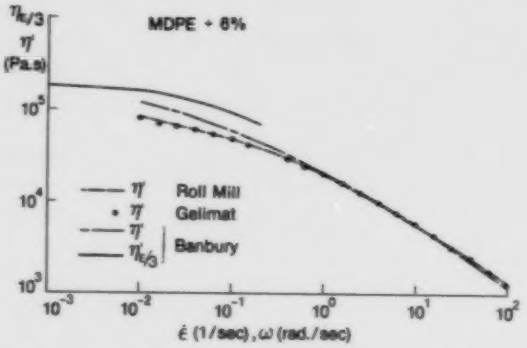

Fig. 7. Comparison of dynamic, η', and elongational, $\eta_e/3$, viscosities vs. frequency, ω, and strain rates, $\dot{\epsilon}$, respectively for MDPE samples containing 6 percent UHMWPE, at 190°C.

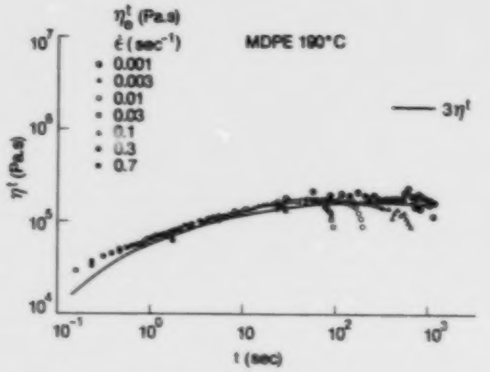

Fig. 8. Comparison of dynamic, $3\eta^t$, and elongational, η_e^t, time dependent viscosities vs. time for MDPE samples, at 190°C.

Tensile Test Results

From the engineering stress-strain curves (*Fig. 11*) the initial modulus, *E*, and the yield stress, σ_y, were calculated. The average values of these parameters *vs.* the concentration of the UHMWPE, *c*, are shown in *Figs. 12* and *13*, respectively. Each point represents the average of 5 to 9 measurements with the standard deviation indicated by the bar. The lines were calculated by the least squares method, taking into account all the data points,

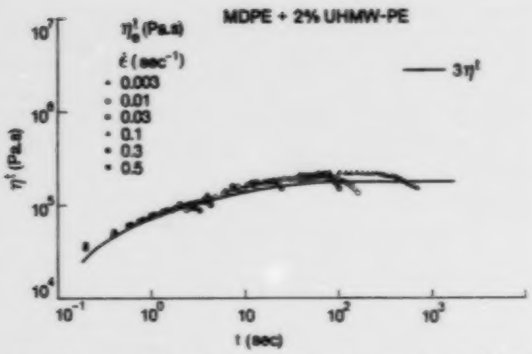

Fig. 9. Comparison of dynamic, $3\eta^t$, and elongational, η_e^t, time dependent viscosities vs. time for MDPE samples containing 2 percent UHMWPE, at 190°C.

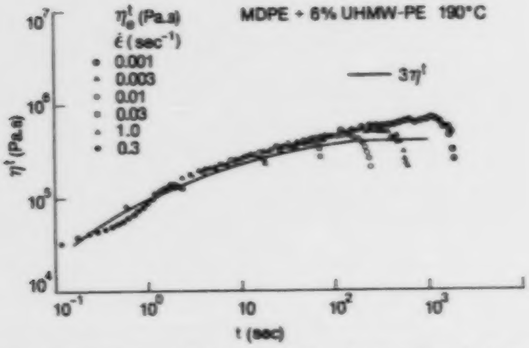

Fig. 10. Comparison of dynamic, $3\eta^t$, and elongational, η_e^t, time dependent viscosities vs. time for MDPE samples containing 6 percent UHMWPE, at 190°C.

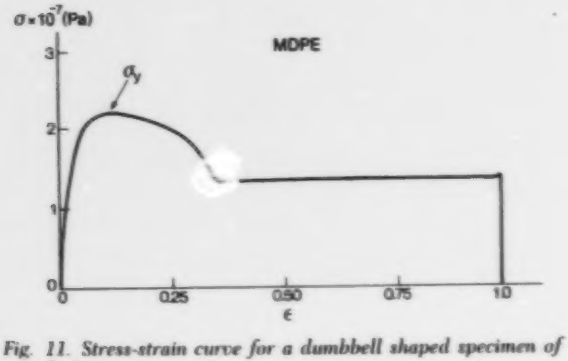

Fig. 11. Stress-strain curve for a dumbbell shaped specimen of sample G-0.

including those omitted in the figures for the sake of clarity.

Size Exclusion Chromatography

In *Table 4* the $\bar{M}_w$ and $\bar{M}_w/\bar{M}_n$ for the granulated specimens are listed. The procedure was described earlier (8). Comparing the data of *Table 1* with *Table 4*, it is observed that within the experimental error range the molecular parameters of MDPE are not affected by the processing. On the other hand, additions of UHMWPE seem to lower the $\bar{M}_w$ and $\bar{M}_w/\bar{M}_n$.

Microscopy

Figures 14 and *15* show the micrographs of the UHMWPE powder and the sample B-6. The photographs were taken in cross-polarized light. The dark, almost circular spots are the nearly-amorphous particles of UHMWPE. The dimension of the powder particles varies from 130 to 250 μm and of a B-6 blend from 16 to 144 μm. *Figure 16* shows the micrograph of sample S-2. It is apparent that while the diameter of the UHMWPE region decreased to 10 to 50 μm, the dissolution method did not produce a homogenous blend. The reason for this is most likely due to the time and temperature used for dissolution (see *Table 2*); the discoloration of the solution was observed after heating for a longer time and/or at a higher temperature. It is worth pointing out that there was no sign of discoloration of MDPE sample solution heated at 165°C for $t = 2$ hrs.

DISCUSSION

Rheological Data

It can be seen in *Figs.* 5 to 7 that the RM and G samples behave very similarly, while those of B

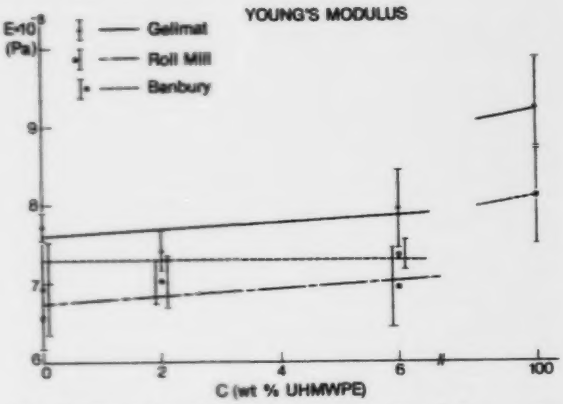

Fig. 12. Young's modulus, E, vs. composition (wt percent of UHMWPE); tensile tests of samples of the three series.

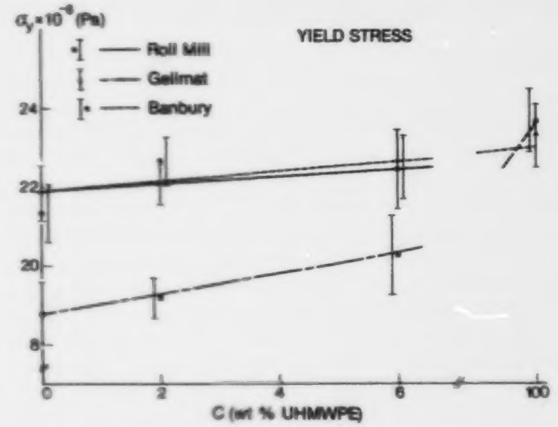

Fig. 13. Yield stress, σ_y, vs. composition (wt percent of UHMWPE); tensile tests of samples of the three series.

Table 4. Coding and Properties of PE Blends

No	Preparation		Code	Density (kg/L)	Property			
	Equipment Code	wt % of UHMWPE			$\bar{M}_w \times 10^{-3}$ by GPC	$\bar{M}_w/\bar{M}_n$ by GPC	$\eta_o \times 10^{-3}$ (Pa.s) Eq 4	Cole-Cole
1	RM	0	RM-0	0.944	267.2	6.55	74.5	67.0
2	RM	0.2	RM-0.2	—	249.5	7.32	77.6	72.0
3	RM	0.6	RM-0.6	—			78.3	74.0
4	RM	2.0	RM-2	0.941			86.6	76.0
5	RM	6.0	RM-6	0.941			116.0	105.
6	G	0	G-0	0.946	261.4	6.56	74.4	65.0
7	G	0.2	G-0.2	—			75.8	70.5
8	G	0.6	G-0.6	—	211.6	5.26	76.4	72.0
9	G	2.0	G-2	0.946			81.7	73.0
10	G	6.0	G-6	0.946			110.0	108.
11	G	100.0	G-100	—			—	—
12	B	0	B-0	0.944	266.4	6.73	47.2	66.0
13	B	2.0	B-2	0.940			97.7	97.5
14	B	6.0	B-6	0.938			167.	+250
15	B	100.0	B-100	—			—	—
16	S	1.8	S-2	—	226.1	5.86	—	—

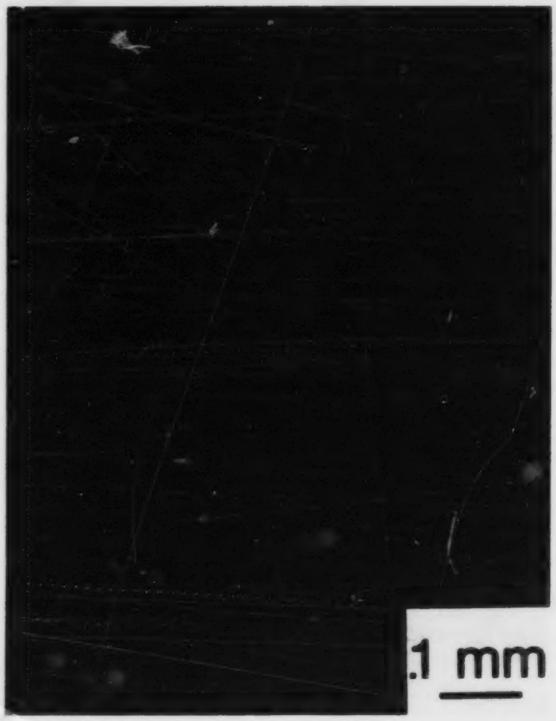

Fig. 14 Optical micrograph of UHMWPE powder; magnification: 125 times.

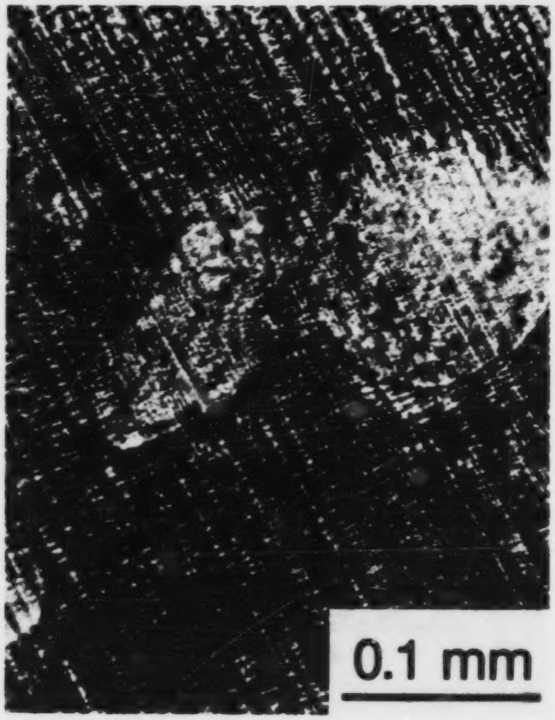

Fig. 15. Optical micrograph of sample B-6; magnification: 310 times.

tend toward higher viscosity values. The transient viscosities (*Figs. 8 to 10*) show a consistent stress increase in shear and elongation. It is worth noting that at $\dot{\gamma} = 10^{-2}$ (s^{-1}) the shear transient data for longer, near equilibrium times, fall systematically below the values observed in the extensional flow. This indicates that the zero shear viscosity, η_o, should be measured at $\dot{\gamma} < 10^{-2}$ (s^{-1}), and its value is higher than η's determined directly within the accessible range of the deformation rates. The same conclusion can be reached from *Figs. 5 to 7*.

There are two methods of calculation of η_o (10): via the relaxation spectrum or from the Cole-Cole type plot of η'' *vs.* η'. Both methods were used. The relaxation spectra, computed from the dynamic RMS data, are presented in *Figs. 17 to 20*.

The relaxation spectrum, $H(\lambda)$ *vs.* λ (λ being the relaxation time) also illustrates the changes in the melt structure obtained by incorporation of the UHMWPE using the three types of mixing equipment. It can be seen that addition of this resin systematically increases the relaxation times. Furthermore (*Fig. 20*), it can be concluded that the B-samples have the highest degree of entanglement. Integration

$$\int_o^\infty H(\lambda)d\lambda = \eta_o \tag{4}$$

Fig. 16. Optical micrograph of sample S-2; magnification: 310 times.

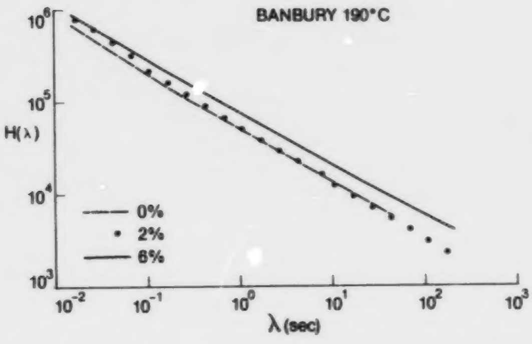

Fig. 17. Relaxation spectra of samples B-0, B-2, and B-6 at 190°C.

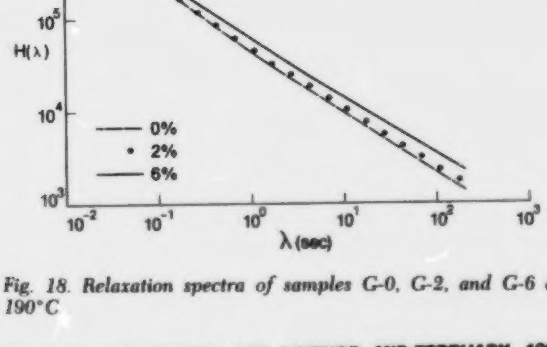

Fig. 18. Relaxation spectra of samples G-0, G-2, and G-6 at 190°C.

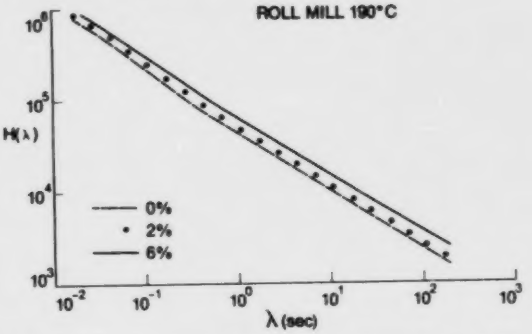

Fig. 19. Relaxation spectra of samples RM-0, RM-2, and RM-6 at 190°C.

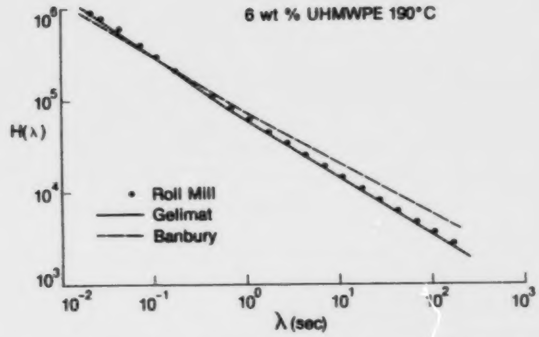

Fig. 20. Comparison of relaxation spectra for samples B-6, G-6, and RM-6.

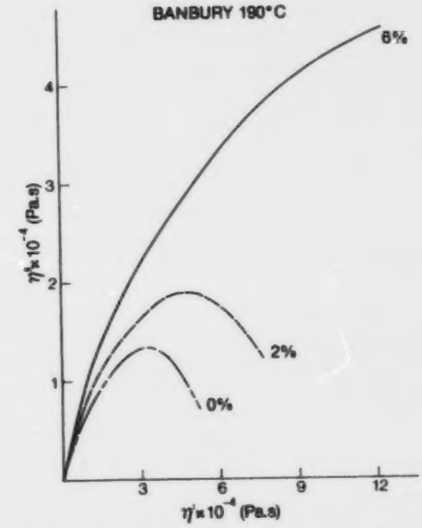

Fig. 21. Imaginary part, η'', vs. real part η' of the complex viscosity for samples B-0, B-2, and B-6 at 190°C.

gives the first set of η_o-values listed in *Table 4*.

The Cole-Cole type dependencies are shown in *Figs. 21* to *23*. The second set of η_o's in *Table 4* was computed from the symmetry principle of these dependencies. The average values of η_o are plotted in *Fig. 24* as $\eta_o(c)/\eta_o(c = 0) = \eta_r$ *vs.* c, where c is the wt percent of UHMWPE. The broken lines are computed from Simha's theoretical equation de-

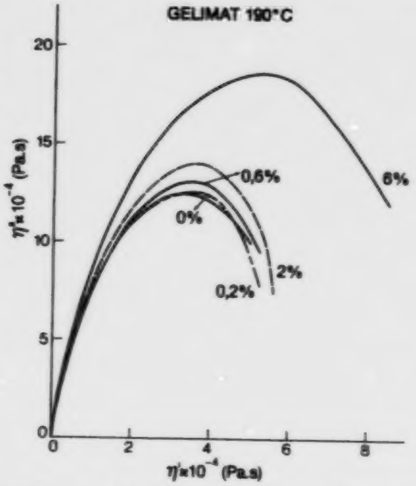

Fig. 22. Imaginary part, η'' vs. real part, η' of the complex viscosity for samples G-0, G-0.2, G-0.6, G-2, and G-6 at 190°C.

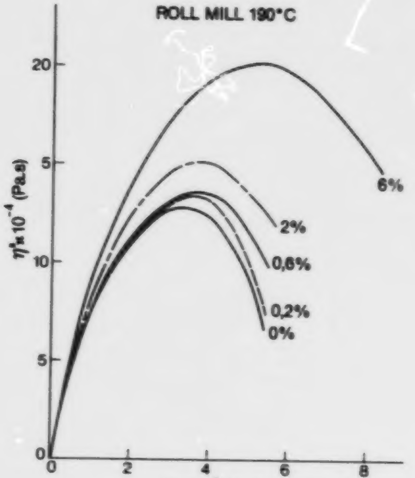

Fig. 23. Imaginary part, η'' vs. real part, η' of the complex viscosity for samples RM-0, RM-0.2, RM-0.6, RM-2, and RM-6 at 190°C.

rived for hard sphere suspensions (11). It can be seen that the theoretical viscosity is much lower than measured for PE-mixtures. Furthermore, it seems that the experimental data for the vanishing concentration do not extrapolate to $\eta_r = 1$. It is tempting to assume that for the RM and G data there is a certain amount of dissolution of UHMWPE which raises the value of $\eta_o(c = 0)$ of the matrix. With this proviso, and taking the maximum packing volume fraction $\phi_m = c_m/100 = 0.144$, one can produce the η_r vs. c curve (middle line in *Fig. 24*) which well approximates these experimental data. However, obviously this value of ϕ_m is unreasonably low. Furthermore, to fit this equation to the B-samples data, much lower values of ϕ_m would still have to be assumed. In short, the η_o results indicate that a significant amount of UHMWPE was dissolved in MDPE.

In order to test the extent of dissolution, the relation derived by one of us (12) for the concentrated solution viscosity at the Flory's θ-conditions can be used:

$$\eta_r = 1 + x\exp\{1.19x\} \tag{5}$$

$$x = c[\eta] \tag{6}$$

To fit the experimental data to these equations, the $[\eta] = 0.005$ and 0.016 (1/g) for the RM/G samples and B ones, respectively, have to be used. These calculated values are significantly smaller than $[\eta]_\theta = 0.39$ (L/g) calculable from the unperturbed dimensions of PE molecules, i.e. only a fraction of this material was dissolved.

For more precision in estimating this amount, using $[\eta]_\theta$, the effective concentrations of UHMWPE can be calculated from *Eq 5*. It can be found that in RM/G only about 0.16 percent of UHMWPE is effectively dissolved and in the Banbury mixer about four times as much (the shear degradation was not taken into account). Using these parameter, the upper curve in *Fig. 24* was computed. Since we are looking for effects of VHMWT on the rheological and mechanical properties of plastics, these dissolved amounts should be sufficient to demonstrate the tendency.

Figures 5 to *7* show that addition of the UHMWPE systematically increases the shear and elongational viscosities. The increases are much more apparent at lower rates of deformation. The UHMWPE has no significant influence of R_T; the values calculated for this parameter are 1.4, 1.3, 1.6 for $c = 0$, 2 and 6 percent in the B-series.

Using the Zeichner and Patel approach (13) a systematic displacement of the cross-over point of G', G'' vs. ω was observed (see Fig. 25). The values of G_x and ω_x, defined respectively as the ordinate and abscissa of the cross-over point, are listed in the *Table 5*. In the same *Table* the "Polydispersity Index", PI, and the relative viscosity, η_r, calculated (13) from G_x and ω_x respectively are shown. It is interesting to see that η_r agrees with the values derived directly from the zero shear viscosities. On

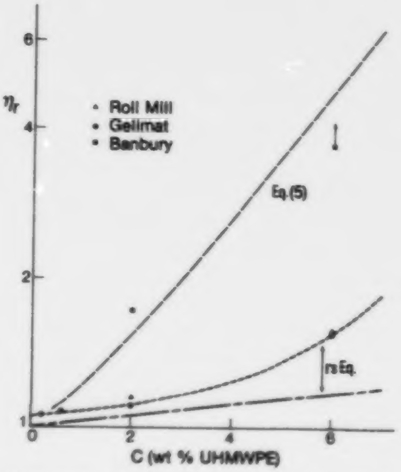

Fig. 24. Relative viscosity, η_r, vs. composition for the three series of samples. See text.

Table 5. Cross Point Parameters for Series—B Blends

c wt % UHMWPE	$G_x \times 10^{-4}$ (Pa)	ω_x (rad/s)	PI calculated (13)	η_r
0	5.0	15	2.00	1
2	4.6	9.7	2.17	1.55
6	3.1	4.2	3.23	3.57

the other hand, the GPC data, which indicated a narrowing of distribution, MWD, on addition of UHMWPE are in direct conflict with PI (PI should be proportional to M_w/M_n). The reason for the apparent narrowing of MWD is the degradative effect of UHMWPE in solution.

The results of the tensile tests for all three series of mixtures seem to show weak increase of the properties with addition of UHMWPE (*Figs. 12* and *13*). The Fisher-test indicates that the increase is statistically non-significant. The tensile testing at a relatively high rate of deformation does not allow evaluation of the effect of the additive. *Figure 13* indicates that the yield stress, σ_y, of Banbury samples behave differently from those of Roll Mill or Gelimat ones. As mentioned earlier it was believed that the yield stress depends primarily on the degree of crystallinity. However, the densities for these blends (*Table 4*) are almost identical, i.e. the degree of crystallinity is therefore expected to be similar for all these mixtures and should not play a significant role in the observed behavior of the yield stress.

It is interesting to note that a different behavior for Banbury samples was also observed in the molten state. The degree of crystallinity therefore becomes a much less attractive explanation. The other source of this behavior may come from the degradation during mixing. Comparing the $\bar{M}_w$ and $\bar{M}_w/\bar{M}_n$ of the virgin MDPE resin (*Table 1*) with those of *Table 4*, one can see that there was no significant change of the molecular weight parameters on processing for any of the three mixers used. Because of the degradation observed in solutions containing UHMWPE it was impossible to collect similar data for the mixtures. The most plausible explanation for the differences between the RM/G and B-series of samples is the chain disentanglement. In fact, it has been reported (14) that the intensive mixer (B) provides much more efficient means for changing the polymer melt structure than the laminar (RM) or kinetic energy (G) ones. It should also be noted that the higher energy input in B-series is responsible for a larger decrease in UHMWPE particle size than that observed for RM/G series.

CONCLUSION

1. It is very difficult to quantitatively incorporate UHMWPE in a molten state; the maximum concentration obtained for a B-6 sample was 0.036 percent.
2. The mechanical test results (tensile, creep, abrasion) are not sensitive to the additions of UHMWPE.
3. The shear and elongational viscosities as well as the storage modulus provide reliable, consistent methods for analysis of the melt composition and structure.
4. The parameter most sensitive to changes in MW and MWD is the cross-over point of the G' and G'' as a function of frequency plot (*Fig. 25*).
5. From the rheological data it can be calculated that the Banbury mixer was most effective in incorporating UHMWPE into MDPE; in this case only 6 percent of the total amount of UHMWPE was dissolved into the matrix with the remaining amount left as dispersed particles.
6. As evidenced by the relaxation spectra some fragmentation of macromolecules did occur in Banbury and Gelimat mixers.
7. Molecular disentanglement during mixing was observed in samples prepared in the Banbury mixer.

The work is in progress.

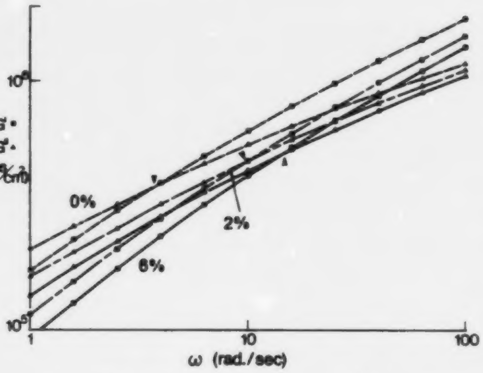

Fig. 25. Loss modulus, G", and storage modulus G' vs. frequency, ω.

REFERENCES

1. J. R. Martin, J. F. Johnson, and A. R. Cooper, *J. Macromol. Sci.—Revs. Macromol. Chem.*, **C8**, 57 (1972).
2. R. W. Nunes, J. R. Martin, and J. F. Johnson, *Polymer Eng. Sci.*, *22*, 205 (1982).
3. L. E. Nielsen, "Mechanical Properties of Polymers and Composites", p. 271, Vol. 2, Marcel Dekker, N.Y., (1974).
4. F. W. Billmeyer Jr., "Textbook of Polymer Science", 2nd ed., J. Wiley and Sons, New York, (1971).
5. A. F. Margolies, *SPE J.*, **27**, 44 (1971).
6. W. M. Birnkraut, G. Braun, and J. Falbe, *J. Appl. Polym. Sci.; Appl. Polym. Symp.*, **36**, 79 (1981).
7. L. A. Utracki and J. Lara, "Melt Rheology of Polyethylenes", presented during the International Workshop on "Extensional Flows", January 24–28 1983, Mülhouse-La Bresse (France).
8. L. A. Utracki and M. M. Dumoulin, *Preprints ACS Org. Coatings Plastics Chem. Div.*, **48**, 859 (1983).
9. L. A. Utracki and B. Fisa, *Polym. Compos.*, **3**, 193 (1982).
10. B. Fisa and L. A. Utracki, *Polym. Compos.*, **5**, 36, 99 (1984).
11. R. Simha, *J. Appl. Phys.*, **23**, 1020 (1952).
12. L. A. Utracki, *Polimery-Tworz. Wielkocz.* (Poland), **9**, 144 (1964).
13. G. R Zeichner and P. D. Patel, Proceedings 2nd World Congress Chem. Eng., **6**, 333 (1981).
14. M. Rokudai, *et al.*, *J. Appl. Polym. Sci.*, **23**, 463, 3289, 3295 (1979); ibid., **26**, 1343 (1981).

DISCUSSION

L. A. Utracki: First, I would like to express our gratitude to Dr. Nelson Wright from Carlew Chemicals, for allowing us to use their GELIMAT. Recently we purchased this mixer and it is being installed.

J. M. Ottino: Do you have any idea about the shape of domains, of particle size? I shall appreciate whatever information you can give me related to the dispersion accomplished by mixing in these three different machines.

M. M. Dumoulin: The size of solid particles of UHMWPE as measured from a couple of micrographs are about 100 to 250 μm. In a 6 percent Banbury sample the particles, as resolidified droplets, are reduced almost by half.

J. M. Ottino: What qualitative difference do you see between these three mixers?

M. M. Dumoulin: First, we see differences in the size of the particles after the blending. From roll mill and GELIMAT, the particles are significantly larger; reduced by maybe 10 percent whereas their size from Banbury was reduced by half.

I. Sanchez: What was the temperature in the Banbury mixer?

M. M. Dumoulin: From 180 to 200°C.

J. M. Ottino: It is known that the droplet breaking mechanism is quite different whether you have a shear or elongational flow. What you are doing is structuring the blend. In many cases you will have elongated blocks, or droplets. With regard to the very interesting increase of the transient viscosity, do you have explanations concerning why it should take place?

L. A. Utracki: The stress build up at low rates of shear, or an increase of the transient viscosity, is a normal behavior of viscoelastic liquids. We wanted to show that these very complex morphological systems give rather simple rheological response. Let me go back to your first statement about the mechanism of mixing. This is a very good point; depending on the type of force-field, extensional or shear, during mixing the mechanism is different. You have to remember that in the present case the difference in molecular weight is about one decade and in viscosity about 2500; i.e., it is very difficult to couple the deforming force to the droplet. We could only hope that the dissolution process will take over and complement the deformation. Throughout the process the droplets remain spherical, indicating that these deformations are insignificant on roll mill where shear field predominates as well as in Banbury where the elongational field exists. In the GELIMAT, as evidenced by the relaxation spectrum, the mixing is accomplished by the kinetic energy heating at high speeds. In this case there are some effects of degradation not detectable by GPC, but apparent in the rheological test data.

J. M. Ottino: Just for the record, I would like to say that during mixing it is common to have a decrease in viscosity. For example, in copolymers, the viscosities will decrease as a function of time.

L. A. Utracki: The transient effects for these blends were very similar to those observed for pure MDPE melt. They were not specific to the structure or size of droplets or dissolution. Moreover, for both MDPE and blends containing 6 percent of UHMWPE the same stress build-up was observed in the elongational and shear modes of deformation. This is a confirmation that nothing extraordinary is happening in these blends. One can treat this system the same way as a single phase polymer melt.

J. Giacomin: I am surprised to see droplets of one polyethylene in another. What do you postulate there? The only difference you have is the molecular weight. The chemical nature is the same. By contrast, in the other systems discussed, the phase separation existed by virtue of gross chemical differences. It surprises me to see droplets being maintained. I cannot understand how the droplets are made visible on your slides.

L. A. Utracki: The micrographs were taken in cross-polarized light.

J. M. Ottino: To start with, in the mixer you have initially large heterogeneities of polymers, then you break them apart to smaller and smaller sizes. Even having the same polymer but one part being deuterated to measure the self-diffusion coefficient (its magnitude probably will be of the order of 10^{-10} cm^2/sec), even with scale of the order of microns and perfect miscibility you would have to wait for days in order to completely homogenize the system. It is not surprising to see domains here.

G. L. Vexler: I would like to ask about the analogy that could arise between your system and high molecular weight PVC mixed with medium or low MW PVC. Do you think there can be an analogy between these two cases?

L. A. Utracki: Yes, I believe that such an analogy exists. It is always a question of dispersion and diffusion. I fully agree with Prof. Ottino's comment. We did not obtain good dispersion because of a large difference in molecular weight and because of the high value of molecular weight the diffusion has been very slow. In the micrographs, we see the particles because the kinetics of crystallization of UHMWPE domains is so much slower then crystallization of MDPE that on the depolarized slide we see the UHMWPE almost as an amorphous body. On the other hand, we tried to do the same kind of analysis using the SEM where we saw very little. I also want to stress that, according to the calculations, the concentration of UHMWPE dissolved in MDPE is about six percent out of the 6 percent added; i.e., out of the total added 6 percent, we dissolved only 6 percent.

Thermally Stimulated Creep of Polyethylene, Polypropylene, Copolymers, and Blends

P. DEMONT, D. CHATAIN, and C. LACABANNE

Laboratoire de Physique des Solides
CNRS Université Paul Sabatier
Toulouse
D. RONARC'H
Division Réseaux Optiques
TIC CNET Lannion
and J.-L. MOURA
AtoChimie, Usine de Mont, France.

The technique of Thermo Stimulated Creep (TSC) has been applied to the study of anelastic properties of polyethylene, polypropylene, their copolymers and blends. In the temperature range −200 to 100°C, complex TSC peaks were observed in all samples, namely around 0°C, about the same temperature as for the homopolymer polypropylene. By applying "fractional stresses", with a convenient choice of the loading program, these peaks have been experimentally resolved. Two components can be distinguished: 1. The "low temperature" component is characterized by mechanical retardation times following a compensation law. It has been attributed to microbrownian motions of polypropylene sequences liberated at the glass transition of the "true" amorphous regions. 2. The "high temperature" component which is influenced by thermal treatment has been assigned to microbrownian motions of polypropylene sequences liberated at the glass transition of the "constrained" amorphous regions. In block polymers, an additional TSC peak is observed around −50°C: it has been associated with the glass transition of ethylene-propylene-rubber (EPR) interphase. The coupling of this interphase with polyethylene and polypropylene phases is insured by diffusion of some ethylene and propylene sequences in EPR. At about −140°C, a TSC peak associated with the low temperature component of the glass transition of polyethylene can be distinguished in all the materials studied.

INTRODUCTION

Within the rapidly growing literature on polymer-polymer blends and copolymers (1–3), blends and copolymers of polyolefins, occupy only a small part, despite the considerable economic interest of those materials caused by their high-impact strength and low temperature toughness (4–9). For these reasons, the micromechanical study of blends, random and block polymers of the most common polyolefins—polyethylene and isotactic polypropylene—has been undertaken. The aim of this work is to characterize the amorphous phase of these materials. The thermostimulated creep technique has been used for this investigation.

After a brief recall of the principle of this technique, data will be presented for blends, block and random copolymers with ethylene content lower than 20 percent.

THERMOSTIMULATED CREEP (TSC)

Principle

The principle of this technique is as follows (10):

- the sample is subjected to a given stress σ at T_σ for a time allowing complete orientation of the mobile units that one wishes to consider.
- the temperature is then lowered to $T_o \ll T_\sigma$ where any molecular motion is completely hindered; then the stress is removed.
- the sample is subsequently warmed up at a controlled rate so that the mobile units can return at random. The strain γ, its time derivative $\dot{\gamma}$, and the temperature T, are recorded *vs.* time t.

If the recovery behavior can be described by a Kelvin-Voigt model, the mechanical retardation time τ can be deduced from measurements of $\dot{\gamma}(T)$ and $\gamma(T)$:

$$\tau(T) = \gamma(T)/\dot{\gamma}(T). \qquad [1]$$

Thermally activated states theory predicts the $\tau(T)$ follows the Arrhenius equation,

$$\tau(T) = \tau_{oa}\exp(\Delta H/kT), \qquad [2]$$

where: τ_{oa} is the pre-exponential factor, ΔH the activation enthalpy, k the Boltzmann constant.

The activation entropy ΔS can be deduced from τ_{oa}:

$$\tau_{oa} = h/kT \exp(-\Delta S/k), \qquad [3]$$

where h is the Planck constant.

In the free volume theories $\tau(T)$ is given by a Vogel equation:

$$\tau(T) = \tau_{ov} \exp\{\alpha(T - T_\infty)\}^{-1}, \qquad [4]$$

where: τ_{ov} is the pre-exponential factor, α is the thermal expansion coefficient of the free volume, T_∞ is the critical temperature at which the molecular motions are frozen. The linearization of $ln\tau(T)$ *vs.* $(T - T_\infty)^{-1}$ allows to determine T_∞, τ_{ov} and α.

In polymers, the model of a single retardation time must be generalized in order to obtain a good fit between theory and experiment; this is generally done by using a distribution of retardation times. The great advantage of the TSC technique is that it allows a detailed study of this distribution.

EXPERIMENTAL

A) Equipment

The specimen, with dimension of 60 mm × 6 mm × 300 μm, is subjected to a shear stress by a torsional balance. The deformation is determined by observing rotation of a light beam reflected by a mirror. The sample is placed in a thermal jacket whose temperature can vary from liquid nitrogen to 500 K. In all experiments, the heating rate was 0.08 K/sec. The strain γ and the temperature T were simultaneously recorded *vs.* time. By taking the time derivative of the strain, the rate of strain $\dot{\gamma}$ was obtained with an accuracy of a few percent.

B) Materials

All polymers have been synthesized in propylene liquid phase with the same catalyst. The polypropylene, free from additive was 97 percent isotactic, with a molecular weight of 452,000 and a polydispersity of 8.1. The Differential Scanning Calorimetry (DSC) has given 163.4°C for the melting temperature at 20°/minute and 50.5 percent for the crystallinity content. The melt index was 2.1, at 230°C under 2.16 kg.

Blends have been prepared from polypropylene and low density polyethylene. The DSC spectrum showed two melting peaks: the one at 160°C corresponding to the melting of polypropylene, the other at 107°C to the melting of low density polyethylene.

Block copolymers contained polypropylene and high density polyethylene. The DSC spectrum recorded at 20°/minute showed two melting peaks of polypropylene and polyethylene respectively at 160 and 120°C.

Random copolymers: Their molecular weights are 428,000 with a poly-dispersity of 6.8. The DSC spectrum indicated only one melting peak; for 2.5 percent ethylene content and 20°/min it was situated at 143°C which is significantly lower than for polypropylene or for block copolymers with the same ethylene content.

C) Procedure

Complex TSC Spectra

In semicrystalline polymers like polyethylene, polypropylene, blends and copolymers, the recorded strain is rather small in the linear region. Moreover, any thermal treatment above glass transitions, may influence the TSC response. So, instead of looking at the recovery behavior as usual, the "true" creep experiments are performed according to the following procedure:

- —the stress σ was applied at the temperature T_o at which the molecular motions are frozen;
- —the sample was warmed up at a controlled rate while γ, T and $\dot{\gamma}$ are simultaneously recorded *vs.* time.

Resolution of the Complex TSC Spectra

The following procedure has been used for the experimental resolution of the complex TSC spectra (11):

- —the stress is applied at the temperature $T_{\sigma on}$ for 2 minutes in order to allow the mobile units with a retardation time lower than $\tau(T_{\sigma on})$ to orientate;
- —the temperature is lowered to $T_{\sigma off} = T_{\sigma on} - 5°$ (or 10°) at which the stress is cut off. Then, the temperature is maintained constant for 2 minutes in order to allow the units with retardation time lower $\tau(T_{\sigma off})$ to return to equilibrium.

The classical TSC cycle gives a spectrum that can be characterized by a single retardation time. By varying $T_{\sigma on}$ in the temperature range, the whole TSC spectrum can be resolved into "elementary spectra" well described by a Kelvin Voigt model.

POLYETHYLENE-POLYPROPYLENE BLENDS

Complex TSC Spectra

Figure 1 shows the TSC spectra of the three blends after annealing for 115 hours at room temperature. The dotted line is for the 5/95 PE-PP, the dashed line for the 10/90 PE-PP, and the solid line for the 20/80 PE-PP. The same shear stress, σ = 2.8 MPa, was applied at T_σ = −190°C, to all samples. In the sample containing 20 percent of polyethylene, a small ill-defined TSC peak was observed around −140°C. It has been attributed to the γ relaxation of the polyethylene chains (5, 12–17). Around 0°C, a complex TSC peak with two components was recorded for all samples. It is due to the polypropylene chains (4, 12, 18–20). Note that the temperature position of its low-temperature component (−6°C) was independent of the composition while its intensity increases with the polyethylene content indicating a decreasing of the degree of crystallinity (12). Around 40°C, the high temperature component of TSC peaks was strongly depressed after a quench from 100°C to liquid nitrogen temperature as shown in *Figure 2* where the dotted line is for 5/95 PE-PP, the dashed line for the 10/90 PE-PP, and the solid line for 20/80 PE-PP. Annealing for 16 hours at room temperature was necessary to observe this peak (20). So, the two components that we have observed in blends, have the characteristic behavior of the double glass transition, $Tg(L)$ and $Tg(u)$, of polypropylene (18, 20–22).

It seems relevant to note that the same features have been observed in other semicrystalline polymers such as poly(vinylidene fluoride) (23) or polyacetylene (24).

FINE STRUCTURE OF THE TSC SPECTRA

By a convenient choice of the parameters (temperature and time) defining the loading program, fractional stresses have been applied to the sample. The complex TSC spectra have been resolved into "elementary" TSC peaks that can be analyzed by making the hypothesis of a single retardation time $\tau(T)$ given by *Eq 1*. The results of the analysis of the various elementary TSC peaks have been reported in *Fig. 3* for the 5/95 PE-PP blend. For each elementary peak, the temperature of the TSC maximum (Tm) is indicated by a small arrow: the best accuracy for determining the temperature dependence of the retardation times is obtained from the experimental points corresponding to the low temperature side of the TSC peaks. Except for the two peaks isolated at 30 and 35°C, the retardation times can be described by the Arrhenius equation (*Eq. 2*). The corresponding parameters τ_{oa} and ΔH are listed in *Table 1*. The five peaks isolated between −17 and 4°C have the same retardation time τ_c at a "compensation temperature" T_c.

$$\tau(T) = \tau_c \exp\left\{\frac{\Delta H}{k}\,(T^{-1} - T_c^{-1})\right\}, \qquad [5]$$

where: $\tau_c = 0.37$ sec. and $T_c = 21°C$, in other words, their activation entropy varies linearly with the activation enthalpy.

It is important to note that for the other PE-PP compositions, T_c remains constant. In semi-crystal-

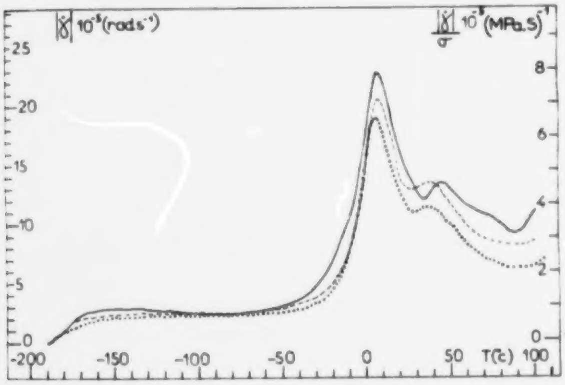

Fig. 1. TSC spectra of annealed polyethylene-polypropylene blends.
···5/95 PE-PP
- - -10/90 PE-PP
——20/80 PE-PP.

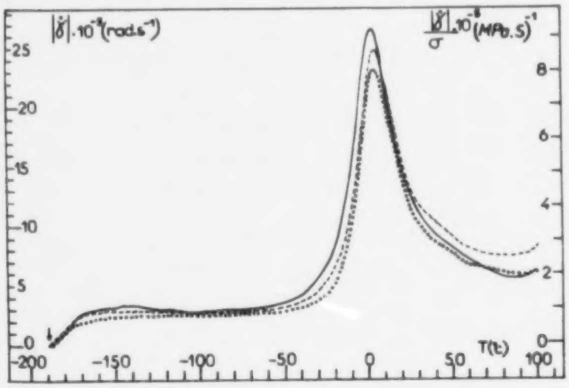

Fig. 2. TSC spectra of quenched polyethylene-polypropylene blends.
···5/95 PE-PP
- - -10/90 PE-PP
——20/80 PE-PP.

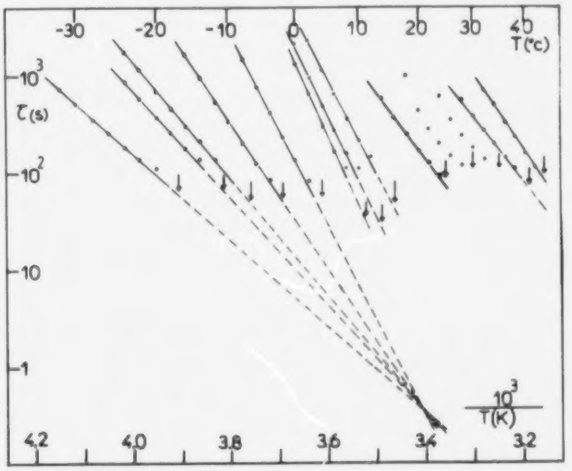

Fig. 3. Arrhenius diagram of the retardation times characterizing the "elementary" TSC peaks isolated in the 5/95 PE-PP blend.

Table 1. Parameters of retardation times following the Arrhenius equation (*Eq. 2*) in 5/95 polyethylene-polypropylene blend.

T_m (°C)	ΔH(eV)	τ_{oa} (sec)
−17	0.90	1.1×10^{-16}
−11	1.09	6.8×10^{-20}
−7	1.20	8.2×10^{-22}
−2	1.49	1.0×10^{-26}
4	1.97	5.0×10^{-35}
11	2.27	1.8×10^{-39}
14	2.10	3.3×10^{-36}
16	1.96	3.1×10^{-33}
25	1.32	3.1×10^{-21}
41	1.29	1.4×10^{-19}
44	1.52	5.0×10^{-23}

line polymers, this behavior is characteristic of the low temperature component of the glass transition (20, 22–27). These processes have been attributed to the microbrownian motions responsible for the glass transition of polypropylene chains situated in the interspherulite regions free from constraints.

For the other processes following an Arrhenius equation, at higher temperature ΔH and ΔS vary independently of each other. Their dependences on thermal treatment, and the relatively low activation entropies, have been attributed to microbrownian motions of polypropylene chains in amorphous regions ordered by the constraints exerted by crystallites.

For the processes isolated at 30 and 35°C, the retardation times can be described by a Vogel equation (*Eq 4*) with $\tau_{o\infty} = 26$ and 13 sec., $\alpha = 4.10^{-2}$ and 2.10^{-2}, and $T_\infty = 11°C$ in both cases. These processes have been attributed to the free volume expansion. For the other composition, the parameters were decreasing when the PE content increased: in the 20/80 PE-PP blend, for example, $T_\infty = -18°C$. The thermal expansion coefficient of the free volume remains at least ten times higher than the empirical WLF value. These processes have been attributed to the liquid-liquid transition of amorphous polypropylene chains (20–22).

POLYETHYLENE-POLYPROPYLENE BLOCK COPOLYMERS

Complex TSC Spectra

Figure 4 shows the TSC spectra of the 6/94 PE-PP block copolymer under a shear stress, $\sigma = 0.5$ MPa, applied to the temperatures indicated by the small arrows in the *figure*. The solid line corresponds to a sample annealed for 115 hours at room temperature; the dashed line to a sample quenched from 100°C to liquid nitrogen temperature. The TSC peak observed around −150°C has been assigned to polyethylene sequences (5, 12–17).

As for the peak at 3°C, it looks like the one observed in blends or in polypropylene; it is probably due to polypropylene sequences. The additional peak around −50°C has been compared with the peak obtained for ethylene-propylene-rubber (EPR) (cf. *Fig. 5*): the former peak is observed 10° lower than the latter. For ascertaining the above hypothesis, a detailed study of the TSC spectra has been performed.

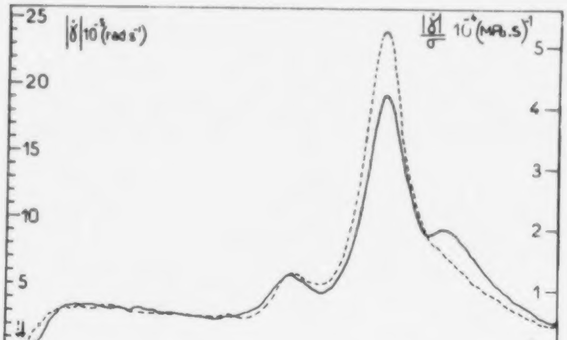

Fig. 4. TSC spectra of the 6/94 PE-PP block copolymer:
——annealed,
- - -quenched.

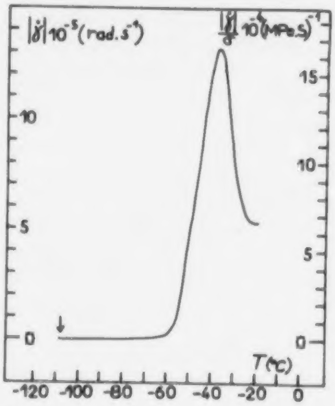

Fig. 5. TSC spectrum of ethylene propylene rubber.

FINE STRUCTURE OF TSC SPECTRA

Fractional stresses have been applied to resolve the complex TSC spectra. The temperature dependence of the retardation times isolated in the peak at −50°C is given by a compensation law (cf. *Eq 5*) with $T_c = -54°C$ and $\tau_c = 19$ sec. The above behavior, which is characteristic of a glass transition, has been attributed to microbrownian motions of EPR chains under constraints from the polypropylene matrix. In fact, this EPR interphase is responsible for the high performances of these materials (28–32). The TSC peak observed at 3°C has been also resolved into elementary processes which are characterized by retardation times plotted *vs.* the reciprocal temperature on the Arrhenius diagram of *Fig. 6*. The small arrows indicate the temperatures of the TSC maximum.

Contrary to the homopolymers and the PE-PP blends, all the retardation times isolated in copolymers are well described by an Arrhenius equation (*Eq 2*). The corresponding parameters have been listed in *Table 2*. Moreover the six processes situated between −12 and 4°C follow a compensation law (*Eq 5*) with $\tau_c = 2.3\,10^{-2}$ sec. and $T_c = 39°C$. This behavior is characteristic of the low temperature component of the glass transition of polypropylene sequences. The high temperature component of this peak is only observed after annealing. As it is characterized by relatively low activation entropies, it has been assigned to the high temperature component of the glass transition of polypropylene sequences due to microbrownian motions in ordered amorphous regions i.e. in the intercrystallite zones.

ETHYLENE PROPYLENE RANDOM COPOLYMERS

Complex TSC Spectra

Figure 7 shows the TSC spectra of the 2.5/97.5

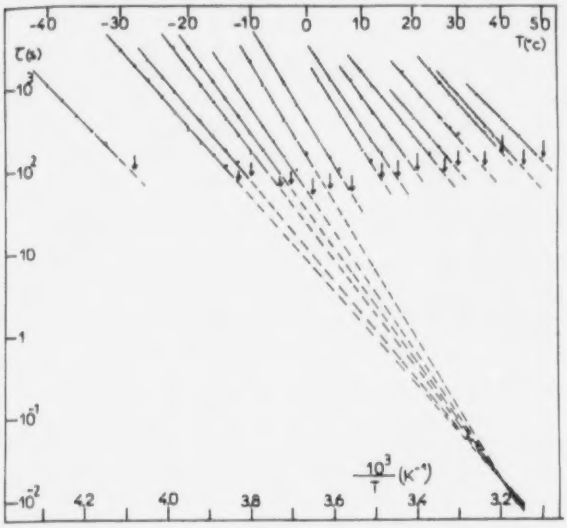

Fig. 6. Arrhenius diagram of the retardation times characterizing the "elementary" TSC peaks isolated in the 6/94 PE-PP block copolymer.

Table 2. Parameters of retardation times following the Arrhenius equation (*Eq. 2*) in 6.94 ethylene-propylene block copolymer.

T_M (°C)	ΔH(eV)	τ_{0M} (sec)
−61	0.62	1.5×10^{-13}
−60	0.86	4.1×10^{-19}
−57	1.06	6.7×10^{-24}
−50	1.02	2.6×10^{-22}
−43	0.95	1.2×10^{-19}
−28	1.05	2.0×10^{-20}
−12	1.12	1.7×10^{-20}
−10	1.17	3.1×10^{-21}
−5	1.29	4.2×10^{-23}
−3	1.37	1.5×10^{-24}
1	1.48	2.5×10^{-26}
4	1.66	3.1×10^{-29}
8	1.65	1.1×10^{-28}
14	1.60	6.6×10^{-27}
17	1.50	7.4×10^{-25}
21	1.42	4.1×10^{-23}
27	1.21	3.5×10^{-19}
30	1.20	1.0×10^{-18}
36	1.13	3.7×10^{-17}
40	1.13	1.0×10^{-16}
45	1.13	1.2×10^{-16}
50	1.00	2.7×10^{-14}

PE-PP random copolymer after annealing 115 hours at room temperature (dashed line). A shear stress of $\sigma = 0.2$ MPa has been applied at the temperatures indicated by the arrows in the *figure*. Since it was difficult to determine the low temperature peak (associated with ethylene segments) a complementary experiment, performed with an applied stress of $\sigma = 6$ MPa, proved its existence at −145°C. So, only a few ethylene groups are involved in this mechanism which is generally associated with the glass transition of ethylene segments (33).

The peak observed around 2°C due to polypropylene is much more intense in random copolymers than in the polypropylene, in blends or in block copolymers. This result is due to low crystallinity of random copolymers. If the copolymer was annealed for 115 hours at room temperature, the peak had two components but only one if it was quenched before the experiment (cf. *Fig. 7*). This behavior is characteristic of the double glass transition of polypropylene (18). These findings will be confirmed by the study of the fine structure of this double TSC peak.

FINE STRUCTURE OF TSC SPECTRA

The temperature dependence of the retardation times isolated in the peak at 2°C are well described by the Arrhenius equation (*Eq* 2). Moreover, the TSC peaks isolated between −16 and −4°C are characterized by retardation times following a compensation law (*Eq* 5) with $T_c = 12$°C and $\tau_c = 0.35$ sec. This component that has been observed at lower temperature than in blends or block copolymers, is also associated with the lowest compensation temperature. Polyethylene sequences might be responsible for the observed plasticization of the mechanical energy loss peak associated with the low temperature component of the glass transition.

The peak observed at 50°C as a shoulder of the preceding one has the same behavior as the ones observed in the same temperature range in blends and block copolymers. It has also be assigned to the microbrownian motions of polypropylene segments in amorphous regions under constraints from crystallites. Nevertheless, the activation entropies obtained in random copolymers are significantly higher than for blends or block copolymers: the constraints exerted on this amorphous phase are the lowest in random copolymers.

DISCUSSION

The morphology of the amorphous phase of ethylene-propylene blends and copolymers has been studied by thermostimulated creep. From the anelastic behavior of these materials, the existence of four amorphous phases has been deduced: polyethylene, free polypropylene, constrained polypropylene, and EPR interphase. Each phase can be identified from its anelastic loss peak associated with its glass transition.

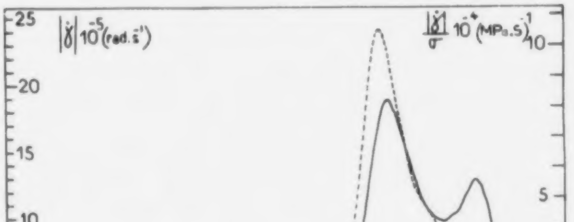

Fig. 7. TSC spectra of the 2.5/97.5 PE-PP random copolymer:
——annealed,
- - -quenched.

Amorphous Polyethylene Phase

The amorphous polyethylene chains are responsible for the small TSC peak observed around −145°C for ethylene contents higher than 5 percent in copolymers and than 20 percent in blends. This peak has been attributed to microbrownian motions of ethylenic sequences free from constraints.

Free Amorphous Polypropylene Phase

The free amorphous polypropylene phase is characterized by the most intense TSC peak observed around 0°C namely, the homopolymer. This component is characterized by retardation times following a compensation law: the higher compensation temperature is obtained in block copolymers.

These TSC peaks have been assigned to microbrownian motions of free amorphous propylenic sequences.

Constrained Amorphous Polypropylene Phase

The constrained amorphous polypropylene phase is responsible for the shoulder of the TSC peak at 0°C which is only observed after annealing for 16 hours at room temperature; in fact, the order induced by constraints exerted by crystallites on this phase, vanishes at 100°C, so this phase is no longer observed after quenching to liquid nitrogen temperature. This unstable phase might be located between crystallites in the polypropylene spherulites. Note that this phase has been found to be less ordered in random copolymers.

Amorphous Interphase

It is responsible for the TSC peak observed around −50°C only in block copolymers. It is important to note that a dielectric loss peak was also observed at the same frequency in the same temperature range. This peak is comparable with the one associated with the glass transition of pure EPR, except for its temperature position; it is shifted towards lower temperature in a significant manner (10^9). So, we might think that the amorphous phase responsible for the TSC peak observed in block copolymers is constituted by an EPR matrix interpenetrated by propylene and ethylene sequences. Such interpenetration of different chains have been found to produce intermediate phases responsible for additional proceses in bi and triblock styrene-isoprene copolymers (34–36). The observed EPR-polypropylene couplings might be attributed to the existence of an intermediate phase resulting from the diffusion of propylene and ethylene sequences in EPR.

REFERENCES

1. D. R. Paul and S. Newman, "Polymer Blends," Academic Press, New York (1978).
2. J. A. Manson and L. H. Sperling, "Polymers Blends and Composites", Plenum Press, New York, (1976).
3. O. Olabisi, L. M. Robeson, and M. T. Shaw, "Polymer-Polymer Miscibility", Academic Press, New York, (1979).
4. A. Plochocki, *Kolloid Z. Z. Polym.*, **208,** 168 (1966).
5. J. L. Zakin, R. Simha, and H. Herskey, *J. Appl. Polym. Sci.*, **10,** 1455 (1966).
6. M. Kryszewski, A. Galeski, T. Pakula, and J. Grebowicz, *J. Coll. Interf. Sci.*, **44,** 85 (1973).
7. O. F. Noel and J. F. Carley, *Polym. Eng. Sci.*, **15,** 117 (1975).
8. R. Deanin and M. F. Sansone, *Polym. Prepr. Am. Chem. Soc. Div. Polym. Chem.* **19,** 211 (1978).
9. A. J. Lovinger and M. L. Williams, *J. Appl. Polym Sci.*, **25,** 1703 (1980).
10. J. C. Monpagens, D. Chatain, and C. Lacabanne, *J. Polym. Sci. Polym. Phys. Eds.*, **15,** 67 (1977).
11. C. Lacabanne, D. Chatrain, and J. C. Monpagens, *J. Macromolec. Sci. Phys.*, **B13,** 537 (1977).
12. C. A. Tuijnman, *J. Polym. Sci. Part C*, **16,** 2379 (1967).
13. R. W. Gray and N. G. Mac Crum, *J. Polym. Sci. Part A2*, 7, 1329 (1969).
14. F. C. Stehling and L. Mandelkern, *Macromolecules*, **3,** 242 (1970).
15. K. H. Illers, *Colloid Polym. Sci.*, **252,** 1 (1974).
16. C. L. Beatty and F. E. Karasz, *J. Macromol. Sci. Rev. Macromol. Chem.* C, **17,** 37 (1979).
17. D. Ronarc'h, *Appl. Phys. Lett.* **37,** 707 (1980).
18. Y. Wada, Y. Hotta, and R. Suzuki, *J. Polym. Sci. Part C*, **23,** 583 (1968).
19. I. Inamura, H. Ochiai, and H. Yamamura, *J. Polym. Sci Polym. Phys. Ed.*, **14,** 1221 (1976).
20. Ph. Demont, D. Chatain, T. Elsayed, C. Lacabanne, D. Ronarc'h, and J. L. Moura, *J. Physiqur, C5 suppl. 10*, **42,** 563 (1981).
21. R. F. Boyer, "Encyclopedia of Polymer Science and Technology", suppl. Vol. II, 745–839 J. Wiley, (1977).
22. M. Jarrigeon, B. Chabert, D. Chatain, C. Lacabanne, and G. Nemoz, *J. Macromol. Sci. B*, **17,** 1 (1980).
23. C. Lacabanne, D. Chatain, T. Elsayed, D. Broussoux, and F. Micheron, *Ferroelectrics*, **30,** 307 (1980).
24. T. Elsayed, J. Elhout, B. Francqis, C. Mathis, D. Chatain, and C. Lacabanne, *J. Physique* (to be published).
25. P. Berticat, AiBui, Hoang The Giam, D. Chatain, and C. Lacabanne, *Makromol. Chem.*, **177,** 1583 (1977).
26. C. Lacabanne, D. Chatain, J. C. Monpagens, A. Hiltner, and E. Baer, *Solid State Commun.*, **27,** 1055 (1978).
27. T. Elsayed, D. Chatain, and C. Lacabanne, "Rheology" Vol. III, Applications, G. Astarita, G. Marucci, and L. Nicolais ed. Plenum Press, New York (1981).
28. J. J. Maurer, *Rubber Chem. Technol.*, **38,** 979 (1965).
29. S. Onogi, T. Asada, and A. Tanaka, *J. Polym. Sci., Part A.2*, **7,** 171 (1969).
30. M. Kryszewski, A. Galeski, T. Pakula, J. Grebowicz, and P. Milczarek, *J. Appl. Polym. Sci.*, **15,** 1139 (1971).
31. F. C. Stehling, T. Huff, C. S. Speed, and G. Wissler, *J. Appl. Polym. Sci.*, **26,** 2693 (1981).
32. M. Kojima, *J. Macromol. Sci., Phys.*, **B19,** 523 (1981).
33. F. P. Reading, J. A. Faucher, and P. D. Whitman, *J. Polym. Sci.*, **57,** 483 (1982).
34. T. Soen, M. Shimomura, T. Uchida, and H. Kawai, *Colloid Polym. Sci.*, **252,** 933 (1974).
35. T. Hashimoto, M. Fujimura, K. Saijo, H. Diamant, and M. Shen, *Adv. Chem. Sci.*, **176,** 257 (1979).
36. A. Todo, H. Uno, K. Miyoshi, T. Hashimoto, and H. Kawai, *Polym. Eng. Sci.*, **17,** 587 (1977).

DISCUSSION

M. Winnik: I am confused—what corresponds to the upper and the lower glass transition temperature?

C. Lacabanne: The physicists who are studying these phenomena are assigning the upper glass transition peak as due to the amorphous phase with some sort of order. It is well-known that for semicrystalline materials there are not only two main phases—the crystalline and amorphous ones, but also the interphase. In this situation one can talk of the interphase in two senses—first, in the same sense as colloid scientists will talk about interphase in block polymers, and second, in a purely physical sense where the amophous phase is subjected to stresses and, as a result, forced into a semi-ordered structure. In fact, this is confirmed by the values of conformational entropies. This concept is very helpful in discussing these meta-stable systems. It seems that there are various types, or various structures of amorphous phases, which may be taken as a measure of the meta-stability.

M. Winnik: What is the T_g of isotactic polypropylene?

C. Lacabanne: Around room temperature. For atactic it is slightly lower—around 0°C.

J. Noolandi: To what degree do these transition temperatures correlate with the transitions in viscoelastic properties? Is there any correlation between what you are measuring in the amorphous phases and the overall measurements of the storage and loss moduli?

C. Lacabanne: Yes, we made this correlation. From our experiments we directly obtain the compliance and the spectrum of retardation times, from which we can get the other spectra. We compared our results with those obtained from dynamic and static experiments in the experimental range of variables and we found good consistent agreement. However, it is always difficult to extrapolate outside the range of measured variables. We have some troubles with polyethylene for which we observed a drastic drop in retardation time spectrum which makes extrapolation and prediction rather difficult. But, in fact, this has been known for some time from dielectric measurements—the T_g does not shift with frequency as one may expect. Excepting these few problems we can reconstruct the mechanical, or viscoelastic, spectra from our data with good accuracy. We can get the mechanical surfaces in good agreement with static or dynamic methods.

L. A. Utracki: This seems to be a very useful technique. If I understand correctly, you are able to measure both the stress recovery and the creep, and calculate the same relaxation, or retardation, spectrum from both of these.

C. Lacabanne: In order to analyze the curve we have to perform the recovery. But we can cross-check the whole complex spectrum obtained either by creep or by recovery. We cannot perform the analysis of the spectrum in creep because we still have a small contribution of the flow. If we wanted to use creep we would have to substract this effect, which is a difficult and uncertain thing to do. We prefer to draw the Arrhenius pattern from the recovery. For the complex spectrum we have something that fits quite nicely. We are applying strains of less than 10^{-3}, i.e., we are well within the linear region.

L. A. Utracki: Pursuing Prof. Winnick's question: you are referring to all the peaks as glass transition temperatures, the upper and lower belonging to polyethylene, to polypropylene or EPR rubber. You consider all these peaks as indication of nothing but glass transitions. Now, two questions: first, can you see any so-called β-peaks? Second, we how that Raymond Boyer has been fighting for his liquid/liquid transitions for years; can you say which of these upper and lower transitions belong to the T_{LL} groups?

C. Lacabanne: To answer the first question—yes, we have in fact investigated the secondary transition. However, here we were concerned only with the glass transitions because the point was to see differences associated with segregation of polyethylene and polypropylene. This is the reason why we have not investigated other transitions. We can look for the secondary transition and we can see them, of course. In regard to the second question, in semi-crystalline materials, by this method we generally see two components around the glass transition temperature. Of course, in a completely amorphous material we see only one T_g, so it is simpler to take an amorphous material and see where the liquid/liquid transition is. In fact, for example we take a PMMA, we will detect a glass transition and an additional peak some 50°C higher. We performed the thermally stimulated current study of PMMA and this peak at high temperature was found to follow the Vogle equation, i.e., it had the same behavior as the liquid/liquid transitions observed by Boyer, so we have identified it as a liquid/liquid transition temperature. However, afterwards there was a strong controversy around this problem and some postulated that what we saw was an artifact of space charges. This is why, in fact, we have performed the mechanical experiments and now we can say that this peak was observed by both methods; it was not associated with irreversible flows, neither was it associated with the space charges. It looks to us as if this is a true transition. We can call it the liquid/liquid transition or anything else, but it is there. From these kinds of experiments we see that the manner in which these transitions behave allows us to identify them through their temperature dependence which follows the Vogle equation. For semi-crystalline materials below T_{LL} we have the two components of the glass transition at lower temperatures.

L. A. Utracki: PMMA is not a very good system for testing this. I think that you must have various lengths of isomeric sequences in PMMA. Somebody will always say that the upper transition may be associated with the presence of stereo-segments in the material. Did you see anything of this sort in strictly amorphous polymer?

C. Lacabanne: We have also investigated polystyrene. If I mentioned PMMA as an example it is because currently we have some problems with polystyrene. To us polystyrene seems to be more complicated than PMMA. It depends on the kind of experiments you are doing.

M. Winnik: This seems to me a very interesting technique that lends itself to analogous kinds of studies that look at free volume in a more direct way. For example, there are a number of studies using spin label probes by ESR spectroscopy especially at the Jet Propulsion Laboratories and also some fluorescent studies at Xerox and some earlier work in our laboratories, where you look either at fluorescence intensities or fluorescence lifetime of a molecule in a polymer matrix. The presence of free volumes allows the molecules to move or be quenched. It affects their lifetime or intensity of emission, so you get some microscopic 10 Å resolution—again a picture of what is happening to the free volume. It seems that you might be able to dope your films with 10^{-2} percent of some probe either as a spin label or luminescence probe that would be sensitive to the β-transition or to the various glass transitions that you observe mechanically.

C. Lacabanne: I agree, it would be a nice experiment.

G. Delmas: If I understood correctly, in one of the samples that you studied you had four components: polyethylene, polypropylene, and copolymers. In chemistry, usually when you have such a mixture either you try to separate, to make the system simpler or, if you cannot because it is too difficult, you add a bit of one component and in this way you see the peak for this component increase. This method is useful for identification. Have you tried this?

C. Lacabanne: Yes, we are just doing this kind of work. First of all, we have extracted the EPR by using xylene and from these data we might be able to get a quantitative interpretation of the shift of the peak. That is the first point. We are also extracting the atactic polypropylene (there is always a small fraction of it present) just to look at the response of this material. This is also coherent with the true atactic material. It is evident that the shift of the various components in the copolymer shows that there is no segregation of the various phases; there is a small penetration of the atactic chains into EPR, of the ethylene chains into EPR, and so on—so various phases are not segregated at all. But this work is now in progress. We have also performed other binary blends by using, for example, EPR and polypropylene and just having the physical blends of these two materials.

G. Delmas: And you can obtain an estimation of the amount of each component you have in your mixture?

C. Lacabanne: That would be more difficult. Perhaps in future, but to date it is still quite difficult.

The Composition-Dependent Glass Transition: Relations Between Temperature, Pressure, and Composition

P. R. COUCHMAN

Department of Mechanics and Materials Science
College of Engineering
Rutgers-The State University of New Jersey
Piscataway, New Jersey 08854

A new predictive relation between pressure and temperature changes on the glass-transition boundary is derived for random solutions. The isobaric version of this relation is integrated to recover a previous theory for the compositional variation of glass-transition temperatures. The isothermal form of the differential equation gives an equation for the compositional variation of glass-transition pressures. An enthalpic definition of the transition boundary provides a relation between excess enthalpies of mixing for the glassy and liquid states for the isobaric and isothermal transitions. Similarly, a definition of the boundary in terms of the solution volume provides a relation between excess volumes of mixing for these two states for the isobaric and isothermal transitions. The primary entropic equation for the composition-dependent isobaric transition gives two hierarchies of approximation, one of which is shown to be preferred for physical reasons. A parallel situation arises for the isothermal transition.

INTRODUCTION

A thermodynamic theory for the composition-dependent isobaric glass transition by the present author has provided, for random solutions, a general method for the calculation of their glass-transition temperatures, T_g, and associated transition increments of heat capacity, ΔC_p, from corresponding properties of the pure components. Solutions and phenomena to which the theory has been applied include: miscible blends of high polymers (1–4); the effect of degree of polymerization on T_g (5–7); the combined variation of blend glass-transition temperatures and increments of heat capacity with overall composition and pure-component molecular mass (8); plasticized linear (9, 10) and network (11) polymers; the effect of cross-link density on T_g (12), and the effect of copolymerization on glass-transition temperatures (13). A more general problem, of which the compositional variation of the isobaric glass-transition constitutes part, is the dependence of the solution glass-liquid boundary on temperature, pressure, and composition. A subsequent section of this paper outlines a thermodynamic description of this problem.

The new theory proceeds from an entropic definition of the solution glass-transition boundary, given in differential form, to a predictive differential relation between temperature and pressure. The isobaric form of this primary equation of the theory can be integrated to recover a previous, related theory for the compositional variation of glass transition temperatures, but by a more direct and compact method. Integration of the isothermal form of the differential equation gives a relation for the compositional variation of glass-transition pressures. For binary solutions, two equations for the coefficient $\partial lnT/\partial lnP$ can be derived and, when compared, give a consistency condition. A comparison between theory and experiment is presented for the isobaric transition for a variety of solutions and for two phenomena within the overall topic of the compositional variation of T_g.

Following these tests of the entropic theory, the solution glass-transition boundary is defined in terms of the solution enthalpy to give relations between excess enthalpies of mixing in the glassy and liquid states for the isobaric transition and for the isothermal transition. Similarly, excess volumes of mixing in the liquid and glassy states are shown to be connected. A comparison of equations obtained from the entropic, enthalpic, and volume-based definitions of the glass-transition boundary demonstrates the relative merit of the two hierarchies of approximation to principal entropic equations for the isobaric and isothermal transitions.

ENTROPIC THEORY

The glass-transition boundary for the solution in temperature-pressure composition $(T - P - X_i)$ space is defined as the set of points for which the entropy of the liquid state, $S^l(T, P, X_i)$, is equal to the entropy of the glassy state, $S^g(T, P, X_i)$. Both S^l and S^g can be written as linear combinations of composition-weighted pure-component entropies,

S_i, and an excess entropy of mixing. For random mixtures, the excess enthalpy and volume of mixing are generally finite and change discontinuously at the glass transition. The excess entropy of mixing, finite except for high polymers (for which it is vanishingly small), is by contrast essentially continuous as the glass transition is traversed.

At fixed but arbitrary composition, the glass-transition boundary for a random solution with c components satisfies the pure-component differential condition

$$\sum_{i=1}^{c} X_i d(S_i^l - S_i^g) = 0 \tag{1}$$

A relation between changes of temperature and pressure on the glass-transition boundary can be derived directly from *Eq 1* and is

$$\sum_{i=1}^{c} X_i \Delta C_{p_i} dlnT + \sum_{i=1}^{c} X_i \Delta C_{T_i} dlnP = 0 \tag{2}$$

In *Eq 2* the ΔC_{p_i} denote pure-component glass-transition increments of heat capacity and the $\Delta C_{T_i} = \Delta \partial S_i/\partial lnP)_T$ their isothermal analogues.

The Isobaric Glass-Transition

If *Eq 2* is integrated at arbitrary but fixed pressure and the boundary conditions $T_g \equiv T_{g_i}$ at $X_i = 1$ are used, in the temperature-independent approximation for the ΔC_{p_i} a previous equation for the compositional variation of glass-transition temperatures (1, 2) is recovered. The denominator of this equation,

$$lnT_g = \frac{\Sigma X_i \Delta C_{p_i} lnT_{g_i}}{\Sigma X_i \Delta C_{p_i}} \tag{3}$$

is ΔC_p for the solution. The symbol Σ is used to indicate the sum over all components of the solution. As discussed later, temperature dependent pure-component heat-capacity increments can be incorporated in the theory through *Eq 2*.

For binary systems the derivative of *Eq 3* with respect to composition,

$$\frac{\partial lnT_g}{\partial X_2} = \frac{\Delta C_{p_1} \Delta C_{p_2} lnT_{g_2}/T_{g_1}}{(X_1 \Delta C_{p_1} + X_2 \Delta C_{p_2})^2} \tag{4}$$

demonstrates that in the absence of compound formation the solution glass transition temperature is monotonic in composition. The second derivative of *Eq 3* with respect to composition,

$$\frac{\partial^2 lnT_g}{\partial X_2^{\,2}} = \frac{2(\Delta C_{p_1} - \Delta C_{p_2}) \Delta C_{p_1} \Delta C_{p_2} lnT_{g_2}/T_{g_1}}{(X_1 \Delta C_{p_1} + X_2 \Delta C_{p_2})^3} \tag{5}$$

indicates that if $T_{g_2} > T_{g_1}$, lnT_g is a concave function of X_2 if, also (as typically then occurs), $\Delta C_{p_2} < \Delta C_{p_1}$. If, however, $T_{g_2} > T_{g_1}$ and $\Delta C_{p_2} > \Delta C_{p_1}$, then lnT_g is a convex function of X_2. If $\Delta C_{p_1} = \Delta C_{p_2}$, lnT_g is linear in composition.

The Isothermal Glass-Transition

At a given composition at fixed temperature, the thermodynamic transition variable is the glass-transition pressure, P_g. In a manner analogous to the derivation of *Eq 3*, the isothermal version of *Eq 2* is integrated in the pressure-independent approximation for the ΔC_{T_i} and the boundary conditions are used to give

$$lnP_g = \frac{\Sigma X_i \Delta C_{T_i} lnP_{g_i}}{\Sigma X_i \Delta C_{T_i}} \tag{6}$$

The pressure-dependence of the ΔC_{T_i} can be included in the theory, for example by writing these as polynomials in pressure. The denominator of *Eq 6* is the transition increment of C_T for the solution,

$$\Delta C_T = \Sigma X_i \Delta C_{T_i} \tag{7}$$

Somewhat more convenient forms of *Eqs 6* and *7* are obtained by the use of a Maxwell relation, from which

$$\Delta C_{T_i} \equiv -P\Delta(V_i\alpha_i) \tag{8}$$

where V_i, α_i are in turn pure-component volumes and isobaric volume expansitivities. The approximation of the ΔC_{T_i} as pressure-independent and the evaluation of the $\Delta(V_i\alpha_i)$ at a common pressure allow *Eqs 6* and *7*, respectively, to be written as

$$lnP_g = \frac{\Sigma X_i \Delta(V_i\alpha_i) lnP_{g_i}}{\Sigma X_i \Delta(V_i\alpha_i)} \tag{9}$$

and

$$-\frac{1}{P}\Delta C_T = \Delta\left(\frac{\partial V}{\partial T}\right) = V\Delta\alpha = \Sigma X_i \Delta(V_i\alpha_i) \tag{10}$$

Strictly, the increments $\Delta(V_i\alpha_i)$ of *Eqs 8* to *10* must be evaluated at the temperature at which the isothermal transition occurs. In practice, this necessitates extrapolating volumetric properties of the pure-component liquid and glassy states. To lesser (zero'th) order, the $\Delta(V_i\alpha_i)$ of *Eqs 9* and *10* may be approximated by increments at the T_{g_i} and some common pressure.

For binary solutions, the derivative

$$\begin{aligned}\frac{\partial lnP_g}{\partial X_2} &= \frac{\Delta C_{T_1} \Delta C_{T_2} lnP_{g_2}/P_{g_1}}{[X_1 \Delta C_{T_1} + X_2 \Delta C_{T_2}]^2} \\ &= \frac{\Delta(V_1\alpha_1)\Delta(V_2\alpha_2) lnP_{g_2}/P_{g_1}}{[X_1\Delta(V_1\alpha_1) + X_2\Delta(V_2\alpha_2)]^2}\end{aligned} \tag{11}$$

demonstrates the absence of absolute extrema in P_g. The compositional curvature of the dependence described by *Eq 9* can be determined from the expression

$$\frac{\partial^2 lnP_g}{\partial X_2^{\,2}} = \frac{\begin{array}{r}2[\Delta(V_1\alpha_1) - \Delta(V_2\alpha_2)]\Delta(V_1\alpha_1) \\ \cdot\Delta(V_2\alpha_2) lnP_{g_2}/P_{g_1}\end{array}}{[X_1\Delta(V_1\alpha_1) + X_2\Delta(V_2\alpha_2)]^3} \tag{12}$$

The present theory is applicable to all phenomena which can be modeled in terms of random solutions. To consider for instance the molecular-mass dependence of P_g, homopolymers of degree of polymerization n are modeled as binary solutions of an oligomer, degree of polymerization m, and n-m mers with properties of the high polymer (5–8). Glass-transition properties of these components are denoted in turn by subscripts m, ∞ to give, for monomolecular polymers,

$$lnP_g = \frac{(n\text{-}m)\Delta(V_\infty\alpha_\infty)lnP_{g_\infty} + m\Delta(V_m\alpha_m)lnP_{g_m}}{(n\text{-}m)\Delta(V_\infty\alpha_\infty) + m\Delta(V_m\alpha_m)} \qquad (13)$$

For polymolecular systems, n would be the number-average degree of polymerization. The effect of compound formation on glass-transition pressures can also be included in the theory. For example, the effect of copolymer composition on P_g can be accounted for by a formal description of these as random mixtures of the three kinds of mer pairs (13), fractions of which are denoted as f_{ii}, f_{jj}, f_{ij}. Similar use of subscripts to distinguish in turn properties of the associated homopolymers and of the fully alternating copolymer give, from *Eq 9*,

$$lnP_g = \frac{f_{ii}\Delta(V_{ii}\alpha_{ii})lnP_{g_{ii}} + f_{ij}\Delta(V_{ij}\alpha_{ij})lnP_{g_{ij}} + f_{jj}\Delta(V_{jj}\alpha_{jj})lnP_{g_{jj}}}{f_{ii}\Delta(V_{ii}\alpha_{ii}) + f_{ij}\Delta(V_{ij}\alpha_{ij}) + f_{jj}\Delta(V_{jj}\alpha_{jj})} \qquad (14)$$

with $V\Delta\alpha$ for the copolymer the denominator of this relation. Conditions for the occurrence of absolute compositional extrema in P_g and $\Delta(V\alpha)$ can be derived by writing the dyad fractions in *Eq 14* as a function of the fraction, f_i, of i mers in the copolymer feed and the monomer reactivity ratios, r_i, r_j, and proceeding as in (13). A considerable simplification of the analysis occurs for ideal azeotropic copolymerizations ($r_i = r_j = 1$) for which $P_{g_{ii}} \simeq P_{g_{jj}}$ and $\Delta(V_{ii}\alpha_{ii}) \simeq \Delta(V_{jj}\alpha_{jj})$. Both the copolymer glass transition pressure and transition increment of $V\alpha$ then pass through an extremum, at $f_i = 1/2$, with values given in turn by

$$lnP_g^* = \frac{\Delta(V_{ii}\alpha_{ii})lnP_{g_{ii}} + \Delta(V_{ij}\alpha_{ij})lnP_{g_{ij}}}{\Delta(V_{ii}\alpha_{ii}) + \Delta(V_{ij}\alpha_{ij})} \qquad (15)$$

and

$$\Delta(V\alpha)^* = \frac{\Delta(V_{ii}\alpha_{ii}) + \Delta(V_{ij}\alpha_{ij})}{2} \qquad (16)$$

Differential Changes of Temperature and Pressure

From *Eqs 2* and *8*,

$$\frac{\partial lnT}{\partial lnP} = -\frac{\Sigma X_i\Delta C_{T_i}}{\Sigma X_i\Delta C_{p_i}} = \frac{P\Sigma X_i\Delta(V_i\alpha_i)}{\Sigma X_i\Delta C_{p_i}} \qquad (17)$$

which can be rewritten as $\partial lnT/\partial P = \Sigma X_i\Delta\cdot(V_i\alpha_i)/\Sigma X_i\Delta C_{p_i}$. For $X_i = 1$, Ehrenfest relations are obtained for the pure components. For binary solutions, the compositional first derivative of *Eq 17* is

$$\frac{d}{dX_2}\left(\frac{\partial lnT}{\partial lnP}\right) = -\left[\frac{\Delta C_{p_1}\Delta C_{T_2} - \Delta C_{p_2}\Delta C_{T_1}}{[X_1\Delta C_{p_1} + X_2\Delta C_{p_2}]^2}\right]$$
$$= P\left[\frac{\Delta C_{p_1}\Delta(V_2\alpha_2) - \Delta C_{p_2}\Delta(V_1\alpha_1)}{[X_1\Delta C_{p_1} + X_2\Delta C_{p_2}]^2}\right] \qquad (18)$$

An alternative form of *Eq 17* for binary solutions can be derived from *Eqs 4* and *11* and the relation

$$\left.\frac{\partial T}{\partial P}\right)_{X_2} = -\left.\frac{\partial X_2}{\partial P}\right)_T \Big/ \left.\frac{\partial X_2}{\partial T}\right)_P \qquad (19)$$

and is

$$\frac{\partial lnT}{\partial lnP} = -\left[\frac{X_1\Delta C_{T_1} + X_2\Delta C_{T_2}}{X_1\Delta C_{p_1} + X_2\Delta C_{p_2}}\right]^2\left[\frac{\Delta C_{p_1}\Delta C_{p_2}lnT_{g_2}/T_{g_1}}{\Delta C_{T_1}\Delta C_{T_2}lnP_{g_2}/P_{g_1}}\right]$$
$$= -\left[\frac{X_1\Delta(V_1\alpha_1) + X_2\Delta(V_2\alpha_2)}{X_1\Delta C_{p_1} + X_2\Delta C_{p_2}}\right]^2 \cdot\left[\frac{\Delta C_{p_1}\Delta C_{p_2}lnT_{g_2}/T_{g_1}}{\Delta(V_1\alpha_1)\Delta(V_2\alpha_2)lnP_{g_2}/P_{g_1}}\right] \qquad (20)$$

A comparison of *Eqs 17* and *20* gives the consistency condition

$$\frac{X_1\Delta C_{T_1} + X_2\Delta C_{T_2}}{X_1\Delta C_{p_1} + X_2\Delta C_{p_2}} = \frac{\Delta C_{T_1}\Delta C_{T_2}lnP_{g_2}/P_{g_1}}{\Delta C_{p_1}\Delta C_{p_2}lnT_{g_2}/T_{g_1}} \qquad (21)$$

or, equivalently,

$$P = -\left[\frac{X_1\Delta(V_1\alpha_1) + X_2\Delta(V_2\alpha_2)}{X_1\Delta C_{p_1} + X_2\Delta C_{p_2}}\right]\left[\frac{\Delta C_{p_1}\Delta C_{p_2}lnT_{g_2}/T_{g_1}}{\Delta(V_1\alpha_1)\Delta(V_2\alpha_2)lnP_{g_2}/P_{g_1}}\right] \qquad (22)$$

COMPARISON OF THEORY AND EXPERIMENT

The theory accounts well for the atmospheric-pressure glass-transition in miscible or compatible blends of polymers (1–4, 8) and, typically, *Eq 3* is sufficiently accurate. *Figures 1* and *2* compare values of T_g given by *Eq 3* to experimental glass-transition temperatures for miscible blends of polystrene (PS) with, in turn, poly(2,6-dimethyl-

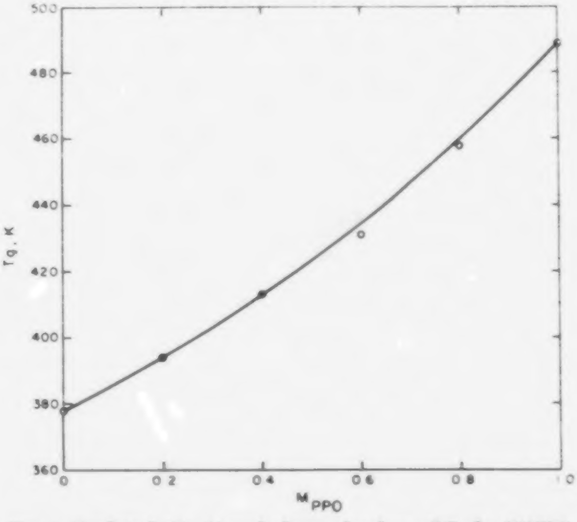

Fig. 1. Predicted (Eq 3) and observed values of T_g for PS/PPO blends vs. mass fraction of PPO. Reproduced with permission from (2).

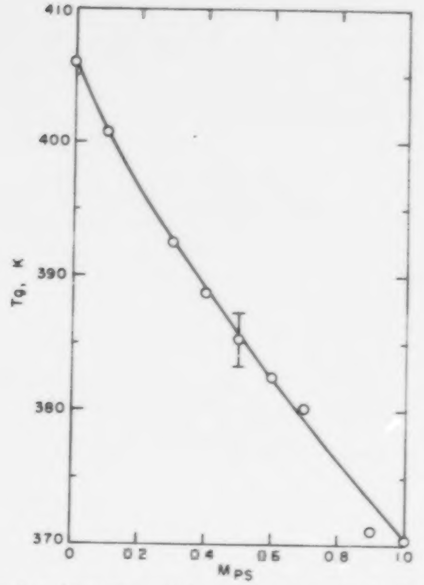

Fig. 2. *Predicted (Eq 3) and observed values of T_g for PS/P-2ClS blends vs. mass fraction of PS. Reproduced with permission from (4).*

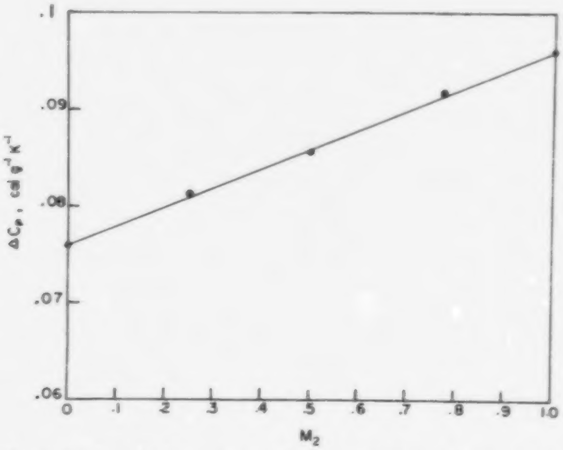

Fig. 3. *Predicted (denominator of Eq 3) and observed (15) values of ΔC_p for PMMA/PSAN blends vs. mass fraction of PSAN.*

1,4-phenylene oxide) (PPO) and poly(2-chlorostyrene) (P-2 C*l*S). *Figure 3* shows that the denominator of *Eq 3* is in good agreement with the experimental value of ΔC_p for compatible blends of poly(methyl methacrylate) (PMMA) with poly(styrene-co-acrylonitrile) (PSAN). For miscible blends of PS with poly(α-methylstyrene) (PαMS) Lau, *et al.* (14) found it necessary to include the temperature-dependence of the ΔC_{p_i} for the predicted glass-transition temperatures to agree with the experimental data. In contrast, Leisz, *et al.* (3) found that their T_g data for PS/PαMS blends is well-accounted for by *Eq 3*. Regardless of the position of PS/PαMS blends in relation to *Eq 3*, it is to be expected that the approximation of the ΔC_{p_i} as temperature-independent might not always be acceptable.

A first-order modification of the principal equation for T_g can be obtained by use of an explicit expression for the ΔC_{p_i} as a function of temperature in the isobaric form of *Eq 2*. If, for example, the first two terms of a typical polynomial representation of heat capacities are used, $\Delta C_{p_i} = \Delta a_i + \Delta b_i T$ with Δa_i and Δb_i constants for each component. Substituting these dependences in *Eq 2*, integrating and using the boundary conditions gives

$$\Sigma X_i [\Delta a_i \ln T_g/T_{g_i} + \Delta b_i (T_g - T_{g_i})] = 0 \qquad (23)$$

The solution glass-transition increment of heat capacity is

$$\Delta C_p = \Sigma X_i \Delta C_{p_i} = \Sigma X_i [\Delta a_i + \Delta b_i T_g] \qquad (24)$$

Additional terms can be included as necessary in the polynomial or other representations of the ΔC_{p_i}.

Experimental data on the compositional variation of T_g at elevated pressures (16) can also be accounted for by the form of *Eq 3*. *Figure 4* compares calculated and experimental glass-transition temperatures at 2 kbar for blends of poly(vinylidene fluoride) (PVF$_2$) with PMMA. Of particular interest here is that the data at elevated pressure can be accounted for by the value of the ratio $\Delta C_{p_1}/\Delta C_{p_2}$ determined from a fit of *Eq 3* to atmospheric pressure data.

To demonstrate further the applicability of the theory, *Figs.* 5 and 6 compare calculated and experimental glass-transition temperatures for, respectively, solutions of PS with styrene hexamer and of a network polymer of styrene (S) and divinyl benzene (DVB) with styrene hexamer. For PS, and S/DVB network polymers plasticized with styrene monomer rather than hexamer, *Eq 3* can underestimate T_g of the solution by a considerable amount (11). An example of this difference between theory

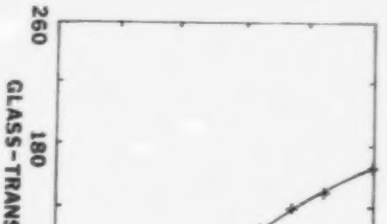

Fig. 4. *Calculated (Eq 3) and observed values of T_g at 2 Kbar for PVF$_2$/PMMA blends vs. weight fraction of PMMA, with the ratio $\Delta C_{p_1}/\Delta C_{p_2}$ determined from a fit of Eq 3 to atmospheric-pressure data (16).*

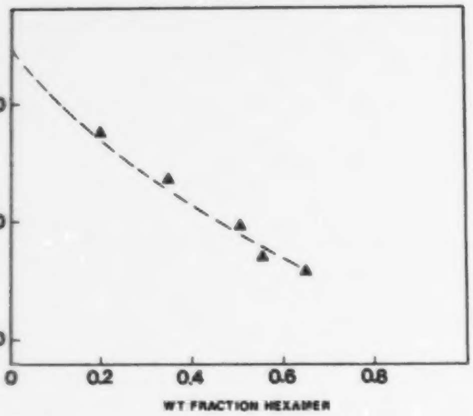

Fig. 5. Predicted (Eq 3) and observed values of T_g in °K for polystyrene plasticized with styrene hexamer. Reproduced with permission from (11).

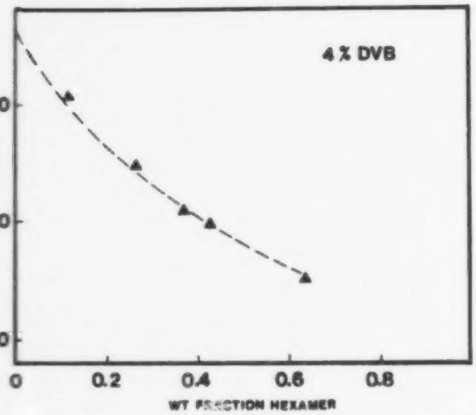

Fig. 6. Predicted (Eq 3) and observed values of T_g in °K for a S/DVB network polymer plasticized with styrene hexamer. Reproduced with permission from (11).

and experiment is shown in *Fig. 7*. The difference between predicted and observed values of T_g may be less than is suggested there, as the glass-transition temperature of ethyl benzene, 111° K (17) was used in lieu of that for styrene monomer (rapid crystallization of the latter makes a value of T_g difficult to determine directly). This value of 111 °K is considerably lower than the value of T_g for styrene deduced from electron spin resonance experiments, 135° K (18), which in turn is lower than a value of 158° K estimated from the present theory applied to the effect of degree of polymerization on T_g (19). These higher values used in *Eq 3* would shift the calculated solution glass transition temperatures toward the data. A further complication is that the definition of T_g as an onset temperature (11) rather than that at which ½ ΔC_p is reached can shift the predicted glass-transition temperature below the experimental data in a composition-dependent manner (8). These problems aside, there remains a discrepancy between the predictions of *Eq 3* and at least some of the data of (11). However, as Moy (11) has shown, and as depicted in *Fig. 7*, allowing for temperature-dependent pure-component heat capacities in the manner leading to *Eq 23* restores agreement between calculated and observed values of T_g. In like manner, theory and experiment can be brought into accord for S/DVB polymers plasticized with styrene and for epoxy network polymers plasticized with water. For these solutions, Δb_1 (polymer) and Δb_2 (diluent) were not determined directly, rather Δb_1 was taken as zero and Δb_2 was determined by a fit of *Eq 23* to the data. The value of Δb_2 so determined was, as expected, characteristic of the diluent and independent of the polymer.

In the nearest-neighbor approximation the glass-transition temperature of a polymer of degree of polymerization n is the same whether this is an actual or effective value, the former arising if all chains have the same length, the latter if there is a solution of a polymer with a corresponding oligomer. *Figures 5* and *8* taken together demonstrate

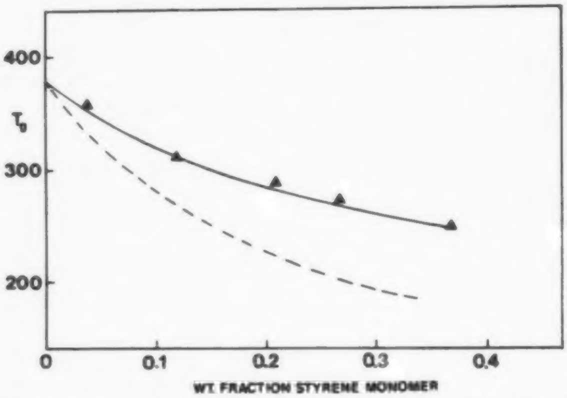

Fig. 7. Calculated (dotted line from Eq 3) and observed values of T_g in °K for solutions of styrene monomer in polystyrene. The full line is a fit of the data to Eq 23, as described in the text. Reproduced with permission from (11).

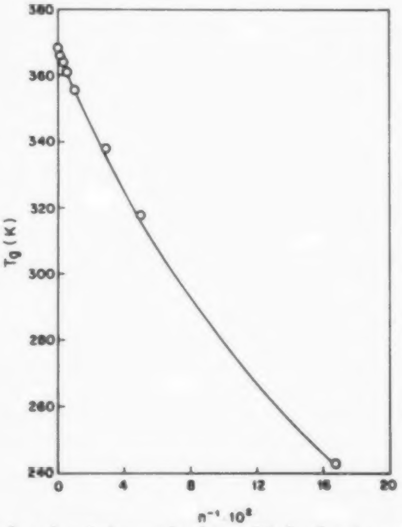

Fig. 8. Predicted and observed values of T_g for fractions of anionic PS vs. inverse degree of polymerization. Reproduced with permission from (5).

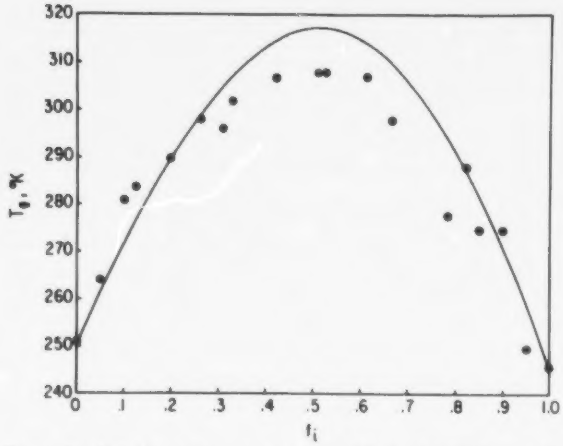

Fig. 9. Predicted and observed values of T_g for EA/VCl$_2$ copolymers vs. mole fraction of ethyl acrylate in the copolymer feed. Reproduced with permission from (13).

that this formal supposition, discussed in detail elsewhere (5–7), is acceptable.

For copolymers with single glass-transitions, as discussed in the section on the isothermal transition and elsewhere for the isobaric transition (13), the nearest-neighbor approximation and the copolymerization equation provide an expression for the copolymer T_g as a function of feed composition. This expression contains glass-transition properties of the two homopolymers and of the fully alternating copolymer, and the reactivity ratios for the two

EXCESS HEATS OF MIXING

In a development parallel to that for the entropy, the solution glass transition boundary is defined as the set of all T, P, X_i for which the enthalpy of the liquid state, H^l, is equal to that of the glassy state, H^g. Pure-component enthalpies and glass-transition properties are then used to give a relation between excess enthalpies of mixing in the liquid and glassy states, respectively $\Delta H_m{}^l$ and $\Delta H_m{}^g$. For the isobaric transition, at T_g

$$\Delta H_m{}^g = \Delta H_m{}^l + \Sigma X_i \Delta C_{p_i}(T_g - T_{g_i}) \qquad (25)$$

where T_g is given by *Eq 3*. For the isothermal transition, at P_g

$$\Delta H_m{}^g = \Delta H_m{}^l - \Sigma X_i \Delta \left(\frac{V_i\beta_i}{2}\right)(P_g - P_{g_i})^2 \qquad (26)$$

where the β_i denote pure-component isothermal bulk compressibilities and the solution glass-transition pressure is given by *Eqs 6* or *9*. In both *Eqs 25* and *26* relations and for *Eqs 27* and *28* below, the pure-component transition increments have been taken as independent of the corresponding transition variable.

EXCESS VOLUMES OF MIXING

The definition that on the glass-transition boundary the volumes of the liquid and glassy states, respectively V^l, V^g, are equal, and the use of pure-component reference states and properties, in the manner of the preceding section, leads to a formal connection between the excess volumes of mixing of these two states, in turn $\Delta V_m{}^l$ and $\Delta V_m{}^g$. For the isobaric transition, at T_g

$$\Delta V_m{}^g = \Delta V_m{}^l + \Sigma X_i \Delta(V_i\alpha_i)(T_g - T_{g_i}) \qquad (27)$$

and for the isothermal transition, at P_g

$$\Delta V_m{}^g = \Delta V_m{}^l - \Sigma X_i \Delta(V_i\beta_i)(P_g - P_{g_i}) \qquad (28)$$

APPROXIMATIONS TO THE PRINCIPAL RELATIONS FOR T_g, P_g

Two initial versions of each of *Eqs 3* and *9* arise from consistent use of a single-term expansion of the kind $ln(1 + y) \cong y$. For *Eq 3* written as $\Sigma X_i \Delta C_{p_i} ln(1 + y) = 0$, where y is in turn $(T_{g_i} - T_g)/T_g$, $(T_g - T_{g_i})/T_{g_i}$, the corresponding relations are

$$T_g = \frac{\Sigma X_i \Delta C_{p_i} T_{g_i}}{\Sigma X_i \Delta C_{p_i}} \qquad (29)$$

and

$$T_g = \frac{\Sigma X_i \Delta C_{p_i}}{\Sigma X_i \Delta C_{p_i} T_{g_i}{}^{-1}} \qquad (30)$$

As is evident from *Eq 25*, for *Eq 29* to be valid, $\Delta H_m{}^l = \Delta H_m{}^g$ at T_g. In contrast, *Eq 30* does not imply a restrictive connection between excess mixing properties and, therefore, is to be preferred over *Eq 29*. In connection with this difference, the continuity of ΔH_{mix} at T_g implies the continuity of ΔV_m and, consequently, that

$$T_g = \frac{\Sigma X_i \Delta(V_i\alpha_i) T_{g_i}}{\Sigma X_i \Delta(V_i\alpha_i)} \qquad (31)$$

For binary solutions, if *Eqs 29* and *31* are equivalent

$$\frac{\Delta(V_1\alpha_1)}{\Delta C_{p_1}} = \frac{\Delta(V_2\alpha_2)}{\Delta C_{p_2}} \qquad (32)$$

or, approximately (20),

$$\frac{dlnT_{g_1}}{dP} = \frac{dlnT_{g_2}}{dP} \qquad (33)$$

No such restriction is implied by *Eq 30*

The two first-order approximations to *Eq 9* are derived in the manner of *Eqs 29* and *30* and are

$$P_g = \frac{\Sigma X_i \Delta(V_i\alpha_i) P_{g_i}}{\Sigma X_i \Delta(V_i\alpha_i)} \qquad (34)$$

and

$$P_g = \frac{\Sigma X_i \Delta(V_i\alpha_i)}{\Sigma X_i \Delta(V_i\alpha_i) P_{g_i}^{-1}} \qquad (35)$$

An expression qualitatively parallel to *Eq 34* also arises if, at P_g, $\Delta V_m{}^l = \Delta V_m$, and is from *Eq 28*

$$P_g = \frac{\Sigma X_i \Delta(V_i\beta_i) P_{g_i}}{\Sigma X_i \Delta(V_i\beta_i)} \qquad (36)$$

If, in the spirit of discussion of *Eq 29*, *Eqs 34* and *36* are equivalent, for a binary solution

$$\frac{\Delta(V_1\beta_1)}{\Delta(V_1\alpha_1)} = \frac{\Delta(V_2\beta_2)}{\Delta(V_2\alpha_2)} \tag{37}$$

or, approximately (20),

$$\frac{dT_{g_1}}{dP} = \frac{dT_{g_2}}{dP} \tag{38}$$

The form of *Eq 35*, unlike that of *Eq 34*, does not imply any restriction on excess properties of mixing. Consequently, *Eq 35* is to be preferred over *Eq 34*.

Secondary approximations to *Eq 3* can be obtained from *Eqs 29* and *30* with $\Delta C_{p_i} = \Delta C_{p_j}$ and are in turn

$$T_g = \Sigma X_i T_{g_i} \tag{39}$$

and

$$T_g^{-1} = \Sigma X_i T_{g_i}^{-1} \tag{40}$$

Equation 39 also arises if, in *Eq 31*, $\Delta(V_i\alpha_i) = \Delta(V_j\alpha_j)$. The antecedent of *Eq 40* is less restrictive than that of *Eq 39*, consequently *Eq 40* is the more acceptable final approximation to *Eq 3*.

Use of the approximation $\Delta(V_i\alpha_i) = \Delta(V_j\alpha_j)$ in *Eqs 34* and *35* gives as secondary versions of *Eq 9*

$$P_g = \Sigma X_i P_{g_i} \tag{41}$$

and

$$P_g^{-1} = \Sigma X_i P_{g_i}^{-1} \tag{42}$$

Equation 41 can also be obtained from *Eq 36* if $\Delta(V_i\beta_i) = \Delta(V_j\beta_j)$. The preferred final approximation to the principal relation for the compositional variation of glass-transition pressures is *Eq 42*.

Two further mixing relations are obtained if $\Delta C_{p_i} = \Delta C_{p_j}$ in *Eq 3* and $\Delta(V_i\alpha_i) = \Delta(V_j\alpha_j)$ in *Eq 9*. For the isobaric and isothermal transitions these are, in turn,

$$lnT_g = \Sigma X_i lnT_{g_i} \tag{43}$$

and

$$lnP_g = \Sigma X_i lnP_{g_i} \tag{44}$$

Figure 10 summarizes the way in which *Eq 3* gives rise to *Eqs 29, 30, 39, 40* and *43*. A similar summary can be obtained for the approximations to *Eq 9* by replacing ΔC_{p_i} and T_{g_i} of this *Figure* by, in turn, $\Delta(V_i\alpha_i)$ and P_{g_i}.

CONCLUSIONS

As demonstrated, it is possible to develop a predictive theory for the composition-dependent glass-transition that is both comprehensive and uses readily-measurable pure-component properties. Although so far the theory has been tested for only the isobaric transition, the adequacy with which experimental data are accounted for suggests the expectation of further success. For certain solutions, the approximation of temperature-independent heat capacities for the isobaric transition is apparently inappropriate but, as outlined in the discussion leading to *Eqs 23* and *24*, the incorporation of temperature-dependent ΔC_{p_i} is, formally, a minor matter and restores good agreement between theory and experiment (11).

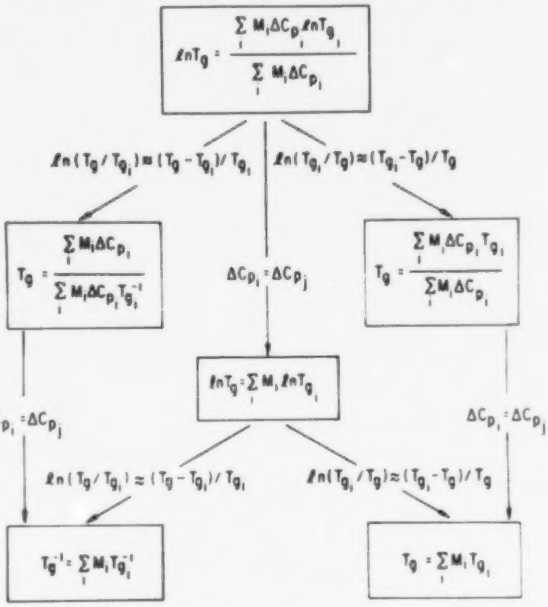
$\ell nT_g = \frac{\sum_i M_i \Delta C_{p_i} \ell nT_{g_i}}{\sum_i M_i \Delta C_{p_i}}$
$\ell n(T_g/T_{g_i}) \approx (T_g - T_{g_i})/T_{g_i}$
$\ell n(T_{g_i}/T_g) \approx (T_{g_i} - T_g)/T_g$
$T_g = \frac{\sum_i M_i \Delta C_{p_i}}{\sum_i M_i \Delta C_{p_i} T_{g_i}^{-1}}$
$\Delta C_{p_i} = \Delta C_{p_j}$
$T_g = \frac{\sum_i M_i \Delta C_{p_i} T_{g_i}}{\sum_i M_i \Delta C_{p_i}}$
$\ell nT_g = \sum_i M_i \ell nT_{g_i}$
$\Delta C_{p_i} = \Delta C_{p_j}$
$\Delta C_{p_i} = \Delta C_{p_j}$
$\ell n(T_g/T_{g_i}) \approx (T_g - T_{g_i})/T_{g_i}$
$\ell n(T_{g_i}/T_g) \approx (T_{g_i} - T_g)/T_g$
$T_g^{-1} = \sum_i M_i T_{g_i}^{-1}$
$T_g = \sum_i M_i T_{g_i}$

Fig. 10. Summary of first- and second-order approximations to Eq 3 and the manner of their derivation from this expression. Reproduced with permission from (8).

The principal first-order relations for, in turn, the isobaric and isothermal transitions can be written in product form as

$$T_g = \prod_{i=1}^{c} (T_{g_i})^{v_i} \tag{45}$$

and

$$P_g = \prod_{i=1}^{c} (P_{g_i})^{u_i} \tag{46}$$

where $v_i = \frac{X_i \Delta C_{p_i}}{\Sigma X_i \Delta C_{p_i}}$, $u_i = \frac{X_i \Delta(V_i\alpha_i)}{\Sigma X_i \Delta(V_i\alpha_i)}$ are the fractional contributions of the pure components to in turn ΔC_p and $V\Delta\alpha$.

All composition-differentials simplify considerably at extremes of composition and become functions of pure-component properties alone. For example, *Eq 4* at $X_2 = 0$ becomes

$$\frac{\partial lnT_g}{\partial X_2} = \frac{1}{T_{g_1}} \frac{\partial T_g}{\partial X_2} = \frac{\Delta C_{p_2}}{\Delta C_{p_1}} ln(T_{g_2}/T_{g_1}) \tag{47}$$

Changing the composition by a differential amount, δX_2, changes the solution glass-transition temperature from T_{g_1} to

$$T_g = T_{g_1}\left[1 + \delta X_2 \frac{\Delta C_{p_2}}{\Delta C_{p_1}} ln(T_{g_2}/T_{g_1})\right] \tag{48}$$

Not only can the first-order principal relation for the isobaric transition be approximated to recover the form of previous empirical and semi-empirical equations for the effect of composition on T_g, but also *Eq 23* and the parallel relation for the isothermal transition can be usefully and conveniently approximated. For $ln(T_g/T_{g_i}) \simeq (T_g - T_{g_i})/T_{g_i}$, *Eq 23* becomes

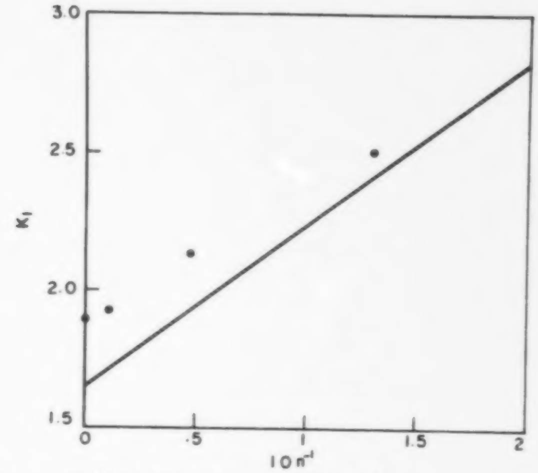

Fig. 11. Predicted (8) and curve-fit (22) values of K_1 (see text) for PPO/PS blends vs. inverse degree of polymerization of PS.

$$T_g = \frac{\Sigma X_i(\Delta a_i + \Delta b_i T_{g_i})}{\Sigma X_i(\Delta a_i T_{g_i}^{-1} + \Delta b_i)} \tag{49}$$

which, for binary solutions, can be rewritten in the form of the Wood equation (21)

$$T_g = \frac{X_1 T_{g_1} + X_2 K_1 T_{g_2}}{X_1 + X_2 K_1} \tag{50}$$

with

$$K_1 = \frac{\Delta a_2 T_{g_2}^{-1} + \Delta b_2}{\Delta a_1 T_{g_1}^{-1} + \Delta b_1} \tag{51}$$

Kwei and Frisch (22) found that their data for miscible blends of PPO with four monodisperse polystyrenes could be fit by the form of *Eq 50*, with K_1 inversely proportional to the degree of polymerization, n, of PS. Using *Eq 51* with $\Delta b_1 = \Delta b_2 = 0$, K_1 is predicted to vary with n^{-1} as shown in *Fig. 11*, in fair agreement with values obtained by fitting *Eq 50* to the data.

For obvious reasons, initial applications of the theory were largely confined to amorphous solutions. The adequacy of the theory to account for the composition-dependent isobaric transition for these systems suggests that it can also be applied to account both qualitatively and quantitatively to this and other aspects of the solution glass-transition in partially crystalline systems.

ACKNOWLEDGEMENT

This research was supported by the National Science Foundation, Polymers Program, through Grant DMR 81-06153.

REFERENCES

1. P. R. Couchman, *Phys. Lett.*, **70A**, 155 (1979).
2. P. R. Couchman, *Macromolecules*, **11**, 1156 (1978).
3. D. M. Leisz, L. W. Kleiner, and P. G. Gertenbach, *Thermochimica Acta*, **35**, 51 (1980).
4. C. L. Ryan, Ph.D. Dissertation, University of Massachusetts (1979).
5. P. R. Couchman, *J. Appl. Phys.*, **50**, 6043 (1979).
6. P. R. Couchman, *J. Mater. Sci.*, **15**, 1680 (1980).
7. P. R. Couchman, *Polym. Eng. Sci.* **21**, 377 (1981).
8. P. R. Couchman, *Macromolecules*, **13**, 1272 (1980).
9. J. R. Fried and S.-Y. Lai, *J. Appl. Polym. Sci.*, **27**, 2869 (1981).
10. H. E. Bair and P. C. Warren, *J. Macromol. Sci.*, **B20**, 381 (1981).
11. P. Moy, Ph.D. Dissertation, University of Massachusetts (1981).
12. C. G. Martin, R. K. Mehta, and S. E. Lott, *Am. Chem. Soc., Div. Polym. Chem., Polym. Prepr.*, **22**, 319 (1981).
13. P. R. Couchman, *Macromolecules*, **15**, 770 (1982).
14. S.-F. Lau, J. Pathak, and B. Wunderlich, *Macromolecules*, **15**, 1278 (1982).
15. K. Naito, G. E. Johnson, D. L. Allara, and T. K. Kwei, *Macromolecules*, **11**, 1260 (1978).
16. D. J. Woan, P. R. Couchman, and J. I. Scheinbeim, to be published.
17. C. A. Angell, J. M. Sare, and E. J. Sare, *J. Phys. Chem.*, **82**, 2622 (1978).
18. P. L. Kumler, S. E. Keinath, and R. F. Boyer, *J. Macromol. Sci.-Phys.*, **B13**, 631 (1977).
19. The glass-transition temperature of styrene monomer was estimated by setting $n = 1$ in the appropriate version of *Eq (3)(5–7)*.
20. A. H. Wilson, "Thermodynamics and Statistical Mechanics," Cambridge University Press, 1957.
21. L. A. Wood, *J. Polym. Sci.*, **28**, 319 (1958).
22. T. K. Kwei and H. L. Frisch, *Macromolecules*, **11**, 1267 (1978).

DISCUSSION

I. Sanchez: Could you again go over the argument, why you are willing to equate the differential of entropy along the transition line and not the volume?

P. Couchman: I am, of course, willing to equate the volumes along the transition line. However, in order to produce a predictive relation from the volume one must make the restrictive assumption of volume additivity, that is, you cannot allow any excess volume of mixing. In contrast, the entropy gives a predictive relation for all random solutions, including those with finite excess volumes and/or enthalpies of mixing. Thus, on the basis of a volume rather than an entropy argument you cannot produce a predictive relation without a severely restrictive assumption, which of course you are free to do. However, one of the consequences of such a restrictive assumption is that the corresponding equation for T_g will be of restricted applicability. Joel Fried (Ph.D., University of Massachusetts, 1976) has shown that for PS/PPO blends, if you use the relation for the compositional variation of T_g derived from the assumption that the excess volume of mixing vanishes, the theory does not agree at all with the experimental data. This is a practical point.

I. Sanchez: In utilization of your equations to describe the effect of molecular weight on T_g, you used an expression for the entropy which has a linear term in n. It has been a point of controversy in the past whether you can do this. Flory argued very strongly that there is a logarithmic term in the entropy. This will not so much affect the curvature of the equation but the extrapolated value of T_g for large n.

P. Couchman: The theory implies that for this problem the entropy expression has both a linear term in n and logarithmic terms containing n. The latter characterize the excess entropy of mixing for a formal model of polymers of degree of polymerization *n*, as random mixtures of oligomers, degree of polymerization *m*, and chains consisting of *n-m* mers which have properties of the high polymer. The logarithmic terms are equal for the liquid and glassy states and cancel in the final expression.

L. A. Utracki: There are some works on T_g of plasticized polymers which indicate that at high concentration of plasticizer there is a cusp, a sort of plateau region.

P. Couchman: Does this perhaps indicate clustering or partial phase separation?

L. A. Utracki: Leon St-Pierre has some evidence regarding this plateau for PVC. This may indicate a sort of volume change. Can this behavior be computed from your theory?

P. Couchman: Not as it is presently constituted. However, the theory can be of use if one plots the theoretical T_g *vs.* the experimental T_g and there is a significant difference.

D. D. Patterson: I think that this cusp behavior was predicted by Kovacs and is supposed to be a general phenomenon.

P. Couchman: To predict strictly means to foretell. What he does is use the free volume for the mixture as an adjustable parameter (A. J. Kovacs, *Adv. Polym. Sci.*, **3**, 394 (1963)). If there is an adjustable parameter it is not a predictive theory.

D. D. Patterson: In the case of this theory $V^E \simeq 0$. If you take different values of the excess volumes then you are going to get slightly different behavior. I think that the problem is that very little experimental data exists to exemplify this behavior. St-Pierre seems to find this behavior in PVC at about 10 percent of plasticizer or a little bit higher.

P. R. Couchman: The theory would not have much to say about that in a predictive fashion, although one could infer from comparison between theory and experiment how the entropy may differ from that of a random mixture; degree of ordering, etc.

D. D. Patterson: Is there any physical reason why T_g as a function of composition should be independent of interactions between two components there?

P. R. Couchman: Yes, the solutions I have considered are random or, for formal purposes, can be described in terms of equivalent random solutions. In connection with the latter, see Ref. 13.

D. D. Patterson: In a polymer system, or indeed in a small molecule system, the entropy of mixing should depend upon differences of free volumes or interactions between the two components.

P. R. Couchman: This is typically a very small correction, which is inconvenient. What you say is true but calculationally a minor effect.

L. A. Utracki: Recently we computed theoretical free volume changes with temperatures and pressures for paraffins and polymers. Plotting the zero shear viscosity of small molecule or polymeric liquids *vs.* this theoretical free volume one gets a master curve for each liquid in a very wide range of pressures and temperatures. This parameter should also control the glass transition behavior. It may be an interesting way to extend your treatment to high pressure regions.

P. R. Couchman: Yes, it sounds intriguing.

Dielectric Properties of Poly(α-Methyl-α-N-Propyl-β-Propiolactone)/Poly(Vinyl Chloride) Blends

TARIQ M. MALIK and ROBERT E. PRUD'HOMME

Groupe de recherche sur les macromolécules
Chemistry Department, Laval University
Quebec (Québec) Canada G1K 7P4

The dielectric properties of miscible blends of poly(vinyl chloride) (PVC) and poly(α-methyl-α-n-propyl-β-propiolactone) (PMPPL) have been investigated at different temperatures above and below T_g. The results were analyzed using the Cole-Cole representation and lead to the conclusion that this mixture does not exhibit micro-scale heterogeneities. Dielectric constant and dielectric loss master curves were constructed using the stress relaxation shift factors determined previously; the same shift factors could be used for the homopolymers and their blends. Similarities between the dielectric master curves and the stress relaxation master curves of PVC, PMPPL, and their blends, are also discussed.

INTRODUCTION

In a previous article (1), we reported the stress relaxation behavior of PMPPL/PVC blends where PMPPL is poly(α-methyl-α-n-propyl-β-propiolactone) and PVC is poly(vinyl chloride). In the linear viscoelastic region, stress relaxation master curves were constructed for each blend at a reference temperature of T_g-25. Time-temperature superposition was found to be satisfactory indicating that these mixtures are thermorheologically simple materials. The stress relaxation master curves of the blends were found to be intermediate between those of PMPPL and PVC. For short times, the influence of PMPPL was predominant. For longer times, a rapid decrease in modulus, similar to that seen for PVC, was observed. The same temperature dependence of the shift factors was found for PMPPL, PVC, and their blends.

This earlier study did not reveal any micro-scale phase separation between the components of the blends but neither did it exclude the possibility of its occurrence. We believe that dielectric relaxation measurements are more sensitive to the presence of any micro-scale phase separation; they can also give additional information about the interactions occurring in PMPPL/PVC blends and about their relaxation processes.

It is the purpose of the present article to report the dielectric relaxation of PMPPL/PVC blends. Master curves of the real and imaginary components of the dielectric constant will be constructed. Attempts will be made to correlate the dielectric properties of these miscible blends with their mechanical relaxation properties. The parameters describing the dispersion curves of the blends, their dipole moments, and their orientation corelation factors will be discussed.

In this study and in the previous one, PVC was chosen because it is a common polymer and because it is known to be miscible with a large number of polyesters (2–4). PMPPL was chosen because it has been shown to be fully miscible with PVC (5, 6), and because it has a very low degree of crystallinity contrary to all other polyesters which are known to be miscible with PVC. In addition, the glass transition temperature, T_g, of PMPPL is conveniently found at 275 K which simplifies somewhat the measurements in the T_g region.

EXPERIMENTAL SECTION

Details concerning the PMPPL and PVC samples used in this study can be found in *Ref.* 5. As a reminder the structural formula of PMPPL is

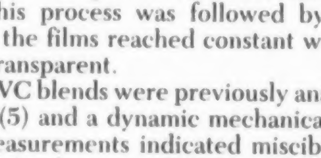

$$\left[-CH_2-\overset{\displaystyle CH_3}{\underset{\displaystyle C_3H_7}{\overset{|}{\underset{|}{C}}}}-\ COO- \right]_n$$

Blends were prepared by the conventional solvent casting technique, using tetrahydrofuran as solvent. Solvent evaporation was conducted for one week at room temperature, under atmospheric pressure. This process was followed by vacuum drying until the films reached constant weight. All films were transparent.

PMPPL/PVC blends were previously analyzed by calorimetry (5) and a dynamic mechanical method (6). Both measurements indicated miscibility, i.e., extensive mixing between PMPPL and PVC, since a single T_g was observed at any composition. The main characteristics of the blends and homopolymers are given in *Table 1*. It can be seen that the 75/25 blend is semi-crystalline. Note that PMPPL

Table 1. Glass transition temperature, melting temperature, density, degree of crystallinity, and enthalpy of fusion of PVC, PMPPL, and their blends (5).

Wt. % PMPPL	T_g (K)	T_m (K)	Density (g/cm^3)	Enthalpy of fusion (J/g)	Degree of crystallinity (%)
0	337.5	—	1.39	0	0
25*	316	—	1.30	0	0
50	305.5	305	1.20	1	1
75*	291	360	1.16	12	13
100	275	370	1.07	27	25

* Values intrapolated from the data of *Ref. 5.*

crystallizes in this blend but the PMPPL crystals do not include PVC. The amorphous phase of this blend is composed of PVC, plus the remaining non-crystalline PMPPL.

All test specimens were annealed at 320 K for two weeks, before the dielectric measurements which were performed with a General Radio 1621 Precision Capacitance System in a frequency range of 0.01 to 100 kHz. The samples were held in a Balsbaugh model LD-3 three terminal cell with electrode diameter of 6.3 cm. An environmental chamber was constructed to regulate the temperature of the cell. A copper-constantan thermocouple was mounted near the sample to monitor its temperature. The temperature stability was better than ±0.5K.

The dielectric constant, ϵ', dielectric loss, ϵ'', and loss tangent, $\tan\delta$, were calculated from the following equations:

$$\tan\delta = G/2\pi fC \qquad (1)$$

$$\epsilon' = C/|Co(1 + \tan^2\delta)| \qquad (2)$$

$$\epsilon'' = \epsilon' \tan\delta \qquad (3)$$

where G is the conductance, C the capacitance, f the frequency, and Co the capacitance of the empty cell.

RESULTS AND DISCUSSION

Figures 1 to *3* show the temperature dependence of the dielectric constant and the dielectric loss of PVC, PMPPL, and a 50/50 PMPPL/PVC blend, in the T_g region. In the three cases, a well-defined maximum is observed in the ϵ'' curve and this maximum is closely related to the T_g of the sample. With increasing frequencies, it shifts to higher temperatures and the intensity of the dielectric loss peak increases. At the same time, the ϵ' curves also shift to higher temperatures with increasing frequencies. Similar data were obtained for 75/25 and 25/75 PMPPL/PVC blends but are not reported here (7).

Similar data are not available in the literature for PMPPL and PMPPL/PVC blends. *Figure 1* can, however, be compared with data published by several groups of workers (8–10) and the agreement is satisfactory [a more extensive list of references on the dielectric behavior of PVC can be found in *Ref. 11*]. However, the curves of *Fig. 1* occur at lower temperatures than those published by others due to the lower T_g of the PVC used in this study (5).

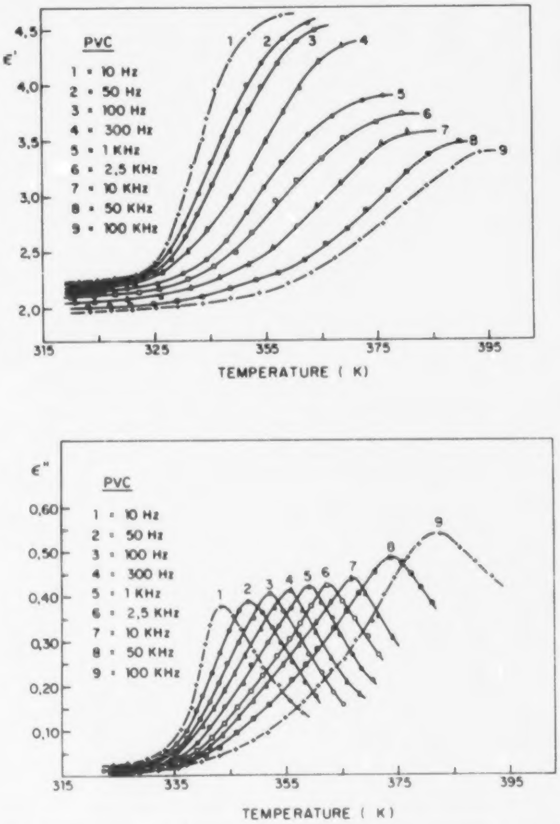

Fig. 1. Temperature dependence of the dielectric constant, ε', and of the dielectric loss, ε", of PVC at different frequencies.

Figures 1 to *3* also show that, at any given frequency, the intensity of the dielectric loss peak increases regularly as a function of the composition of the blend. It is low for PMPPL and much higher for PVC. This increase is due to an increase of the dipole moment concentration of the mixture. At the same time, at any given frequency, the position of the dielectric loss peak shifts toward higher temperatures with increasing PVC concentrations. Assuming that the maximum of the ϵ'' curve is equal to T_g, *Fig. 4* shows that T_g increases linearly as a function of composition. This result confirms previous calorimetric (5) and dynamic mechanical (6) measurements. The presence of a single T_g for PMPPL/PVC blends, whose value is intermediate between those of PMPPL and PVC, indicates the miscibility of the mixture (3, 4). However, this result cannot be taken as a proof of the micro-scale homogeneity of the mixture since the measurement of T_g is not a molecular measurement. Moreover, the dilatometric curves of the blends are broadened as compared to those of PMPPL and PVC suggesting some micro-scale heterogeneities (5). Additional comments on this matter will be made in the rest of this paper.

Figure 5 shows the complex plane plots, also called Cole-Cole plots, for the local mode relaxation

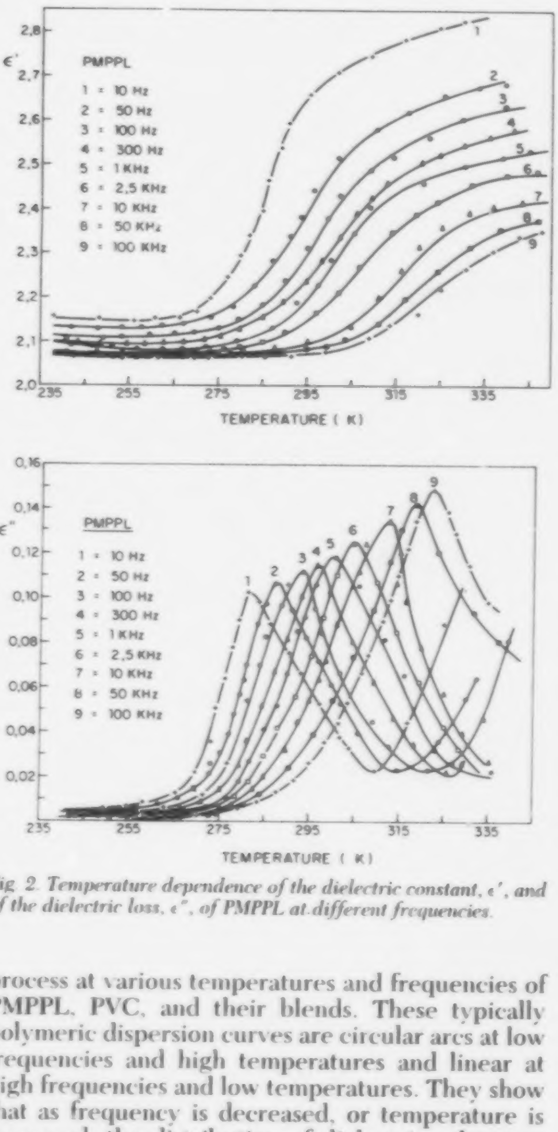

Fig. 2. Temperature dependence of the dielectric constant, ε', and of the dielectric loss, ε", of PMPPL at different frequencies.

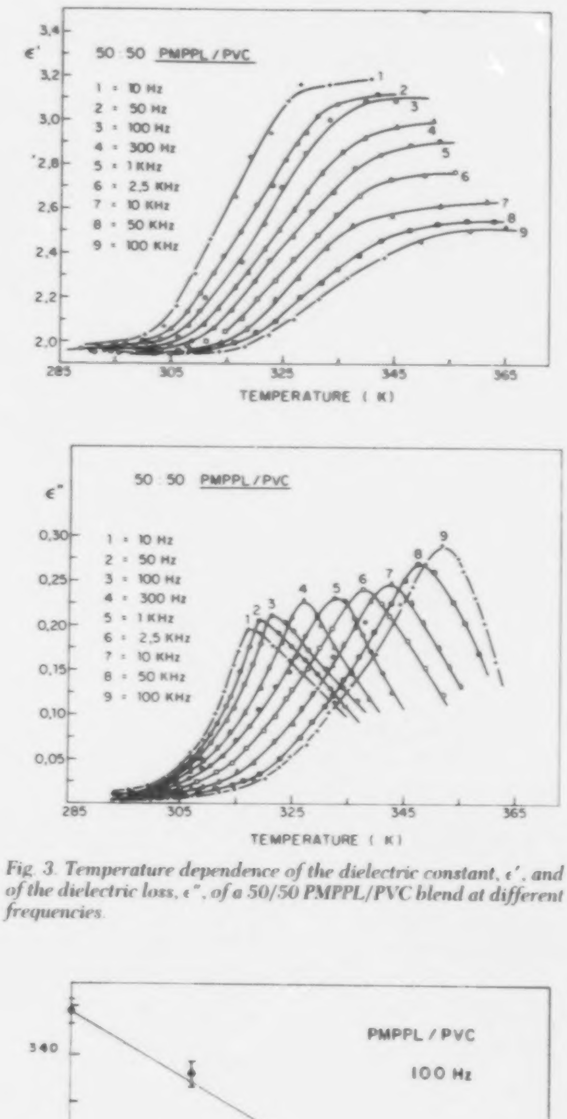

Fig. 3. Temperature dependence of the dielectric constant, ε', and of the dielectric loss, ε", of a 50/50 PMPPL/PVC blend at different frequencies.

process at various temperatures and frequencies of PMPPL, PVC, and their blends. These typically polymeric dispersion curves are circular arcs at low frequencies and high temperatures and linear at high frequencies and low temperatures. They show that as frequency is decreased, or temperature is increased, the distribution of dielectric relaxation times becomes narrower; at low frequencies or high temperatures, the relaxation process can eventually be described by a single relaxation time (11, 12).

The limiting low and high frequency dielectric constants ϵ_R and ϵ_U, respectively, can be taken as the low and high frequency intercepts with the horizontal axis by extrapolation of the curves. This result is predicted by the Cole-Cole equation (11–14):

$$\epsilon^* = \epsilon_u + \frac{\epsilon_R - \epsilon_U}{[(1 + i\omega\tau)^{1-\alpha}]^\beta} \qquad (4)$$

where ϵ^* is the complex dielectric constant, ω is the angular frequency, and τ the relaxation time. α is a parameter measuring the departure from a single relaxation time. β is a second parameter taking into account the deviation of the Cole-Cole plot from a circular arc. α and β must be in a range from zero to unity.

In this work, the parameter α was determined by fitting the low frequency data with a semi-circle, the center of the semi-circle being approximately on the same vertical axis as the maximum of the Cole-Cole plot (11). Values of α thus obtained are given in *Table 2*.

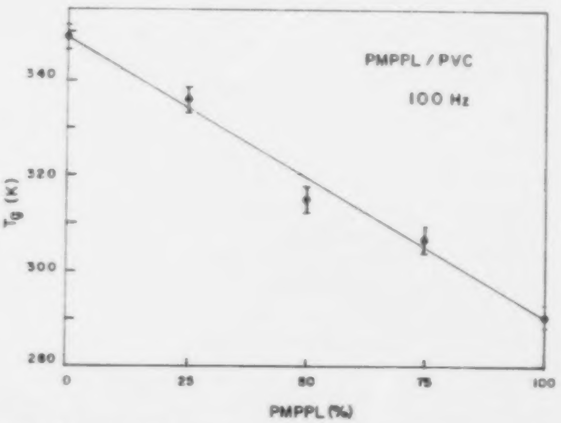

Fig. 4. Composition dependence of the glass transition temperature of PMPPL/PVC blends measured dielectrically.

Normalized curves of the dielectric loss can be produced by plotting ϵ''/ϵ_m'' *vs.* log (f/fm) where

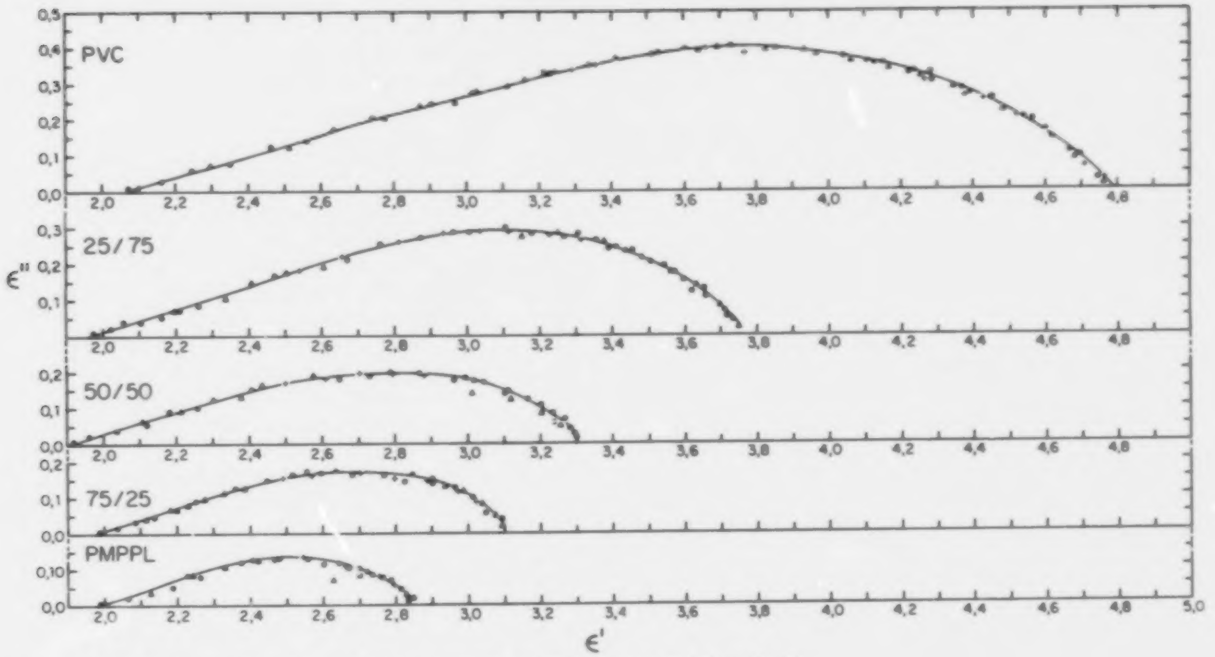

Fig. 5. Cole-Cole representation of the dielectric properties of PMPPL, PVC, and their blends.

Table 2. Parameters describing the normalized dispersion curves of PMPPL/PVC blends

Wt. % PMPPL	Width at half-height	$\Delta H/\Delta L$	α
0	3.15	1.13	0.37
25	3.20	1.19	0.38
50	3.35	1.23	0.40
75	3.40	1.39	0.43
100	3.50	1.33	0.44

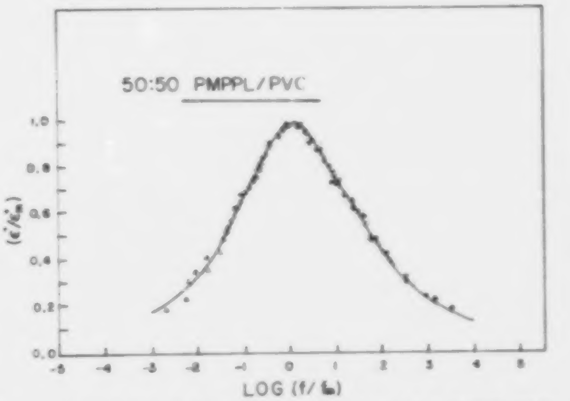

Fig. 6. Normalized dielectric loss data of a 50/50 PMPPL/PVC blend.

ϵ_m'' is the maximum value of ϵ'', at a frequency *fm*. Normalized dispersion curves of this sort were constructed for PMPPL, PVC, and several blends, and *Fig.* 6 shows an appropriate example for a 50/50 PMPPL/PVC blend. A single well-defined α peak is observed and both the horizontal and vertical superpositions are satisfactory. Similar conclusions were reached for PMPPL, PVC, and the other blends (7).

The width at half-height of each normalized dispersion curve was determined and is reported in *Table* 2. *Table* 2 also gives the ratio $\Delta H/\Delta L$ where ΔH and ΔL are the distances in decades from the center of the plot (where log (f/fm) equals zero) to the curve at half-height, on the high frequency side and the low frequency side, respectively. $\Delta H/\Delta L$ is then a measure of the asymmetry of the dispersion curve, $\Delta H/\Delta L$ being equal to unity for a symmetrical curve.

Table 2 shows that the width at half-height, $\Delta H/\Delta L$ and α are significantly larger for PMPPL than for PVC. This is due to the low dipole moment of the PMPPL repeat unit as compared to that of PVC and to its crystallinity. The presence of crystallinity is known to broaden the dispersion curve of a polymer and to increase its asymmetry (10, 15–18). It also reduces its relaxation strength defined by $(\epsilon_R - \epsilon_U)$, as can be seen from *Fig.* 5 and as suggested in the literature (16, 17).

Table 2 also shows that the width at half-height, $\Delta H/\Delta L$ and α of the blends are intermediate between those of PMPPL and PVC and that these parameters increase slightly but regularly with increasing PMPPL concentrations. This result contrasts with those found by Wetton et al. (19) and Alexandrovich et al. (20) on P(pCS-S)/PPO and P(pCS-S)/PS blends, respectively (PPO is poly(phenylene oxide), PS is poly(styrene), and P(pCS-S) is a copolymer of p-chlorostyrene and styrene). It is also different from the results found by Akiyama et al. on various mixtures (21). These authors have found broader normalized dispersion curves for the blends than those of any of the unblended polymers or copolymers. The P(pCS-S)/PPO and P(pCs-S)/PS blends are, however, miscible since they exhibit a single T_g by calorimetric, dynamic mechanical, and dielectric measurements. The broadening effect was interpreted primarily as arising from a wide range of local concentrations which are present in the miscible blends; in other words it was interpreted as arising from a micro-scale phase separation. Since PMPPL/PVC blends do not exhibit any broadening of this sort, it is suggested here that they are homogeneous at micro-scale level.

The magnitude of the orientation polarization of bulk polymers depends not only on the dipole moments of the monomer units but also on correlations between dipoles. From experimental measurements of the dielectric constant and loss, the effective dipole moment of a polymer chain can be calculated. For that purpose, one generally uses the Onsager equation (11)

$$\mu_e^2 = \frac{9kT}{4\pi N}\,\frac{(2\epsilon_R + \epsilon_U)(\epsilon_R - \epsilon_U)}{\epsilon_R(\epsilon_U + 2)^2} \qquad (5)$$

where ϵ_R and ϵ_U are the limiting values of ϵ' (see *Eq. 4*), T is the temperature, k the Boltzmann constant, N is the number of repeat units per unit volume, and μ_e is the effective dipole moment per repeat unit. *Equation 5* does not take into account correlations between dipoles which are most important for polymers. Frohlich (22) considered this factor and arrived at an expression which is obtained by substituting *Eq. 6* into *Eq. 5*:

$$\mu_e^2 = g\,\mu_o^2 \qquad (6)$$

In this last equation, μ_o is the permanent dipole moment of the repeat unit. This value is generally estimated by the dipole moment in the gas phase of a model compound. The factor g is the orientation correlation function which is expressed by

$$g = 1 + \sum_{i,i \neq j}^{No} \overline{\cos \gamma_{ij}} \qquad (7)$$

where the factor $\overline{\cos \gamma_{ij}}$ is the average of the cosine of the angle between dipole i, considered as being fixed in space, and dipole j. Summation over i is done for all No dipoles, taking into account all correlations between the dipoles of the sample. Obviously, a random correlation leads to $\overline{\cos \gamma_{ij}} = 0$ and $g = 1$.

Table 3 gives the values of μ_e^2 and g calculated for PMPPL, PVC, and their blends, using *Eqs. 5* and *6*. It also gives all parameters required for this calculation: ϵ_R, ϵ_U, and μ_o. The model compound dipole moments of the homopolymers, in the gas phase, were calculated from the group contribution method outlined by Smyth (23). The density values reported in *Table 3* were taken from *Ref. 5*. The μ_o values for the blends were calculated by the following equation:

$$\mu_o^2 = X_1\,\mu_{o1}^2 + X_2\,\mu_{o2}^2 \qquad (8)$$

where the X_i's are the weight fractions and the μ_{oi}'s the gas phase permanent dipole moments of the homopolymers.

Table 3 shows that the effective dipole moment per repeat unit of PVC is higher than that of PMPPL indicating a higher dipole moment of the C-Cl group than that of the C = 0 group. It also shows a g value of 0.25 for PVC as compared to 0.30 for PMPPL indicating a higher correlation of dipoles in the PVC chain due to hindered rotation. This correlation phenomenon is likely the result of specific interactions between PVC repeat units, i.e., intramolecular and/or intermolecular hydrogen bonding and dipole-dipole interactions.

Finally, *Table 3* shows that the μ_e^2 and g values of the blends are intermediate between those of the homopolymers and that, within experimental error, they change linearly as a function of blend composition. Similar results were found by Wetton et al. (19) and Alexandrovich et al. (20). This indicates that the local conformational states of PVC and PMPPL are unperturbed by the presence of the other polymer. This result is different from that reported by Alexandrovich et al. (24) on random copolymers of pCS and S where a maximum in g was seen as a function of the comonomer composition. Put another way, copolymerization leads to chain expansion of the polymer molecules, but not blending. However, miscibility of PMPPL/PVC blends is known to be possible due to specific interactions between the two polymers (3–5). These specific interactions do not seem to be strong enough to significantly perturb the chain conformation of any one polymer in the blend as compared to that of the homopolymer. It is suggested here that the miscibility phenomenon results from weak interactions between the polymer repeat units.

DISCUSSION AND CONCLUSIONS

In a previous work (1), we showed that the shift factor temperature dependence of PVC, PMPPL, and their blends was the same when constructing stress relaxation master curves, using Ferry's reduced variable method (24) at a reference temperature of T_g-25. This result indicated that all relaxation times depend similarly on temperature, despite different distributions of relaxation times for each sample (25, 26). A similar analysis can be made using the dielectric relaxation data.

For this purpose, the dielectric constant and dielectric loss values have been normalized in the form of $(\epsilon' - \epsilon_U)/\epsilon_R - \epsilon_U)$ and $\epsilon''/(\epsilon_R - \epsilon_U)$ functions. *Figure 7* shows the frequency dependence of the dielectric

Table 3. Dipole moment, orientation correlation factor and other parameters of PMPPL/PVC measured at (T_g + 15)

Wt. % PMPPL	T_o (K) (T_g + 15)	Density (g/cm^3)	μ_o (D)	ϵ_R	ϵ_U	μ_e^2 (D^2)	g
0	352.5	1.39	2.05	4.80	2.06	1.05	0.25
25	331	1.30	1.97	3.78	1.92	1.00	0.26
50	320.5	1.20	1.89	3.34	1.95	0.96	0.27
75	306	1.16	1.81	3.12	1.99	0.92	0.28
100	290	1.07	1.73	2.86	1.94	0.89	0.30

constant normalized function of PVC. This master curve was obtained at a reference temperature T_o of (T_g + 15) by shifting the curves horizontally (no vertical shift was required since the function was previously normalized). The superposition is satisfactory.

Then, using the shift factors b_T determined empirically from *Fig. 7*, the frequency dependence of the dielectric loss normalized function of PVC was found. This master curve is shown in *Fig. 8*. The superposition is again satisfactory indicating that the same shift factors can be used for the dielectric constant and the dielectric loss functions.

Figure 9 shows the temperature dependence of the shift factor a_T determined in *Ref. 1* from stress relaxation measurements. The error bars at both ends of the curve indicate the uncertainty of these measurements. Note that this shift factor curve is a master curve since it applies equally well to PVC, PMPPL, and their blends (1). The data points of *Fig. 9* are the dielectric shift factors b_T determined by constructing *Fig. 7*. Within experimental error, they agree with the a_T curve despite the use of slightly different reference temperatures in both series of experiments: $T_o = T_g - 25$ in the stress relaxation measurements and $T_o = T_g + 15$ in the dielectric measurements.

We have then assumed that the a_T shift factor master curve of *Fig. 9* applies to the dielectric data not only of PVC but also of PMPPL and PMPPL/PVC blends. As a representative example, the dielectric constant and dielectric loss master curves of a 50/50 PMPPL/PVC blend are shown in *Fig. 10*. Satisfactory superposition is obtained using the shift factors of *Fig. 9*. The same sort of agreement was found for PMPPL and two PMPPL/PVC blends of 75/25 and 25/75 compositions (7).

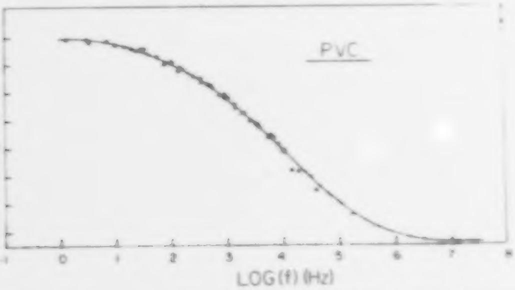

Fig. 7. Dielectric constant master curve of PVC at a reference temperature of 352.5 K (T_g + 15).

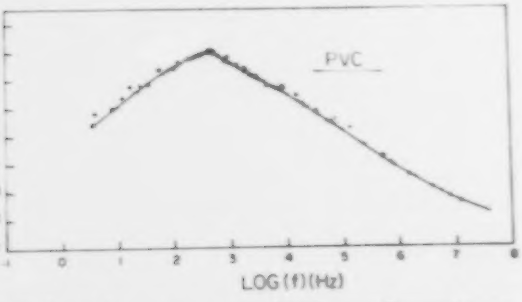

Fig. 8. Dielectric loss master curve of PVC at a reference temperature of 352.5 (T_g + 15).

At this point, it must be mentioned that a large number of authors have reported dielectric data for PVC and plasticized PVC's and have attempted to treat these results with the Cole-Cole method or the reduced variable methods (8–11, 15, 25–28 and others cited in *Ref. 11*). From this mass of somewhat contradictory results, it can be concluded that the superposition methods can be applied to PVC, but within a limited temperature range. This conclusion is also valid for most polymers (25, 29). The results presented in *Figs. 5–8* and *10* indicate that, within the frequency and temperature ranges used in this paper, the superposition methods can be applied satisfactorily.

Figure 11 shows a comparison of the dielectric constant master curves of PMPPL, PVC, and their blends at a reference temperature of T_g + 15. It is seen that the position and shape of the master curves change systematically with blend composition and that the master curves of the blends are located in between those of PMPPL and PVC. However, at low frequencies, the blend master curves are slightly closer to that of PMPPL and at high frequencies, they are slightly closer to that of PVC. One must keep in mind that PMPPL and the 75/25 blend are semicrystalline materials whereas the other blends and PVC are amorphous (*Table 1*). The higher dielectric constants of the former at high frequencies are certainly due to their degree of crystallinity.

Figure 11 is reminiscent of the stress relaxation master curves of PMPPL/PVC blends that were presented in *Ref. 1*. Both series of curves exhibit the same features and emphasize the strong influence of PMPPL on PVC properties, without showing any indication of micro-phase separation of the

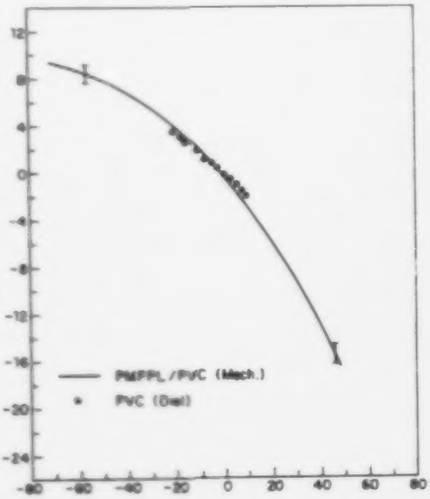

Fig. 9. Shift factors vs. (T-T_o) of PMPPL/PVC blends. The line was obtained from stress relaxation measurements. The data points were obtained by constructing Figs. 7 and 8.

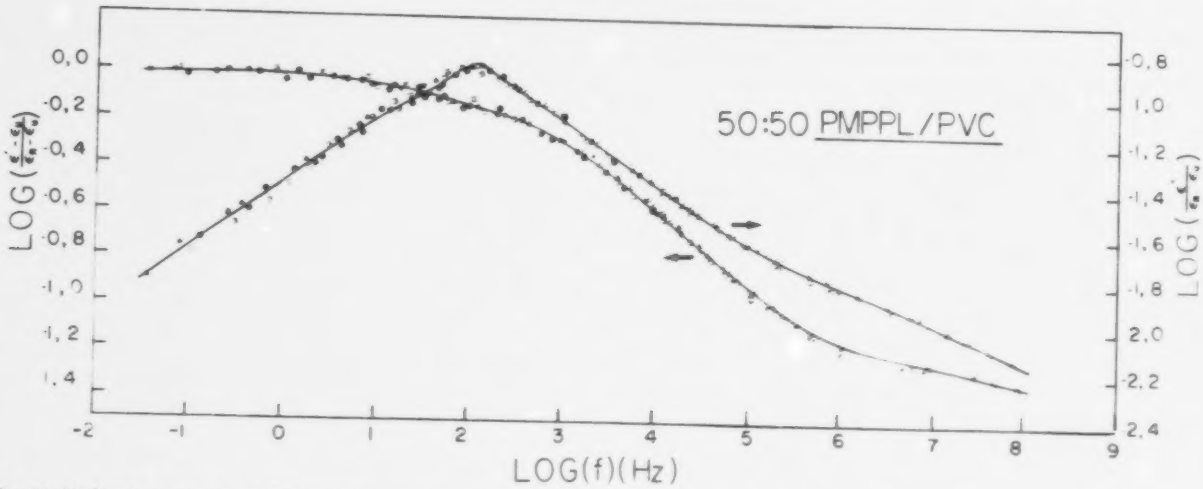

Fig. 10. Dielectric constant and dielectric loss master curves of a 50/50 PMPPL/PVC blend at a reference temperature of 320.5 K.

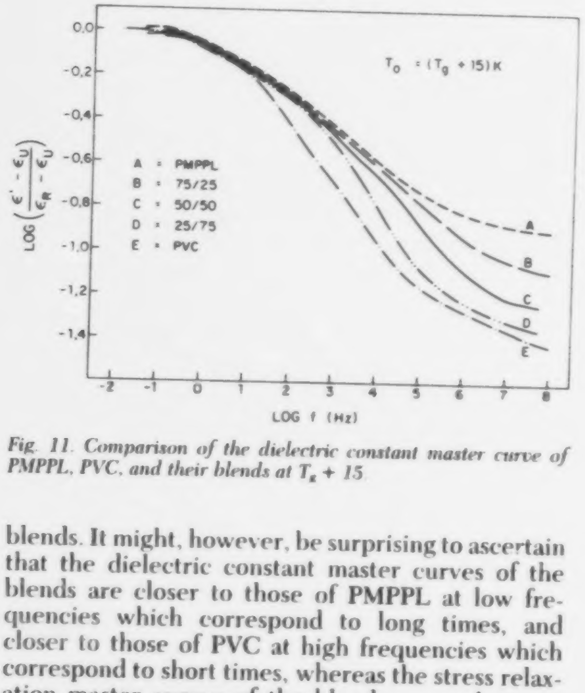

Fig. 11. Comparison of the dielectric constant master curve of PMPPL, PVC, and their blends at T_g + 15.

blends. It might, however, be surprising to ascertain that the dielectric constant master curves of the blends are closer to those of PMPPL at low frequencies which correspond to long times, and closer to those of PVC at high frequencies which correspond to short times, whereas the stress relaxation master curves of the blends were closer to those of PMPPL at short times and closer to those of PVC at long times. This apparent contradiction results from the fact that the dielectric experiments are analogous to creep experiments rather than to relaxation experiments (11, 25). Short time relaxation processes correspond to long time creep processes and vice versa.

The apparent activation energy, ΔH_a, of the α process can be calculated from the Arrhenius equation:

$$f = f_o \exp(-\Delta H_a/RT) \tag{8}$$

where f is the measuring frequency, f_o is the frequency when T approaches infinity, and T is the temperature corresponding to the maximum of the ϵ'' curve. The data obtained for PMPPL, PVC, and

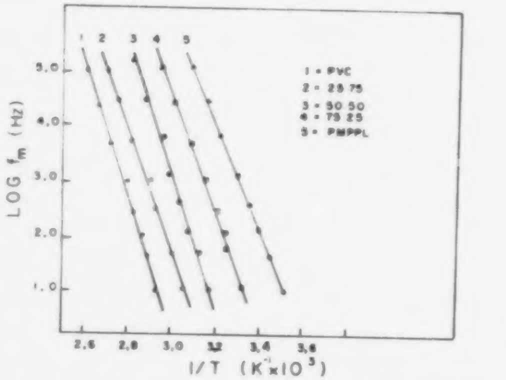

Fig. 12. Arrhenius plot of the dielectric loss peak of PMPPL, PVC, and their blends.

Table 4. Energy of activation of PMPPL/PVC blends.

Wt. % PMPPL	ΔH_a (kJ/mol) Arrhenius	ΔH_a (kJ/mol) WLF	C_1^o	C_2^o (K)
0	239 ± 16	200 ± 20	8.7	103
25	226 ± 20	175 ± 17	9.6	105
50	224 ± 12	161 ± 25	9.3	114
75	200 ± 15	137 ± 11	8.3	107
100	180 ± 12	134 ± 15	13.6	147

their blends are plotted in *Fig. 12* according to *Eq. 8*. Straight lines are obtained. ΔH_a was calculated from their slopes and is reported in *Table 4*.

ΔH_a values were also calculated from the Williams-Landel-Ferry (WLF) equation

$$\Delta H_a = \frac{2.303 C_1^o C_2^o R T_g^2}{(C_2^o + T_g - T_o)^2} \tag{9}$$

where C_1^o and C_2^o are two constants which were determined by the classical graphical method suggested by Ferry (25) and T_o is the reference temperature. The ΔH_a's obtained from *Eq. 9* and the C_1^o and C_2^o constants used in this calculation are given in *Table 4*.

Table 4 shows a fair agreement between the ΔH_a's obtained by the two methods. In both cases, there is a regular decrease from the higher value found for PVC to a lesser value for PMPPL. This decrease is mainly due to the decrease of T_g of the blends having higher PMPPL contents (30–32). This relation is clearly seen in *Eq. 9* where it is shown that ΔH_a is proportional to T_g^2. The ΔH_a's of PVC reported in *Table 4* are in good agreement with those of the literature. Values of 180 and 330 kJ/mol were reported by Sears and Darby (33) and Diaz Calleja and Gomez Ribelles (34) to mention just two examples. Several other examples can be found in the literature and most of them are in the 180–330 kJ/mole range (8–11, 15, 33).

Finally, a few words must be said about the micro-scale miscibility of PMPPL/PVC blends. We have already mentioned that a broadening of the DSC curves of these blends, in the T_g region, was interpreted as indicating the presence of local heterogeneities in the mixtures (5). On the other hand, stress relaxation measurements do not present any indication of micro-phase separation (1).

The measurements presented in this article support the stress relaxation results. We have already said that the parameters μ_r^2 and g change smoothly with composition indicating that the local conformation states of PMPPL and PVC are unperturbed by the blending process. In addition, the dispersion parameters α and $\Delta H/\Delta L$ also change smoothly with composition in contrast to the observation of significant increases of these parameters for other miscible polymer/polymer blends and for random copolymers (19–21). All these measurements strongly suggest that the PMPPL/PVC blends are as homogeneous mixtures as possible.

In addition, polymers that obey the time-temperature superposition principle are called thermorheologically simple materials whereas those that do not are called thermorheologically complex materials (25, 35). Usually, homogeneous materials are thermorheologically simple while heterogeneous materials, i.e., block copolymers, immiscible blends, and ionomers, are thermorheologically complex (25, 35–39). The satisfactory superposition of the dielectric data of PMPPL/PVC blends at T_o indicates that these blends are thermorheologically simple materials and suggests that they form homogeneous mixtures.

This conclusion implies that the broadening of the DSC curves may result from reasons other than the presence of local heterogeneities. This idea was recently suggested by Prest and Roberts and supported experimentally (40). They demonstrated that the broadening of the DSC curves of a miscible blend was due to differences in the structural properties of the glass rather than as the result of a change in the distribution of relaxation processes. This may constitute a valid explanation of the broadening of the DSC curves of PMPPL/PVC blends.

ACKNOWLEDGEMENTS

The authors thank the National Sciences and Engineering Research Council of Canada and the Ministry of Education of the Province of Quebec (FCAC program) for the research grants that supported this work.

REFERENCES

1. T. M. Malik and R. E. Prud'homme, *Macromolecules*, **16**, 311 (1983).
2. R. E. Prud'homme, *Polym. Eng. Sci.*, **22**, 90 (1982).
3. D. R. Paul and S. Newman, ed., "Polymer Blends," Academic Press, N.Y. (1978).
4. O. Olabisi, L. M. Robeson, and M. T. Shaw," Polymer-Polymer Miscibility," Academic Press, N.Y. (1979).
5. M. Aubin and R. E. Prud'homme, *Macromolecules*, **13**, 365 (1980).
6. M. Aubin, D. Bussières, D. Duchesne, and R. E. Prud'homme, in "Polymer Compatibility and Incompatibility: Principles and Practice," K. Solc, ed., Harwood Academic Publ., N.Y. (1982).
7. T. M. Malik, Ph.D. Thesis, in preparation.
8. R. M. Fuoss, *J. Am. Chem. Soc.*, **63**, 378 (1941).
9. E. R. Fitzgerald and R. F. Miller, *J. Colloid Sci.*, **8**, 148 (1953).
10. Y. Ishida, *Kolloid Z.*, **168**, 29 (1960).
11. N. G. McCrum, B. E. Read, and G. Williams, "Anelastic and Dielectric Effects in Polymer Solids," Wiley, London (1967).
12. K. S. Cole and R. H. Cole, *J. Chem. Phys.*, **9**, 341 (1941).
13. S. Haviliak and S. Negami, *J. Polym. Sci.*, **C14**, 99 (1966).
14. S. Haviliak and S. Negami, *Polymer*, **8**, 161 (1967).
15. S. Saito, *Kolloid Z.*, **189**, 116 (1963).
16. Y. Ishida, K. Yamafuji, and M. Takayanagi, *Kolloid Z.*, **189**, 97 (1963).
17. K. Sawada and Y. Ishida, *Rep. Prog. Polym. Phys. Japan*, **17**, 437 (1974).
18. H. Adachi, K. Adahi, Y. Ishida, and T. Kolako, *J. Polym. Sci., Polym. Phys. Ed.*, **17**, 851 (1979).
19. R. W. Wetton, W. J. MacKnight, J. R. Fried, and F. E. Karasz, *Macromolecules*, **11**, 158 (1978).
20. P. S. Alexandrovich, F. E. Karasz, and W. J. MacKnight, *J. Macrom. Sci.-Phys.*, **B17**, 501 (1980).
21. S. Akiyama, Y. Komatsu, and R. Koneko, *Polymer J.*, **7**, 172 (1975).
22. H. Frohlich, "Theory of Dielectrics," Oxford University Press, London (1958).
23. C. P. Smyth, "Dielectric Behavior and Structure," McGraw-Hill, N.Y. (1955).
24. P. S. Alexandrovich, F. E. Karasz, and W. J. MacKnight, *Polymer*, **21**, 488, (1980).
25. J. D. Ferry, "Viscoelastic Properties of Polymers," 3rd Ed., Wiley, N.Y. (1980).
26. J. D. Ferry, M. L. Williams, and E. R. Fitzgerald, *J. Phys. Chem.*, **59**, 403 (1955).
27. M. L. Williams, *J. Phys. Chem.*, **59**, 95 (1955).
28. J. D. Ferry and E. R. Fitzgerald, *J. Colloid Sci.*, **8**, 224 (1953).
29. J. D. Ferry and S. Strella, *J. Colloid Sci.*, **13**, 459 (1958).
30. H. W. Starkweather, Jr., *Macromolecules*, **14**, 1277 (1981).
31. P. J. Phillips, *J. Polym. Sci., Polym. Phys. Ed.*, **17**, 409 (1979).
32. J. M. Pochan, C. L. Beatty, and D. F. Pochan, *Polymer* **20**, 879 (1979).
33. J. K. Sears and J. R. Darby, "The Technology of Plasticizers," Wiley, N.Y. (1982).
34. R. Diaz Calleja and J. L. Gomez Ribelles, *Polym. Eng. Sci.*, **22**, 845 (1982).
35. D. G. Fesko and N. W. Tschoegl, *J. Polym. Sci.*, **C35**, 51 (1971).
36. D. Kaplan and N. W. Tschoegl, *Polym. Eng. Sci.*, **14**, 43 (1974).
37. D. G. Fesko and N. W. Tschoegl, *Int. J. Polym. Mater.*, **3**, 51 (1974).
38. C. K. Lim, R. E. Cohen, and N. W. Tschoegl, *Adv. Chem. Series*, **99**, 397 (1971).
39. A. Eisenberg and M. King, "Ion-Containing Polymers," Academic Press, N.Y. (1977).
40. W. M. Prest, Jr., and F. J. Roberts, Jr., Proceedings of the IUPAC 28th Macromolecular Symposium, Amherst, July 1983, p. 664.

DISCUSSION

L. A. Utracki: Could you say a few words about the experimental method used to determine the viscoelastic relaxation spectrum from the mechanical test data?

R. E. Prud'homme: I must, first of all, mention that the relaxation measurements were done in the region of linear viscoelasticity which was determined experimentally for each sample. It turned out, for most samples and at most temperatures, to be below 1 percent in strain. We then used a classical Instron tester, with temperature regulation, for the relaxation measurements which were tedious, but quite simple.

G. L. Vexler: What kind of mixing mechanism have you used? A Brabender plastograph or something else?

R. E. Prud'homme: We prepared all samples from THF solutions. This method leads to homogeneous mixtures, as determined by DSC. Our purpose was to prepare samples which were as homogeneous as possible. For that purpose, solution casting is appropriate.

M. Winnik: Just a brief question: how did you remove the solvent to ensure homogeneous mixing?

R. E. Prud'homme: With polyesters and PVC, the removal of the last trace of solvent is a problem. It requires leaving the sample in a vacuum oven until it reaches a constant weight.

M. Winnick: I was just curious, if you wanted to ensure intimate mixing whether you would want to remove the solvent as rapidly as possible rather than slowly?

R. E. Prud'homme: Recently we examined mixtures of aromatic polyesters with chlorinated polymers, like PVC. We discovered that, whatever the rate of evaporation, a two-phase material is found from some solvents, but a homogeneous mixture is generated from other solvents. The critical parameter is the thermodynamic quality of the solvent, not its rate of evaporation. If the solvent is properly chosen, a homogeneous mixture will be found whatever the rate of evaporation. This topic has been discussed by D. D. Patterson in two recent papers: *Macromolecules*, **10**, 1021 (1977) and *Polymer Engineering and Science* **22**, 64 (1982).

Analysis of Transient Sorption and Permeation of Small Molecules in Multiphase Polymer Systems

J. M. OTTINO *and* N. SHAH

Departments of Chemical Engineering
and
Polymer Science and Engineering
University of Massachusetts
Amherst, Massachusetts 01003

The transport of small molecules (gases) in incompatible polymer blends, semi-crystalline polymers, and filled polymer systems is usually examined in terms of transient sorption and permeation experiments which yield effective values of diffusivity and permeability. From a modeling standpoint these complex systems can be regarded as composites with complex morphology whereas the gas can be considered as a molecular probe of the morphology and especially its connectedness. In this paper we present a brief review of transport descriptions in prototype ordered and disordered systems with special emphasis on simulation of transient measurements. The simulations presented are selected in such a way as to aid in the interpretation of experimental results obtained by sorption and permeation and in the construction and evaluation of morphologies with desired effective transport properties.

INTRODUCTION

In many applications one would like to describe the transport of permeants through heterogeneous polymer systems of various degrees of complexity. However, the current level of understanding is very incomplete; there are no comprehensive experimental studies and an almost complete absence of modeling (1).

According to the level of scrutiny, the polymeric materials of interest might contain heterogeneities ranging from tens of Angstroms to several microns; they might be mechanically interspersed polymers with morphology dependent upon processing conditions, semi-crystalline polymers, and even filled systems where the filler can be glass, graphite, carbon black, etc. (2). The permeants can be small, non-interactive gas molecules, vapors, and even liquids which could induce swelling, crystallization, crazing, etc. (3). From a general viewpoint, multiphase polymer systems have a rich morphological structure and the transport laws within microdomains are in many cases only imperfectly understood (3).

In spite of this variety of problems, or probably due to it, the transport of permeants in multiphase polymer systems has received disproportionately little attention. Admittedly, experiments are hard to interpret and general enough theories difficult to conceptualize and generate. However, recent theoretical advances in the area of transport in disordered systems (4, 5) should shed some light on this subject and aid in the interpretation of classical experimental techniques.

The objective here is to present a few aspects of this problem from a general viewpoint. First, we briefly describe possible morphologies and transport laws at the microscale level. We then concentrate on the transport of non-interacting species (gases) in prototype blends of different degrees of morphological complexity. The transport laws at the microscale are assumed linear. The results presented are selected in such a way as to aid in the interpretation of experimental results obtained via sorption and permeation and in the construction and evaluation of morphologies with desired effective transport properties.

MORPHOLOGIES OF INTEREST

If a system is such that the transport coefficient, D, within a continuum framework, is a discontinuous function of space, i.e.

$$D(\underline{x}) = \begin{cases} D_1 \text{ if } \underline{x} \text{ is in region 1} \\ D_2 \text{ if } \underline{x} \text{ is in region 2} \\ \text{etc.} \end{cases} \qquad (1)$$

we then have a system with sharp boundaries and the regions 1, 2, ... are termed *domains* (or phases) (throughout our presentation we assume that the length scale of the domains is much larger than the length scale of the penetrant. However, the term domain should be interpreted in an abstract sense). The domains (or phases) may or may not be simply connected, one of them may be discontinuous or in the binary case both may be continuous, etc. If the interfacial regions, say between domains "1" and

"2", are provided some identity and preferential diffusion occurs along boundaries the system can still be described by the above relation. In this case, regions of simply-connected, disconnected or multiply-connected *surfaces* contribute to diffusion.

Systems such as (1) can be perfectly ordered, examples are regular arrays of spheres, ellipsoids, etc., different types of regular or semi-regular lattices, layered structures, and several kinds of bicontinuous structures. At the other extreme we have random and chaotic systems, with random arrangement of randomly shaped phases such as in the conceptual representations of composites in Effective Medium Theory (6, 7), Voronoi tessellations (8), and percolation theory (9).

In percolation theory (9), "phases" are distributed randomly in regular networks or trees in such a way that the underlying topology is constant whereas in the Voronoi tessellation the topology is also variable (8). Some degree of order can be introduced by means of correlated percolation (9) and a rich variety of structures can be obtained via regular or irregular cellular structures (of which the Voronoi tessellation is a particular case). More ordered systems are those in which we can recognize order at particular scales. For example, small scale order and large scale disorder are observed in many real systems. Even more ordered structures would correspond to blends with order resembling the different degrees of order in liquid crystals. The variety of morphologies is enormous and the bridge in between perfectly ordered, partially ordered, and perfectly random structures is not clear; there is no complete mathematical theory of classification of disorder.

Generalizations are possible. For example, most of the previous systems can be the precursors of systems with diffuse boundaries. The boundaries can be selected in such a way that they mimic real systems where a smooth concentration gradient exists in between phases (say over length scales much larger than molecular scales) but where the regions are still clearly distinguishable. The extreme mixing case would correspond to nearly compatible systems where D is a smooth function of position. Polymeric systems undergoing phase separation bridge these two extremes.*

Throughout this work we will focus on perfectly ordered and perfectly disordered systems.

TRANSPORT LAWS WITHIN DOMAINS

The transport laws within domains can be divided according to whether the domains are rubbery or glassy and these can be further divided according to the size of the molecule of the permeant (10). If we restrict ourselves to low pressures and small molecules, the transport in rubbery polymers is well understood. We have

$$\text{rate of relaxation} \gg \text{rate of diffusion},$$

diffusion controls, and boundary conditions are rapidly established. The diffusion coefficient is nearly constant and the solubility obeys Henry's law. The classical scaling laws with square root of time behavior are obeyed (11). For example,

$$\text{mass uptake} = \text{const. } t^{1/2}, \text{ for small time in sorption experiments}$$

$$\text{penetration distance} = \text{const. } t^{1/2}$$

For slightly larger molecules we might have some concentration dependence but diffusion is still Fickian and independent of time (we should note here that the diffusion coefficient can not be an *explicit* function of time). This case is also termed *Case I* diffusion.

Solute diffusion in glassy polymers is dominated by relaxation. We have

$$\text{rate of relaxation} \ll \text{rate of diffusion},$$

and the polymer responds slowly to the presence of the penetrant. Boundary conditions can be time dependent, solubility may present positive and negative deviations from Henry's law, and effective diffusion coefficients appear to be time dependent. Two cases are distinguished, *Case II* with

$$\text{mass uptake} = \text{const. } t, \text{ in sorption experiments}$$

$$\text{penetration distance} = \text{const. } t,$$

and super *Case II* with

$$\text{mass uptake} = \text{const. } t^n,$$

in sorption experiments, with $n > 1$ (12, 13).

The boundary conditions between domains are in general given by partition functions expressing the equality of chemical potential and continuity of flux. A special case corresponds to an impervious domain (effectively satisfied when $D_1/D_2 \to 0$). In this case the interfacial boundary condition corresponds to zero flux at the boundary.

SCENARIO

In order to highlight the role of morphology we will restrict ourselves to idealized blends governed by linear transport laws at the microdomain scale. Under these conditions our goal is to obtain the effective diffusion coefficient for the transport of a species in the blends, i.e., for a binary blend with domains A and B, we seek

$$Deff = f(D_A, D_B, S_A, S_B, \phi_A, \phi_B, \text{morphological parameters}) \tag{2}$$

where D_A and D_B are the diffusion coefficients of the permeating species in domains A and B, S_A and S_B are the solubilities, and ϕ_A and ϕ_B, the volume fractions of the domains. (We take $D_A/D_B < 1$)

Theoretical analysis can be conducted at two levels: steady and non-steady state. Most steady state analyses to date have been conducted on infinite (or periodic) systems. For example, the assumption of an infinite system is implicit in EMT (7) and the numerical experiments in percolation theory are presented in the limit of infinitely large samples; the theory has not been adequately developed for finite systems.

---

*Polymer blends can have morphologies that are quenched or are at equilibrium. For example, a mechanically mixed, untreated blend will have a quenched morphology that depends on processing whereas a carefully prepared and annealed blend might achieve an equilibrium morphology.

The classical transport experiments in polymers are sorption and permeation and the measured outputs are weight gain and flux *vs.* time respectively (14). Several means have been devised to obtain effective diffusion coefficients from these data (14). However, it has been noted that on occasion the values obtained by different methods differ by up to an order of magnitude (14). Also, it has been noted that the values obtained by different methods of analysis of either the sorption or permeation experiments can give different values. No thorough analysis of these effects has yet been reported in the literature.

Experimental analyses are inherently non-steady state in nature. Non-steady state simulations give additional information and serve to highlight experimental limitations and the relationship between transport and morphology.

STEADY STATE ANALYSIS

Analysis can be carried out in terms of theories suited for ordered and disordered systems. However, real systems are most likely to be neither ordered nor completely disordered.

A simple analysis of transport of small molecules in polymer blends in terms of Effective Medium Theory is given by Sax and Ottino (1). The EMT result for a conductive—non-conductive network of coordination number z was combined with the analysis of Davis (15) to account for the proper driving force, i.e., the gradient of the chemical potential. The model was applied to a large set of data of permeation in blends of PVC and several rubbery polymers obtained by Ranby *et al.* (16–19). Assuming the media to be completely random the coordination number, z was calculated by forcing

$$(Deff)_{\text{exp}} = [Deff(z)]_{\text{theory}}$$

at all volume fractions. In general, the coordination number at low volume fractions was unrealistically large and decreased towards 4–6 for $\phi_B \gtrsim 0.4 (D_A < D_B)$. Thus, the degree of connectedness of the rubbery phase at low volume fractions is higher than predicted by a model assuming complete chaos; the rubbery component tends to percolate, i.e., to form sample spanning clusters at volume fractions much smaller than those predicted by Effective Medium Theory.

Ranby's data was also analyzed in terms of simple models assuming locally ordered microstructures (lamellae, cylinders, etc.) and large scale disorder. This analysis reinforced the conclusion obtained by EMT. At low volume fractions of the rubbery component the models assuming lamellar and cylindrical microstructural arrangements gave, in general, a fair description of the system whereas models assuming spherical non-overlapping microdomains often failed to predict the correct value for the initial slope $dDeff/d\phi_B$.

The above results could have been anticipated. Based on some microscopy observations Ranby (20) indicated that the melt blending of PVC and the rubbers produced structures where the grains of PVC tended to be coated by the rubbers. Indeed, it seems to be easy to create sample spanning clusters of the less viscous material. (See Example 1, next section)

Compatibility seems to decrease the thickness of these sample spanning clusters and *Deff* decreases if the volume fraction is held constant. Under normal conditions changing the compatibility seems to provide a method for changing *Deff*.

SIMPLE EXTENSIONS OF PERCOLATION THEORY

In the context of percolation theory, the transport of species occurs in idealized regular or irregular randomized lattices. The classical problem is the prediction of *Deff* as a function of the fraction of conductive bonds (bond percolation problem). The results can be easily generalized to account for more practical situations. Let us introduce the methodology by means of three simple examples; the generalization to other cases should be obvious.

Example 1. In a highly idealized situation consider a $2D$ (two dimensional) blend of A and B, $D_A/D_B = 0$, where the highly conductive material occupies randomly the space between grains of A as shown in *Fig. 1*. The problem can be viewed as a bond percolation problem in a square lattice. If ϕ_B' is the fraction of conductive bonds (number of bonds of B/total number of bonds) and ϕ_B is the area fraction of B (area occupied by B/total area), the relationship between ϕ_B' and ϕ_B is (to a first order approximation)

$$\phi_B \cong \frac{2\phi_B'\left(\dfrac{\delta}{l}\right)}{1 - 2\phi_B'\left(\dfrac{\delta}{l}\right)}$$

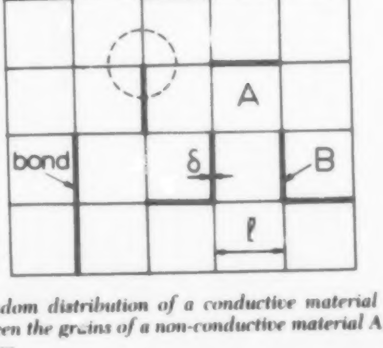

Fig. 1. Random distribution of a conductive material B in the space between the grains of a non-conductive material A, on a 2D square lattice.

The square lattice percolates at $\phi_B'^C = 0.5$ (bond percolation). If $\delta/l = 0.1$ then $\phi_B^C = 0.111$. Thus a blend can be made conductive at small volume fractions by dispersing the highly conductive material between the grain boundaries of the impervious material.

Example 2. Consider a square $2D$ blend composed of fused square grains of size l of a highly conductive material B, some of which are coated with a thin layer of thickness δ of a non-conductive material A, $D_A/D_B = 0$ (see *Fig. 2*). The problem can be viewed as site percolation in a square lattice. If ϕ_A' is the fraction of non-conductive sites (i.e., number of coated squares/total number of squares) and ϕ_A is the area fraction of A (i.e. area of A/total area) we have (to a first order approximation)

$$\phi_A \cong 4\phi_A' \left(\frac{\delta}{l}\right)$$

The site percolation fraction is $\phi_B'^C = 0.591$. The lattice will become nonconductive if $\phi_A' \geq 0.409$. If $\delta/l = 0.1$, the blend will be non-conductive if $\phi_A \geq 0.164$. Thus, a blend can be made non-conductive at small volume fractions by random coating of the conductive grains with the impervious material.

Example 3. Consider a $3D$ blend of A and B, $D_A/D_B = 0$, composed of fused cubic grains of size l of an impervious material A some of which have the "edges" randomly replaced with highly conductive needles of B of diameter δ ($\delta \ll l$). The problem can be viewed as bond percolation in a three dimensional cubic network and the analysis is similar to the previous examples.

Generalizations are possible; however, they should be managed with care. The new problems have to correspond to a classical bond or site percolation problem. For example, coating impervious $3D$ cubes with a conductive material (generalization of Example 2) or placing conductive needles on the edges of Voronoi polygons (generalization of Example 3) do not correspond to any classical problem.

NON-STEADY STATE ANALYSIS

Transient diffusion in disordered media is richer in structure than steady state and tends to a time independent limit only after a relaxation time, characteristic of the morphology, has elapsed. The starting point of the analysis is the so-called Master Equation (21) applied to a carefully selected two or three dimensional cellular or network representation (tessellation) of the blend in question.

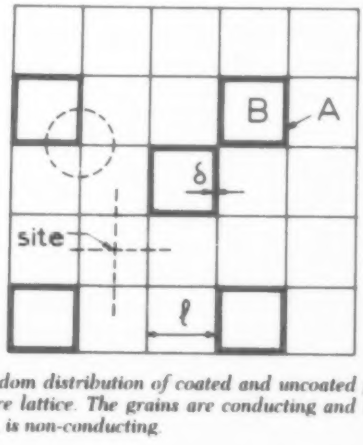

Fig. 2. Random distribution of coated and uncoated grains of B in 2D square lattice. The grains are conducting and the coating material, A, is non-conducting.

In these representations the resistance to diffusion is located only in certain planes and bonds. The equation describing the time evolution of concentration in the cell or site i is given by:

$$\left\{\frac{dC_i}{dt} = \sum_j \left(W_{ij}C_j - W_{ji}C_i\right)\right\} \qquad (3)$$

where the subscript j runs from 1 to the number of nearest neighbors of the cell or site in question. W_{ij} is the transfer rate from the cell or site j to i whereas W_{ji} is the transfer rate from the cell or site i to j. The values of W_{ij} (frequency) are computed from the properties of the microstructure of the medium as well as the transport properties of the individual domains. The spatial distribution of the W_{ij}'s (if the W_{ij} are arranged in form of a matrix) describes the topology of the medium (i.e., connectedness of domains).

Figure 3 shows several examples of basic tessellations of space. A basic tessellation is a subdivision of two of three dimensional space by means of regular, semi-regular, or irregular convex polytopes; polygons in two dimensions, $2D$, polyhedra in three dimensions, $3D$ (22). (Basic tessellations do not define any particular physical process and they can be interpreted to represent different diffusion processes. They are just constructs that serve as a base state for the definition of a physical problem representing some real polymer blend).

The number of edges (in $2D$) or faces (in $3D$) of a given cell describes its connectivity and is called its coordination number, z. There are only three regular tessellations in $2D$ (triangle ($z = 3$), square ($z = 4$), hexagon ($z = 6$)) and only one in $3D$ (cubic ($z = 6$)). The classical irregular tessellation is the Voronoi tessellation (8). It has both random geometry and topology. In $2D$ Voronoi tessellations, the minimum z is 3 and the average is 6. In $3D$ the minimum z is 4 and the average is 15.46. A network is defined by lines intersecting the walls of the cell (dual network). Thus, the dual network of a square tessellation in $2D$ is a square network, the dual of a hexagonal tessellation in $2D$ is a triangular network ($z = 6$), etc. (22). The dual network of a Voronoi tessellation has both a random geometry and topology (22). The coordination number of the dual network is equal to the coordination number of the polygons.

The sides of a tessellation in $2D$ and the edges of the polygons in $3D$ define still another network. For example, in $2D$, the network defined by the square tessellation has $z = 4$, the hexagonal tessellation, $z = 3$, and the Voronoi $z = 3$ ($z \geq 4$ is extremely improbable). In $3D$, we have $z = 6$ for the cubic tessellation and $z = 4$ for the Voronoi tessellation ($z \geq 5$ is extremely improbable). Each

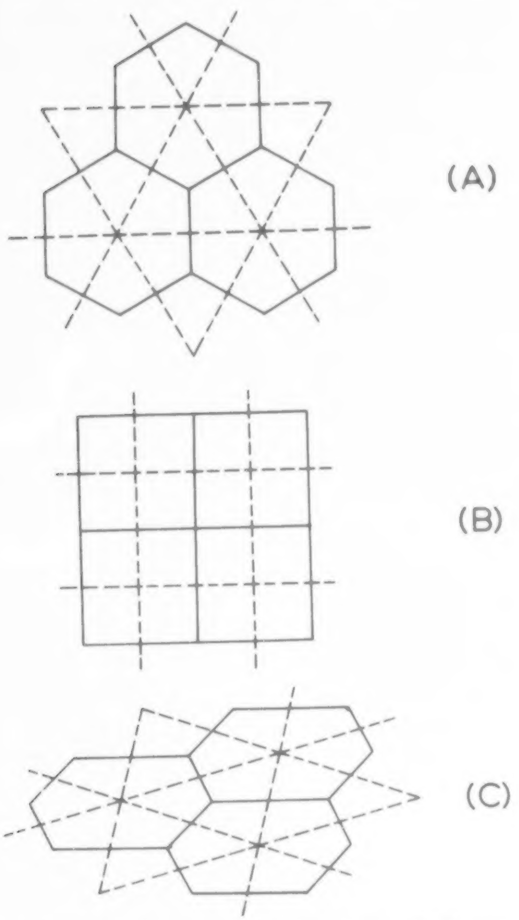

Fig. 3. Examples of the basic tessellations of space. Dual networks are shown with broken lines: (a) regular hexagonal, (b) square, (c) generalized hexagonal.

of these constructs might represent one of several transport problems which in turn define the field of W_{ij}. Some examples are given next. The special case of cellular systems is described by Mohanty *et al.* (23).

Example 4. Transport in media with arbitrarily shaped and randomly dispersed phases and $D_A/D_B = 0$ (see *Fig. 4*). If the shape of domains is known we can superimpose a grid and set $W_{ij} = 0$ if the bond is in the interior of A, and W_{ij} = const. if the bond is in B. Some kind of decision for bonds cutting across the boundary of the phases has to be made. Transport in random binary blends is simulated by random distribution of a bimodal population of W_{ij}. The results are expected to be a function of the coordination number of the network.

Example 5. Grain boundary diffusion in a system where a highly conductive material occupies preferentially the spaces between the grains of a nonconductive material (see *Fig. 1*). Construct a cell as indicated in *Fig. 1* (dashed lines) and set W_{ij} = const. if the bond is of material B and zero if it is not. This can be easily generalized to $3D$. The W_{ij}'s are randomly distributed.

Example 6. A variation on grain boundary diffusion. A more complex example is obtained by fusing impervious squares of A, some of which are coated, with a layer of conductive material B (the reverse of example shown in *Fig. 2*). Construct a cell as indicated in *Fig. 2* (dashed lines) and set W_{ij} = const. if the bond is of B. The W_{ij}'s *are not* randomly distributed.

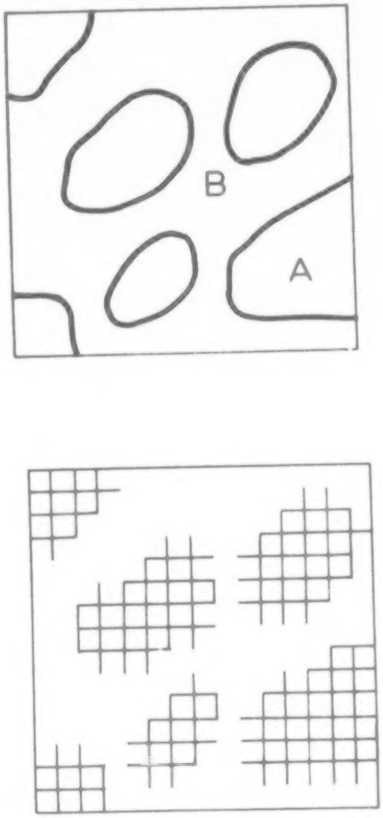

Fig. 4. Media with arbitrarily shaped and randomly dispersed phases.

Evaluation of W_{ij} (Transfer Rates)

In general, W_{ij} is given by

$$W_{ij} = \frac{D_{ij}A_{ij}}{V_i\delta_{ij}} = \frac{\text{Diffusion coefficient}}{(\text{characteristic length})^2}$$

Two main cases are identified here:

Diffusion in network and network-like structures (see Example 5)

D_{ij} = diffusion coefficient of species in the material of bonds
A_{ij} = cross sectional area of bonds
δ_{ij} = length between sites i and j
V_i = volume of the cell around site i

Cellular media (see Mohanty *et al.* (23))

D_{ij} = diffusion coefficient of species i in the wall connecting cell i and cell j
A_{ij} = area of contact between cell i and cell j

δ_{ij} = thickness of the wall separating cells i and j
V_i = volume of cell i

Most of the results given in this paper are presented in terms of the dimensionless time, $\tau \equiv tW^{\circ}_{ij}$, where W°_{ij} is a reference transition rate.

SOLUTIONS OF THE MASTER EQUATION

Under special conditions the system of equations (3) can be solved analytically. If the field W_{ij} is uniform the system can be solved for some regular and semi-regular infinite systems by means of generating functions. Aris (24) solved the system for two dimensional generalized hexagons whereas Mohanty *et al.* (23) presented the result for three dimensional generalized hexagons. In both cases the transfer was assumed to occur across the walls of the polytopes (i.e., transfer along bonds in the network dual). If the field of W_{ij}'s is a stochastic function of position, general solutions for infinite lattices by using Laplace transforms are presented by Webman (4) and Sahimi *et al.* (5). Other cases have to be solved numerically.

EFFECTIVE DIFFUSION COEFFICIENTS

For engineering applications, the equations governing transport at the microscale (Master Equation) are replaced by an equation describing behavior at an intermediate scale much larger than the microstructural level but much smaller than macroscopic dimensions. The equation for the average concentration at any site in the lattice is replaced by that for the average concentration over the intermediate scale. The average concentration is smooth and at this scale the composite behaves as a structured continuum.

In general, the lattice representing a random composite will have a considerable amount of disorder, that is, variation in the bond transition rates. It has been shown by Sahimi *et al.* (5) that the effective bond transition rate for such a lattice will be time dependent and will constitute the memory kernel of a generalized Master Equation. The effective diffusion coefficient in the corresponding equation for the intermediate-scale structured continuum will, therefore, also be a function of time.

It must be noted that the lattice itself does not possess any memory. It is only when the system behavior is characterized by a single coefficient, *Deff*, that a memory effect has to be taken into account.

Deff(t) has been obtained by several investigators in different ways. Webman (4) and Sahimi *et al.* (5) obtained *Deff* analytically on the basis of a single-bond effective medium approximation for the potential in infinite disordered lattices subjected to an injection type initial condition. The same problem was studied in infinite ordered and disordered lattices by Mohanty, *et al.* (23) by using an equation of the type

$$\frac{\partial c}{\partial t} = Deff(t)\nabla^2 c$$

rather then the form suggested by Sahimi *et al.* (5). However, the time dependence obtained for the case W_{ij} = uniform is a consequence of the discretization of the continuum and not of intrinsic memory effects.

According to recent analysis (4, 5, 25) the following results have been obtained: if $D_A/D_B = 0$, $\phi_B < \phi_B{}^C$, *Deff*(t) tends to zero as $t \rightarrow \infty$ and a delta function of contaminant obtains a final radius that diverges as $|\phi_B - \phi_B{}^C|^{-1}$ (4). If $D_A/D_B = 0$, $\phi_B > \phi_B{}^C$, *Deff*(t) tends to a constant value *Deff*(∞). The time scales to approach *Deff*(∞) depend strongly on the proximity of ϕ_B to $\phi_B{}^C$. If $\phi_B \gtrsim \phi_B{}^C$, the time scale for steady state diverges as $|\phi_B - \phi_B{}^C| - \gamma_T$. According to Davis (24), $\gamma_T = 2.5$–3.6 in $2D$ and $\gamma_T = 1.7$–3.4 in $3D$. Webman gives $\gamma_T = 2$ for $3D$. If $\phi_B > \phi_B{}^C$, the steady state is approached in time scales $|Deff(\infty)a_v{}^2|^{-1}$, where a_v is the intermaterial area per unit volume in $3D$ or perimeter per unit area in $2D$, a measure of distances between clusters (25).

The behavior of *Deff*(∞) has been well-studied also. Near $\phi_B{}^C$, for $\phi_B > \phi_B{}^C$, $Deff(\infty)\alpha(\phi_B - \phi_B{}^C)\gamma_E$. The reported values of γ_E are: $\gamma_E = 1.1$ to 1.3 in $2D$, $\gamma_E \cong 1.6$ in $3D$ for all tessellations.

A few general statements can be made (see section on Steady State Analysis): $\phi_B{}^C$ is smaller, the larger the coordination number (8, 9, 22). At a given $\phi_B > \phi_B{}^C$, *Deff*(∞) is larger, the larger the coordination number. At a given $\phi_B > \phi_B{}^C$, *Deff*(∞) increases as topological disorder decreases (for example, *Deff*(∞) hexagonal > *Deff*(∞) Voronoi). However, the percolation threshold for both the hexagonal and Voronoi tessellations is the same. This indicates that the average coordination number is the dominant parameter (22). In terms of simulations, the hexagonal representation is an inexpensive way of modeling transport in a Voronoi tessellation. Consequently, most of the results presented in this paper are computed in terms of hexagonal tessellations.

It is not surprising to observe memory effects in media with complex morphology at intermediate scales and transition to Fickian behavior at large scales, especially near the percolation point. The coherence length, ζ, (26) provides a good measure of the suitable length scale for averaging. In a disordered composite, morphological properties and quantities of interest such as concentration averaged over length scales $\gg \zeta$ will approach the continuum limit. The coherence length diverges according to:

$$\zeta \alpha |\phi_B - \phi_B{}^C| - \gamma_\zeta$$

where $\gamma_\zeta = 1.2$ to 1.3 in $2D$ and $\gamma_\zeta = 0.8$ to 0.9 in $3D$.

EFFECTIVE DIFFUSION COEFFICIENTS IN TERMS OF SORPTION AND PERMEATION

We have seen that non-Fickian behavior and memory effects arise from morphological effects even though the constitutive equations for the microstructural subparts of the composite are linear. It is then important to examine the behavior of the effective diffusion coefficient as obtained by the classical experimental techniques of sorption and permeation. The important points to be covered by such an analysis are:

- Most previous analyses considered the case $D_A/D_B = 0$. Polymer blends of interest have $D_A/D_B = 10^{-1}$ to 10^{-3}. Can percolation be detected under these conditions?
- Since $D_A/D_B = 0$, most previous analysis did not consider the solubility distribution among phases. A realistic analysis should include this effect.
- Polymer blends present an enormous array of morphologies highly dependent upon the method of preparation: studies including partially ordered systems, diffusion along grain boundaries, etc., are needed.
- There are at least three different techniques with which the effective diffusion coefficient is estimated from sorption experiments (half-time, initial slope, moment). Are all of them equivalent if the medium has complex morphology? A similar question can be posed for differential permeation.
- Most previous analyses have concentrated on infinitely large systems. However, in reality as well as in experimental model systems the system inhomogeneities might be comparable to the size of the system (especially near the phase inversion point). Analyses for thin films are needed.
- Finally the most important question is the following: Can percolation be safely detected in systems with $D_A/D_B \neq 0$ and finte solubility ratio by means of sorption and/or permeation?

Only a few important points pertaining to the above questions will be covered here.

SIMULATIONS OF SORPTION AND PERMEATION

All the results presented here have been obtained by simulations on 2*D* hexagonal tessellations, whose cells are marked *A* or *B* in an ordered or chaotic manner. *Figures* 5 to 9 illustrate the data obtained by simulation of sorption and differential permeation in a chaotic composite, with the constraint that $D_A/D_B = 0$.

The time dependence of the flux, F_t, of a permeant through composites with different area fractions of *B* is shown in *Fig.* 5. F_t is measured by the rate at which the concentration in the last layer of cells on the downstream side is depleted by the diffusion of the permeant into the gas phase. These curves have been used to relate the half-time, $\tau_{1/2}$, for each composite to the area fraction of *B*, ϕ_B. This relationship has been plotted in *Fig.* 6.

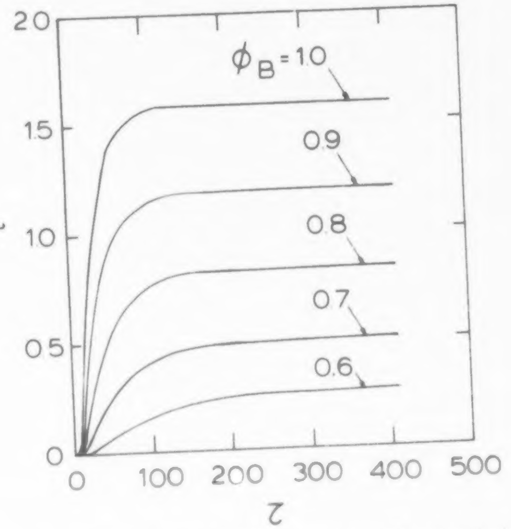

Fig 5 Permeation through a 2D hexagonal tessellation with chaotic morphology and $D_A/D_B = 0$ Number of exposed cells per face = 15, tesselation is 18 cells thick Dimensionless flow rate, F_t, vs. dimensionless time, τ

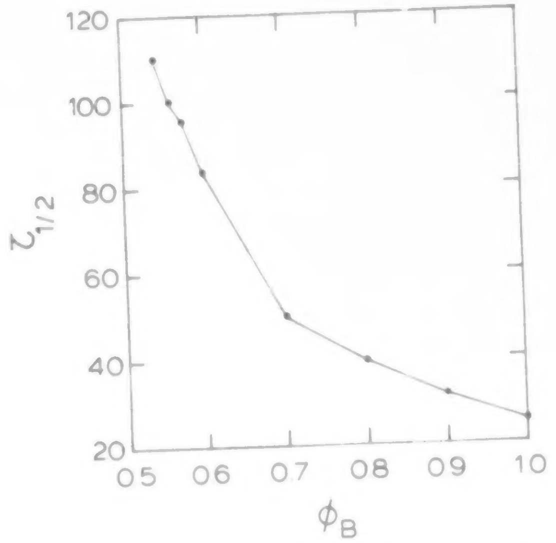

Fig 6 Permeation through a 2D hexagonal tessellation with chaotic morphology and $D_A/D_B = 0$ Number of exposed cells per face = 15; tessellation is 18 cells thick Half-time, $\tau_{1/2}$, vs area fraction, ϕ_B.

Since the effective diffusion coefficient, *Deff*, is inversely proportional to $\tau_{1/2}$, the ϕ_B-dependence of *Deff* can be easily estimated by the half-time method. *Figure* 7 illustrates this dependence by means of the effective volume fraction, $\phi_B{}^E$, defined as $Deff/D_B$. All these results have been obtained for a single set of composites created randomly (one realization).

The time-dependence of the fractional mass uptake, M_t/M_∞, of a permeant in such composites with different area fractions, ϕ_B, is shown in *Fig.* 8. M_t is the dimensionless mass of the permeant in the com-

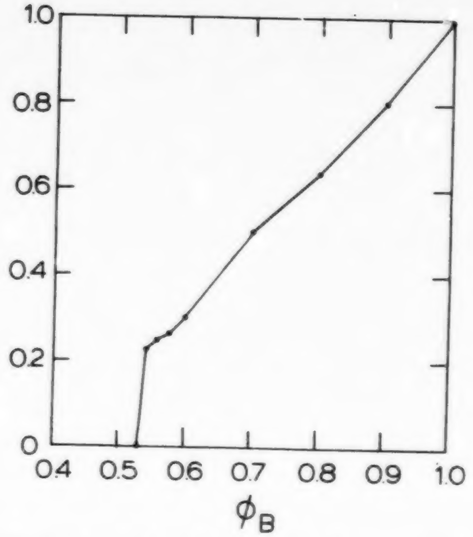

Fig. 7. Permeation through a 2D hexagonal tessellation with chaotic morphology and $D_A/D_B = 0$. Number of exposed cells per face = 15; tessellation is 18 cells thick. Conductivity factor, ϕ_B^E, vs. area fraction, ϕ_B.

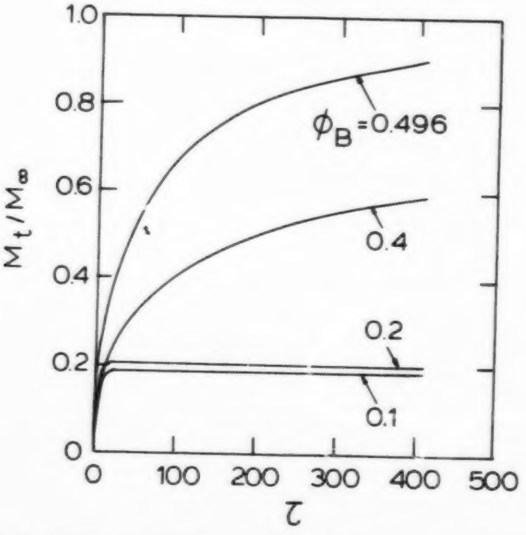

Fig. 8. Sorption in a 2D hexagonal tessellation with chaotic morphology and $D_A/D_B = 0$. Number of exposed cells per face = 15; tessellation is 18 cells thick. Fractional mass uptake, M_t/M_∞, vs. dimensionless time, τ.

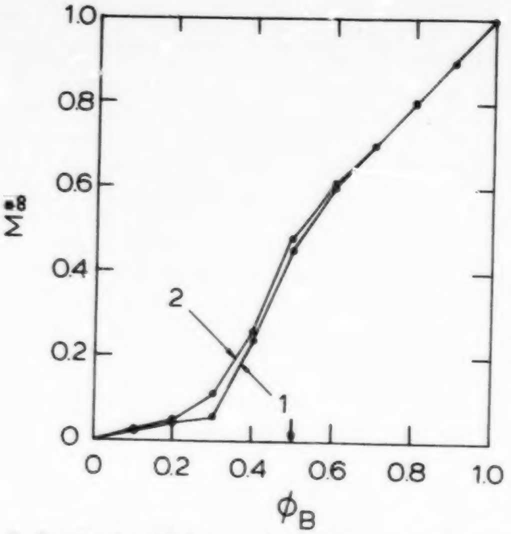

Fig. 9. Sorption in a 2D hexagonal tessellation with chaotic morphology and $D_A/D_B = 0$. Equilibrium mass uptake, M_∞^*, vs. area fraction, ϕ_B. Two realizations: Curve 1: number of exposed cells per face = 15; tessellation is 18 cells thick; Curve 2: number of exposed cells per face = 14; tessellation is 14 cells thick. The arrow indicates the reported percolation threshold for this tesselation.

posite at time τ and M_∞ is the dimensionless mass of the permeant present in the composite at equilibrium with the gas phase if all the conductive phase were accessible. Below the percolation threshold, a differential permeation experiment indicates that the effective diffusion coefficient is zero in such composites. However, the mass uptake in composites with low values of ϕ_B is non-zero. A non-zero value of *Deff* can be obtained from this data if the initial slope method (14) or the half-time method is used. Hence, the two experiments provide contrasting conclusions. In such cases, it is advisable to perform differential permeation experiments if the diffusive properties of the whole film are of interest and sorption experiments only if its sorptive capacity is of interest. The actual equilibrium mass uptake, M_∞^*, in these composites has been shown in *Fig. 9*. As expected, above the percolation threshold, M_∞ is directly proportional to ϕ_B. Below the threshold, the relationship is non-linear and M_∞ is a measure of the fraction of the phase *B* that can be reached from the boundary. This fraction is nonzero for films of finite thickness. Thus, a sorption experiment provides a method for probing the morphology of composites with $\phi_B < \phi_B{}^C$.

We have seen that memory effects appear in disordered composites (see Section on Effective Diffusion Coefficients). Over and above these effects, the coupling between the morphology and the imposed boundary conditions may also produce time-dependent effective diffusion coefficients. An extreme example of this phenomenon is obtained on comparison of the simulations of sorption, desorption, and differential permeation in random and laminated (ordered) composites having the same composition (with $D_A/D_B = 0.275 \times 10^{-2}$). *Figure 10* shows the time-dependence of the mass uptake in three such composites. For the layered composites, the initial slope method provides a value characteristic of the outer layers. *Figure 11* illustrates the depletion of mass from these composites due to desorption. The rate of desorption from laminated composites is similarly dependent on the properties of the outer layers. The difference between the random and the laminated composites is even greater when subjected to differential permeation boundary conditions. This is illustrated by *Fig. 12*.

All the above simulations were carried out in composites which were thick enough compared to the lengths of the exposed faces to prevent forma-

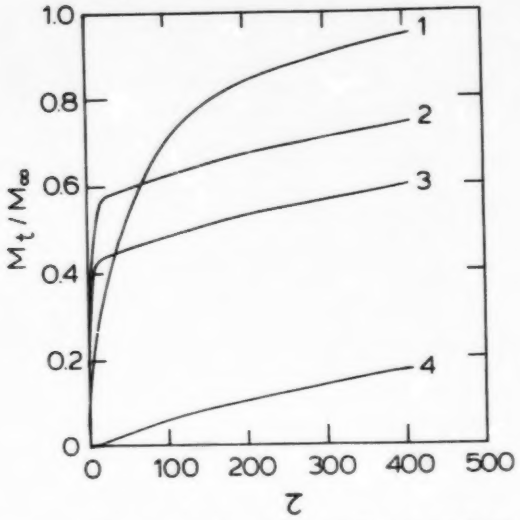

Fig. 10. Sorption in a 2D hexagonal tessellation and $D_A/D_B = 0.275 \times 10^{-2}$. Number of exposed cells per face = 14; tessellation is 14 cells thick; area fraction is 0.5714. Fractional mass uptake, M_t/M_∞, versus dimensionless time, τ. Curve 1: chaotic morphology; Curve 2: laminate BAB; Curve 3: laminate BABAB; Curve 4: laminate ABA.

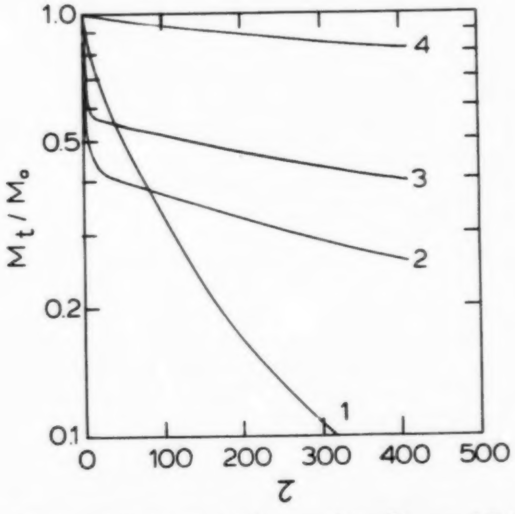

Fig. 11. Desorption from a 2D hexagonal tessellation and $D_A/D_B = 0.275 \times 10^{-2}$. Number of exposed cells per face = 14; tessellation is 14 cells thick; area fraction ϕ_B is 0.5714. Dimensionless average concentration M_t/M_o, vs. dimensionless time, τ. Curve 1: chaotic morphology; Curve 2: laminate BAB; Curve 3: laminate BABAB; Curve 4: laminate ABA.

tion of sample-spanning clusters below the percolation threshold.

CONCLUSIONS

The experimental or numerical evaluation of an effective diffusion coefficient for a given blend must be carried out on the basis of its intended use. The morphology of the blend can be such that the coefficients obtained by sorption and differential permeation differ significantly. Such differences are magnified for small samples, close to but below the percolation threshold. The morphology can also be responsible for temporal variations in the calculated effective diffusion coefficients. In blends with complex morphologies, temporal variations are due to averaging over length scales which are much larger than those of the heterogeneities (coherence length). Additional effects arise due to large scale ordering such as skin-core effects, etc.

In the conductor—non-conductor composites studied in this article, the behavior of certain quantities near the percolation threshold is significantly different from that reported for infinitely large systems. For example, the effective diffusion coefficient does not start with zero slope. This serves to illustrate the distinction between finite and infinite conductor—non-conductor composites.

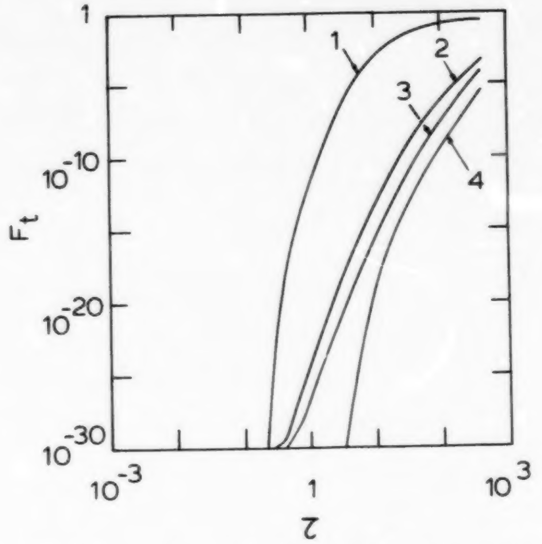

Fig. 12. Permeation through a 2D hexagonal tessellation and $D_A/D_B = 0.275 \times 10^{-2}$. Number of exposed cells per face = 14; tessellation is 14 cells thick; area fraction = 0.5714. Dimensionless flow rate, F_t, vs. dimensionless time, τ. Curve 1: chaotic morphology; Curve 2: laminate BAB; Curve 3: laminate BABAB; Curve 4: laminate ABA.

ACKNOWLEDGEMENT

The authors wish to acknowledge the financial support of the National Science Foundation, Polymers Program (DMR-8020244) and U.S. Army Research Office.

REFERENCES

1. J. Sax and J. M. Ottino, *Polym. Eng. Sci.*, **23**, 165 (1983).
2. R. M. Barrer, Chap. 6 in "Diffusion in Polymers", J. Crank and J. S. Park, eds., Academic Press (1968).
3. T. K. Kwei and T. T. Wang, in "Permeability of Films of Coatings", p. 37. H. B. Hopfenberg, ed., Plenum (1974).
4. I. Webman, *Phys. Rev. Lett.*, **47**, 1496 (1981).
5. M. Sahimi, B. D. Hughes, L. E. Scriven, and H. T. Davis, *J. Chem. Phys.*, **78**, 6849 (1983).
6. H. T. Davis, L. R. Valencourt, and C. E. Johnson, *J. Am. Ceramic Soc.*, **58**, 446 (1975).
7. R. Landauer, *J. Appl. Phys.*, **23**, 779 (1952).
8. P. H. Winterfeld, L. E. Scriven, and H. T. Davis, *J. Phys. C: Solid State Phys.*, **14**, 2361 (1981).

9. S. Kirkpatrick, *Rev. Mod. Phys.*, **45,** 574 (1973).
10. S. A. Stern and H. L. Frisch, *Ann. Rev. Mater. Sci.*, **11,** 523 (1981).
11. J. Crank, "The Mathematics of Diffusion", Oxford University Press (1956).
12. T. Alfrey, Jr., E. F. Gurnie, and W. D. Lloyd, *J. Polym. Sci.*, *C*, **12,** 249 (1966).
13. C. H. M. Jacques, H. B. Hopfenberg, and V. T. Stannett, in "Permeability of Films and Cotings", p. 73. H. B. Hopfenberg, ed., Plenum (1974).
14. R. M. Felder and G. S. Huvard, "Methods of Experimental Physics", *16C*, R. Fava, ed., Academic Press (1980).
15. H. T. Davis, *J. Am. Ceram. Soc.*, **60,** 499 (1977).
16. Y. J. Shur and B. Ranby, *J. Appl. Polym. Sci.*, **19,** 1337 (1975).
17. Y. J. Shur and B. Ranby, *J. Appl. Polym. Sci.*, **19,** 2143 (1975).
18. Y. J. Shur and B. Ranby, *J. Appl. Polym. Sci.*, **20,** 3105 (1975).
19. Y. J. Shur and B. Ranby, *J. Appl. Polym. Sci.*, **20,** 3121 (1975).
20. B. Ranby, *J. Polym. Sci., Symp. No. 51*, 89 (1975).
21. L. E. Reichl, Chap. 6 in "A Modern Course in Statistical Physics" University of Texas Press (1980).
22. P. H. Winterfeld, Ph.D. Thesis, University of Minnesota, Minneapolis (1981).
23. K. K. Mohanty, J. M. Ottino, and H. T. Davis, *Chem. Eng. Sci.*, **37,** 905 (1982).
24. R. Aris, *Arch. Rat. Mech. Anal.*, **70,** 203 (1979).
25. H. T. Davis, Proceedings 28th Macromolecular Symposium IUPAC, 739 (1982).
26. S. Kirkpatrick, in "American Institute of Physics/AIP Conference Proceedings" No. 40, p. 99, J. C. Garland and D. B. Tanner, eds., American Institute of Physics, New York (1978).

DISCUSSION

L. Piche: Yesterday I had a discussion with Prof. Lacabanne. We were looking at the expressions she gets for relaxation times and in this context we made a reference to spin glasses. I know of Kirkpatrick's work in Toulouse on spin glasses. I was wondering what is your point of view on this subject.

J. M. Ottino: The treatment of spin glasses is somewhat related to percolation theory that was developed in the context of these problems, electron hopping in semiconductors, and so on. As to how to use some of these concepts to study the distribution of relaxation times, I have no idea.

L. Piche: You do not have any idea how to translate the experiments which are done in spin glasses to relaxation in polymeric systems?

J. M. Ottino: I have not given too much thought to that. I would be willing to speculate but I do not have any concrete information right now.

I. Sanchez: My question is a very naive one. Is there a simple way to understand why sorption should be different from permeation? Is it that sorption makes use of all the dead ends in the pathway as well as of those that do not lead to dead ends whereas for permeation only the pathways are important?

J. M. Ottino: Yes, that is exactly the correct explanation.

L. A. Utracki: If one is making incompatible polymer blends, the morphology is determined by composition and the method of preparation. Generally speaking when one goes from polymer *A* to polymer *B* throughout the whole range of composition, first there is a region of solubility, then the dispersed phase appears, usually as spherical particles with a certain distribution of particle sizes. Around 35 percent the morphology changes to interconnecting regions. Usually the two homopolymers form interconnecting lamellar or fibrillar structures. The sequence is the same if one considers polymer *A* dispersed in polymer *B*, i.e., there is a symmetry of behaviour. Now the question is, if I want to reduce the permeability of polymer *A* by adding polymer *B* what would be the desired morphology and desired concentration according to your theoretical calculations?

J. M. Ottino: I would like to expand your question. Let us consider the case of electrical conductivity in composites of metals and polymers. Let us suppose we have a non-conductive polymer which we want to make conductive. Furthermore, let us say that we are not interested in the mechanical properties. How to make it conductive? One possible answer to this problem is to "squeeze" the conductive phase in between the grains of the other, non-conductive phase.

Now let us consider the reverse situation: having a conductive polymer which you want to make non-conductive. What you can do is to place thin, insulating regions between the conductive grains of polymer to break the electrical conductivity pathways, or in practical terms, to coat some of the polymer grains with the insulator and then fuse all grains together. One of my figures in the paper illustrates this situation. The theory can tell you precisely how much of the non-conductor you need. The concentration is not high—I think it can well be below 10 vol. percent.

This approach has been used in the area of conductive polymers. For example, some people have been able to make a non-conductive polymer conductive by coating its uniform size, spherical grains with less than 1 percent of silver, then compressing them into a desired form. They generated a monolayer of conductive silver pathways in over 99 percent pure polymer; from the point of view of electrical conductivity its performance changed drastically whereas the other properties remained unaffected. It seems to me that the same concept can be used to modify the gas permeability.

L. A. Utracki: This is a very attractive concept.

Society of Plastics Engineers

Executive Office, 14 Fairfield Drive, Brookfield Center, CT 06805, U.S.A.
(203) 775-0471
Telex No. 643-712

EMBERSHIP
PPLICATION

I am applying for:

☐ Membership
☐ Reclassification
(no charge)
☐ Reinstatement
(initiation fee not required)

AME: ______________________
First Middle Last

ATE OF BIRTH: ______________________
Month Day Year

DDRESS:
l in both addresses and check your preferred mailing address.

COMPANY (spell out name)
____
____
____
ity State (Prov.) Zip

OSITION: ______________________

HOME ______________________
____
City State (Prov.) Zip

ob Function
hat is the *primary* end product manufactured or service
erformed at your company location?

lease Check your Primary job function (check one only).

- ____ 01 Production or Manufacturing Engineering
- ____ 02 Design or Design Engineering
- ____ 03 Purchasing
- ____ 04 Sales or Marketing
- ____ 05 Research or Development Engineering
- ____ 06 General or Corporate Management
- ____ 07 Other (Specify)

DIVISIONS

My free primary Division choice is ______________________
check (✓) others below as secondary Divisions (cost -$4 each).

- ____ 21 Color and Appearance
- ____ 22 Extrusion
- ____ 23 Injection Molding
- ____ 24 Electrical and Electronic
- ____ 25 Thermoforming
- ____ 26 Engineering Properties and Structure
- ____ 27 Vinyl Plastics
- ____ 28 Thermoset
- ____ 29 Thermoplastics Materials & Foams (Nonvinyl)
- ____ 30 Blow Molding
- ____ 31 Plastics in Automotive
- ____ 33 Plastics Analysis
- ____ 34 Decorating
- ____ 35 Moldmaking and Mold Design
- ____ 36 Medical Plastics
- ____ 37 Marketing (in formation)
- ____ 38 Polymer Modifiers & Additives (in formation)

Grade	Requirements
Senior Member	Minimum of twelve (12) experience credits and current continuous membership in the Society for a minimum of two (2) years.
Member	Minimum of six (6) experience credits.
Affiliate Member	Less than six (6) experience credits.
Student Member	Regularly enrolled FULL-TIME student in a course of study in plastics.

Check below the membership grade for which you believe details of your experience in plastics qualifies you (see grades above).

☐ Student Member ☐ Member
☐ Affiliate Member ☐ Senior Member

Statement of Fees *(U.S. FUNDS ONLY)*

MEMBERSHIP YEAR: 7/1 thru 6/30

$10.00 INITIATION FEE MUST BE ATTACHED IN ORDER TO PROCESS YOUR APPLICATION. INITIATION FEE IS SEPARATE FROM ANNUAL DUES.

- **SENIOR MEMBER, MEMBER, AFFILIATE**

Annual Dues: 7/1 - 6/30	$45.00
If joining after 12/31	$22.50
If joining after 4/1	$10.00 (initiation fee only)

- **STUDENT MEMBER**
  Annual Dues: whenever joining $8.00 (no initiation fee/ not pro-rated)
- **REINSTATED MEMBER**
  Annual Dues: whenever reinstated $45.00 (no initiation fee/ not pro-rated)

I wish to join the ______________________ Section.

REFERENCES The Bylaws require the names of three references who are familiar with your work. One of them should be a member of the Society. Assistance in providing member-references will be given on request. Signatures are not necessary.

1. (Member-Sponsor) ______________________
2. ______________________
3. ______________________

STATEMENT OF COLLEGE WORK

Years attended		Institution	Major	Degree	Education Credits
From	To				

RECORD OF QUALIFYING EXPERIENCE IN PLASTICS

DATES				Give your title, name and location of employer. List in chronological order. Describe duties fully and state any important engineering work you have done in each position. If space is not sufficient, use separate sheet.	Time in years (a)	% in plastics (b)	Qualifying experience (a x b)
From		To					
Mo.	Yr.	Mo.	Yr.		yrs./mo.		yrs./mo.
						SUB-TOTAL	

CREDENTIALS COMMITTEE APPROVAL ONLY Approved Grade	
(S)	Date
(S)	Date
Office use only:	Division
ID#	Job Class
Grade	Date Elected
Section	

Total education and experience credits. ▶ ______

I certify that the statements made in this application are correct. I agree, if elected, to be governed by the Constitution and Bylaws of the Society and to promote the objectives of the Society.

____
Signature in ink. Date

If applying for Member or Senior Member, please complete *in detail:*

STATEMENT OF COLLEGE WORK

Years attended		Institution	Major	Degree	Experience Credits (see notes below)
From	To				

RECORD OF QUALIFYING EXPERIENCE IN PLASTICS

DATES				Give your title, name and location of employer. List in chronological order. Describe duties fully and state any important engineering work you have done in each position. If space is not sufficient, use separate sheet.	Time in years (a)	% in plastics (b)	Qualifying experience (a x b)
From		To					
Mo.	Yr.	Mo.	Yr.				
					yrs./mo.		yrs./mo.

SUB-TOTAL

Total education and experience credits. ▶

Grade	Requirements
Senior Member	Minimum of twelve (12) experience credits and current continuous membership in the Society for a minimum of two (2) years.
Member	Minimum of six (6) experience credits.
Affiliate Member	Less than six (6) experience credits.
Student Member	Regularly enrolled FULL-TIME student in a course of study in plastics.

CREDENTIALS COMMITTEE APPROVAL ONLY	Approved Grade
(S) Date	
(S) Date	

Experience Credits
Grade of Membership . . .

Membership grades are based on expeience credits which are earned as follows:

1. **Experience credits earned for education.**
   Maximum credits allowable for education shall be six (6). Use highest degree credits ONLY.

Doctorate in science or engineering	**6 credits**
Masters in science or engineering	**5 credits**
Bachelors in science or engineering	**4 credits**
Any degree other than above	**2 credits**
Associate or Adjunct in Plastics	**2 credits**
Associate or Adjunct (awarded by Community College or equivalent for two-year course of studies, without specializing in plastics).	**1 credit**

When filling in the "Statement of College Work" above place the corresponding number of credits earned in the right-hand column.

2. **Experience credits** are determined by the proportion of time involved in actual technical and engineering duties in plastics for each position held. For instance, if only three of the five years you worked for the XYZ Co. comprised technical or engineering duties, then three (3) years (60% of 5 yrs.) would constitute the "Qualifying Experience" you would enter in years and months in the right-hand column under "Record of Qualifying Experience in Plastics."
   Please detail carefully the engineering skill required for each position to help the Credentials Committee judge experience as "qualifying."

When you have determined the number of credits which you believe you have earned, consult the following member grade requirements. Indicate on the reverse side the grade of membership for which you believe you are qualified.

INFORMATION FOR AUTHORS

Submission of original and review articles is encouraged. There is no limit on length. Three copies of the manuscript should be submitted, which should be typed, one side only, double space, with at least a 1-inch margin. Submission will be taken to imply that the paper has not been previously published, that it is not being considered elsewhere for publication, and that if accepted it will not be published elsewhere in the same form, in any language, without the consent of the editor or publisher. Authors must agree to transfer copyright to the publisher when an article is accepted for publication. Unless notified to the contrary by the authors, the publisher assumes that the act of submitting the article signifies the authors' agreement to such copyright transfer to the publisher. The journal carries a voluntary page charge. Each manuscript should include:

A separate title page, headed by a concise, meaningful title (avoid abbreviations) for the paper. This page should provide:

- The name and affiliations of each contributing author at the time the paper was prepared.
- Indicate by asterisk any changes of address for each author since article preparation.
- Acknowledgment of any prior oral presentation and original source of the material.

A separate abstract page, consisting of a single paragraph of 100–200 words to include the title and the names and addresses of the authors. Define any abbreviations for substances or methods (such as ABS, SAXS, etc.).

A list of references, on a separate page at the end of the text, numbered in order of text citation. The references are to be abbreviated in the form used in Chemical Abstracts using the names of all authors preceded by initials; see Bibliographic Guide for Editors and Authors, American Chemical Society, Washington, D.C.

- Within the text, the reference citations are typed in parentheses in line with the main copy (no superscripts or subscripts), thus:

  According to Young, et al. (1)...

- In the list of references the general style is as follows:

For periodicals:

1. S. S. Young, J. L. White, E. S. Clark and Y. Oyanogi, *Polym. Eng. Sci.*, 20, 798 (1980).

The journal name and volume are to be underlined and the year is placed in brackets. The issue number is given only when needed for identification. The article name is eliminated unless the reference is unclear without it.

For books: The title to be spelled out in full.

5. H.-G. Elias, "Macromolecules," Ch. 1, Vol. 2, Plenum Press, New York (1977). (Include the state when the city is not identifiable.)

A list of nomenclature, identifying symbols and abbreviations, commonly desirable at the end of the text. Footnotes are to be avoided.

Equations, numbered and typed in the appropriate place in the text. Where symbols cannot be typed, write them neatly in ink.

Tables, each typed on a separate page, with a heading, and numbered with arabic numerals that correspond to the order in which they are cited in the text. The tables should be inserted in the manuscript after the references and before the figures.

Figures, assembled at the end of the manuscript and preceded by a typed list of captions that explain them. Please also supply a set of original figures or sharp glossy photos thereof, on 8½ × 11 paper or attached to sheets of this size, one sheet for each figure. Each should be identified on the front edge or on the back (photographs) with the name of the first author and the figure number (e.g., Smith, Fig. 1). Originals are to be prepared with high contrast India ink and to bear uniformly stencilled notations. Line drawings and photos should be of a quality suitable for good photographic reproduction and retained legibility upon size reduction to one quarter. Manuscript transmittal letter should indicate if the figures need be returned.

Send manuscripts to:
Roger S. Porter, Editor
POLYMER ENGINEERING AND SCIENCE
℅ Polymer Science & Engineering
University of Massachusetts
Amherst, Massachusetts 01003

For information concerning publication dates, page charges and reprint orders contact:
Editorial Dept.
Society of Plastics Engineers
14 Fairfield Drive
Brookfield Center, Connecticut 06805